Dynamic Stability Analysis of Tensegrity Domes

(Analiza stateczności dynamicznej kopuł typu tensegrity)

by

Maryna Solovei

A thesis submitted in partial satisfaction of the requirements for the degree of Doctor of Philosophy in Civil Engineering, Geodesy and Transportation in the Graduate Division of the Kielce University of Technology

Supervisor

DSc., PhD., Eng. Paulina Obara

Kielce 2024

I am deeply grateful to my supervisor

Professor Paulina Obara

for the invaluable supervision, support

and tutelage during my PhD study

I also would like to offer my special thanks to

Dr. Justyna Tomasik

for the insightful comments and suggestions

Thesis Abstract

The dissertation thesis concerns the dynamic stability analysis of tensegrity domes. The consideration includes the most known tensegrity domes, i.e., Geiger dome and Levy dome. These structures are distinguished from the traditional cable-strut steel domes by the presence of some unusual features. These domes are characterized by the presence of a self-equilibrated set of forces (the initial prestress), that stabilize the infinitesimal mechanisms. The analysis of tensegrity domes includes the influence of the initial prestress level on structure response. Considered domes with different structural modifications to compare their behaviour are presented. The modifications include different types of upper sections (open or closed upper sections) and additional circumferential cables (only in the case of the Geiger domes). Three types of analyses are performed, i.e., static, dynamic, and dynamic stability analysis. The influence of the initial prestress level on the static parameters (displacements, stiffness, and maximum effort), dynamic parameters (natural and free frequencies), and most importantly, the distribution and range of the unstable regions are considered.

The analysis proved that the ability to control static and dynamic parameters with initial prestress is possible only in the case of the existence of an infinitesimal mechanism or mechanisms. Additionally, structures with a larger number of infinitesimal mechanisms are more sensitive to the change in the initial prestress level. In the case of the Geiger domes, structural modifications caused reducing a number of mechanisms, thus influence of the initial prestress level. For the Levy dome, the change of the upper section (from a closed one to an open one) resulted in the appearance of one local infinitesimal mechanism, however, the behaviour is similar to the structure without the mechanism.

The analysis of the unstable regions showed, that the widest unstable regions appear at the minimum prestress level. Nonetheless, the increase in the initial prestress level results in the complete or partial narrowing of unstable regions. Additionally, the shape and range of the unstable region are also connected to the external load situation.

The thesis concluded with answers to the questions asked at the beginning of the consideration and summarized with advantages and disadvantages of the considered structures. The summary includes the authors' design guidelines for the future application of tensegrity domes in civil engineering.

Thesis Abstract (in Polish)

Rozprawa doktorska dotyczy analizy stateczności dynamicznej kopuł tensegrity. Rozważania obejmują najbardziej znane kopuły tensegrity, tj. kopułę Geigera i kopułę Levy'ego. Konstrukcje te różnią się od tradycyjnych stalowych kopuł cięgnowych obecnością pewnych nietypowych cech. Kopuły te charakteryzują się obecnością samozrównoważonego układu sił wewnętrznych (wstępnego sprężenia), który stabilizuje nieskończenie małe mechanizmy. Analiza kopuł tensegrity obejmuje wpływ stanu samonaprężenia na odpowiedź konstrukcji. Przedstawiono różne, znane z literatury, modyfikacje strukturalne, w celu porównania wpływu tych modyfikacji na zachowanie kopuł. Analizowane są kopuły z środkowym pierścieniem (otwarta górna sekcja) lub bez (zamknięta górna sekcja). Dodatkowo, w przypadku kopuł Geigera, uwzględniono dodatkowe kable obwodowe łączące górne węzły. Przeprowadzono trzy rodzaje analiz, tj. analizę statyczną, analizę dynamiczną i analizę stateczności dynamicznej. Rozważono wpływ wstępnego sprężenia na parametry statyczne (przemieszczenia, sztywność i maksymalne wytężenie), parametry dynamiczne (częstotliwości drgań własnych i swobodnych), a przede wszystkim na rozkład obszarów niestateczności.

Analiza wykazała, że możliwość kontroli parametrów statycznych i dynamicznych za pomocą wstępnego sprężenia jest możliwa tylko w przypadku istnienia mechanizmu infinitezymalnego (lub mechanizmów). Dodatkowo, konstrukcje z większą liczbą mechanizmów infinitezymalnych są bardziej wrażliwe na zmianę poziomu wstępnego sprężenia. W przypadku kopuł Geigera modyfikacje strukturalne spowodowały zmniejszenie liczby mechanizmów, a tym samym wpływ naprężenia wstępnego. W przypadku kopuł Levy'ego zmiana górnej sekcji (z zamkniętej na otwartą) spowodowała wystąpienie jednego, lokalnego mechanizmu infinitezymalnego, jednak zachowanie tej kopuły jest podobne do struktury bez mechanizmu.

Analiza stateczności dynamicznej wykazała, że najszersze obszary niestateczne występują przy niskim poziomie wstępnego sprężenia. Niemniej jednak wzrost poziomu wstępnego sprężenia powoduje częściowe lub całkowite zwężenie obszarów niestateczności.

Rozprawę zakończono odpowiedziami na postawione na początku rozważań pytania oraz podsumowano zalety i wady rozważanych konstrukcji. Dodatkowo, w podsumowanie zawarto sugerowane wytyczne projektowe, dotyczące przyszłego zastosowania kopuł tensegrity w inżynierii lądowej.

TABLE OF CONTENTS

Abbreviations and symbols (in order of appearing in the text)

${}^{0}C$	Initial configuration
t	Time
${}^{t}C$	Actual configuration at the moment t
Δt	Time increment
${}^{t+\Delta t}C$	Actual configuration at the moment $t + \Delta t$
A_0	Initial cross-section
l_0	Initial length
A	Cross-section
l	Length
$\mathbf{q}$	Nodal coordinates vector
$\mathbf{Q}$	Nodal forces vector
q_i	Displacement
Q_i	Nodal force
$\mathbf{K}_T$	Tangential stiffness matrix
$\mathbf{R}$	Residual force vector
$\mathbf{F}$	Inertial forces vector
$\mathbf{K}_L$	Linear stiffness matrix
$\mathbf{S}$	Initial prestress vector
$\mathbf{K}_G$	Geometry stiffness matrix that depends on the initial prestress vector $\mathbf{S}$
$\mathbf{N}$	Axial forces vector
$\mathbf{K}_{GN}$	Geometry stiffness matrix that depends on the axial forces vector $\mathbf{N}$
$\mathbf{K}_{NL}$	Non-linear stiffness matrix
$\mathbf{K}_{ui}$	Displacement stiffness matrix
S	Initial prestress level
$\mathbf{y}_s$	Self-stress state
σ_0	Initial stress

N	Axial force
E	Young modulus
Δ_{ui}	Displacement increment
N'	Actual axial force
n	Number of elements
m	Number of degrees of freedom
$\mathbf{B}$	Extension matrix
$\boldsymbol{\sigma}$	Stress vector
$\mathbf{D}$	Compatibility matrix
$\mathbf{H}$	Diagonal matrix of eigenvalues of the compatibility matrix **D**
$\mathbf{y}_i$	Eigenvector of the compatibility matrix **D** corresponded to zero eigenvalue of the matrix **H**, responsible for the self-stress state
μ_i	Zero eigenvalue of the compatibility matrix **D**
$\mathbf{L}$	Diagonal matrix of eigenvalues of the linear stiffness matrix $\mathbf{K}_L$
$\mathbf{x}_i$	Eigenvector of the linear stiffness matrix $\mathbf{K}_L$ corresponded to zero eigenvalue of the matrix **L**, responsible for the mechanism
γ_i	Zero eigenvalue of the linear stiffness matrix $\mathbf{K}_L$
σ_i	Eigenvalues of the linear stiffness matrix $\mathbf{K}_L$ and the geometric stiffness matrix $\mathbf{K}_G$
$\mathbf{z}_i$	Eigenvector of the linear stiffness matrix $\mathbf{K}_L$ and the geometric stiffness matrix $\mathbf{K}_G$
$\mathbf{O}$	Diagonal matrix of eigenvalues σ_i of the stiffness matrix consisted of linear matrix $\mathbf{K}_L$ and geometric matrix $\mathbf{K}_G$
$\boldsymbol{\Gamma}$	Set of all elements of the structure
$\boldsymbol{g}_i$	Set of elements of the structure with the same length
e_l	First element in the set of elements of the structure with the same length
e_z	Last element in the set of elements of the structure with the same length
$\pm S_i$	i-th level of the initial prestress
S_{max}	Maximum level of initial prestress

F	Fitness function
F_1	Component of fitness function related to the stiffness matrix
F_2	Component of fitness function related to the equilibrium of nodes
EN	Equilibrium of nodes
S_{ix}	Force projection on x axis
S_{iy}	Force projection on y axis
S_{iz}	Force projection on z axis
S_{min}	Minimum level of initial prestress
N_{Rd}	Load-bearing capacity
W_{max}	Maximum effort of elements
GSP	Global Stiffness Parameter
$\mathbf{K}_S$	Secant stiffness matrix
$\tilde{\mathbf{q}}$	Amplitude vector
f	Frequency
$\mathbf{M}$	Mass matrix
P	Constant part of the periodic load
P_t	Amplitude of the periodic load
θ	Load frequency
Ω	Natural frequency of the structure loaded with a constant part of the load
$\ddot{\mathbf{q}}$	Acceleration vector
υ	Pulsatility index
η	Resonant frequency of the external load vibrations
α	The angle of inclination of cables of the load-bearing girder
β	The angle between perimeter cables
ng	Number of load-bearing girders
ns	Number of struts
nm	Number of infinitesimal mechanisms
$W_{max,C}$	Maximum effort of cables

$W_{max,S}$	Maximum effort of struts
P_z	Vertical load applied according to z axis
P_{xy}	Plane load applied on plane of x and y axes
ρ	Steel density
f_{total}	Total number of frequencies dependent on the initial prestress
f_{nm}	Number of frequencies that correspond with the mechanism
f_{add}	Number of additional frequencies dependent on the initial prestress
A_η	The area of the unstable region
λ	Non-dimensional parameter that measures changes in areas of unstable regions depending on the initial prestress level

1. Introduction

1.1. Subject of consideration

Tensegrity domes are composed of compressed (struts) and tensed (cables) elements. The struts never touch and are surrounded by a continuous network of cables. There are some characteristic features that distinguishes them from the traditional rod-like structures. The immanent features are self-stress state and infinitesimal mechanism. The self-stress state can be defined as a system of self-equilibrated forces that satisfy the homogeneous equation of equilibrium (the initial prestress). The absence of these forces makes the tensegrity structure unstable, i.e., geometrically variable. The initial prestress must be introduced to the structure to stiffen the existing infinitesimal mechanism and ensure stabilization. The self-stress state depends only on the geometry of the structure, and is independent of external loads. The infinitesimal mechanisms, unlike finite mechanisms, describe the local geometric variability to the infinitesimal displacements. Changing the initial prestress allows controlling the behaviour of the tensegrity system under various loads and influences the stiffness of the structure.

The idea of tensegrity was mainly associated with art, and to a lesser extent with architecture, and consequently, with construction. In recent years, the interest of architects and engineers in the practical application of these solutions has increased: “Tensegrity: from Art to Structural Engineering” [1]. This is confirmed by numerous scientific works on the design of tensegrity systems, opening new perspectives for construction and application.

Currently, many research teams worldwide are working on tensegrity structures. It is impossible to list all the scientists, but the leaders include René Motro (France), Robert E. Skelton (USA), Hidenori Murakami (USA), Bin-Bing Wang (Singapore), and Y. Kono (Japan). Important monographs on tensegrity include: “An Introduction to Tensegrity” [2], “Tensegrity: Structural Systems for the Future” [3], “Tensegrity Systems” [4], “Art and Ideas” [5], and “Tensegrity Structures: Form, Stability, and Symmetry” [6].

In Poland, relatively few researchers are involved in tensegrity structures. Wacław Zalewski, considered a pioneer, designed the roof of Supersam in Warsaw in 1962 and the roof of the sports hall in Katowice in 1971. The first use of tensegrity as a bridge structure was the KL-03 footbridge over the S-7 Salomea – Wolnica route in Magdalenka, designed by Bogusław Markocki [7, 8]. The only monograph published in Polish on tensegrity structures is Zbigniew Bieniek's work [9] “Tensegrity – Integrating Tension in Architectural Systems.” This monograph is contributory in nature. Bieniek presented geometrically diverse systems and structures for use in construction technology. He also supplemented the current classification of tensegrity systems by adding a new class, θ (theta), which includes systems with a disjoint network of tendons. Bieniek's research is primarily architectural and focuses on the search and presentation of morphological methods for shaping these structures [10-17]. In turn, Wojciech Gilewski deals with tensegrity from a mechanical perspective [18-29]. Under his supervision, three doctoral theses have been completed on the use of tensegrity structures in bridge construction [30], the possibility of using tensegrity as an intelligent structure [31], and the potential use of tensegrity structures in building construction [32]. In the cooperation with Al Sabouni-Zawadzka the research on orthotropic tensegrity models [33-36] and metamaterials [37, 38] was conducted. From the experimental point of view, works regarding the effect of prestressing [39], tensegrity towers [40], and the dynamic response of tensegrity structures [41] were presented by Małyszko and Rutkiewicz.

Attempts to apply tensegrity structures in construction date back to the origins of the idea itself. Among the first constructions were geodesic domes, patented by Fuller in 1954 [42]. These domes are characterized by high load-bearing capacity with minimal use of construction materials. Unfortunately, they require complex analyses due to large deformations, susceptibility to dynamic loads, and the necessity to analyze individual assembly phases. Additionally, the process of prestressing the structure is challenging [43, 44].

In recent years, there has been an increase in interest in the application of tensegrity structures in construction. It applies to both standard and non-standard applications. This increase is due to the enhanced design and execution capabilities, which are related to the development of advanced computational techniques and the advancement of construction technologies and materials.

Standard applications refer to the use of the tensegrity concept for building domes, plates, towers, masts, bridges, and footbridges. Non-standard applications involve intelligent construction and the use of the tensegrity concept in creating innovative materials, so-called metamaterials.

The research topic addressed is dictated by the need to supplement the existing literature, in which the problem of parametric resonance of tensegrity structures has not been highlighted so far. From an engineering point of view, the technical significance of instability areas is particularly large because if the load parameters fall within the designated area, oscillations with increasing amplitude occur. These oscillations are dangerous in terms of the durability of the structure. There is extensive literature on parametric vibrations that essentially resolves all the basic issues. Nonetheless, tensegrity structures are a special example of constructions. They are characterized by an additional parameter, the state of self-stress, which affects the shape and extent of these areas. In this work, surface tensegrity structures, such as double-layer grids and domes, whose application in construction is increasingly common, will be analyzed.

1.2. Purpose, scope and assumptions of the work

The **research problem** involves the analysis of the behavior of tensegrity domes subjected to a periodic load. Particularly, the influence of the initial prestress level on the structure's static and dynamic parameters is considered.

The **research hypothesis** is formulated as follows:

1. Control of static and dynamic parameters is only possible for tensegrity domes that exhibit an infinitesimal mechanism.
2. Structural modifications can both improve and impair domes' response to the external load.
3. The initial prestress level affects the distribution of dynamic unstable regions in tensegrity domes subjected to periodic loads.

The **research purpose and scope** are to investigate the behavior of tensegrity domes under the influence of loads (time-independent and periodic). To achieve this aim, the following questions must be answered:

i. How does initial prestress impact the static parameters of the domes with and without infinitesimal mechanisms?
ii. What is the relation between the initial prestress level and vibration frequencies that correspond to the infinitesimal mechanisms?
iii. What is the relation between the initial prestress level and vibration frequencies that do not correspond to the infinitesimal mechanisms?
iv. How does the initial prestress level influence the distribution and range of unstable regions?
v. How does the position and value of the external load influence the static and dynamic responses of the dome?
vi. How does structural modification influence the static and dynamic responses of the dome?
vii. What are the design guidelines for the application of tensegrity domes?

The following **assumptions** were adopted for the research:

- the structure material (steel) is continuous, uniform, and isotropic,
- constitutive equations are linear,
- structure consists of only stressed elements (cables) and only compressed elements (struts),
- all elements are straight and of comparable length,
- the structures are initially prestressed, by means no cable is loose (the sag effect on the effective elasticity modulus is neglected),
- the minimum prestress level ensures only tension forces in the cables in each computational situation,
- tensed elements create a continuous net, whereas, compressed elements never touch, thus are not subjected to large buckling loads,
- nodes are ideal ball joints,
- supporting bonds are fixed, and scleronomic,
- loads are conservative,
- large displacement gradients are possible,
- the elements assumed to be weightless in the static considerations,
- the impact of dumping was omitted in the dynamic considerations.

Theoretical studies and numerical simulations are conducted. Since tensegrity structures without considering the initial prestress level are geometrically variable, their analysis using commercial software is more complicated. Additionally, the inclusion of initial prestress is only feasible by introducing the appropriate axial load to all elements. The numerical analysis in this work utilizes a computational procedure encompassing the analysis of geometrically nonlinear rode systems. This procedure is based on the finite element method and allows for a comprehensive analysis at any initial prestress level defined in the pre-stressed tensegrity element.

The computational module is written in the Mathematica environment, which simplifies operations through the use of its built-in functions and commands. The solution of the algebraic nonlinear system of equations executed using the Newton-Raphson method is implemented in the mentioned environment. The program allows for the flexible definition of the construction geometry, material parameters, initial stresses, and loads and will enable tracking the behavior of selected static, geometric, and dynamic parameters.

1.3. Dissertation draft

The work consists of seven main chapters, whereas the first chapter contains the introduction to the subject of consideration (**Chapter 1**).

Chapter 2 presents the general concept of tensegrity structures. This part focuses on the history and evolution of tensegrity, covering the development from the idea to its application, including the first originators and their successors. The chapter includes a thorough literature review of existing research on tensegrity structures and also discusses the current state of knowledge in the field of dynamic stability analysis of tensegrity. To present the research subject in detail about tensegrity domes, the chapter delves into the origin, history, analysis, and application of cable-strut tensegrity domes.

Chapter 3 focuses on the geometrically nonlinear mathematical model applied to the analysis of tensegrity systems. It presents the equilibrium equations for a single finite element and for the complex structure. The presented description is further applied to the qualitative and quantitative analyses of the tensegrity domes.

The main subject of **Chapter 4** is the qualitative and quantitative analysis of the tensegrity structures. The qualitative analysis focuses on the identification of self-stress states (initial prestress) and infinitesimal mechanisms. Two methods of the analysis are described, i.e., spectral analysis of truss matrices and genetic algorithm. In turn, the quantitative analysis is divided into static, dynamic, and dynamic stability analyses. This assessment concerns the influence of the initial prestress level on the static parameters (displacements, stiffness, and maximum effort of the structure) and dynamic parameters (natural and free frequencies), and on the distribution of the unstable regions.

Chapter 5 is focused on the first type of the analyzed tensegrity domes, i.e., the Geiger dome. The history of the first appearance, patented geometry, and up-to-date research are provided. The several variants of considered domes are presented, i.e., small-scale domes, real-scale domes, and examples from the literature. Qualitative and quantitative analyses are performed.

Chapter 6 describes the second type of analyzed tensegrity domes, i.e., the Levy dome. The introduction covers the first inventor, design solutions, and literature review. Next, the geometry of the analyzed structures, i.e., small-scale domes, real-scale domes, and examples from the literature is provided. The qualitative and quantitative analyses are performed.

The thesis is finished with **Chapter 7** which highlights the main conclusions and achievements of the work. In particularly, answers the questions from Chapter 1.2.

A list of figures, tables, and references are provided at the end of the work, along with the calculation program developed in the Mathematica and Python environments.

2. Concept and application of tensegrity structures

2.1. Introduction

Tensegrity systems are novel solutions in the field of civil engineering. Initially considered only as works of art, they later gained popularity among scientists worldwide. These structures are characterized by their characteristic features, i.e., self-stress state and infinitesimal mechanism, which are important in the context of the potential use of tensegrity systems as adaptive and deployable "smart structures". Due to their unique properties, tensegrity systems can be implemented in various areas of science.

Furthermore, tensegrity structures offer several advantages over traditional engineering solutions. Their lightweight nature makes them ideal for applications where weight is a critical factor, such as in aerospace engineering and portable architectural structures. The inherent flexibility and adaptability of tensegrity systems also make them suitable for dynamic environments where traditional static structures might fail. In addition to their practical applications, tensegrity systems also hold aesthetic value due to their visually striking and intricate designs. This blend of form and function has led to their use in innovative architectural projects, where structural integrity and artistic appeal are equally prioritized. Architects and engineers are increasingly exploring tensegrity principles to create sustainable and energy-efficient buildings, leveraging the minimal material usage and optimal load distribution inherent to these structures.

In conclusion, tensegrity systems represent a significant advancement in structural engineering, offering a unique combination of strength, flexibility, and efficiency. Their potential for adaptation, deployability, and aesthetic integration makes them a promising area of study and application, poised to address some of the most pressing challenges in modern engineering and beyond.

2.2. Historical review

The first tensegrity structure is considered to be a sculpture made by Kenneth Snelson in 1948. It presented the original concept of "self-stressed structures composed of rigid struts and cables, with compressive and tensile forces that form an integrated whole" [45]. Initially, the idea was associated mainly with art and to a small extent with architecture and construction. Hugh Kenner was the first person who brought tensegrity from the world of art to the technical sciences. In his book [46], he initiated the systematic study of tensegrity systems, performed static analysis, and developed a prestressed configuration of *the expanded octahedron*. At the same time, Anthony Pugh elaborated on the practical principles of building simple tensegrity systems in his book [2]. The main advantage of these works was raising awareness of tensegrity structures and laying the foundation for further research.

In 1978, the British engineer Christopher Calladine noticed that the existence of an infinitesimal mechanism in a frame that fulfills Maxwell's rule [47] implies an appropriate self-stress state. In the absence of a self-stress state, the stiffness of the mechanism is zero. Infinitesimal mechanisms in tensegrity structures are stiffened by introducing the self-stress state [48, 49]. New research initiated by Calladine was continued by Pellegrino [50, 51] and Hanaor [52, 53]. Pellegrino and Calladine developed new methods for segregating rigid struts, identifying mechanisms, and detecting when the self-stress state is beneficial [54]. They refined the method of segregation of first-order mechanisms and high-order mechanisms. The study of infinitesimal mechanisms, self-stress states, geometry, and stability of tensegrity was continued by Murakami et al. [55-57].

A key issue in the study of tensegrity structures is their susceptibility to the initial prestress. The problem of finding the appropriate initial prestress has been investigated by many researchers. Existing methods for determining the appropriate initial prestress can be divided into exact and approximate (including numerical methods). The first numerical solution was proposed by Murakami and Nishimura [58-60] for *dodecahedral* and *icosahedral* modules of tensegrity structures. Numerical methods were also applied by Motro and Pellegrino, though they were effective only for some computational problems. Over time, the development of other methods began to emerge, known as "form-finding methods" [61-66]. These methods involve determining the configuration of the elements that result in a stable self-stress state in the system. The most frequently used methods are analytical solutions [19], nonlinear programming [50], dynamic relaxation [67], force density method [68], and many others. A comprehensive overview of the form-finding methods was provided in [64, 69, 70]. The search for new forms of tensegrity structures is defined as a qualitative analysis and is a main step in the analysis of tensegrity structures.

The influence of the self-stress state, and more specifically, the influence of the initial prestress level, on the behaviour of the structure is considered the next step in the analysis of tensegrity structures (quantitative analysis). The static response of tensegrity structures to external loads has been studied by many scientists [53, 55, 56, 58, 59, 71-78]. Due to the flexibility of the systems, the research required a nonlinear approach. Nonlinear analysis revealed emergent properties and strong anisotropy in tensegrity systems. Among other findings, procedures for optimizing of stiffness-to-mass ratio for symmetric and asymmetric structures were developed [79-83]. Most of the research is concentrated on theoretical studies [69, 73, 84] and small-scale models are rarely used for actual tests [53, 74, 85, 86]. The dynamic response of the tensegrity systems, on the other hand, is still under study. The literature review distinguished the following areas of research:

- methods directed at designing and searching for stable construction forms,
- algorithms that change the shape of the structure: optimization algorithms used to generate new topologies; the new topology aims to achieve the desired performance criteria, such as the level of stiffness,
- methods of controlling the shape of the structure: examining how the structure changes its shape under the influence of external forces,
- parametric analysis that considers the influence of the initial prestress level on the dynamic behaviour of the structure.

Significant progress in the dynamic research of tensegrity structures was made in the 1990s. The use of controlled structures was considered, particularly in the area of ensuring reliability, failure resistance, and control over the model. The first paper on controlling tensegrity structures was presented by Skelton and Sultan [87]. Soon after, other researchers continued the investigation of active control of tensegrity structures [88-95]. The purpose of research on active control was to reduce vibration in the system and increase efficiency. The influence of the initial prestress level of the tensegrity modules [58, 96, 97], six-strut spherical modules [98], tensegrity grids [99], and clustered systems [100] has been investigated.

Currently, interest in tensegrity structures has increased in the fields of applied sciences and engineering. These structures are often called “structures of the future” [3] and are seen as potential solutions to various problems. In recent years, architects and engineers have been looking for practical applications of tensegrity systems [1]. Tensegrity systems have found wide application in aviation and aerospace engineering due to their relatively low weight and high resistance to vibrations. The use of tensegrity has been considered in components of satellites [101], spacecraft [102, 103], telescopes [104], antennas [95], robots, and damping systems. In civil engineering, the application of tensegrity was initially limited to architectural elements [9, 43, 105, 106]. Gradually, they were implemented in the dome structures [29, 107-111] and the construction industry [27, 32]. Notably, tensegrity structures have been implemented in bridges [30, 31, 112-114] and coverings [115].

Tensegrity structures are also used in biology and biomechanics, mostly to determine the behaviour and functioning of cells [116], and to design robots and artificial intelligence systems [80, 81, 92, 117]. Additionally, the tensegrity system has been used in the design of new materials, known as metamaterials [17, 37, 38, 118-121].

2.3. Tensegrity domes

The prestressed cable-strut domes are an example of tensegrity structures. These structures can have some tensegrity features, but their genesis is not directly related to tensegrity. The first application of such a solution was the roof of the auditorium in Utica, in the United States, completed in 1959. The supporting structure of the roof, with a span of 76.2 m, consisted of radially placed flat girders composed of pairs of tensioned tendons supported by vertical, compressed struts. The girders were connected in internal rings with a diameter of 7 m. The tendons are anchored around the circumference in a rigid reinforced concrete ring. Prestressing ensured that the struts remained compressed and the tendons stretched. The lower tendons were of major importance in terms of the load-bearing capacity of the structure, and the upper ones allowed for the introduction of prestressing forces [122].

The first tensegrity cable-strut dome is considered to be the Geiger dome, patented in 1988 [115]. Geiger combined Fuller's tensegrity principle with the principle of creating compressed cable networks, and thus presented a new non-triangular spatial system of elements. The new patented system was called “Cabledome”. The main principle behind Geiger’s dome is that all tension is achieved through the roof structure by means of tensed cables and discontinuous compressed struts. The original structure consisted of radial trusses, with tensed and compressed elements. One of the main advantages of such a structure is that its weight per square meter does not change as the span increases, and can be successfully used in long-span roofs. Unlike high-profile Fuller domes, the Geiger domes have a low-profile configuration that reduces wind lift, and uneven snow settling, and uses less roofing material. After its appearance, the Geiger dome was the subject of many theoretical and experimental studies [29, 123-126]. The further configurations were presented by Terry [111], Hanaor [53, 73, 108], and others. As well as new design solutions, the analysis of tensegrity domes was the major area of interest. The geometrically nonlinear analysis of tensegrity systems [71], the prestress problem [104, 127], the equilibrium conditions [128, 129], and other aspects were studied.

An example of the implementation of the Geiger dome is the roof of the 1986 Olympic Hall in Seoul (*KSPO Dome*). The roof supporting structure of 120 m span consisted of radially arranged flat girders, as in the case of the auditorium in Utica in the United States. However, in this solution, instead of the lower rope, the struts are based on the diagonal and lower circumferential cables (Fig. 2.1) [109, 130-132]. The load was transferred from the central tension ring, through a series of radial ridge cables and the tension hoops, to the peripheral clamping ring.

Fig. 2.1. Olympic Hall roof in Seoul during the construction [132]

Another example of a tensegrity dome is the roof of the Sports Hall in Katowice (*Spodek* by Wacław Zalewski). The structure is a modified Geiger dome (Fig. 2.2). Unlike the typical solution, in this case, the roof structure with a span of 126 m uses a system of elements with lower and upper radial cables. The roof consists of 120 strut-cable girders, and a dome is supported on the inner ring, illuminating the interior of the hall [32, 133-135].

a)  b) 

Fig. 2.2. *Spodek* Hall in Katowice during the construction: a) upper section [136], b) side view [137]

It is also worth mentioning the first tensegrity structure by W. Zaleski *Supersam* roof in Warsaw (Fig. 2.3). In contrast to structures in a radial system, the supporting structure was composed of several parallel girders. The girders were composed of steel struts and top and bottom chords. The vertical load of the cover was taken up by the lower tensed chords.

Fig. 2.3. Roof of *Supersam* in Warsaw [138]

A slightly different solution for the cable dome, compared to Geiger, was developed by Matthys Levy. Levy's dome consisted of a network of tendons connected at nodes, equally spaced along the meridians. Levy's idea was used to build a stadium cover in Atlanta (*Georgia Dome*) in the United States in 1992 [110, 139-142]. This is an example of the largest existing dome in the world - the dome was built on an ellipse plan with dimensions of 227x185 m, with an area of 37,200 m^2 (Fig. 2.4). To improve the mechanical behavior of the cable dome, the additional hoop cables and changing the arrangement of the struts on the diagonal struts were used.

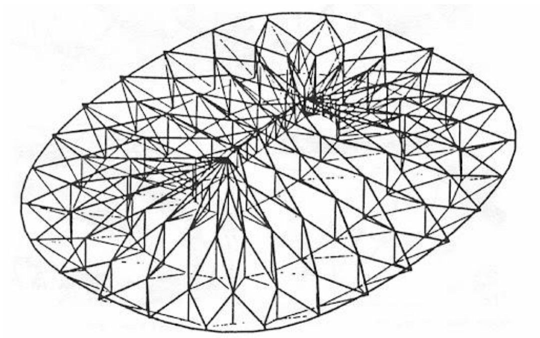

Fig. 2.4. Structure of *Georgia Dome* roof [139]

An interesting example of cable covering is the *White Rhino* membrane roof supporting structure in Chiba (Japan), built in 2001 (Fig. 2.5). The name of the structure refers to the external appearance of the roof, which resembles a rhinoceros. The structure is based on two modified three-strut trapezoidal modules of different dimensions, with an added central vertical strut. The height of the larger module is 9 m, and the length of the base side is 12 m. The dimensions of the smaller module are 6 m and 9 m, respectively. The modification of the modules involves the addition of seven additional elements, i.e., six tendons and one strut. Three additional cables extend between the six unconnected vertices of the module. In turn, the added strut is connected to the module using three further cables and constitutes a form of roof support. Additional elements do not change shape but affect the nature of the structure and improve its stiffness. The modification leads to the disappearance of the infinitesimal mechanism. These elements limit the large deformation of the membrane and transfer the load from the roof membrane to the rigid truss frame [143-145].

A lot of different structures that consist of tensed cables and compressed struts can have tensegrity features. The detailed analysis was provided in [32].

Fig. 2.5. *White Rhino* structure [143]

3. Geometrically nonlinear mathematical model

3.1. Introduction

The qualitative analysis of classical lattice structures can be carried out assuming small displacements, i.e., a linear geometric model, or second-order theory, i.e., a quasi-linear model. However, in the case of tensegrity systems, both these approaches are inadequate. The important feature of the tensegrity structure, which is related to the stiffening of the structure under the influence of an external load, is not considered in either approach. If an external load causes the displacement in accordance with the form of the infinitesimal mechanism, additional prestress of the structure occurs - tensile forces generate additional tensile forces in the cables and compressive forces in the struts. In such circumstances, the initial response cannot be used to determine the behavior of the structure. Therefore, the analysis should be carried out assuming the hypothesis of large displacements (third-order theory).

Tensegrity systems are spatial lattice systems in an initial prestress. The structure consists of tensed cables and compressed struts, and cables do not have compression rigidity. The elements are rectilinear with comparable length. The main tensegrity feature is stabilizing the existing infinitesimal mechanisms by means of the initial prestress. The second one is the size of the displacements, which can be large even if the deformations are small. Taking into account the above-mentioned tensegrity features, a geometrically non-linear model was adopted to describe the behaviour of the structure. The model is characterized by large gradients of displacements and small strain gradients. Due to the presence of the initial prestress in tensegrity structures, the additional condition of the initial stresses [146] was considered [71, 147-150] As a basis for formulating the tensegrity lattice equations, the partially non-linear theory of elasticity in Total Lagrangian – TL (Lagrange's stationary description) approach was adopted.

3.2. Model of tensegrity element

Tensegrity systems can be classified as truss structures. However, due to an existing self-stress state, the truss element is modified taking into account the initial stress σ_0.

The space finite tensegrity element in an undeformed configuration (initial) ${}^{0}C$ and deformed configurations (actual) ${}^{t}C$ and ${}^{t+\Delta t}C$ (Fig. 3.1) is considered. In the initial configuration, the cross-sectional area and the length are relatively A_0 and l_0, whereas in the actual configuration, they are A and l [148, 151].

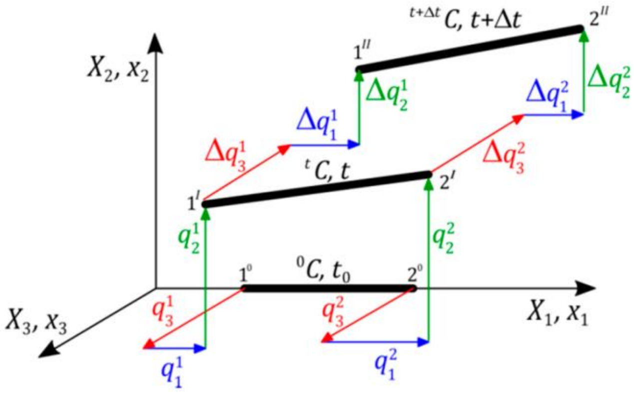

Fig. 3.1. Space finite tensegrity element [151]

The static equilibrium equation in the incremental version is formulated in the actual configuration at the moment $t + \Delta t({}^{t+\Delta t}C)$. The tensegrity element is described by the vector of nodal coordinates and corresponding vector of nodal forces:

$$ {}^{t+\Delta t}\mathbf{q}^e = {}^t\mathbf{q}^e + \Delta\mathbf{q}^e, \quad {}^{t+\Delta t}\mathbf{Q}^e = {}^t\mathbf{Q}^e + \Delta\mathbf{Q}^e \tag{3.1} $$

where ${}^t\mathbf{q}^e = [q_1^1 \quad q_2^1 \quad q_3^1 \quad q_1^2 \quad q_2^2 \quad q_3^2]^T$ and ${}^t\mathbf{Q}^e = [Q_1^1 \quad Q_2^1 \quad Q_3^1 \quad Q_1^2 \quad Q_2^2 \quad Q_3^2]^T$ are relatively a vector of nodal coordinates and the vector of nodal forces in the actual configuration at the moment $t({}^tC)$, whereas $\Delta\mathbf{q}^e = [\Delta q_1^1 \quad \Delta q_2^1 \quad \Delta q_3^1 \quad \Delta q_1^2 \quad \Delta q_2^2 \quad \Delta q_3^2]^T$ is a vector of displacement increments and $\Delta\mathbf{Q}^e = [\Delta Q_1^1 \quad \Delta Q_2^1 \quad \Delta Q_3^1 \quad \Delta Q_1^2 \quad \Delta Q_2^2 \quad \Delta Q_3^2]^T$ is a vector of nodal forces increments.

The variation formulation of the virtual work principle, between two infinitely close times t and $t + \Delta t$, leads to the incremental static equilibrium equation:

$$ \mathbf{K}_T^e(\mathbf{q}^e)\Delta\mathbf{q}^e = \mathbf{R}^e + \Delta\mathbf{Q}^e; \quad \mathbf{R}^e = {}^t\mathbf{Q}^e - \mathbf{F}^e \tag{3.2} $$

where $\mathbf{K}_T^e(\mathbf{q}^e)$ is a tangential stiffness matrix, $\mathbf{R}^e$ is a residual force vector, and $\mathbf{F}^e$ is an inertial forces vector.

The tangential stiffness matrix:

$$ \mathbf{K}_T^e(\mathbf{q}^e) = \mathbf{K}_L^e + \mathbf{K}_G^e + \mathbf{K}_{NL}^e(\mathbf{q}^e); \quad \mathbf{K}_{NL}^e(\mathbf{q}^e) = (\mathbf{K}_{u1}^e + \mathbf{K}_{u2}^e) \tag{3.3} $$

consists of the linear $\mathbf{K}_L^e$, quasi-linear $\mathbf{K}_G^e$, and non-linear $\mathbf{K}_{NL}^e(\mathbf{q}^e)$ parts. The quasi-linear part, called the geometry stiffness matrix, consists of two components $\mathbf{K}_G^e = \mathbf{K}_G^e(A_0\sigma_0) + \mathbf{K}_{GN}^e(N)$, where $\mathbf{K}_G^e(A_0\sigma_0)$ depends on $S = A_0\sigma_0$, which results from the initial stress σ_0, and $\mathbf{K}_{GN}^e(N)$ depends on the axial force N, which results from external loads. All parts of the stiffness matrix (3.3) can be expressed as follows:

$$\mathbf{K}_L^e = \frac{EA_0}{l_0}\begin{bmatrix} \mathbf{I}_0 & -\mathbf{I}_0 \\ -\mathbf{I}_0 & \mathbf{I}_0 \end{bmatrix},\ \mathbf{K}_G^e(A_0\sigma_0) = \frac{S}{l_0}\begin{bmatrix} \mathbf{I} & -\mathbf{I} \\ -\mathbf{I} & \mathbf{I} \end{bmatrix},$$

$$\mathbf{K}_{GN}^e(N) = \frac{N}{l_0}\begin{bmatrix} \mathbf{I} & -\mathbf{I} \\ -\mathbf{I} & \mathbf{I} \end{bmatrix}, \mathbf{K}_{u1}^e = \frac{EA_0}{{l_0}^2}\begin{bmatrix} \mathbf{I}_1 & -\mathbf{I}_1 \\ -\mathbf{I}_1 & \mathbf{I}_1 \end{bmatrix}, \mathbf{K}_{u2}^e = \frac{EA_0}{{l_0}^3}\begin{bmatrix} \mathbf{I}_2 & -\mathbf{I}_2 \\ -\mathbf{I}_2 & \mathbf{I}_2 \end{bmatrix} \tag{3.4}$$

where:

$$\mathbf{I} = \begin{bmatrix} 1 & 0 & 0 \\ 0 & 1 & 0 \\ 0 & 0 & 1 \end{bmatrix},\ \mathbf{I}_0 = \begin{bmatrix} 1 & 0 & 0 \\ 0 & 0 & 0 \\ 0 & 0 & 0 \end{bmatrix},\ \mathbf{I}_1 = \begin{bmatrix} 2\Delta_{u1} & \Delta_{u2} & \Delta_{u3} \\ \Delta_{u2} & 0 & 0 \\ \Delta_{u3} & 0 & 0 \end{bmatrix},$$

$$\mathbf{I}_2 = \begin{bmatrix} (\Delta_{u1})^2 & \Delta_{u1}\Delta_{u2} & \Delta_{u1}\Delta_{u3} \\ \Delta_{u1}\Delta_{u2} & (\Delta_{u2})^2 & \Delta_{u2}\Delta_{u3} \\ \Delta_{u1}\Delta_{u3} & \Delta_{u2}\Delta_{u3} & (\Delta_{u3})^2 \end{bmatrix} \tag{3.5}$$

where: $\Delta_{ui} = q_i^2 - q_i^1$ for $i = 1,2,3$.

The residual force vector $\mathbf{R}^e$ depends on the inertial force vector:

$$\mathbf{F}^e = (S+N)\begin{bmatrix} -\mathbf{I}_{F1} \\ \mathbf{I}_{F1} \end{bmatrix};\ \mathbf{I}_{F1} = \begin{bmatrix} 1 + \frac{\Delta_{u1}}{l_0} \\ \frac{\Delta_{u2}}{l_0} \\ \frac{\Delta_{u3}}{l_0} \end{bmatrix} \tag{3.6}$$

Due to the fact that the initial configuration is not deformed, the axial force N is not a real force. It is the component of the second symmetrical Pioli–Kirchhoff stress tensor, whereas the real force is defined on the basis of the Cauchy tensor and it is:

$$N' = N\frac{l}{l_0} \tag{3.7}$$

3.3. Model of tensegrity structure

Tensegrity structure considered as n -element space truss ($e = 1,2,\ldots,n$), with m degrees of freedom $\mathbf{q}(\in \mathbb{R}^{m\text{x}1})$:

$$\mathbf{q} = [q_1 \quad q_2 \quad \cdots \quad q_m]^T \tag{3.8}$$

The incremental static equilibrium equation for the structure takes the form:

$$\mathbf{K}_T(\mathbf{q})\Delta\mathbf{q} = \Delta\mathbf{P} + \mathbf{R} \tag{3.9}$$

where $\mathbf{P}(\in \mathbb{R}^{m\text{x}1})$ is an external load vector, and $\mathbf{K}_T(\mathbf{q})(\in \mathbb{R}^{m\text{x}m})$ is a tangent stiffness matrix of a structure:

$$\mathbf{K}_T(\mathbf{q}) = \mathbf{K}_L + \mathbf{K}_G(\mathbf{S}) + \mathbf{K}_{GN}(\mathbf{N}) + \mathbf{K}_{NL}(\mathbf{q}); \;\; \mathbf{K}_{NL}(\mathbf{q}) = \mathbf{K}_{u1} + \mathbf{K}_{u2} \tag{3.10}$$

where $\mathbf{K}_G(\mathbf{S})$ is a geometry stiffness matrix that depends on self-equilibrated internal forces **S**:

$$\mathbf{S} = \mathbf{y}_S S \tag{3.11}$$

where S is the initial prestress level and $\mathbf{y}_S(\in \mathbb{R}^{n\times 1})$ is an eigenvector related to the zero eigenvalue of the compatibility matrix (see section 4.2.1). Additionally, the tangent stiffness matrix $\mathbf{K}_T(\mathbf{q})(\in \mathbb{R}^{mxm})$ consists of the geometry stiffness matrix $\mathbf{K}_{GN}(\mathbf{N})$ that depends on the axial forces **N** and the non-linear displacement stiffness matrix $\mathbf{K}_{NL}(\mathbf{q})$.

The residual force vector $\mathbf{R}(\in \mathbb{R}^{mx1})$ in (3.9) results from the aggregation. In equilibrium, it is equal to zero ($\mathbf{R} = \mathbf{0}$), whereas in a process of iteration, a norm $\|\mathbf{R}\|$ is the “distance” from the equilibrium state. The iterative process converges if $\|\mathbf{R}\| \to 0$.

4. Analysis of tensegrity structures

4.1. Introduction

The complete analysis of tensegrity structures is a two-step process. The first step, qualitative analysis, concerns the identification of the immanent features of the structure, i.e., self-stress states and infinitesimal mechanisms. A thorough qualitative analysis allows for proper classification, and, as a result, a better understanding of the behaviour of the structure. According to [22, 148], the following characteristics can be distinguished in the tensegrity structures:

- it is a truss (*T*),
- there is a self-stress state, that stabilizes the structure (*SS*),
- there is an infinitesimal mechanism, stiffened by the self-stress state (*M*),
- the struts extremities are not touching each other, nonetheless, cables create a continuous net (*D*),
- compressed struts are surrounded by tensed cables (*I*),
- tensed cables have no rigidity for compression (*C*).

The presence of characteristics listed above classified tensegrity structure as:

- ideal tensegrity (*T*, *SS*, *M*, *D*, *I*, *C*),
- “pure” tensegrity (*T*, *SS*, *M*, *I*, *C*),
- structures with tensegrity features of class 1 (*T*, *C*, *SS*, *M*),
- structures with tensegrity features of class 2 (*T*, *SS*, *C*, *I* or *D*).

From an engineering perspective, it is very important that the structures have all six features. Nonetheless, all tensegrity structures possess benefits related to the ability to control various parameters, except the structures with tensegrity features of class 2. The second step in the analysis of tensegrity structures is a quantitative approach. The analysis concerns the impact of the initial prestress on the behaviour of the structure. The approach can be performed for the static and dynamic parameters. In the case of the static analysis, the influence of the initial prestress level on displacements, maximum effort of structure, and stiffness of the structure is investigated. For the dynamic analysis, the influence of the initial prestress on the natural and free vibrations is explored. Finally, the dynamic stability analysis examines the influence of the initial prestress level on the limits of the instability regions of the structure.

4.2. Qualitative analysis

The qualitative analysis is the first step to understand the unique properties of tensegrity structures. This assessment is required to determine the immanent features such as infinitesimal mechanisms and self-stress states which stabilize the mechanisms [54, 96, 152]. The qualitative analysis can be performed using the existing form-finding methods. The methods often used include, e.g., the spectral analysis of truss matrices [152], genetic algorithms [153], iteration method [154], the force density method [63], the dynamic relaxation [77], and the singular value decomposition (SVD) of the extension matrix **B** [28, 148, 155].

Two of the mentioned above methods are used in the work. The first method chosen to perform the evaluation is a spectral analysis of the truss matrices. This method allows not only the identification of self-stress states and the mechanisms, but also to determine if the mechanism is infinitesimal or not. As a result, the method determines all existing self-stress states of the structure and verifies whether any existing state provides stability to the structure, i.e., introduces the appropriate forces to elements (struts are compressed, cables are tensed) and ensures the stable equilibrium of the structure. If none of the identified self-stress states correctly defines the elements in a structure, a superimposed state is necessary. Sometimes, the solution of this problem (superposition) can be difficult to obtain, then, the second method can be applied. The genetic algorithm (GA), can be used in cases when the existing self-stress state is not sufficient, and an appropriate set of forces must be introduced to the structure. The GA method allows identifying a correct self-stress state for the structure.

4.2.1. Spectral analysis of truss matrices

The identification of characteristic tensegrity features is performed using the spectral analysis of the truss matrices. The equilibrium equation can be presented in the form of stresses [28]:

$$\mathbf{B}^T\boldsymbol{\sigma} = \mathbf{P} \tag{4.1}$$

where $\mathbf{B}(\in \mathbb{R}^{nxm})$ is an extension matrix, $\boldsymbol{\sigma}(\in \mathbb{R}^{nx1})$ is a stress vector, $\mathbf{P}(\in \mathbb{R}^{mx1})$ is an external load vector.

The system of stress equations (4.1) is presented after symmetrization of the equilibrium equations in the form:

$$\mathbf{DS} = \mathbf{BP} \tag{4.2}$$

where $\mathbf{D} = \mathbf{B}\mathbf{B}^T$ is a compatibility matrix, $\mathbf{S}(\in \mathbb{R}^{nx1})$ is a longitudinal forces vector (initial prestress vector).

The spectral analysis of compatibility matrix $\mathbf{D}(\in \mathbb{R}^{nxn})$ leads to identifying the self-stress states of the structure:

$$(\mathbf{D} - \mu\mathbf{I})\mathbf{y} = 0 \tag{4.3}$$

where μ are eigenvalues and **y** are eigenvectors of the compatibility matrix **D.**

The eigenvalues can be expressed as:

$$\mathbf{H} = \{\mu_1 \quad \mu_2 \quad \cdots \quad \mu_n\} \tag{4.4}$$

The self-stress state can be considered as an eigenvector $\mathbf{y}_S = \mathbf{y}_i(\mu_i = 0)$ related to the zero-eigenvalue appearing in the matrix (4.4).

The spectral analysis of linear stiffness matrix $\mathbf{K}_L(\in \mathbb{R}^{mxm})$ identifies the mechanisms of the structure:

$$(\mathbf{K}_L - \gamma\mathbf{I})\mathbf{x} = 0 \tag{4.5}$$

where γ are eigenvalues and **x** are eigenvectors of the stiffness matrix $\mathbf{K}_L$.

The eigenvalues expressed as:

$$\mathbf{L} = \{\gamma_1 \quad \gamma_2 \quad \cdots \quad \gamma_m\} \tag{4.6}$$

The mechanism can be understood as an eigenvector $\mathbf{x}_i(\gamma_i = 0)$ related to the zero eigenvalue of the matrix (4.6).

If the self-stress state $\mathbf{y}_i(\mu_i = 0)$ is defined, the geometric stiffness matrix $\mathbf{K}_G(\mathbf{S})(\in \mathbb{R}^{mxm})$ is built, where $\mathbf{S} \equiv \mathbf{y}_i(\mu_i = 0)$. The full solution of the eigen problem is provided by the spectral analysis of the stiffness matrix in terms of the effect of self-equilibrated forces **S**:

$$(\mathbf{K}_L + \mathbf{K}_G(\mathbf{S}) - \sigma\mathbf{I})\mathbf{z} = 0 \tag{4.7}$$

where σ are eigenvalues and **z** are eigenvectors of matrix (4.7).

If the eigenvalues of (4.7):

$$\mathbf{O} = \{\sigma_1 \quad \sigma_2 \quad \cdots \quad \sigma_n\} \tag{4.8}$$

are positive numbers, the mechanism is infinitesimal and the structure is stable. Zero eigenvalues are related to finite mechanisms, whereas negative eigenvalues are responsible for the instability of the structure.

In the case of tensegrity domes, several self-stress states may occur in the structure, but none of them will stiffen the infinitesimal mechanism. Nonetheless, the superposition of self-stress states allows introducing the symmetric self-stress state $\mathbf{y}_s$ to reduce the mechanism.

4.2.2. Genetic algorithm

The genetic algorithm is one of the most popular computational algorithms for searching problems based on the mechanics of natural selection and genetics. For the tensegrity systems, genetic algorithm is commonly used as form-finding method for regular [153, 156, 157] and irregular [158-160] structures. Nonetheless, it can also be used as tool for determination the values of initial prestress for the existing structures [161]. An initial random population of feasible solutions evolves to create a better solution based on genetic operators, i.e., parent selection, crossover, or mutation. Then provide the best-selected solution, e.g., set of self-equilibrated forces in elements.

The first part of the algorithm relies on the selection of appropriate groups of elements. The selection can be completed automatically or manually. The automatic selection usually consists of the length selection. The groups of elements are divided according to their length and type. This method can be less precise for structures with elements of comparable lengths. The manual selection is more complicated and involves creating groups manually. Due to the specificity of tensegrity structures, the selection is conducted in a mixed way, i.e., partly automatically and partly manually. Two types of the element groups (tensed or compressed) are used. These groups lead to different definitions in the encoding procedure. An automatic selection was then completed within these groups based on the length selection. The set of all elements $\mathbf{\Gamma}$ is divided into the sets of elements with the same length $\boldsymbol{g}_i$:

$$\boldsymbol{g}_i = \{e_l, \cdots, e_z\}, \quad \boldsymbol{g}_i \in \mathbf{\Gamma} \tag{4.9}$$

where e_l and e_z are, respectively, the first and last element of group. For each group of elements $\boldsymbol{g}_i$, the normalized longitudinal force in element S^e is equal to:

$$S^e = \frac{\pm S_i}{S_{max}}, \tag{4.10}$$

where $\pm S_i$ is a value of i-th initial prestress level (“+” for tensed element, “–” for compressed element) and S_{max} is a maximum value of the initial prestress.

The initialization of the population based on the given parameters is required. As in the first step, it can be completed in two ways, i.e., automatically or manually. For the purpose of this work, the initial population is prepared automatically by encoding the number of solutions in the populations and a number of searched genes. Obtaining an optimal result requires significant computational effort. Genetic operators are used for the natural selection of valuable solutions. The leading operators in the genetic algorithm are: selection, crossover and mutation. The selection operator prefers better solutions (chromosomes) to pass its genes to the algorithm without mutation. The crossover combines the features of the genes of two parents to form two outcomes. The mutation operator is applied on the chromosome generated from the crossover operation with the probability of mutation. There are several methods for genetic operators. The following parameters were proposed:

- parent selection methods: steady state selection (in each generation, a few good chromosomes are selected to create a new offspring; then, some of the bad (with low fitness) chromosomes are removed, and the new offspring is placed in their place; the rest of the population survives to the new generation),
- crossover type: scattered (it randomly selects the gene from one of two parents),
- mutation type: random (the values of some genes change randomly; the number of genes is specified on the basis of the mutation number of genes or the percentage of genes to mutate; for each gene, a random value is selected according to the range specified by the minimum and maximum value),
- number of genes: the number of the groups of elements,
- percentage of genes to mutate: 10.

For chosen operators, the following parameters must be specified, i.e.:

- population size,
- number of generations,
- solutions in the population.

The entire procedure consists of constant reevaluation of provided values, to obtain the best-fitted solution in the result (Fig. 4.1).

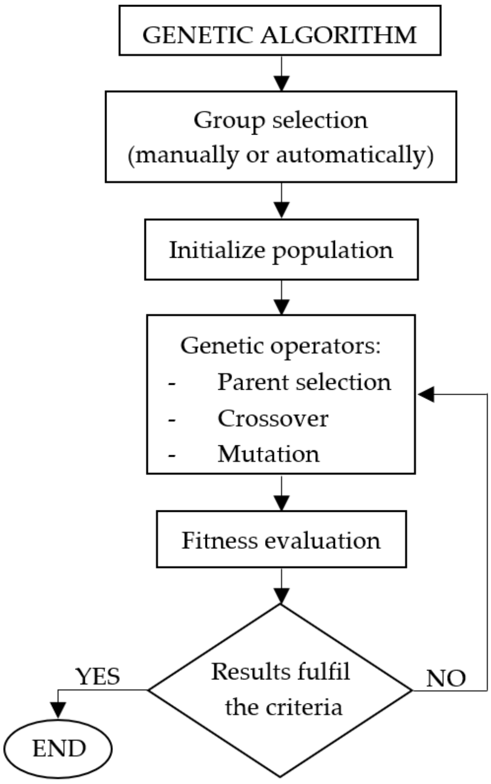

Fig. 4.1. Genetic algorithm procedure

The most critical part of the genetic algorithm is the fitness function. This function determines how the obtained solution fits this particular problem. In the case of seeking of the self-stress state, the fitness function proposed in this paper is equal to:

$$F = F_1 \cdot F_2 \tag{4.11}$$

where the components F_1, F_2 are described as follows:

$$F_1 = \begin{cases} 0, & if \text{ the stiffness matrix } [\mathbf{K}_L + \mathbf{K}_G(\mathbf{S})] \text{is not positive definite} \\ 1, & if \text{ the stiffness matrix } [\mathbf{K}_L + \mathbf{K}_G(\mathbf{S})] \text{is positive definite} \end{cases},$$
$$F_2 = \frac{1}{\sqrt{EN}} \tag{4.12}$$

where EN is the equilibrium of nodes. There is no physical interpretation of the equilibrium of nodes, which, for the sake of simplicity, was assumed as:

$$EN = \sum_{i=1}^{n} [(S_{ix})^2 + (S_{iy})^2 + (S_{iz})^2] \tag{4.13}$$

where S_{ix}, S_{iy}, S_{iz} are force projections.

The feasible solution is obtained by maximizing the fitness function (4.11). The values of the fitness function should increase with the number of generations. The appropriate solution has to satisfy the stable equilibrium.

4.3. Quantitative analysis

The quantitative analysis includes static, dynamic, and dynamic stability analyses. The impact of the initial prestress on static and dynamic parameters is analyzed, as well as the behaviour of the structure under external load. The analysis starts with an identification of the maximum (S_{max}) and minimum (S_{min}) levels of initial prestress. The maximum level of initial prestress (S_{max}) depends on the maximum effort of the structure (W_{max}), where W_{max} depend on the load-bearing capacity (N_{Rd}) and maximum normal force (N_{max}). The assumption is to not exceed the range $\mathrm{W}_{max} < 1$. The minimum levels of initial prestress (S_{min}) depends only on the geometry of the structure and load conditions. The S_{min} level is selected when the elements in the structure appropriately identified, i.e., cables are tensed and struts are compressed.

4.3.1. Static analysis

The static analysis of the traditional lattice structures can be performed assuming small displacements, i.e., a linear geometric model. The quasi-linear model (second-order theory) is also inadequate. Both approaches do not take into account the stiffening of the structure under the influence of external load. In tensegrity structures, the load causes displacements in accordance with the form of the infinitesimal mechanism that induces additional prestress of the structure – tensile forces generate additional tension in the cables and compression in the struts. For such regimes, the initial response should not be used to determine the behavior of the structure. Therefore, the analysis must be carried out with the assumption of the hypothesis of large displacements (third-order theory).

To illustrate the influence of external loads on the stiffening, two approaches are used. The applied methods are the quasi-linear approach (second-order theory):

$$[\mathbf{K}_L + \mathbf{K}_G(\mathbf{S})]\mathbf{q} = \mathbf{P} \tag{4.14}$$

and non-linear approach (third-order theory):

$$[\mathbf{K}_L + \mathbf{K}_S]\mathbf{q} = \mathbf{P}, \quad \mathbf{K}_S = \mathbf{K}_G(\mathbf{S}) + \mathbf{K}_{GN}(\mathbf{N}) + \mathbf{K}_{NL}(\mathbf{q}) \tag{4.15}$$

The analysis concerns the influence of the initial prestress level S ($\mathbf{S} = \mathbf{y}_s S$) on the displacements $\mathbf{q}$ and normal forces $\mathbf{N}$. Additionally, the following parameters are determined:

– maximum effort of the structure W_{max}:

$$\mathrm{W}_{max} = N_{max}/N_{Rd} \tag{4.16}$$

– stiffness of the structure described by the Global Stiffness Parameter (GSP):

$$GSP = \frac{[\mathbf{q}(S_{min})]^T \mathbf{K}_\mathrm{S}(S_{min})\mathbf{q}(S_{min})}{[\mathbf{q}(S_i)]^T \mathbf{K}_\mathrm{S}(S_i)\mathbf{q}(S_i)} \tag{4.17}$$

where $\mathbf{K}_S(S_{min})$ and $\mathbf{q}(S_{min})$ are a secant stiffness matrix and a design displacement vector with a minimum initial prestress level, and $\mathbf{K}_S(S_i)$ and $\mathbf{q}(S_i)$ at *i*-th prestress level.

4.3.2. Dynamic analysis

The ability to control not only the static, but also dynamic parameters is an important feature of tensegrity structures. The dynamic response of the tensegrity system investigated using the modal analysis [75, 82, 162, 163]. The impact of the initial prestress level on natural and free vibrations is analyzed. In case of the vibrations, the time independent external load is treated as an initial disturbance of the equilibrium state. Taking into account the harmonic motion $\mathbf{q}(t) = \tilde{\mathbf{q}}\sin(2\pi f t)$, where $\tilde{\mathbf{q}}(\in \mathbb{R}^{m\mathrm{x}1})$ is an amplitude vector, and the non-linear equation of motion is as follows:

$$[\mathbf{K}_L + \mathbf{K}_G - (2\pi f)^2\mathbf{M}]\tilde{\mathbf{q}} = \mathbf{0} \tag{4.18}$$

where $\mathbf{M}(\in \mathbb{R}^{m\mathrm{x}m})$ is a consequent mass matrix, f is a natural $(f_i(0))$ or free $(f_i(P))$ frequency of vibrations.

In the case of natural vibrations $(f_i(0))$, the geometry stiffness matrix depends only on the self-equilibrium system of longitudinal forces $\mathbf{S}$, consequently $\mathbf{K}_G = \mathbf{K}_G(\mathbf{S})$. For tensegrity domes characterized by infinitesimal mechanisms, the omission of the influence of prestress $(\mathbf{S} = \mathbf{0})$ in (4.18) leads to zero natural frequencies. The number of them is equal to the number of the infinitesimal mechanisms, and the forms of vibrations correspond to the forms of mechanisms.

In the case of free vibrations $(f_i(P))$, the geometry stiffness matrix depends additionally on the longitudinal forces $\mathbf{N}(\in \mathbb{R}^{n\mathrm{x}1})$ caused by the external load:

$$\mathbf{K}_G = \mathbf{K}_G(\mathbf{S}) + \mathbf{K}_{GN}(\mathbf{N}) \tag{4.19}$$

In order to calculate the axial forces, a geometrically nonlinear model must be used, assuming the hypothesis of large displacements, i.e., nonlinear theory of elasticity in terms of the Total Lagrangian (TL). The following equation need to be solved:

$$[\mathbf{K}_L + \mathbf{K}_G(\mathbf{S}) + \mathbf{K}_{GN}(\mathbf{N}) + \mathbf{K}_{NL}(\mathbf{q})]\mathbf{q} = \mathbf{P} \tag{4.20}$$

where $\mathbf{K}_{NL}(\mathbf{q})(\in \mathbb{R}^{mxm})$ is a non-linear displacement stiffness matrix.

4.3.3. Dynamic stability analysis

Dynamic instability analysis (or dynamic instability) leads to the identification of the resonance frequencies of periodic loads and, consequently, to the determination of parametric resonance regions (unstable regions). The most common technical application problem is the analysis of unstable regions at a given constant value P of periodic load:

$$P(t) = P + P_t \cos(\theta t) \tag{4.21}$$

where P_t is an amplitude and θ is a frequency of the periodic load. The instability regions occur at the free frequencies Ω_i, Ω_j of structures loaded by constant values:

$$\Omega = \frac{\Omega_i}{k} \quad \text{or} \quad \Omega = \frac{\Omega_i \pm \Omega_j}{2k} \qquad k = 1,2,\ldots;\ i \neq j \tag{4.22}$$

The first case (4.22_1) represents periodic resonances, and the second one (4.22_2) – combined resonances. From the technical point of view, the main instability regions are most important, i.e., periodic resonances of the first order ($k = 1$).

The study of structural instability problems leads to nonlinear issues that solved by iterative or incremental-iterative analysis of large displacement gradients. However, in the case of dynamic instability analysis, the nature of motion is studied. A quasi-linear approach is sufficient to determine the conditions under which the motion is of an unsteady nature, with solutions that increase indefinitely with time. Admittedly, the determination of the magnitude of the amplitudes of these oscillations can only be obtained from nonlinear equations of vibration, no less, without knowing the magnitude of the amplitudes, the quasi-linear theory gives a sufficiently complete and accurate view of the issue of instability.

The equation of motion with time-varying coefficients with the inclusion of periodic load (4.21) takes the following form:

$$\mathbf{M}\ddot{\mathbf{q}}(t) + [\mathbf{K}_L + P(t)\mathbf{K}_G]\mathbf{q}(t) = \mathbf{0} \tag{4.23}$$

where $\ddot{\mathbf{q}}(t)(\in \mathbb{R}^{m\text{x}1})$ is an accelerator vector.

The boundaries of the stable and unstable regions (Ince-Strutt maps) are determined by the periodic solutions of the equation of motion (4.23). The problem of dynamic instability analysis leads to determining the conditions under which equation of motion has non-zero solutions. The dynamic instability analysis is carried out using the harmonic balance method [148, 164] that leads to equation:

$$\det\left\{\mathbf{K}_L + \left(1 \pm \frac{1}{2}\frac{P_t}{P}\right)\mathbf{K}_G - \frac{\theta^2}{4}\mathbf{M}\right\} = 0 \tag{4.24}$$

which solution leads to the determination of the main unstable regions $A_\eta(S_i)$ at i-th initial prestress level in the plane of a pulsatility index υ and a resonance frequency η:

$$\upsilon = \frac{P_t}{P}, \quad \eta = \frac{\theta}{2\pi} \tag{4.25}$$

The influence of the initial prestress level S on the distribution and range of parametric resonance regions is determined using the nondimensional parameter λ. This parameter measures the changes in areas of unstable regions as the initial prestress level increases:

$$\lambda = \frac{A_\eta(S_i)}{A_\eta(S_{min})} \tag{4.26}$$

where $A_\eta(S_{min})$ is an area at the minimum initial prestress level.

5. Geiger domes

5.1. Introduction

The origin of the Geiger dome starts with a patent of a roof structure presented by David Geiger [115] in 1973. The structure was described as a "curved roof on cable spans" with a simple design and eventually transformed into a cable-strut dome. Geiger's research aimed to combine the principle of tensegrity systems with load-bearing membrane surfaces and achieve maximum spans with a minimum construction weight. The re-evaluation of Fuller's pioneering work led to an innovative stadium roof enclosure that would be as economical as an air-supported structure (Fig. 5.1).

a) b)

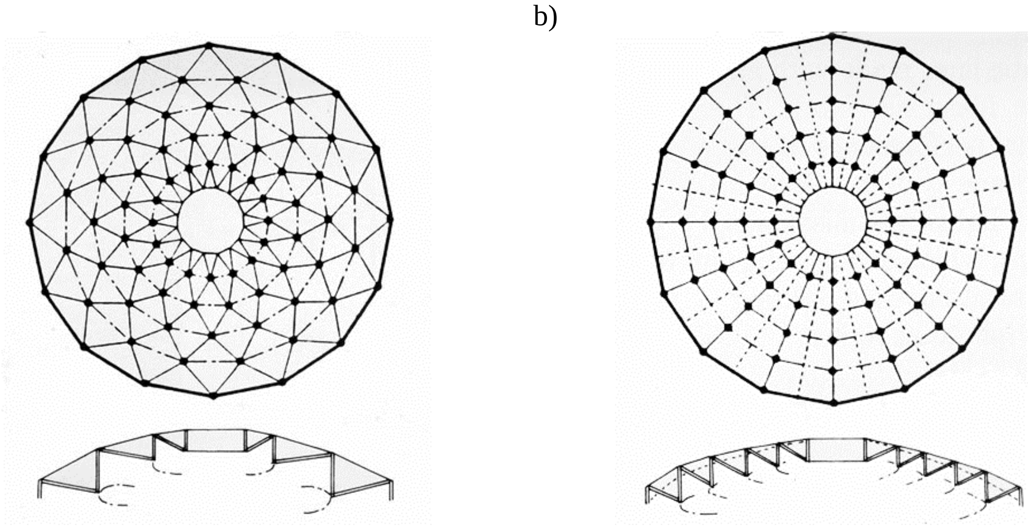

Fig. 5.1. Design of tensegrity dome by: a) Fuller, b) Geiger [130]

The patent of the Geiger dome (implemented on the roof of the Olympic Hall in Seoul) [109, 130, 131] consisted of a system of eight flat repeating load-bearing girders that were not touching at the center (open upper section) and three tension hoops covered with a membrane (Fig. 5.2a). The load-bearing girders are connected with circumferential cables. After its first appearance, the Geiger dome was the main subject of many scientific works. The first modifications of the Geiger dome led to adjusting the cable layout and providing additional cables. The modification was presented by Kim et al. [165] and relied on the additional intersecting bracing cables (Fig. 5.2b). In later works, the crossing cables were removed and only the additional circumferential cables were left [166] (Fig. 5.2c). The original geometry of the Geiger dome motivated other scientists to create new shapes (generate new topologies) [76, 80, 167], and present new form-finding [154, 168, 169] and optimization methods [80, 170, 171]. New cable dome types appeared, based on a Geiger dome patent [123, 172]. As part of an experimental study, different construction methods [173] and shape-forming processes [85, 174] were presented. The new topology aimed to achieve the desired performance criteria and enable control of parameters such as stiffness [78] and stability performance [175-177].

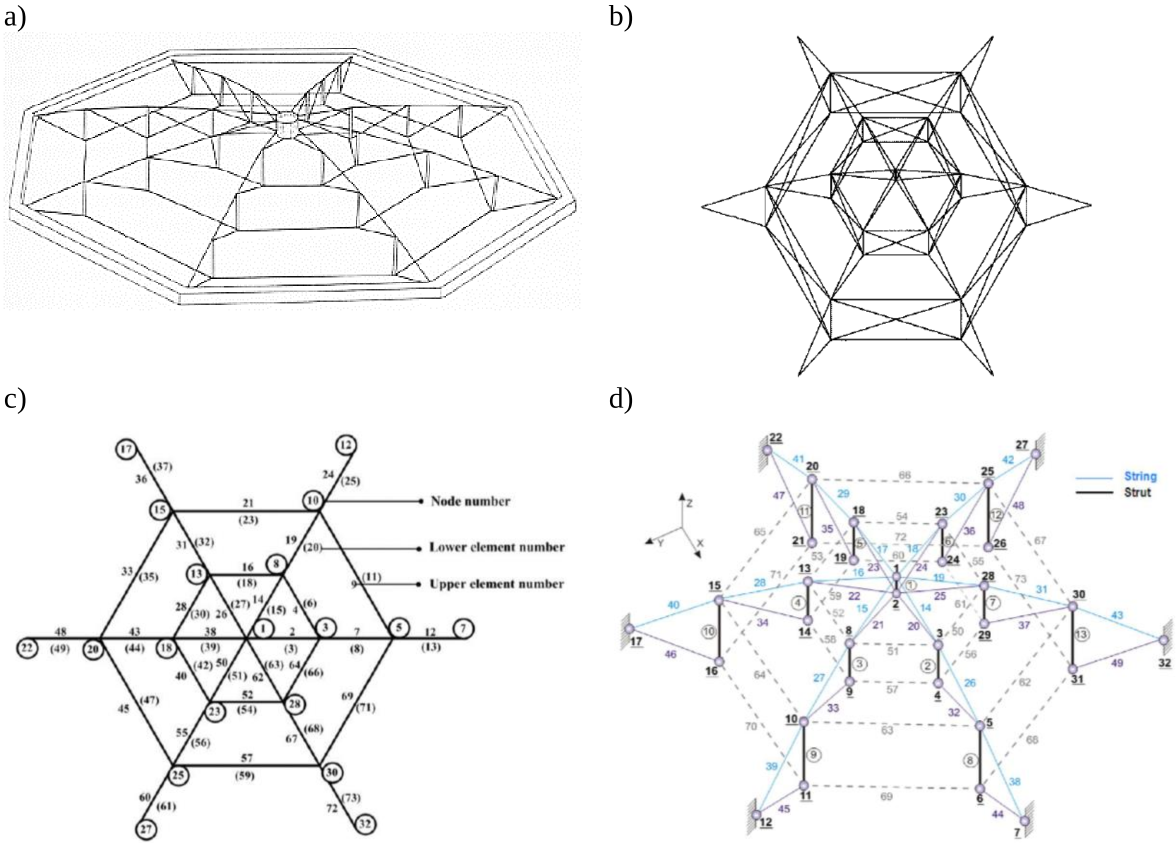

Fig. 5.2. Geometry of the Geiger dome: a) original patent implemented in Seoul Arena [130], b) braced dome [165], d) modified dome [125] c) modified dome [166]

A stable configuration of a cable-strut dome structure consists of an appropriate geometry solution and state of initial prestress that provides stability to elements. In the case of a “pure tensegrity” structure, the initial prestress occurs naturally, stiffens the structure, and reduces infinitesimal mechanisms. In the case of the original Geiger dome, not all existing self-stress states meets those criteria. For the domes with additional modifications, the self-stress state must be accurately derived using the appropriate methods [83, 178-183]. Introducing an appropriate self-stress state allows for further analysis of the dome. Due to a non-conventional shape, the investigation of the structure’s response to different load conditions is significant, including simple load conditions, like a self-weight [126], and also more complex ones, for example, non-uniform snow load [184]. That is why the failure analysis and behaviour of the domes must be thoroughly analyzed [185-188].

The static analysis of tensegrity domes includes the influence of the initial prestress level on the structure's response. The literature review shows works that study the influence of the self-stress state on the displacements [76, 78], effort, and stiffness of the structure [155]. The dynamic analysis of the Geiger domes, on the other hand, is a subject that is still understudied. The papers that include dynamic analysis of the Geiger dome focused mostly on the natural frequencies analysis [55, 56, 148], and only one type of dome was always concerned. More widely the dynamic analysis was presented in [125, 148, 189, 190]. The papers, the subject of which was the complete dynamic analysis of the Geiger dome also appeared [124, 191].

In this work, static and dynamic analysis is performed on the Geiger domes. The differences are in the geometry of a load-bearing girder and the different numbers of girders in the dome structure are presented. The upper section of girder is presented in two variants, i.e., close upper section type A and open upper section type B. The domes presented with a regular cable layout (according to Geiger patent) [115] – regular Geiger domes, and with additional circumferential cables (according to [166]) – modified Geiger domes. The domes with different number of girders are analyzed. The names of analyzed domes are acronyms: R – regular dome, M - modified dome, G – Geiger dome, the number – the number of load-bearing girders, and letter A or B – girders type, e.g., "RG 6A" is the regular Geiger dome with 6 girders type A.

5.2. Geometrical design

The geometry of the Geiger dome consists of uniformly distributed flat load-bearing girders. Two geometrical designs are proposed. First, own solutions are presented (section 5.2.1). The proposed designs are the main subject of further analysis. Next, due to the Geiger dome's popularity, the solutions known from the literature are considered (section 5.2.2).

5.2.1. Proposed design solutions

The proposed design solutions contain small-scale domes. The load-bearing girder consists of cables (elements: 1, 2, 3, 4, 5, 6) and struts (elements: S1, S2, S3) located in the same plane (Fig. 5.3). The flat load-bearing girders are connected into a spatial structure with permanent circumferential cables (elements: C1, C2, C3, C4) and by additional cables (marked in blue), that are optional in the structure (elements: C5, C6). Fig. 5.3 presents the geometry of a regular flat girder – type A (Fig. 5.3a) and modified (with cables C5, C6) – type B (Fig. 5.3b). The node coordinates of a load-bearing girder are presented in Table 5.1. The diameter of 12 m and the height of 3.25 m of all domes were adopted. Domes are supported in every external node of the lowest section of the girder. The geometry of domes consisting of six load-bearing girders is presented in Fig. 5.4. In this work, in addition to domes with six load-bearing girders, the domes with 8 (Fig. 5.5), 10 (Fig. 5.6) and 12 (Fig. 5.7) load-bearing girders are considered.

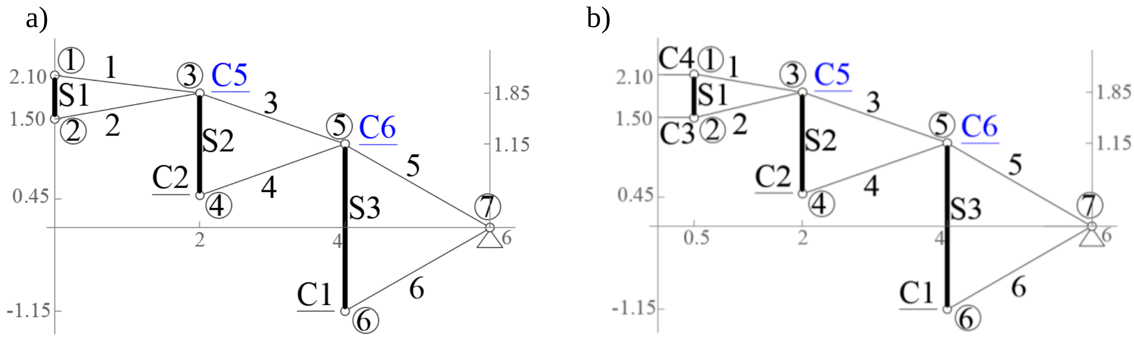

Fig. 5.3. Load-bearing girder of the Geiger dome: a) type A, b) type B

Table 5.1. Node coordinates [m] of the load-bearing girders of the Geiger dome

Coordinate	Type of girder	Number of nodes						
		1	2	3	4	5	6	7
x	A	0.0		2.0		4.0		6.0
	B	0.5						
z	A and B	2.1	1.5	1.85	0.45	1.15	-1.15	0.0

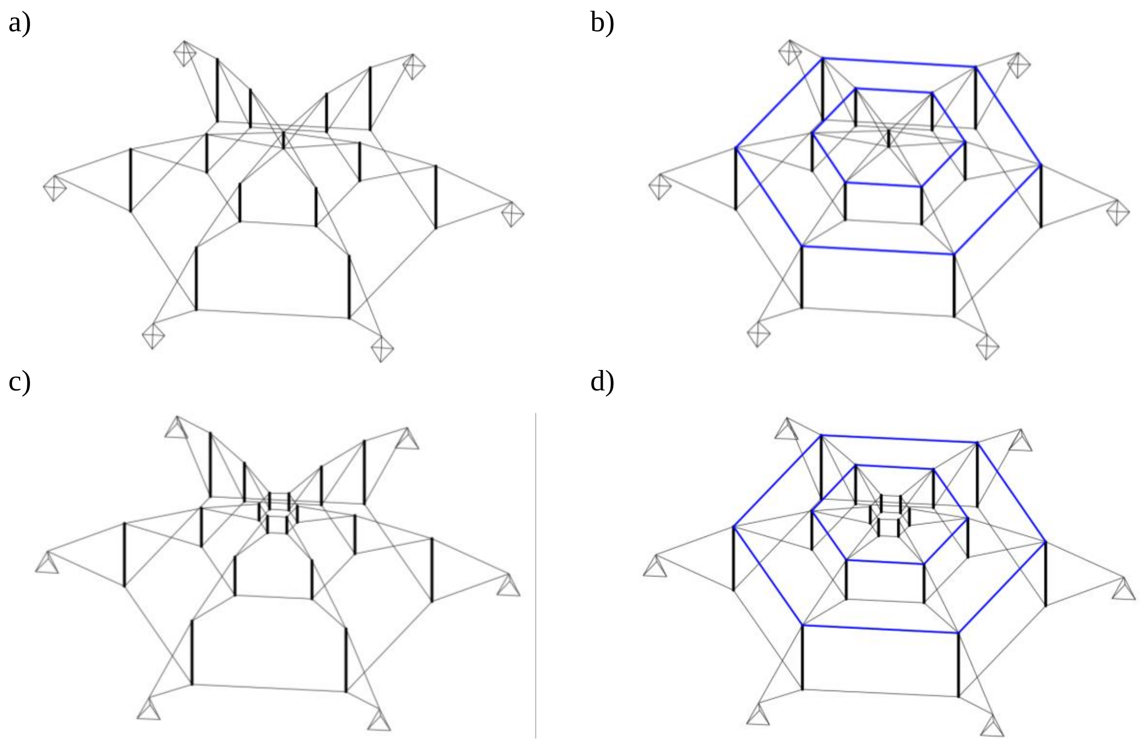

Fig. 5.4. Geiger dome: a) RG 6A, b) MG 6A, c) RG 6B, d) MG 6B

a) b) c) d)

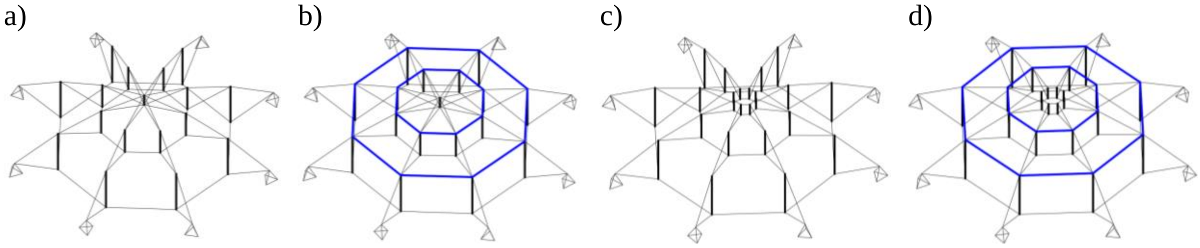

Fig. 5.5. Geiger dome: a) RG 8A, b) MG 8A, c) RG 8B, d) MG 8B

a) b) c) d)

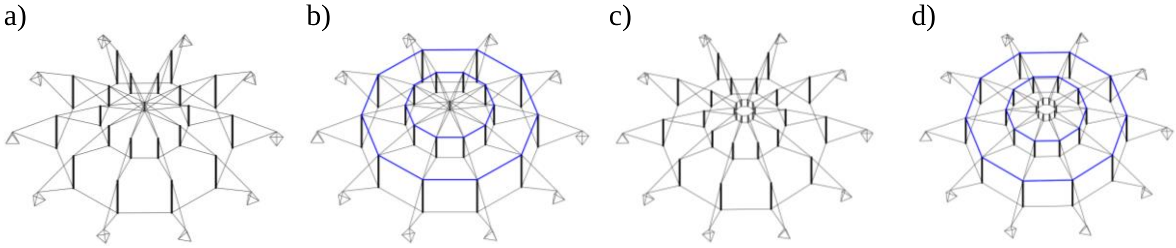

Fig. 5.6. Geiger dome: a) RG 10A, b) MG 10A, c) RG 10B, d) MG 10B

a) b) c) d)

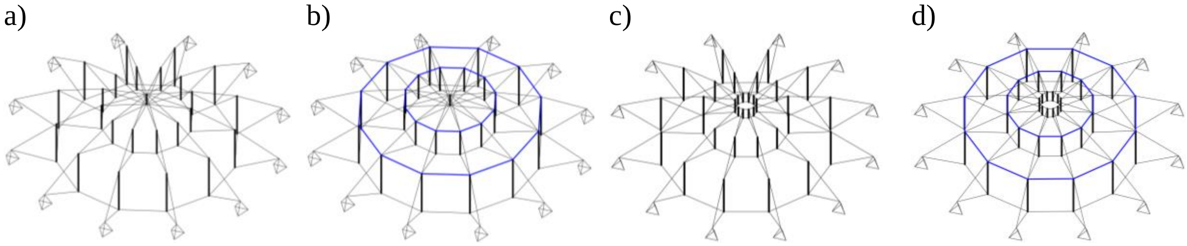

Fig. 5.7. Geiger dome: a) RG 12A, b) MG 12A, c) RG 12B, d) MG 12B

5.2.2. Solutions from the literature

A large group of scientists is investigating the Geiger dome. Each work contains different solutions for the girder geometry and structural system of a dome. Three examples of domes with similar geometry, i.e., 12 load-bearing girders, regular cable layout, type B (RG 12B) are shown. First, the dome presented by Jiang et al. [178] (Fig. 5.8) is considered. The dome is approximated to a large-span structure with a width of 100 m and a height of 8.5 m. The dome is supported in every external node of the lowest section. The node coordinates for a load-bearing girder are presented in Table 5.2.

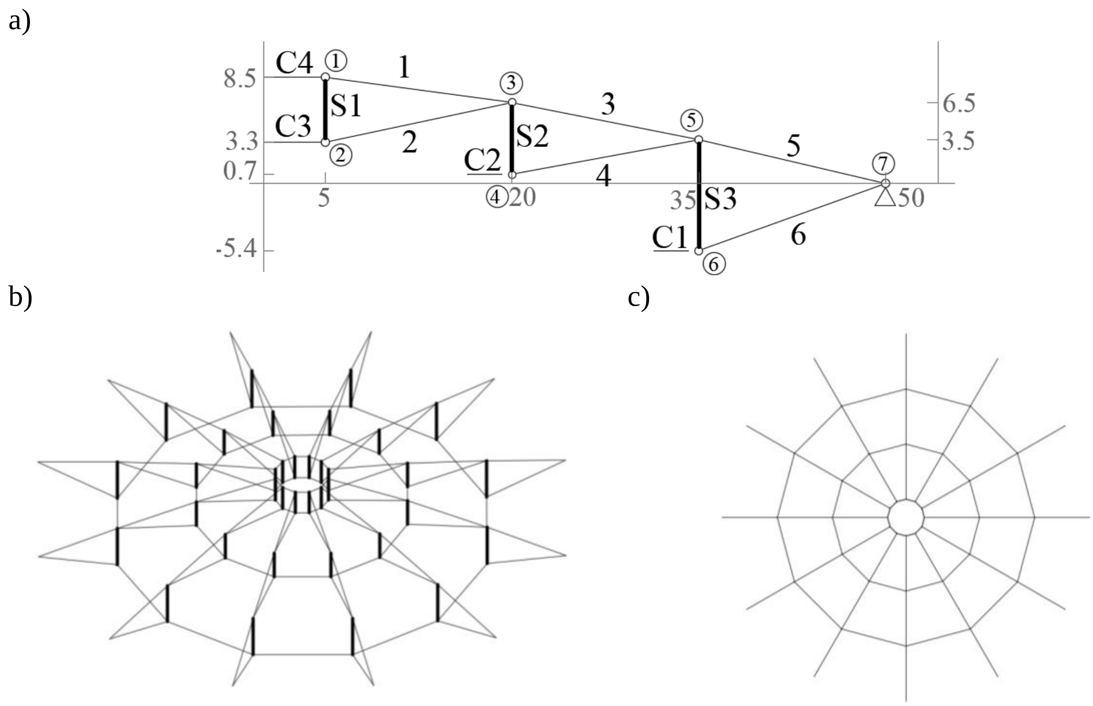

Fig. 5.8. Geiger dome by Jiang et al. [178]: a) geometry of a girder, b) 3D view, c) top view

Table 5.2. Node coordinates [m] of the load-bearing girder of the Geiger dome by [178]

No. of node	**1**	**2**	**3**	**4**	**5**	**6**	**7**
x	5		20		35		50
z	8.5	3.3	6.5	0.7	3.5	-5.4	0.0

The second example is dome presented by Yuan et al. [180] (Fig. 5.9). The dome is 130 m wide and 8 m high. The structure is supported in every external node of the load-bearing girder.

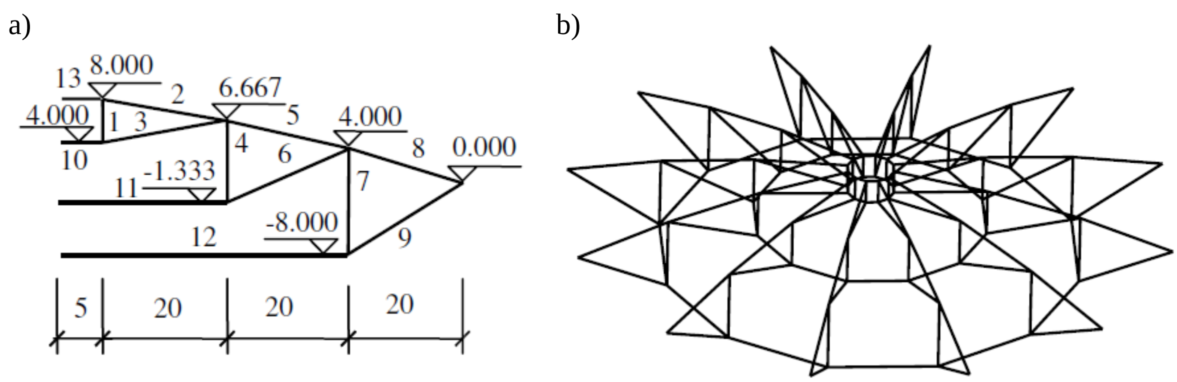

Fig. 5.9. Geiger dome by Yuan et al. [180]: a) geometry of a girder, b) 3D view

The third example is presented by Malerba et al. [168] (Fig. 5.10) has similar load-bearing girder to the one provided in [180]. The dome is also 130 m high and 8 m wide (measuring from the level of supports).

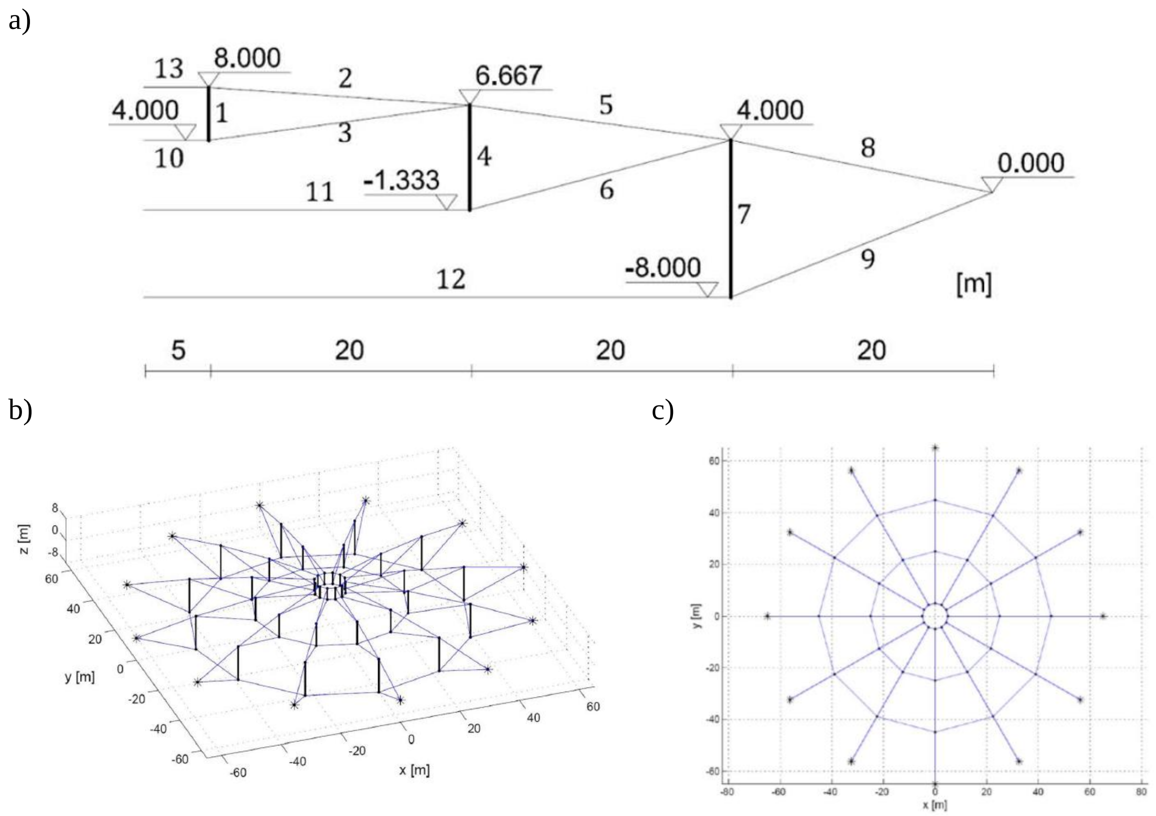

Fig. 5.10. Geiger dome by Malerba et al. [168]: a) geometry of a girder, b) 3D view, c) top view

5.3. Qualitative analysis

The qualitative analysis of the Geiger dome relies on the identification of existing infinitesimal mechanisms and self-stress states. These characteristics are not dependent on the external loads, the cross-section of the elements, or the physical properties of a structure. Only the geometry of a dome is essential. The identification of self-equilibrium forces can be performed using several methods. In the case of regular domes, forces are calculated directly from the node equilibrium (section 5.3.1). For modified domes, different methods must be considered, e.g., spectral analysis (section 5.3.2) genetic algorithm, and others (section 5.3.3).

5.3.1. Exact solution

In the case of simple and statically determinate tensegrity structures, the equations for the determination of the values of self-equilibrium forces (self-stress state) can be derived from the node equilibrium. In the case of Geiger domes, only the regular domes (RG) are suitable to derive the formulas. The formulas on self-equilibrated forces (Table 5.3) depend on the angle of inclination of cables of the girder – α (Fig. 5.11a, b), the angle between perimeter cables – 2β (Fig. 5.11c, d), and the number of load-bearing girders ng. With these ready-to-use formulas (Table 5.3), the self-stress state can be easily derived for each Geiger dome of a regular type (RG). It allows proceeding with the next steps of the analysis and reduces the calculation time.

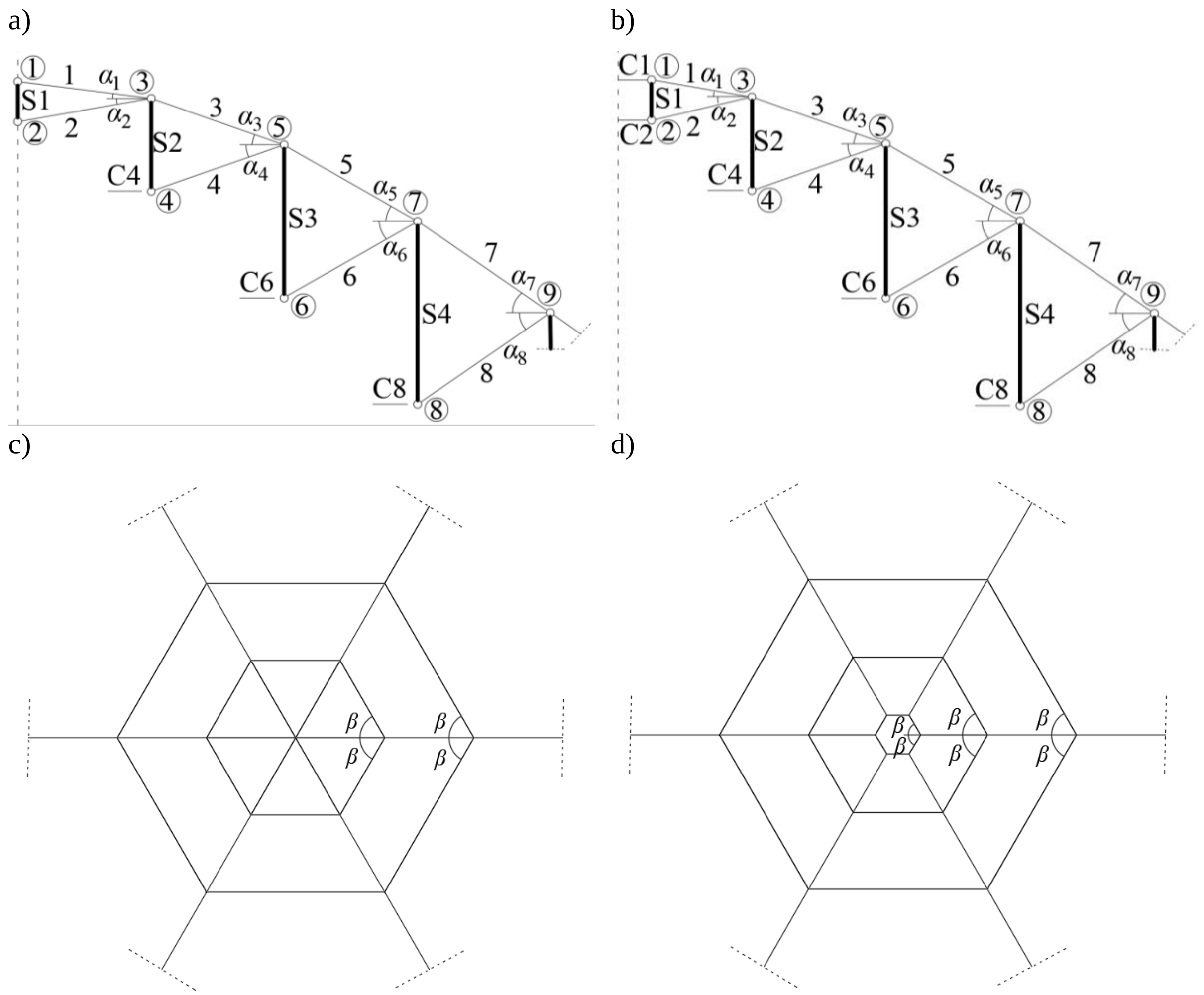

Fig. 5.11. View on geometry of the regular Geiger dome: a) load-bearing girder type A, b) load-bearing girder type B, c) top view on type A dome, d) top view on type B dome

Table 5.3. Formulas on self-equilibrium forces (self-stress state) for the regular Geiger dome

Type A	Type B
$N_1 = \text{constant}$ $N_i = N_{i-1}\dfrac{\sin(\alpha_{i-1})}{\sin(\alpha_i)};\quad i = 2,4,6,8\ ...$ $N_j = \dfrac{N_{j-2}\cos(\alpha_{j-2}) + N_{j-1}\cos(\alpha_{j-1})}{\cos(\alpha_j)};\quad j = 3,5,7\ ...$	

Table 5.3. Formulas on self-equilibrium forces (self-stress state) for the regular Geiger dome - Continued

Type A	Type B
$N_{Ck} = 0.5N_k \dfrac{\cos(\alpha_k)}{\cos(\beta)}; \quad k = 4,6,8\ldots$	
	$N_{C1} = 0.5N_1 \dfrac{\cos(\alpha_1)}{\cos(\beta)}$ $N_{C2} = 0.5N_2 \dfrac{\cos(\alpha_2)}{\cos(\beta)}$
$N_{S1} = ngN_2 \sin(\alpha_2)$	$N_{S1} = N_2 \sin(\alpha_2)$
$N_{Sr} = N_{2r} \sin(\alpha_{2r}); \quad r = 2,3,4\ldots$	

5.3.2. Spectral analysis of truss matrices

The qualitative analysis of regular and modified Geiger dome types A and B is performed using the spectral analysis of the linear stiffness matrix and compatibility matrix (see section 4.2.1). The consideration involves the identification of self-stress states and infinitesimal mechanisms of a structure. The summarized results for considered domes, i.e., RG ngA, MG ngA, RG ngB, MG ngB, where $ng = \{6, 8, 10, 12\}$ number of load-bearing girders, are contained in Table 5.4.

Table 5.4. Results of the qualitative analysis of Geiger domes

No. of the load-bearing girders (ng)	No. of nodes	No of d.o.f	No. of elements (n)	No. of struts (ns)	No. of mechanisms (nm)	No. of self-stress states
Type A						
6	32	78	61 (73)	13	18 (8)	1 (3)
8	42	102	81 (97)	17	22 (8)	1 (3)
10	52	126	101 (121)	21	26 (8)	1 (3)
12	62	150	121 (145)	25	30 (8)	1 (3)
Type B						
6	42	108	78 (90)	18	31 (21)	1 (3)
8	56	144	104 (120)	24	41 (27)	1 (3)
10	70	180	130 (150)	30	51 (33)	1 (3)
12	84	216	156 (180)	36	61 (39)	1 (3)

(.) – the results for the modified domes (MG)

The modification of cable layout leads to a reduction of the number of infinitesimal mechanisms, at the same time increasing the number of self-stress states. In the case of the regular Geiger dome (RG), the number of infinitesimal mechanisms (nm) depends on the number of bearing girders, i.e., the number of struts (ns). The dependency is defined as follows:

$$\text{type A: } nm = ns + 5; \qquad \text{type B: } nm = 0.5(n - ns) + 1 \tag{5.1}$$

The number of mechanisms of a modified dome type A is not depending on the number of girders, eight mechanisms were identified for each dome. On the other hand, the number of mechanisms of modified dome type B (MG ngB) can be calculated as:

$$nm = ns + 3 \tag{5.2}$$

The number of self-stress states is not depending on the number of load-bearing girders. Regular domes (RG) are featured by one self-stress state (Table 5.5). The self-stress state obtained from the spectral analysis is the same as one obtained through the formulas on self-equilibrated forces (Table 5.3). In turn, the modified domes (MG) are featured by three self-stress states. In the case of the modified Geiger domes (MG), superimposed self-stress states (Table 5.6) were used for further analysis. The values of obtained self-stress states were normalized in the way that force in the longest strut is equal to -1. The form of the infinitesimal mechanism of Geiger domes indicates a tendency to tilt (Fig. 5.12).

Table 5.5. Values of self-stress state $\mathbf{y}_S$ of the regular Geiger domes (RG)

Type A						**Type B**					
el.	$\mathbf{y}_S$	**el.**	$\mathbf{y}_S$	**el.**	$\mathbf{y}_S$	**el.**	$\mathbf{y}_S$	**el.**	$\mathbf{y}_S$	**el.**	$\mathbf{y}_S$
S1	-0.380[6] -0.507[8] -0.634[10] -0.761[12]	**1**	0.511	**C1**	1.739[6] 2.272[8] 2.814[10] 3.359[12]	**S1**	-0.085	**1**	0.514	**C1**	1.739[6] 2.272[8] 2.814[10] 3.359[10]
S2	-0.304	**2**	0.368	**C2**	0.869[6] 1.136[8] 1.407[10] 1.679[12]	**S2**	-0.304	**2**	0.372	**C2**	0.869[6] 1.361[8] 1.407[10] 1.679[12]
S3	-1.000	**3** **4**	0.921			**S3**	-1.000	**3** **4**	0.921	**C3**	0.362[6] 0.473[8] 0.586[10] 0.699[12]
		5 **6**	2.006					**5** **6**	2.006	**C4**	0.507[6] 0.663[8] 0.821[10] 0.979[12]

[6] dome with 6 girders; [8] dome with 8 girders; [10] dome with 10 girders; [12] dome with 12 girders

Table 5.6. Values of self-stress state $\mathbf{y}_S$ of the modified Geiger domes (MG)

Type A						**Type B**					
el.	$\mathbf{y}_S$	**el.**	$\mathbf{y}_S$	**el.**	$\mathbf{y}_S$	**el.**	$\mathbf{y}_S$	**el.**	$\mathbf{y}_S$	**el.**	$\mathbf{y}_S$
S1	-0.228$^{(6)}$ -0.304$^{(8)}$ -0.379$^{(10)}$ -0.455$^{(12)}$	**1**	0.306	**C1**	1.739$^{(6)}$ 2.272$^{(8)}$ 2.814$^{(10)}$ 3.359$^{(12)}$	**S1**	-0.051	**1**	0.308	**C1**	1.739$^{(6)}$ 2.272$^{(8)}$ 2.814$^{(10)}$ 3.359$^{(12)}$
S2	-0.265	**2**	0.220	**C2**	0.756$^{(6)}$ 0.988$^{(8)}$ 1.223$^{(10)}$ 1.461$^{(12)}$	**S2**	-0.265	**2**	0.223	**C2**	0.756$^{(6)}$ 0.988$^{(8)}$ 1.223$^{(10)}$ 1.461$^{(12)}$
S3	-1.000	**3** **4**	0.801			**S3**	-1.000	**3** **4**	0.801	**C3**	0.217$^{(6)}$ 0.283$^{(8)}$ 0.351$^{(10)}$ 0.419$^{(12)}$
		5 **6**	2.006					**5** **6**	2.006	**C4**	0.303$^{(6)}$ 0.396$^{(8)}$ 0.491$^{(10)}$ 0.586$^{(12)}$
				C5	0.236$^{(6)}$ 0.308$^{(8)}$ 0.381$^{(10)}$ 0.455$^{(12)}$					**C5**	0.236$^{(6)}$ 0.308$^{(8)}$ 0.381$^{(10)}$ 0.455$^{(12)}$
				C6	0.227$^{(6)}$ 0.297$^{(8)}$ 0.368$^{(10)}$ 0.439$^{(12)}$					**C6**	0.227$^{(6)}$ 0.297$^{(8)}$ 0.368$^{(10)}$ 0.439$^{(12)}$

$^{(6)}$ dome with 6 girders; $^{(8)}$ dome with 8 girders; $^{(10)}$ dome with 10 girders; $^{(12)}$ dome with 12 girders

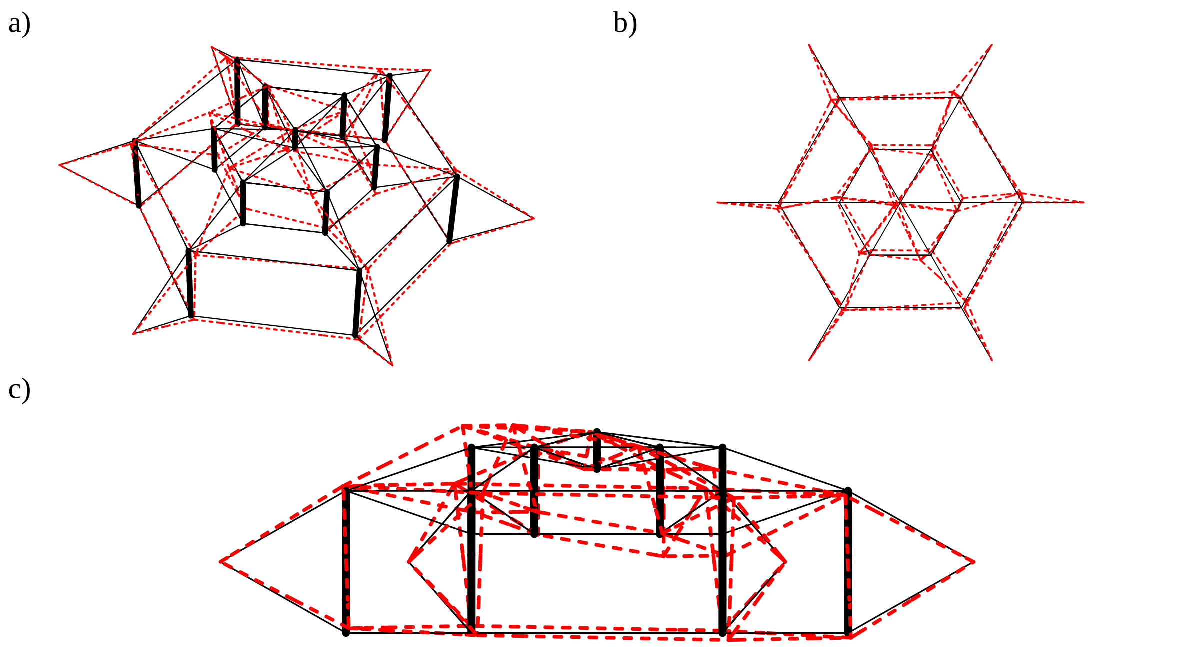

Fig. 5.12. Form of first infinitesimal mechanism of MG 6A dome: a) 3D view, b) top view, c) side view

The qualitative analysis of Geiger domes determined following tensegrity features, i.e., the dome is a truss (*T*), with a continuous net of tensed cables (*C*), and discontinues net of compressed struts (*D*) surrounded by cables, and it features the existence of the self-stress state (*SS*) and infinitesimal mechanism (*M*). Nonetheless, not every existing self-stress state stiffens the mechanism and a superimposed self-stress state must be introduced to the structure. Therefore, the analyzed Geiger domes are classified as structures with tensegrity features of class 1.

5.3.3. Genetic algorithm

The qualitative analysis of the regular type B Geiger dome (RG 12B) (Fig. 5.8) was also performed using the genetic algorithm. The procedure described in section 4.2.2 was implemented to calculate the values of self-equilibrated forces. In the case of the genetic algorithm, the calculations were performed in two series to obtain more accurate results. The algorithms parameters were selected as follows:

- population size: 1000 (Series 1), 1100 (Series 2),
- number of generations: 100 (Series 1), 150 (Series 2),
- solutions in the population: 200 (Series 1), 250 (Series 2),
- number of genes: equals the number of groups of elements.

The results obtained by the genetic algorithm were compared to one obtained by exact methods in paper [182]. The effectiveness of qualitative methods presented in sections 5.3.1 and 5.3.2, has been assessed by comparison with the method used by Jiang et al. [178], i.e., catenary equation-based component force balancing method. Summarized results are provided in Table 5.7. The original values from the paper (Original) were normalized (Norm.) in a way that the value in the longest strut is equal to -1 for a comparison.

Table 5.7. Values of self-stress state of the Geiger dome obtained by different methods

Groups of Elements	**Jiang et al. [178]**			**Present Study**				
	Original	**Norm.**	***Relative Error***	**Exact Solution**	**GA Series 1**	***Relative Error***	**GA Series 2**	***Relative Error***
1	431.514	1.274	1%	1.284	1.315	2%	1.488	16%
2	269.694	0.796	2%	0.814	1.163	43%	0.736	10%
3	701.205	2.069	2%	2.109	2.486	18%	2.235	6%

Table 5.7. Values of self-stress state of the Geiger dome obtained by different methods - Continued

Groups of Elements	**Jiang et al. [178]**			**Present Study**				
	Original	**Norm.**	***Relative Error***	**Exact Solution**	**GA Series 1**	***Relative Error***	**GA Series 2**	***Relative Error***
4	751.292	2.217	2%	2.255	2.336	4%	2.240	1%
5	1452.497	4.287	3%	4.401	4.826	10%	4.511	2%
6	941.433	2.778	6%	2.952	2.952	0%	2.940	0%
C1	1818.387	5.367	0%	5.366	5.359	0%	5.329	1%
C2	1451.127	4.283	0%	4.282	4.416	3%	4.273	0%
C3	833.467	2.459	0%	2.459	2.527	3%	2.848	16%
C4	520.917	1.537	0%	1.537	2.213	44%	1.372	11%
S1	−57.534	−0.169	0%	−0.169	−0.201	19%	−0.197	17%
S2	−140.228	−0.414	0%	−0.414	−0.524	27%	−0.402	3%
S3	−338.833	−1.000	0%	−1.000	−1.000	0%	−1.000	0%

The method provided in [178] gives the 0% error in groups of circumferential cables (C*i*) and struts (S*i*), whereas values for girder cables (*i*) are subjected to errors up to 6%. In the case of the genetic algorithm, the accuracy of the obtained results is highly dependent on the parameters of the algorithm, higher convergence could be achieved by increasing these parameters. Obtained values are considered satisfactory, and meet the requirement of stable equilibrium (the equilibrium of nodes is close to zero).

5.4. Quantitative analysis

The quantitative assessment is the second step of the analysis of tensegrity structures. It is a parametric analysis leading to the determination of the impact of the initial prestress level on the behaviour of the structure under external load. Unlike the qualitative analysis, the results of the quantitative analysis depend on the material and the cross-sections of the elements. It is assumed that cables are made of steel S460N. The "Type A" cables with Young modulus 210 GPa [192] are used. The struts are made of hot-finished circular hollow sections (steel S355J2) with Young modulus 210 GPa. The density of steel is equal $\rho = 7860\ \mathrm{kg/m^3}$.

The quantitative assessment is carried out in terms of static, dynamic, and dynamic stability analysis. All cases concern the small-scale domes. Static analysis is provided for small-scale domes consisted of six load-bearing girders (section 5.2.1). The qualitative analysis of the small-scale domes was performed in section 5.3.2. Dynamic analysis is provided for domes consisting of different numbers of load-bearing girders, i.e., 6, 8, 10, and 12 girders are considered. In turn, dynamic stability analysis is provided for small-scale Geiger domes considered in the static analysis.

In the case of small-scale domes, four variants of geometry are considered, i.e., dome types RG 6A, RG 6B, MG 6A, and MG 6B (Fig. 5.3). The cables with the diameter $\phi = 20$ mm and load-bearing capacity $N_{Rd} = 110.2$ kN are taken into account. For struts, there are rods with a diameter $\phi = 76.1$ mm and thickness $t = 2.9$ mm, with lengths 0.6 m, 1.4 m, and 2.3 m, and load-bearing capacity $N_{Rd} = 224.3$ kN, 170.5 kN, and 107.1 kN respectively. The external load is applied in different positions, i.e., in $\mathbf{P}^{(i)}$, where $i = 1, 2, 3$ (Fig. 5.13). Two values of load are considered, i.e., $\mathbf{P}^{(i)} = \{1\ \mathrm{kN},\ 5\ \mathrm{kN}\}$. The analysis includes time-independent and periodic type of external load. The minimum prestress level is highly dependent on the load value and position of load application (Table 5.8). For some load positions, a higher prestress level is required in comparison to others. In turn, the value of the maximum prestress level (S_{max}) depends on the load-bearing capacity of the most stressed elements. For all structures, it was assumed that S_{max} = 50 kN. The maximum effort of cables is $W_{max,C}$ = 0.95, and the maximum effort of struts is $W_{max,S}$ = 0.48.

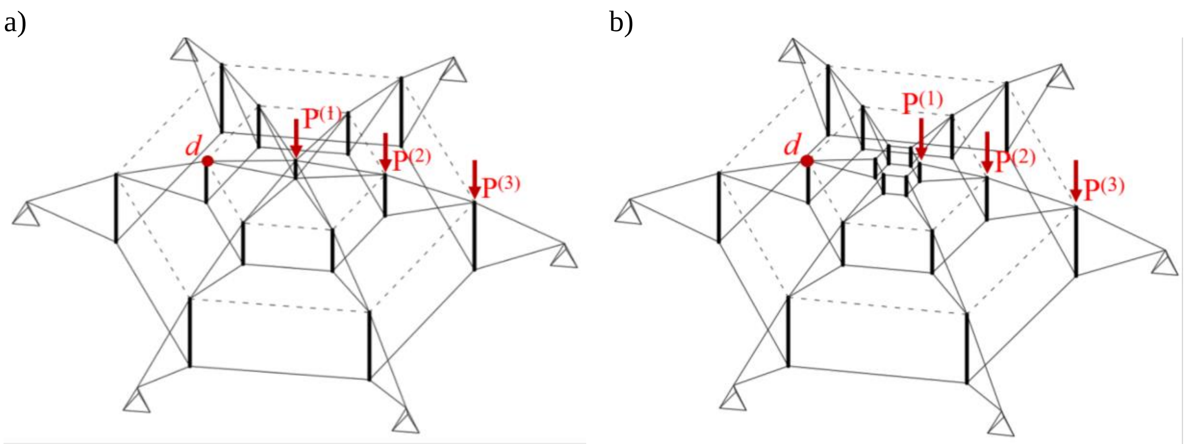

Fig. 5.13. Position of the external load on the load-bearing girder: a) type A, b) type B

Table 5.8. S_{min} values of the Geiger domes under external load

A	Load value						B	Load value					
	$P = 1$ kN			$P = 5$ kN				P = 1 kN			P = 5 kN		
	Load position			Load position				Load position			Load position		
	$\mathbf{P}^{(1)}$	$\mathbf{P}^{(2)}$	$\mathbf{P}^{(3)}$	$\mathbf{P}^{(1)}$	$\mathbf{P}^{(2)}$	$\mathbf{P}^{(3)}$		$\mathbf{P}^{(1)}$	$\mathbf{P}^{(2)}$	$\mathbf{P}^{(3)}$	$\mathbf{P}^{(1)}$	$\mathbf{P}^{(2)}$	$\mathbf{P}^{(3)}$
	S_{min} [kN]			S_{min} [kN]				S_{min} [kN]			S_{min} [kN]		
R	2	5	5	8	22	24	R	2	2	2	2	2	2
M	3	8	12	11	34	36	M	14	10	2	41	26	2

A – type A, B – type B, R – regular dome, M – modified dome

Additionally, to check the possibility of relating results to the real-scale objects, static analysis is performed on the realistic-scale Geiger dome. The realistic-scale dome geometry was obtained by the rescaling of the small-scale dome, and resulted in the same self-stress values (Table 5.6).

In the charts the following symbols are used: II – second-order theory, III – third-order theory, 1 – external load equal to 1 kN, 5 – external load equal to 5 kN, s – struts, c – cables, R – regular dome, M – modified dome, A – type A, B – type B, G1 – realistic dome with symmetrical load, G2 – realistic dome with asymmetrical load. For example, the caption "RA 1(II)" stands for the regular dome type A loaded with force 1 kN analyzed using the second-order theory, and "G1 (II)" stands for the realistic dome with symmetrical load analyzed using the second-order theory.

5.4.1. Static analysis of small-scale domes

Static analysis of Geiger domes concerns the impact of the initial prestress level on the behaviour of the structure under time-independent external load. In particular, the influence of initial prestress level S on the displacements (q_x, q_z), maximum effort of structure W_{max}, and stiffness parameter GSP is analyzed. The displacements are measured for the node located on the girder opposite to the location of the loaded node (node *d*) (Fig. 5.13). The examples are in order to compare the static response of different dome types. Firstly, regular and modified domes type A are compared (Example 1), then regular domes type A and B (Example 2), and, at the end, regular and modified domes type B (Example 3) are considered.

Example 1

<u>*Subject of the comparison:*</u> RG 6A (Fig. 5.14a) and MG 6A (Fig. 5.14b) domes – behaviour under the symmetrical load

<u>*Aim of the comparison:*</u> Whether the modification of the structure matter in the case of symmetrical load?

a) **RG 6A**
$\mathrm{P} = 1\ \mathrm{kN} \rightarrow S_{min} = 2\ \mathrm{kN}$
$\mathrm{P} = 5\ \mathrm{kN} \rightarrow S_{min} = 8\ \mathrm{kN}$

b) **MG 6A**
$\mathrm{P} = 1\ \mathrm{kN} \rightarrow S_{min} = 3\ \mathrm{kN}$
$\mathrm{P} = 5\ \mathrm{kN} \rightarrow S_{min} = 11\ \mathrm{kN}$

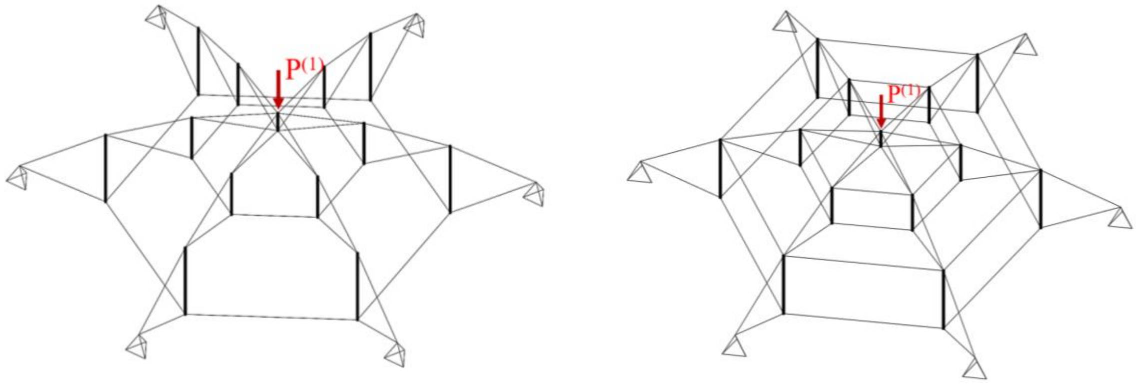

Fig. 5.14. External load application in the case of position $\mathbf{P}^{(1)}$ for: a) RG 6A, b) MG 6A

In order to compare the influence of the initial prestress on the static parameters of the RG 6A and MG 6A domes (Fig. 5.14), firstly the impact of the initial prestress on the plane displacement q_x (Fig. 5.15) and vertical displacement q_z (Fig. 5.16) is considered. In the case of presented type of load, the influence of the initial prestress level on the displacements is absent. The domes are insensitive to the initial prestress. The results obtained from the second-order theory and third-order theory are fully convergent. The increasing of the external load results in a small increasing of displacements. The influence of the initial prestress level on the maximum effort of elements W_{max} (Fig. 5.17) is almost linear, small non-linearity can be noticed at low levels of the prestress. The effort of the elements linearly increases with an increasing of the initial prestress. The GSP parameter, on the other hand, stays constant at value 1, and does not depend neither on the initial prestress level nor external load value (Fig. 5.18).

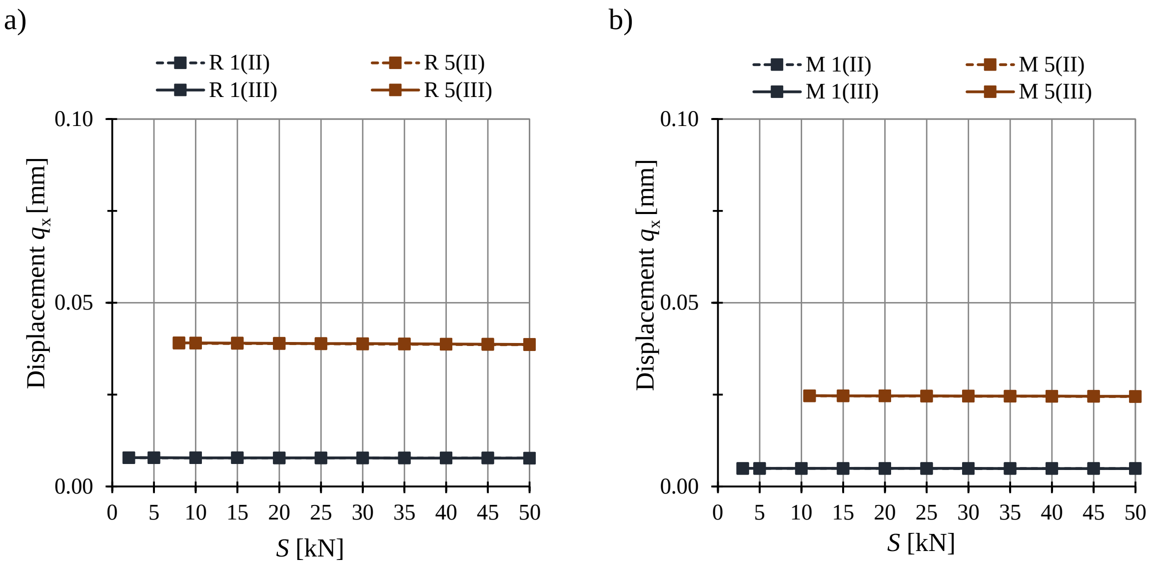

Fig. 5.15. Impact of the initial prestress S on the displacement q_x in the case of the load position $\mathbf{P}^{(1)}$ for: a) RG 6A, b) MG 6A

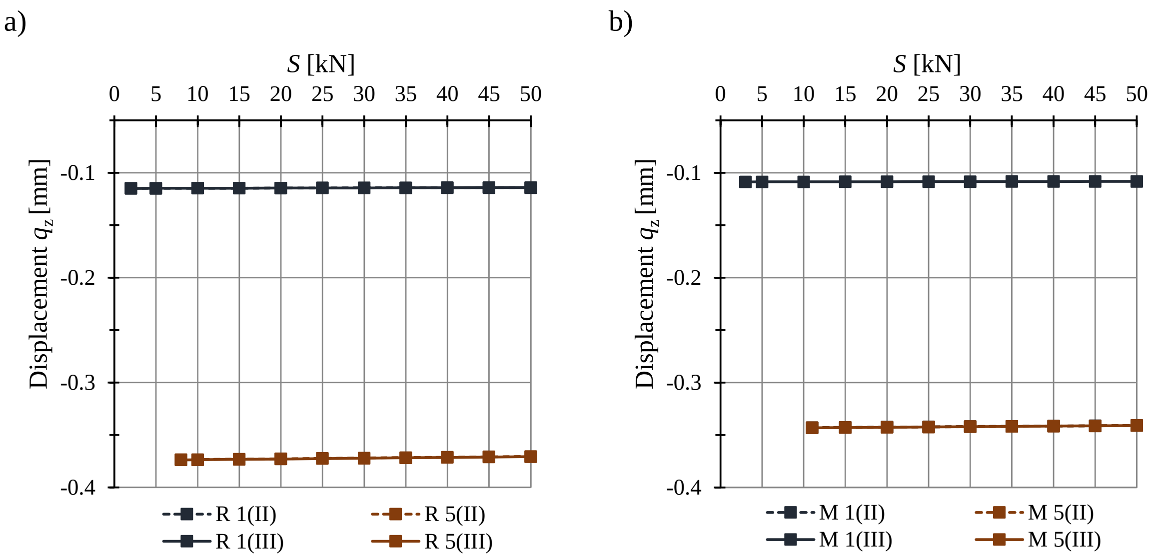

Fig. 5.16. Impact of the initial prestress S on the displacement q_z in the case of the load position $\mathbf{P}^{(1)}$ for: a) RG 6A, b) MG 6A

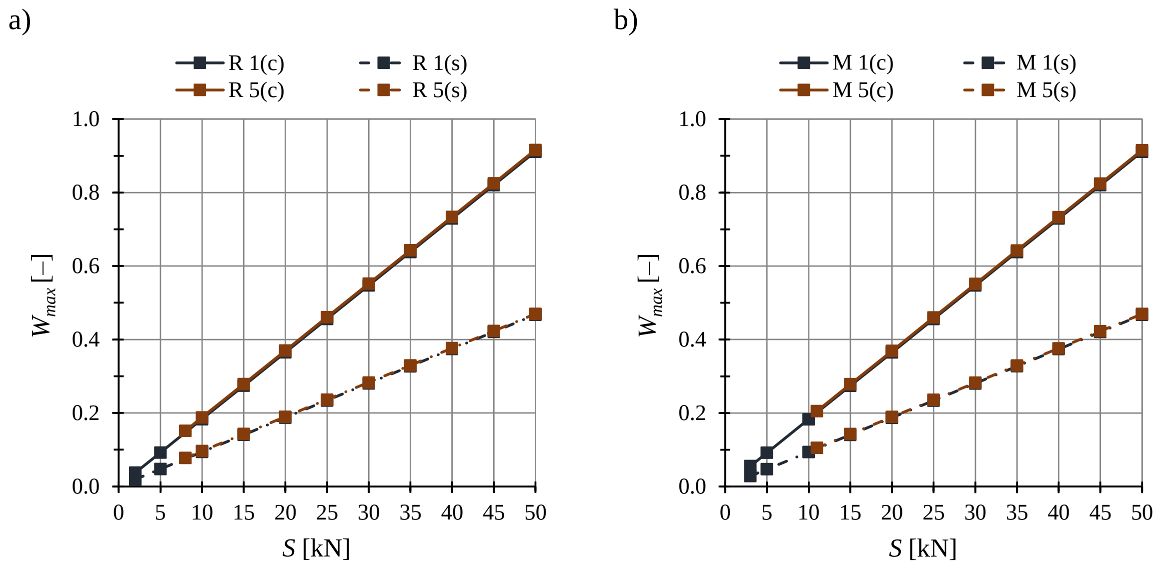

Fig. 5.17. Impact of the initial prestress S on the maximum effort of structure W_{max} in the case of the load position $\mathbf{P}^{(1)}$ for: a) RG 6A, b) MG 6A

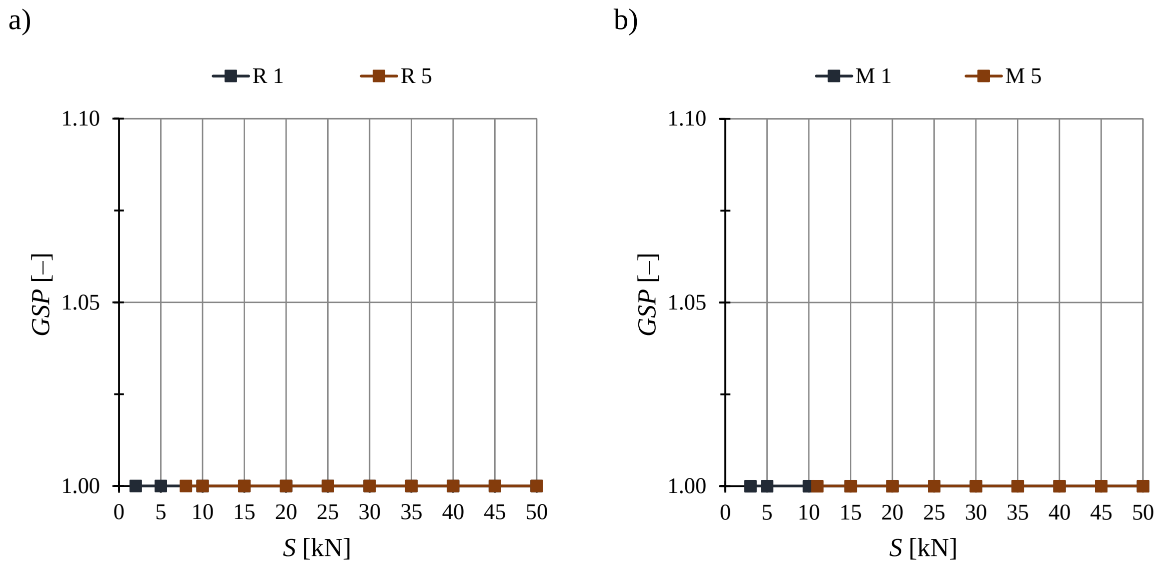

Fig. 5.18. Impact of the initial prestress S on the GSP parameter in the case of the load position $\mathbf{P}^{(1)}$ for: a) RG 6A, b) MG 6A

Conclusion of the comparison: The behaviour of regular and modified domes type A under the symmetrical load is very similar. The main differences remain only in the values of the minimum prestress. In the presented example, the direction of the applied load is inconsistent with the direction of the infinitesimal mechanisms of the structures, thus not affecting the structure. The additional circumferential cables do not contribute to the static response of the dome.

Example 2

<u>Subject of the comparison:</u> RG 6B (Fig. 5.19a) and MG 6B (Fig. 5.19b) domes – behaviour under asymmetrical load

<u>Aim of the comparison:</u> Whether the modification of the structure matter in the case of asymmetrical load?

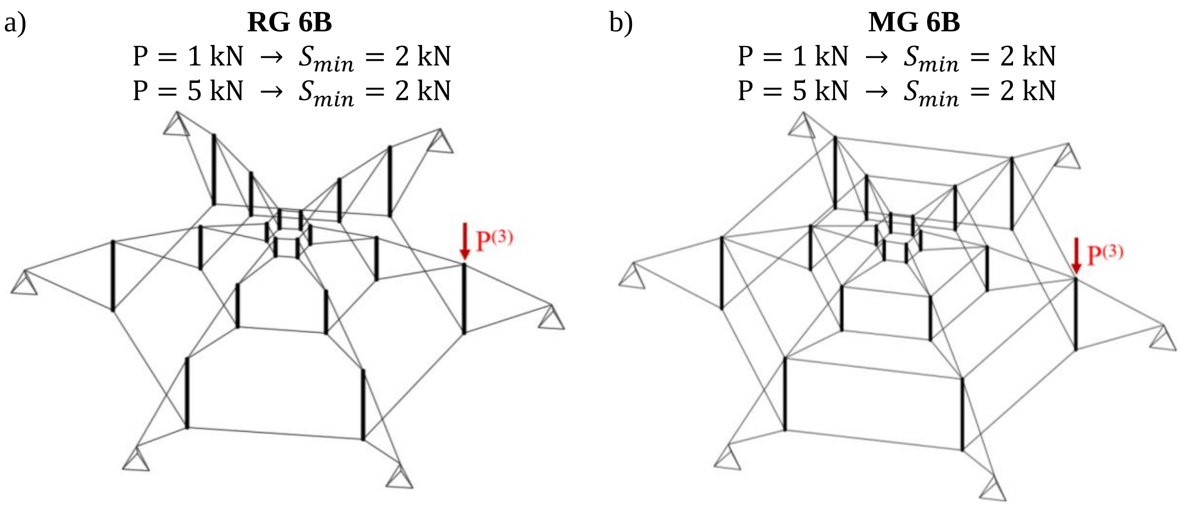

Fig. 5.19. External load application in the case of position $\mathbf{P}^{(3)}$ for: a) RG 6B, b) MG 6B

The second example focuses on the differences in the behaviour of RG 6B and MG 6B domes. The influence of the initial prestress on static parameters in the case of load position $\mathbf{P}^{(3)}$ is considered. The impact of initial prestress on the displacement q_x (Fig. 5.20) and q_z (Fig. 5.21) is similar for both structures. The discrepancy in results obtained from the second- and third-order theory is at the low levels of initial prestress. The nonlinearity increases with an increase of the external load. In the case of the maximum effort of structure W_{max} (Fig. 5.22), the impact of the initial prestress is nonlinear. The impact on the GSP parameter (Fig. 5.23) is considered as linear in the case of low external load, and nonlinearity appears after introducing higher load. Additionally, the increase of the external load results in the decrease of the stiffness of the structure. In the case of initial prestress level $S = 50$ kN, the decrease is around 60% for both domes. The domes characterized by the same level of stiffness.

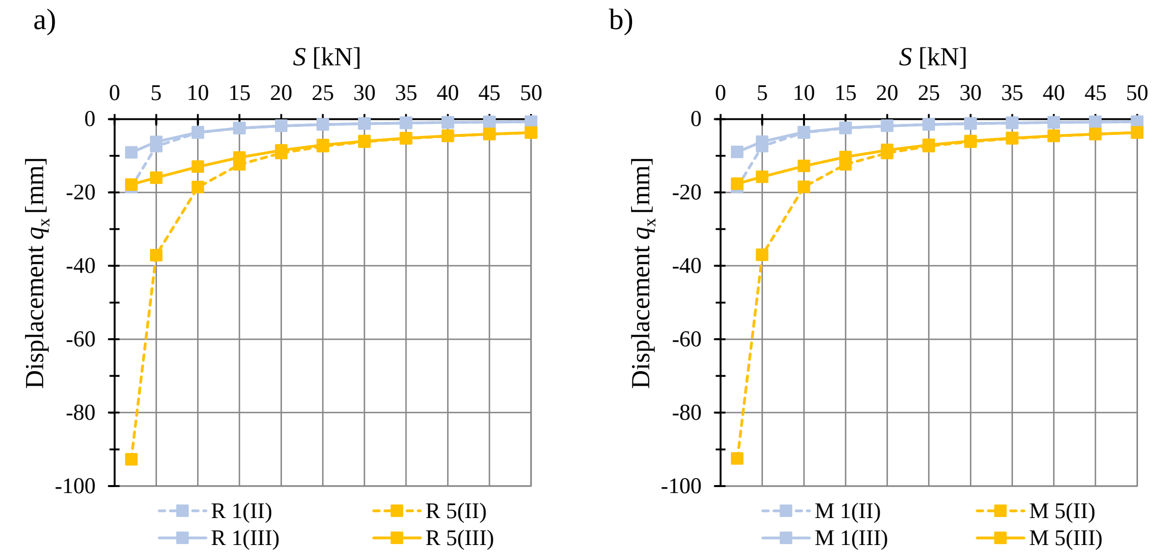

Fig. 5.20. Impact of the initial prestress S on the displacement q_x in the case of the load position $\mathbf{P}^{(3)}$ for: a) RG 6B, b) MG 6B

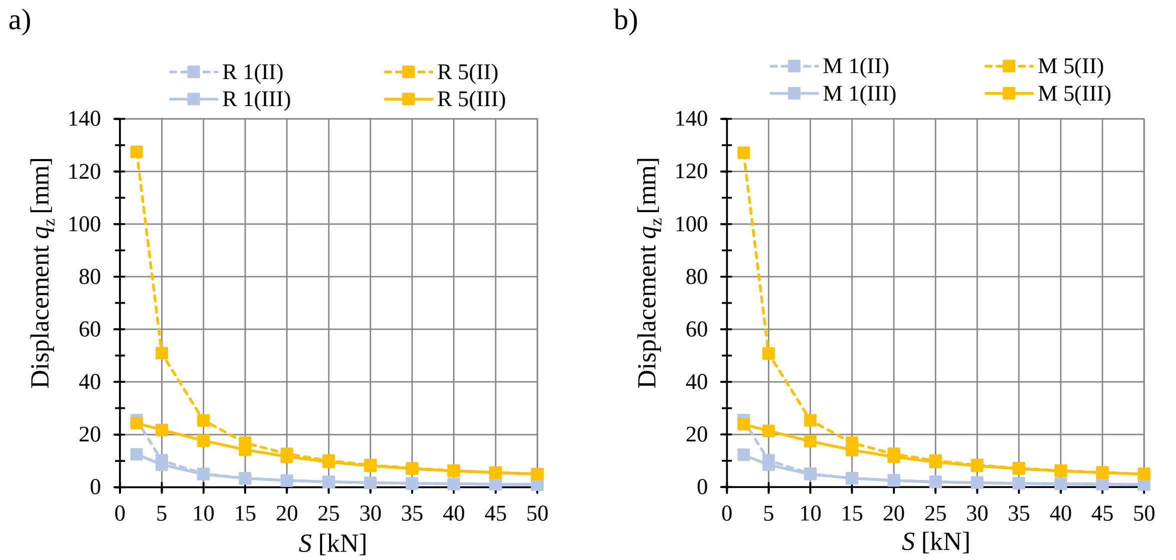

Fig. 5.21. Impact of the initial prestress S on the displacement q_z in the case of the load position $\mathbf{P}^{(3)}$ for: a) RG 6B, b) MG 6B

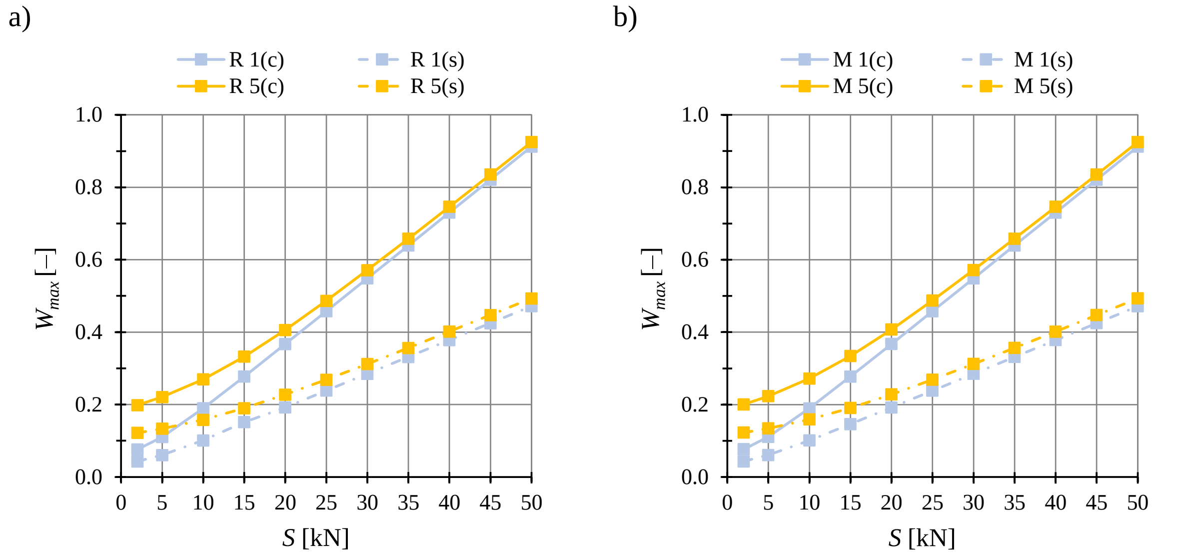

Fig. 5.22. Impact of the initial prestress S on the maximum effort of structure W_{max} in the case of the load position $\mathbf{P}^{(3)}$ for: a) RG 6B, b) MG 6B

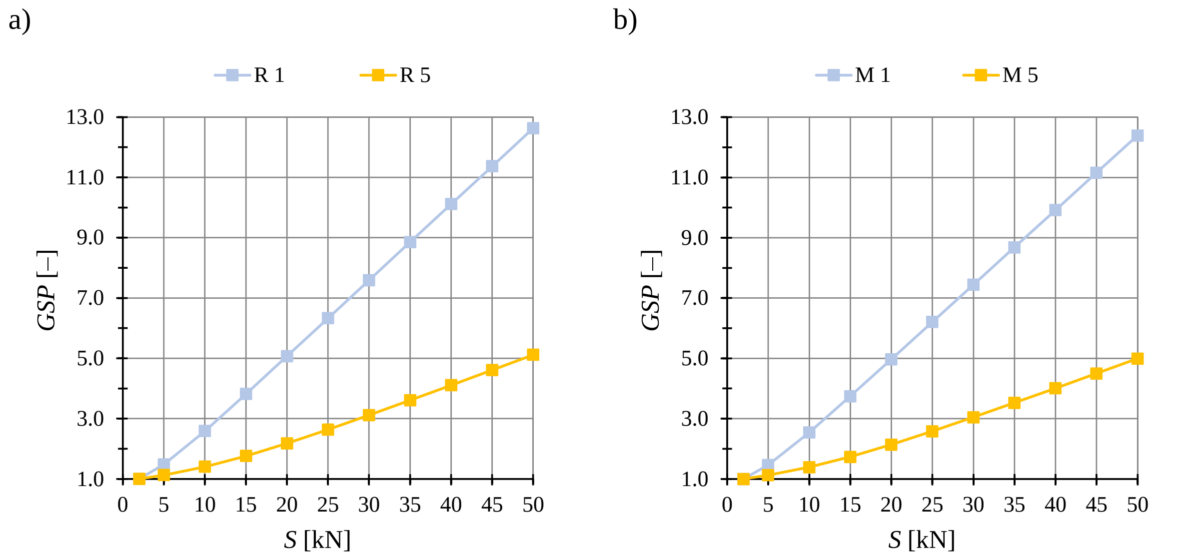

Fig. 5.23. Impact of the initial prestress S on the GSP parameter in the case of the load position $\mathbf{P}^{(3)}$ for: a) RG 6B, b) MG 6B

Conclusion of the comparison: The analysis of regular and modified Geiger domes aims to evaluate the influence of the additional circumferential cables on the static response of the structure. Nonetheless, static analysis showed similar behaviour of considered domes. The impact of the initial prestress on static parameters is the same regardless of the presence of additional cables. The discrepancy in the values obtained from the second- and third-order theory are significant only at the low levels of initial prestress (from S_{min} to $S = 20$ kN). Both domes characterized by the same minimum prestress level. In conclusion, the RG 6B dome is a better design solution and the dome modification is not affecting the static response of the structure.

Example 3

<u>*Subject of the comparison:*</u> RG 6A (Fig. 5.24a) and RG 6B (Fig. 5.24b) domes – behaviour under asymmetrical load

<u>*Aim of the comparison:*</u> Whether the upper section type matter in the case of asymmetrical load?

a) **RG 6A**
P = 1 kN $\rightarrow$ S_{min} = 5 kN
P = 5 kN $\rightarrow$ S_{min} = 22 kN

b) **RG 6B**
P = 1 kN $\rightarrow$ S_{min} = 2 kN
P = 5 kN $\rightarrow$ S_{min} = 2 kN

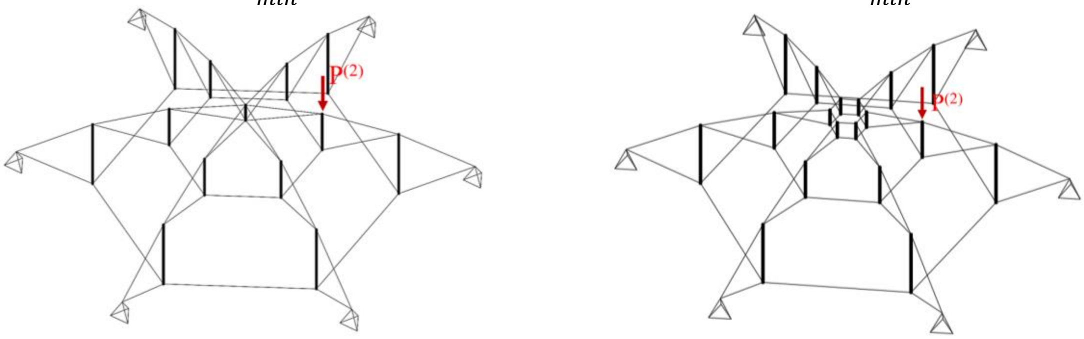

Fig. 5.24. External load application in the case of position $\mathbf{P}^{(2)}$ for: a) RG 6A, b) RG 6B

The third example focuses on the differences in the behaviour of RG 6A and RG 6B domes. The influence of the initial prestress level on static parameters in the case of load position $\mathbf{P}^{(2)}$ is considered (Fig. 5.24). In contrast to *Example 1*, the impact of the initial prestress on the plane displacement q_x (Fig. 5.25) and vertical displacement q_z (Fig. 5.26) can be observed. There are also differences in the results obtained from second-order theory (II) and third-order theory (III) in the case of the RG 6B dome. The biggest discrepancy is at the low initial prestress levels, which increase with an increase in external load. Nonetheless, comparing the displacements of RG 6A and RG 6B domes for the same prestress level (Table 5.9), the differences between theories are similar.

Table 5.9. Displacement q_x for RG 6A and RG 6B domes

	P = 1 kN		P = 5 kN	
	Minimum possible initial prestress level for both domes			
	S = 5 kN		S = 22 kN	
	RG 6A	RG 6B	RG 6A	RG 6B
	Displacement q_x [mm]			
Second-order theory (II)	-18.53	-13.37	-21.04	-15.19
Third-order theory (III)	-15.43	-10.39	-19.54	-13.63
RE*	20.09%	28.68%	7.68%	11.45%

RE* – relative error: $[(q_x(\mathrm{III}) - q_x(\mathrm{II})/q_x(\mathrm{III})) \cdot 100\%]$

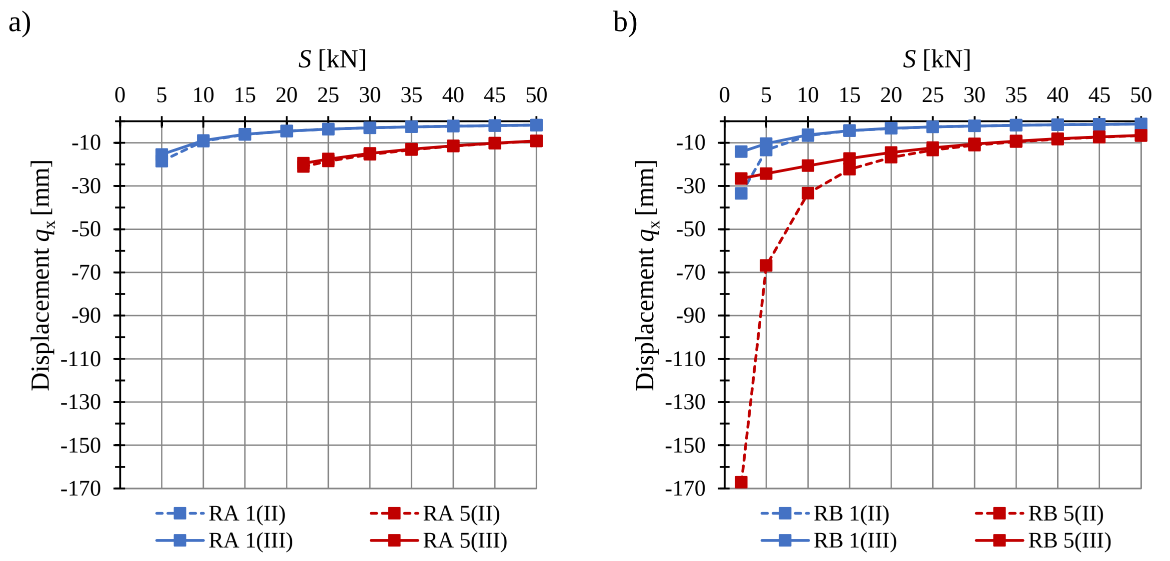

Fig. 5.25. Impact of the initial prestress S on the displacement q_x in the case of the load position $\mathbf{P}^{(2)}$ for: a) RG 6A, b) RG 6B

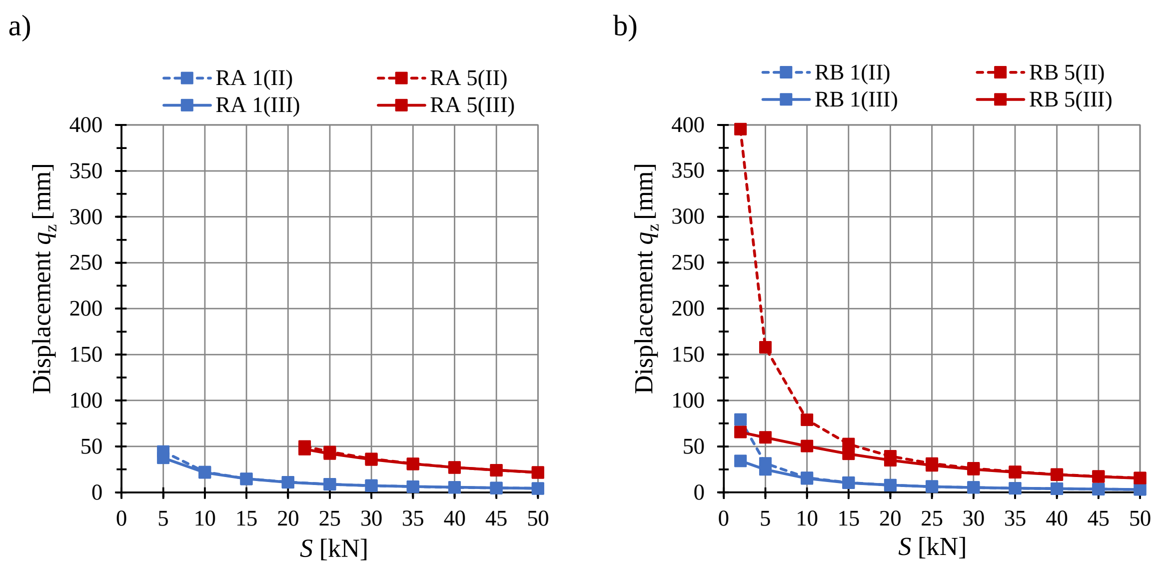

Fig. 5.26. Impact of the initial prestress S on the displacement q_z in the case of the load position $\mathbf{P}^{(2)}$ for: a) RG 6A, b) RG 6B

Comparing the maximum effort of structure W_{max}, for the RG 6A dome the effort is not dependent on the external load and increases linearly (Fig. 5.27a). In turn, for the RG 6B dome the situation is opposite, the effort of the structure depends on the external load, and at the low levels of prestress, the nonlinear behaviour can be observed (Fig. 5.27b).

The GSP parameter is highly dependent on the value of the external load (Fig. 5.28b). The increase from 1kN to 5kN resulted in a decrease in the stiffness of the structure by up to 75% for the RG 6A dome, and up to 60% for the RG 6B dome (in the case of the initial prestress level $S = 50$ kN). Comparing stiffness increase from $S = 5$ kN to $S = 50$ kN (for P = 1 kN), the increase is up to 8-fold for the RG 6A dome and 11-fold for the RG 6B dome. In the case of P = 5 kN (range from $S = 22$ kN to $S = 50$ kN) the increase is 2-fold and almost 5-fold respectively.

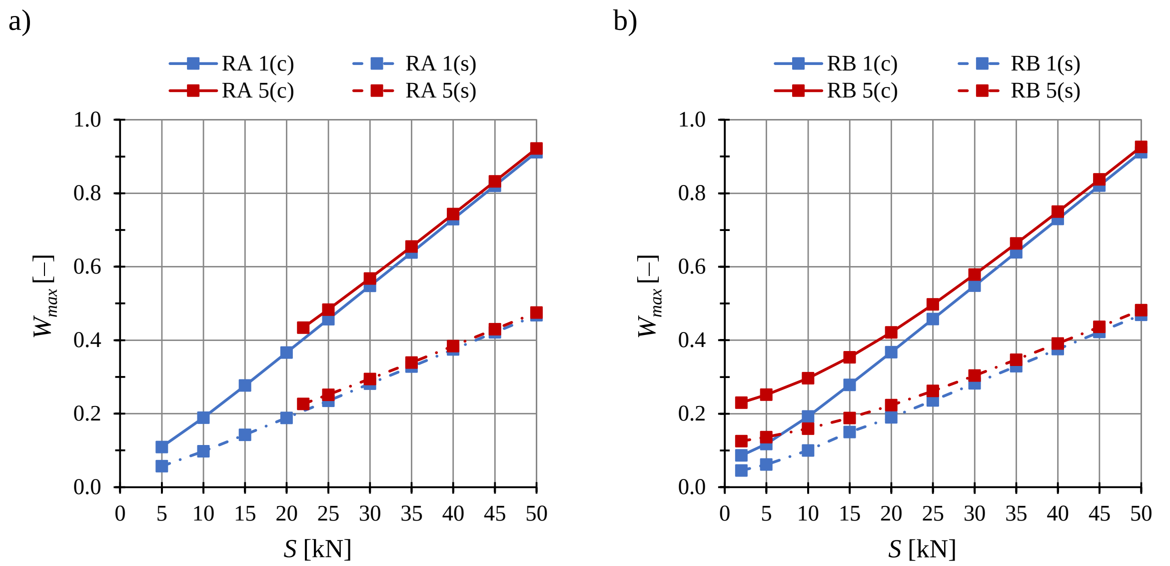

Fig. 5.27. Impact of the initial prestress S on the maximum effort of structure W_{max} in the case of the load position $\mathbf{P}^{(2)}$ for: a) RG 6A, b) RG 6B

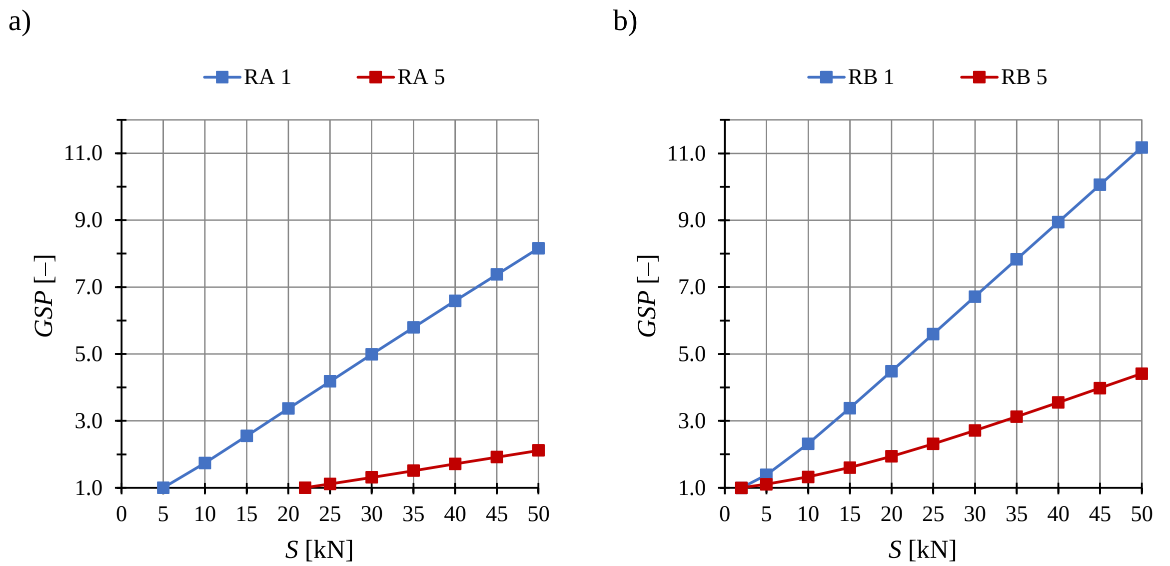

Fig. 5.28. Impact of the initial prestress S on the GSP parameter in the case of the load position $\mathbf{P}^{(2)}$ for: a) RG 6A, b) RG 6B

<u>*Conclusion of the comparison:*</u> The behaviour of domes RG 6A and RG 6B is different due to different prestress conditions. In the case of the RG 6B dome, the external load is not affecting the minimum prestress level. A low prestress level is sufficient to obtain the appropriate distribution of forces in the elements. In turn, for the RG 6A dome, the load value affects the

minimum prestress level, the appropriate distribution of forces can be obtained only by introducing higher prestress. The RG 6A dome minimum prestress level is 150% and 1000% (for 1kN and 5kN load respectively) of the minimum prestress level of the RG 6B dome. The RG 6B dome can be considered as better solution. The increased number of elements (different type of upper section) results in the higher impact of the initial prestress level and easier control of the dome parameters.

5.4.2. Static analysis of the realistic-scale dome

In the case of realistic-scale dome, one variant of geometry is chosen. The modified Geiger dome, with upper section (type A), and six load-bearing girders is considered (MG 6A) (Fig. 5.4d). The dome is 20 m wide and 3.5 m high (measuring from the level of support) (Fig. 5.29). The structure consists of 73 elements, i.e., 13 struts and 60 cables. The struts are designed as tubes CHS 127x5.6. Due to the different lengths, the struts were divided into three groups, i.e., six struts of 3.83 m length, six struts of 2.33 m length, and one strut of 1 m length, with the maximum load-bearing capacity of $N_{Rd} = 418$ kN, 640 kN, and 741 kN, respectively. In turn, the cables are assumed to be made of “D42” with a maximum load-bearing capacity of $N_{Rd} = 504.4$ kN. Two variants of load are considered. In the first case, the load was applied symmetrically (Fig. 5.30a) (G1), whereas in the second – asymmetrically (Fig. 5.30b) (G2). In both cases, the vertical (z-direction) forces (P_z) and plane ones (P_{xy}) are assumed to be the nominal value of 1 kN ($P_x = P_y = 0.707$ kN). The minimum prestress level for the dome is equal to S_{min}= 21 kN, whereas the maximum prestress level was assumed as S_{max} = 190 kN. The maximum effort of structure is W_{max} = 0.91.

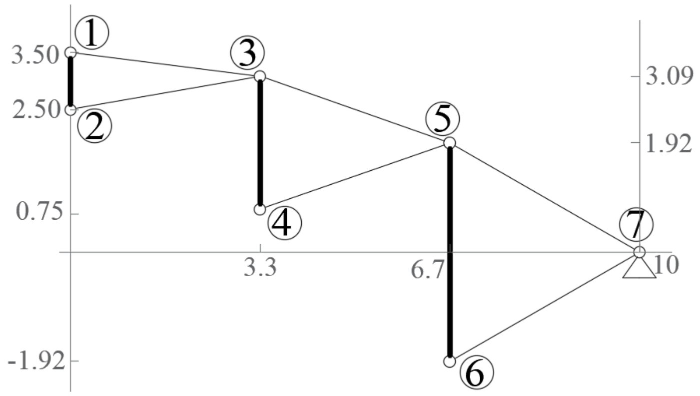

Fig. 5.29. Load-bearing girder of the realistic-scale Geiger dome

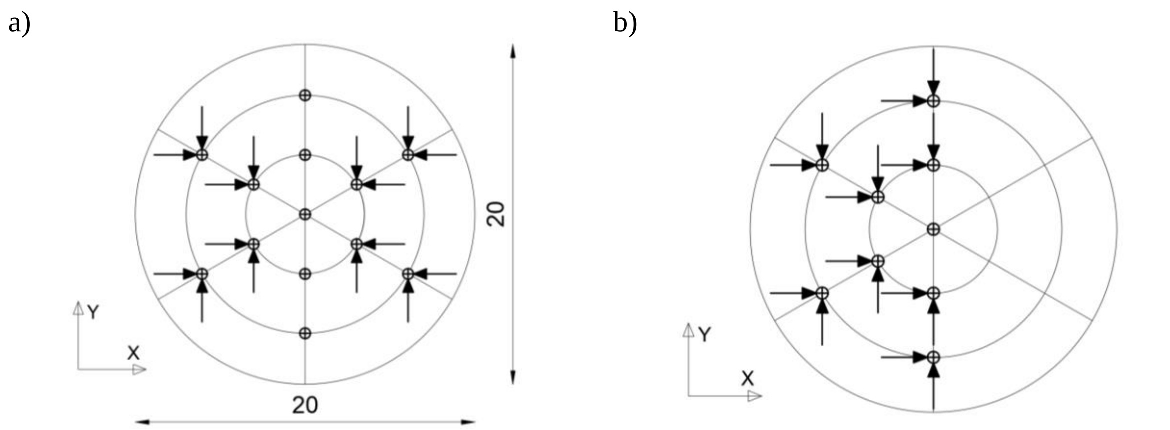

Fig. 5.30. Scheme of the applied load of the realistic-scale Geiger dome: a) symmetrical (G1), b) asymmetrical (G2)

The static analysis of the realistic-scale Geiger dome concerns the impact of the initial prestress level S on the displacements q_x and q_y of the top node 1 (Fig. 5.29), maximum effort of structure W_{max}, and stiffness parameter GSP.

Firstly, the displacements are presented (Fig. 5.31). For the symmetrical load (G1), the displacements q_x and q_y depend on the initial prestress level and additionally on the load variant. The displacements decrease as the initial prestress increases. However, in the case of the asymmetrical load (G2), the displacements are higher than in the case of a symmetrical load (G1). This type of load causes displacements consistent with the infinitesimal mechanisms. The conducted analyses show that the influence of nonlinearity is significant at low values of initial prestress. As prestressing forces increase, the differences between the calculations performed according to the second and third-order theory become smaller. However, in the case of the assumed low load values, results are similar.

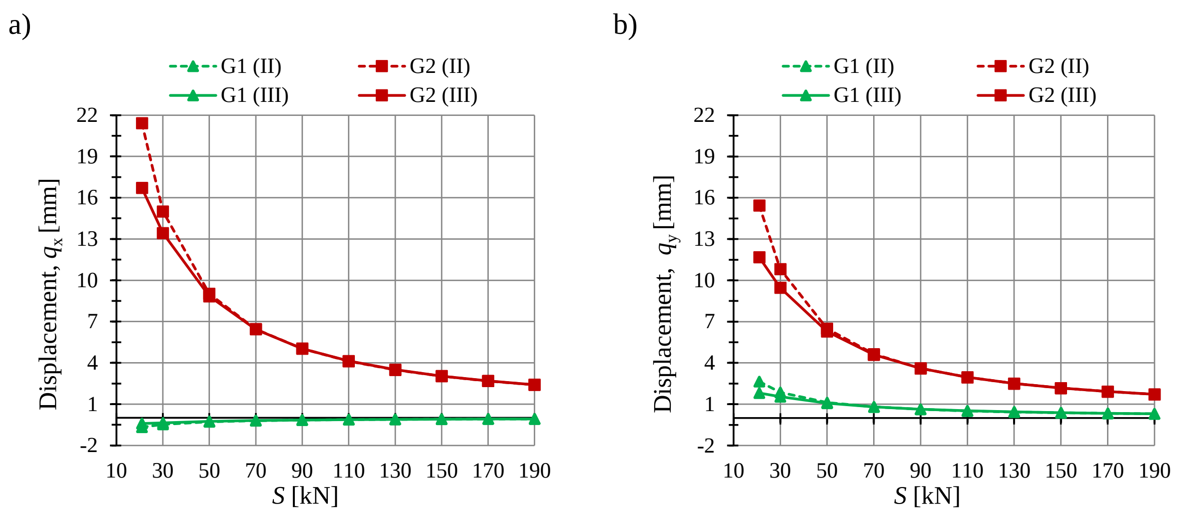

Fig. 5.31. Impact of initial prestress S on the displacement: a) q_x, b) q_y

Next, the maximum effort of the structure (W_{max}) and GSP parameter (Fig. 5.32b) is calculated (Fig. 5.32a). Small nonlinearity can be noticed at the low initial prestress levels, due to a low external load. Nonetheless, the load type is not affecting considered parameters.

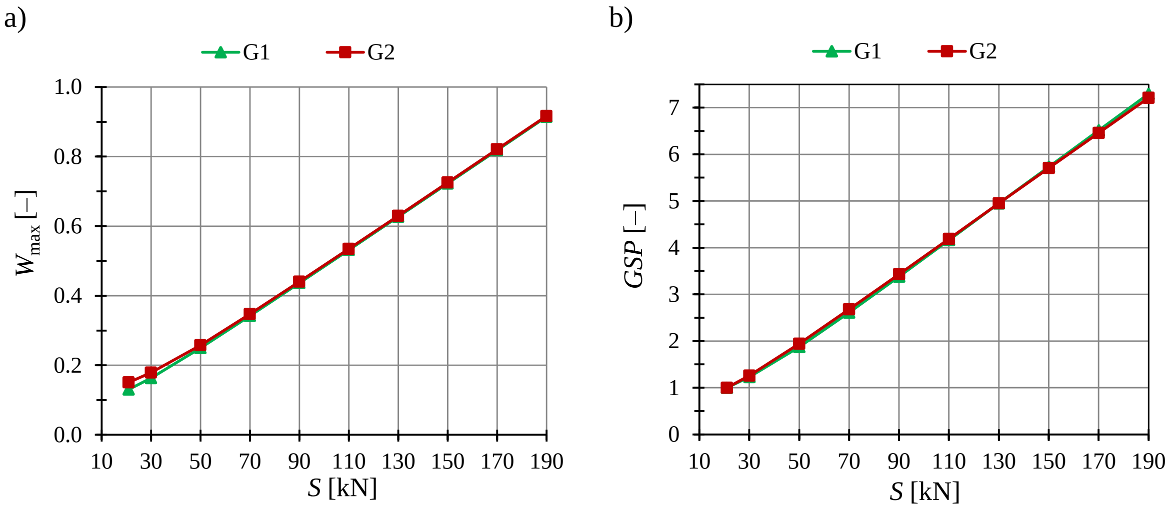

Fig. 5.32. Impact of initial prestress S on the: a) maximum effort of structure W_{max}, b) GSP parameter

The external load nature (symmetrical or asymmetrical) has a great impact on the displacements of the structure. The asymmetrical load (G2) is consistent with the infinitesimal mechanism and causes bigger displacements than in the case of symmetrical load (G1). In turn, parameters such as maximum effort of structure or stiffness are not dependent on the load nature.

5.4.3. Dynamic analysis

The dynamic analysis of the Geiger domes includes the analysis of both natural and free frequencies of the structure. The assessment divided onto three parts that contain natural frequencies that correspond to the infinitesimal mechanisms (Example 1), additional natural frequencies that depend on the initial prestress (Example 2), and free frequencies (Example 3).

Example 1

<u>*Subject of the comparison:*</u> RG ngA, RG ngB, MG ngA, MG ngB domes ($ng = \{6,8,10,12\}$) - natural frequencies correspond to the infinitesimal mechanisms

<u>*Aim of the comparison:*</u> (1) How does the initial prestress level impact the natural frequencies corresponding to the infinitesimal mechanisms? (2) Whether the number of load-bearing girders impacts the natural frequencies corresponding to the infinitesimal mechanisms? (3) How does

the design solution (regular or modified, open or closed upper section) impact the dome behaviour?

The dynamic analysis concerns the small-scale Geiger domes provided in section 5.4.1. The consideration includes domes with a different number of load-bearing girders (ng), i.e., $ng = \{6,8,10,12\}$. It is commonly known that, in the case of tensegrity structures, the number of natural frequencies depending on the self-stress state is equal to a number of infinitesimal mechanisms (nm). The number of existing infinitesimal mechanisms of small-scale domes was determined in the section 5.3.2. Fig. 5.33 presents the influence of the initial prestress level on the first ($f1$) and last (fnm) natural frequency of considered domes. A zero prestress ($S = 0$) results in zero frequencies. However, after increasing the level of initial prestress, frequencies increase nonlinearly. The level of the first natural frequency $f1$ is similar for each considered dome $f1 = 5.1$ Hz ÷ 6.5 Hz for S_{max}. The smallest discrepancy between the first and last natural frequency at the maximum prestress level is noted for the MG 6A dome and equals around 7 Hz, thus, the biggest discrepancy is for the RG 12B dome – around 68 Hz. The natural frequencies that correspond to the infinitesimal mechanisms are characterized by high sensitivity to the changes in the initial prestress level.

In the case of RG ngA domes (Fig. 5.33a), the increasing number of load-bearing girders is not affecting the first natural frequency $f1$ and last natural frequency fnm. For MG ngA (Fig. 5.33b), the situation is similar, however, a small discrepancy can be noted (around 0.5 ÷ 2 Hz for the $S_{max} = 50$ kN). In turn, for the regular and modified domes of type B (RG ngB and MG ngB) (Fig. 5.33c, d) an increase in the number of load-bearing girders results in the increase in the value of the last natural frequency fnm. Moreover, the last natural frequency fnm of the regular domes is at least 20% higher than the natural frequencies of the modified domes.

It should be noted, that the forms of vibrations, in the case of $S = 0$, realize the forms of the infinitesimal mechanisms. Although each form of vibration is unique, some natural frequencies are characterized by the same values. As an example, the MG 6A dome is characterized by eight different forms of vibrations (corresponding to the infinitesimal mechanism) (Fig. 5.34), but six different frequencies ($f_2 = f_3$ and $f_5 = f_6$) (Table 5.10) (the frequencies that are characterized by the same values are grouped in gray). In the case of other domes, it is the same.

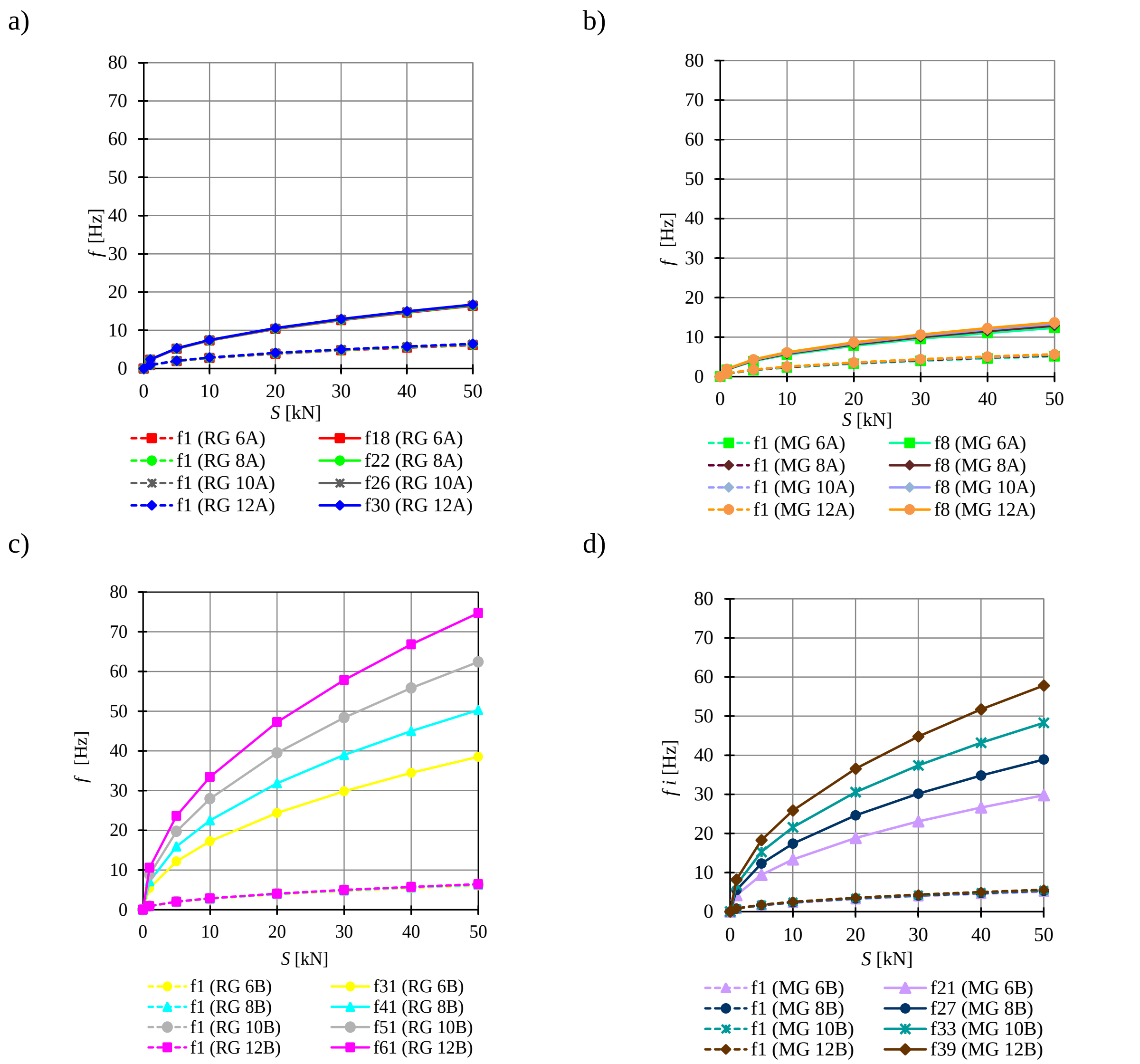

Fig. 5.33. Influence of the initial prestress S on the natural frequency f of: a) RG ngA, b) MG ngA, c) RG ngB, d) MG ngB

Table 5.10. Values of natural frequencies corresponding to the mechanism of MG 6A dome

S [kN]	f_i [Hz]							
	f_1	f_2	f_3	f_4	f_5	f_6	f_7	f_8
0	0	0	0	0	0	0	0	0
1	0.726	0.842	0.842	1.044	1.247	1.247	1.262	1.747
5	1.632	1.883	1.883	2.335	2.788	2.788	2.821	3.906
10	2.296	2.662	2.662	3.302	3.943	3.943	3.990	5.524
20	3.247	3.764	3.764	4.670	5.575	5.575	5.463	7.813
30	3.976	4.608	4.608	5.720	6.827	6.827	6.911	9.569
40	4.591	5.319	5.319	6.604	7.882	7.882	7.980	11.049
50	5.133	5.945	5.945	7.384	8.811	8.811	8.922	12.353

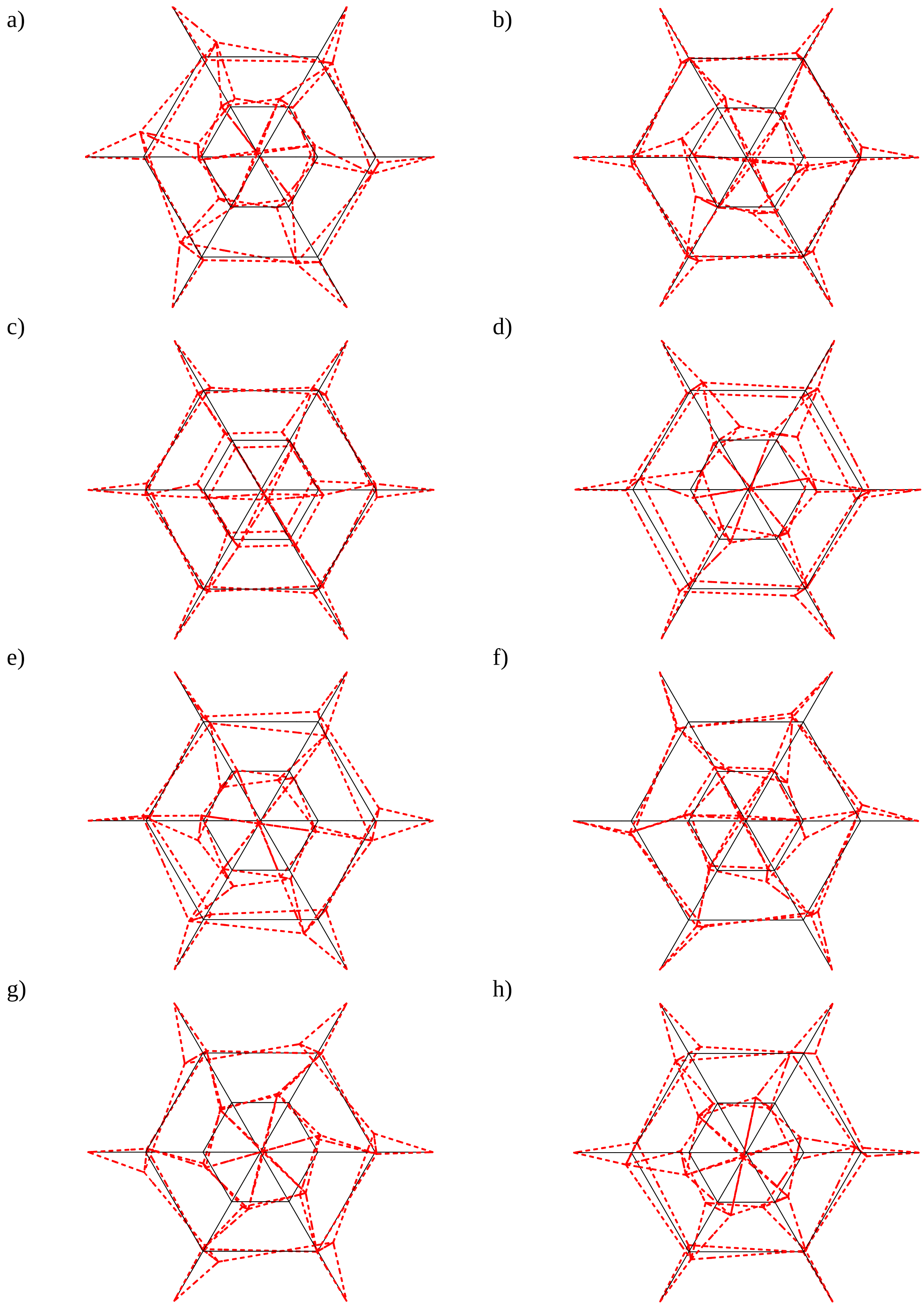

Fig. 5.34. Forms of vibrations for the MG 6A dome for frequency: a) f_1, b) f_2, c) f_3, d) f_4, e) f_5, f) f_6, g) f_7, h) f_8

<u>Conclusion of the comparison:</u> The natural frequencies corresponding to the infinitesimal mechanisms are characterized by a high sensitivity to the change in the initial prestress level. Additionally, the impact of the prestress is nonlinear. The number of load-bearing girders affects only the last natural frequency fnm of the type B domes (open section), especially regular ones (RG ngB). The first natural frequency $f1$ remains on the same level for each considered dome and is not affected by the number of load-bearing girders.

Example 2

<u>Subject of the comparison:</u> RG ngA, RG ngB, MG ngA, MG ngB domes ($ng = \{6{,}8{,}10{,}12\}$) - additional natural frequencies dependent on the initial prestress

<u>Aim of the comparison:</u> (1) Whether the initial prestress level impact the next natural frequencies that not correspond to the infinitesimal mechanism? (2) Whether the number of load-bearing girders impacts the natural frequencies that not correspond to the infinitesimal mechanisms? (3) How the design solution (regular or modified, open or close upper section) impacts the dome behaviour?

As was stated earlier, the number of natural frequencies depending on the initial prestress level is equal to a number of the infinitesimal mechanisms (f_{nm}). Nevertheless, for the type A Geiger domes (RG ngA and MG ngA) it is different. In this case, the number of dependent frequencies f_{total} is greater and depends on the number of girders (ng):

$$f_{total} = f_{nm} + f_{add}; \qquad f_{add} = (ng - 3) \tag{5.3}$$

In Fig. 5.35 and Fig. 5.36 the last frequency corresponding to the infinitesimal mechanism (f_{nm}), the next additional dependent on the prestress (f_{add}) and the first independent of prestress ($f_{total+1}$) ones are shown. In the absence of prestress ($S = 0$) the frequency f_{nm} is equal to zero, and after introducing prestress S the values f_{nm} increase in nonlinear way. Whereas, the behaviour of additional frequency depended on prestress (f_{add}) is different. In the absence of prestress f_{add} is not zero and dependence on the prestress is almost linear. The smallest dependency on the initial prestress level is noted for the $f19 = f20$ of the RG 6A dome, the difference between $S = 0$ and $S = 50$ kN is 5.7 Hz. The biggest dependency, thus, is for $f39$ of the RG 12A dome, the difference is 16.1 Hz. The additional natural frequencies characterized by a little sensitivity to the change in the initial prestress level, comparing to the natural frequencies, corresponded to the infinitesimal mechanism. It should be noted, the number of frequencies f_{add}, and the sensitivity on the initial prestress changes, depends on the number of girders. More sensitive to the changes are higher frequencies.

In turn, the value of the first frequency independent of prestress $(f_{total+1})$ for all Geiger domes type A does not depend neither on the number of loads-bearing girders nor initial prestress level. The value varies $f_{total+1} = 42.7$ Hz ÷ 44.7 Hz.

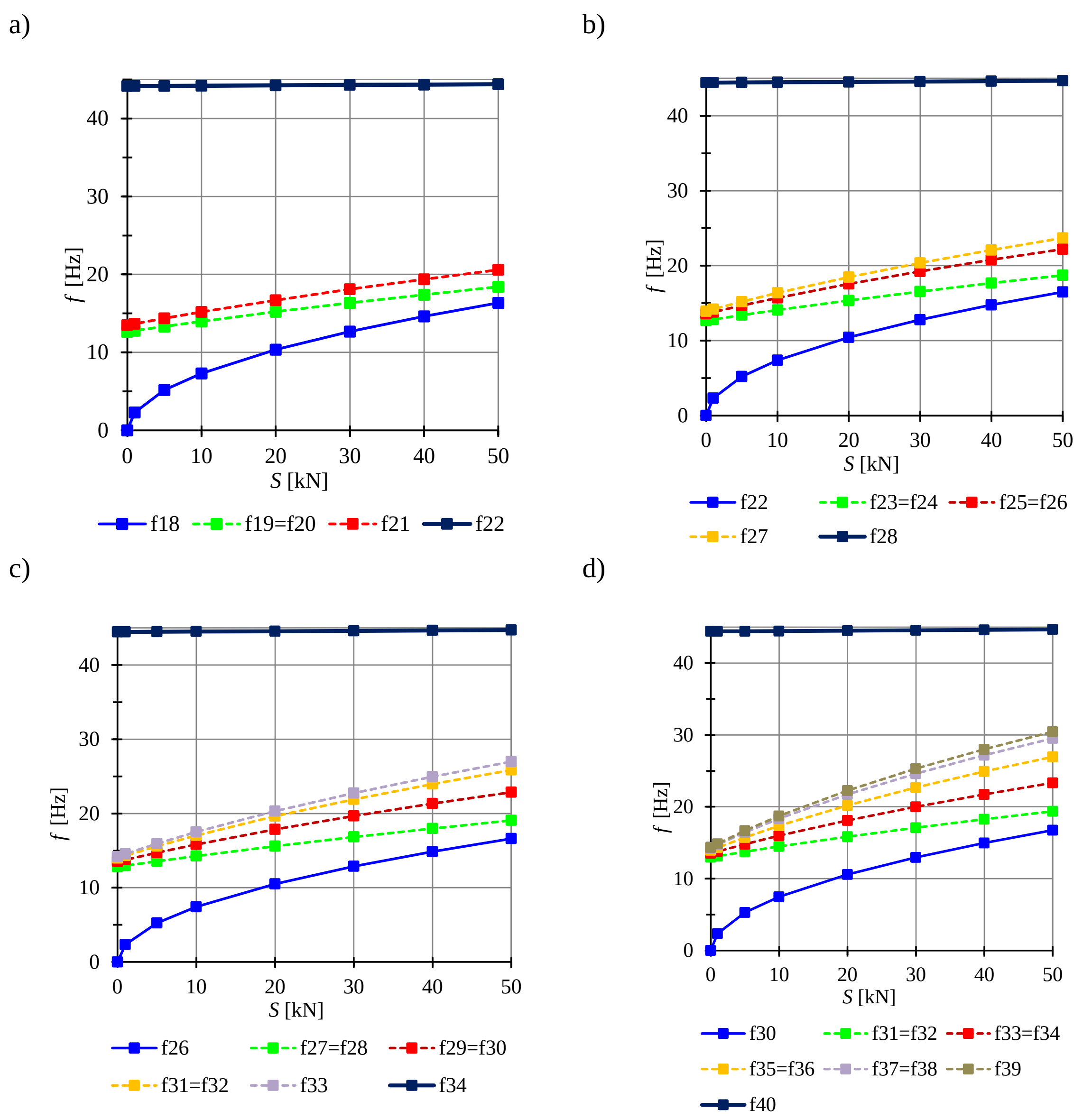

Fig. 5.35. Influence of the initial prestress *S* on the natural frequencies f_{nm}, f_{add}, and $f_{total+1}$ of: a) RG 6A, b) RG 8A, c) RG 10A, d) RG 12A

In the case of the domes type B, the natural frequencies that do not correspond to the infinitesimal mechanism are independent of the initial prestress level. It means that, independent of the number of loads-bearing girders, the number of dependent frequencies is equal:

$$f_{total} = f_{nm} \tag{5.4}$$

For all Geiger domes type B, the value of the first frequency independent of prestress are not depended neither on the number of loads-bearing girders nor the initial prestress level, and the range equals $f_{total+1}$ = 40.9 Hz ÷ 42.2 Hz.

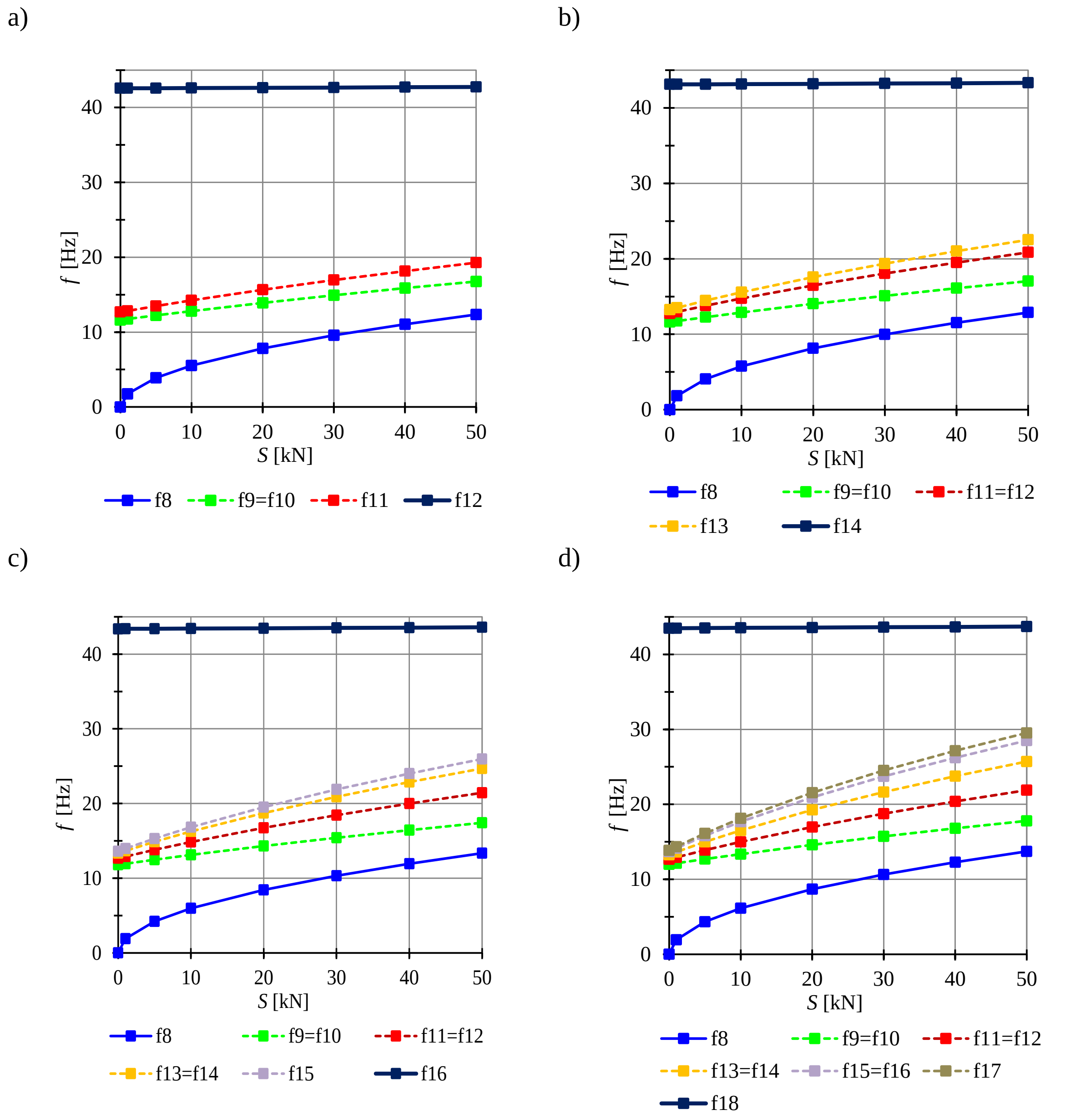

Fig. 5.36. Influence of the initial prestress S on the natural frequencies f_{nm}, f_{add}, and $f_{total+1}$ of: a) MG 6A, b) MG 8A, c) MG 10A, d) MG 12A

<u>*Conclusion of the comparison:*</u> The additional natural frequencies that depend on the initial prestress level occur only in the case of type A domes and highly depend on the number of load-bearing girders. However, in comparison to the natural frequencies corresponding to the

infinitesimal mechanisms, they are characterized by little sensitivity to the initial prestress level and the impact of prestress is linear. In turn, in the case of type B domes, the number of natural frequencies depended on the initial prestress level equal to the number of infinitesimal mechanisms.

Example 3

<u>*Subject of the comparison:*</u> RG 6A, RG 6B, MG 6A, MG 6B domes - free frequencies

<u>*Aim of the comparison:*</u> (1) How does the initial prestress level impact free frequencies? (2) How do the value and position of load impact free frequencies?

The analysis of free frequencies of the structure with different variants (value and position) of load was performed. Tables 5.10-5.13 contain values of the first $f_1(P)$ and last $f_{nm}(P)$ frequency that correspond to the infinitesimal mechanisms. The increasing of the external load results in the decreasing of the minimum prestress level S_{min} value, except for the RG 6B dome (Table 5.11). The behaviour of this dome is unique, and the S_{min} value do not depend on the load value nor the position and always equals 2 kN. In other cases, the increase of the load is significantly affecting the values of the S_{min}. In the case of the domes type A (RG 6A, MG 6A), the S_{min} value decreases when the load position changes from the $\mathbf{P}^{(1)}$ to the $\mathbf{P}^{(3)}$. For example, in the case of load P = 5 kN, the minimum prestress level changed from 8 kN to 24 kN for RG 6A dome (Table 5.12), and from 11 kN to 36 kN for MG 6A dome (Table 5.13). For the MG 6B dome, the situation is the opposite. The minimum initial prestress level is changing from 41 kN to 2 kN for MG 6M dome (Table 5.14).

Table 5.11. Natural $f_i(0)$ and free $f_i(P)$ frequencies [Hz] for the dome RG 6B

S [kN]	$f_1(0)$	$f_1(P)$						$f_{31}(0)$	$f_{31}(P)$					
		$\mathbf{P}^{(1)}$		$\mathbf{P}^{(2)}$		$\mathbf{P}^{(3)}$			$\mathbf{P}^{(1)}$		$\mathbf{P}^{(2)}$		$\mathbf{P}^{(3)}$	
		1 kN	5 kN	1 kN	5 kN	1 kN	5 kN		1 kN	5 kN	1 kN	5 kN	1 kN	5 kN
0	0.00							0.00						
1	0.86							5.45						
2	1.22	1.73	2.75	1.82	2.78	1.69	2.57	7.71	10.81	17.04	11.30	17.60	10.88	17.16
5	1.92	2.08	2.90	2.14	2.97	2.06	2.75	12.18	13.04	17.99	13.38	18.57	13.19	18.20
10	2.72	2.74	3.20	2.76	3.29	2.74	3.10	16.69	17.23	19.91	17.34	20.45	17.41	20.26
20	3.85	3.84	3.95	3.84	4.01	3.84	3.90	23.06	24.21	24.64	24.22	24.94	24.53	25.16
30	4.72	4.70	4.71	4.70	4.74	4.70	4.69	28.02	29.68	29.51	29.68	39.63	29.81	30.04
40	5.44	5.43	5.41	5.43	5.43	5.43	5.40	32.23	34.31	33.97	34.31	34.02	34.42	34.46
50	6.09	6.08	6.05	6.08	6.06	6.08	6.04	35.94	38.39	38.00	38.38	38.01	38.49	38.46

Table 5.12. Natural $f_i(0)$ and free $f_i(P)$ frequencies [Hz] for the dome RG 6A

S [kN]	$f_1(0)$	$f_1(P)$						$f_{18}(0)$	$f_{18}(P)$					
		$\mathbf{P}^{(1)}$		$\mathbf{P}^{(2)}$		$\mathbf{P}^{(3)}$			$\mathbf{P}^{(1)}$		$\mathbf{P}^{(2)}$		$\mathbf{P}^{(3)}$	
		1 kN	5 kN	1 kN	5 kN	1 kN	5 kN		1 kN	5 kN	1 kN	5 kN	1 kN	5 kN
0	0.00							0.00						
1	0.86							2.31						
2	1.22	1.15						3.27	3.17					
5	1.93	1.89		2.07		1.68		5.17	5.10		5.58		5.81	
8	2.45	2.41	2.23	2.48		2.33		6.54	6.49	6.31	6.68		6.84	
10	2.73	2.71	2.57	2.75		2.66		7.32	7.27	7.10	7.38		7.51	
20	3.87	3.85	3.76	3.86		3.84		10.35	10.31	10.18	10.33		10.38	
22	4.06	4.04	3.96	4.04	4.10	4.03		10.85	10.82	10.69	10.83	11.08	10.88	
24	4.24	4.22	4.14	4.22	4.26	4.21	3.78	11.34	11.30	11.18	11.32	11.50	11.35	12.00
30	4.74	4.72	4.65	4.72	4.72	4.72	4.46	12.67	12.64	12.53	12.65	12.73	12.67	13.10
40	5.47	5.45	5.40	5.46	5.43	5.45	5.31	14.63	14.61	14.51	14.61	14.61	14.63	14.84
50	6.11	6.10	6.05	6.10	6.07	6.10	6.01	16.36	16.34	16.25	16.34	16.31	16.35	16.46

Table 5.13. Natural $f_i(0)$ and free $f_i(P)$ frequencies [Hz] for the dome MG 6A

S [kN]	$f_1(0)$	$f_1(P)$						$f_8(0)$	$f_8(P)$					
		$\mathbf{P}^{(1)}$		$\mathbf{P}^{(2)}$		$\mathbf{P}^{(3)}$			$\mathbf{P}^{(1)}$		$\mathbf{P}^{(2)}$		$\mathbf{P}^{(3)}$	
		1 kN	5 kN	1 kN	5 kN	1 kN	5 kN		1 kN	5 kN	1 kN	5 kN	1 kN	5 kN
0	0.00							0.00						
1	0.73							1.75						
3	1.26	1.19						3.03	3.02					
5	1.62	1.56						3.91	3.90					
8	2.05	1.99		2.08				4.95	4.94		5.27			
10	2.30	2.26		2.31				5.52	5.52		5.73			
11	2.41	2.35	2.22	2.39				5.79	5.79	5.79	5.95			
12	2.51	2.46	2.34	2.49		2.51		6.05	6.05	6.05	6.17		6.06	
20	3.25	3.22	3.12	3.23		3.23		7.81	7.81	7.80	7.85		7.80	
30	3.98	3.96	3.88	3.96		3.96		9.57	9.56	9.55	9.58		9.56	
34	4.23	4.22	4.19	4.20	4.20	4.23		10.19	10.18	10.17	10.22	10.44	10.25	
36	4.36	4.35	4.33	4.32	4.32	4.36	4.31	10.48	10.48	10.45	10.52	10.71	10.56	10.47
40	4.59	4.58	4.51	4.58	4.55	4.58	4.54	11.05	11.05	11.04	11.05	11.22	11.04	11.03
50	5.13	5.12	5.06	5.12	5.08	5.12	5.09	12.35	12.35	12.34	12.35	12.45	12.34	12.32

Table 5.14. Natural $f_i(0)$ and free $f_i(P)$ frequencies [Hz] for the dome MG 6B

S [kN]	$f_1(0)$	$f_1(P)$						$f_{21}(0)$	$f_{21}(P)$					
		$\mathbf{P}^{(1)}$		$\mathbf{P}^{(2)}$		$\mathbf{P}^{(3)}$			$\mathbf{P}^{(1)}$		$\mathbf{P}^{(2)}$		$\mathbf{P}^{(3)}$	
		1 kN	5 kN	1 kN	5 kN	1 kN	5 kN		1 kN	5 kN	1 kN	5 kN	1 kN	5 kN
0	0.00							0.00						
1	0.72							4.21						
2	1.02					1.41	2.16	5.96					8.64	13.21
5	1.61					1.76	2.33	9.42					10.56	14.20
10	2.28			2.32		2.29	2.61	13.32			13.56		13.52	15.87
14	2.70	2.69		2.72		2.66	2.92	15.77	18.91		15.71		15.66	17.45
20	3.23	3.22		3.22		3.13	3.28	18.84	20.72		18.77		18.85	19.61
26	3.68	3.67		3.55	3.72	3.69	3.68	21.48	22.67		21.33	21.65	21.47	21.65
30	3.96	3.94		3.94	3.97	3.94	3.94	23.08	23.92		22.97	23.08	23.06	23.33
40	4.57	4.55		4.55	4.54	4.56	4.53	26.65	27.06		26.54	26.42	26.63	26.72
41	4.62	4.61	4.57	4.61	4.58	4.69	4.59	26.98	27.31	32.27	26.97	26.79	27.16	26.91
50	5.11	5.09	5.06	5.09	5.07	5.10	5.06	29.79	30.01	33.81	29.69	29.47	29.77	29.79

The biggest discrepancy between natural and free frequencies is noticeable at the low levels of the initial prestress, especially for the last frequency corresponding to the mechanism. In the case of RG 6B dome, the difference between natural and free frequencies is the biggest, up to 55% (in the case $\mathbf{P}^{(3)} = 5$ kN and $S = 2$ kN), because of the lowest S_{min} value for each load case. The situation is similar for MG 6B dome in case of the same load case and prestress level. Nevertheless, the increasing of the initial prestress level results in the convergence of the values of natural and free frequencies. In the case of the prestress level $S = 50$ kN, the difference in the first frequency is around 1.6% and 1%, and about 0.8% and 11% for the last frequency, for the dome type A and B respectively.

Conclusion of the comparison: The free frequencies of the dome are highly dependent on the initial prestress level. The dependency on the load value and position is significant only in low levels of initial prestress, an increase in the initial prestress level results in a decrease in the sensitivity of the free frequencies to the load.

5.4.4. Dynamic stability analysis

The dynamic stability analysis of a small-scale six-girder Geiger domes is considered (see section 5.4.1). Particularly, the influence of the initial prestress level on the shape and range of unstable regions is analyzed. A few examples are provided in order to compare the behaviour of different domes under the periodic load. Firstly, the RG 6A and MG 6A domes are compared (Example 1), then the RG 6A and RG 6B (Example 2), and the RG 6B with MG 6B domes (Example 3) are considered. The consideration is concluded with summarized results for all domes (Example 4).

Example 1

<u>*Subject of the comparison:*</u> RG 6A (Fig. 5.37a) and MG 6A (Fig. 5.37b) domes – unstable regions

<u>*Aim of the comparison:*</u> (1) Does the initial prestress level affect unstable regions for the type A domes? (2) Does the structure modification of type A domes (Fig. 5.37b) affect unstable regions?

a) **RG 6A**
P = 1 kN → S_{min} = 5 kN
P = 5 kN → S_{min} = 22 kN

b) **MG 6A**
P = 1 kN → S_{min} = 8 kN
P = 5 kN → S_{min} = 34 kN

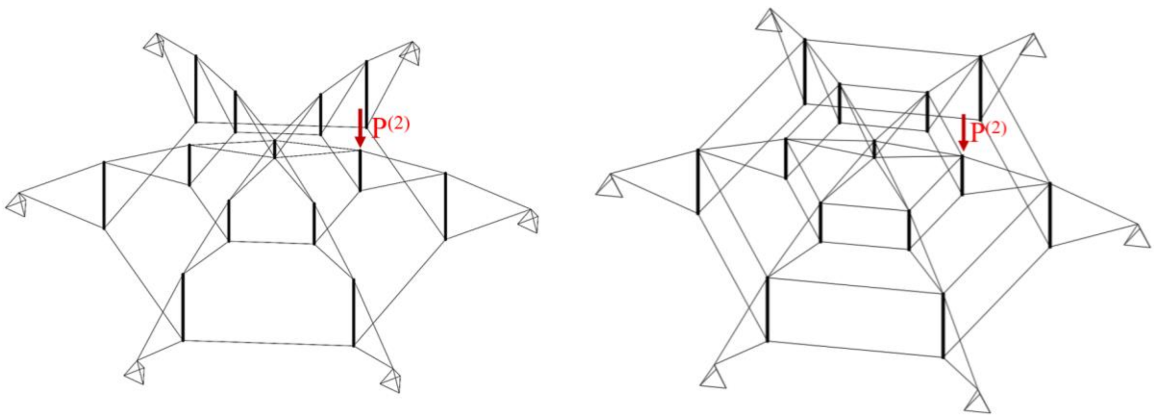

Fig. 5.37. External load application in the case of position $\mathbf{P}^{(2)}$ for: a) RG 6A, b) MG 6A

The first example concerns influence of the initial prestress level on the unstable regions of the RG 6A and MG 6A domes. The load position $\mathbf{P}^{(2)}$ is considered in order to avoid the symmetrically distributed external load. The selected instability regions are presented for three levels of initial prestress, and two load variants P = 1 kN (Table 5.15) and P = 5 kN (Table 5.16). The results indicate quite similar behaviour of regular and modified domes. In the case of first load variant (P = 1 kN) (Table 5.15) the domes are characterized by the similar S_{min} level, and the impact of the initial prestress level on the limits of instability regions is comparable. The biggest instability regions are noted for the last resonant frequency corresponded to the infinitesimal mechanism (η18 for RG 6A, and η8 for MG 6A). For both domes, the resonant frequencies increase with an increase of the initial prestress level, and the instability regions narrows. Unlike in the case of load variant P = 5 kN, for P = 1 kN the instability regions occurred only for S_{min} level of initial prestress, however, not for the all-selected frequencies (in case of modified dome). The increase of load value has great impact on the increase of resonant frequencies of the domes. The resonant frequencies for the P = 5 kN are two times the resonant frequencies for P = 1 kN.

Table 5.15. Limits of chosen four main instability regions of the RG 6A and MG 6A domes for P = 1 kN (R – RG 6A dome, M – MG 6A dome)

<table>
<tr><th></th><th>S_{min} [kN]</th><th>S = 15 kN</th><th>S = 25 kN</th></tr>
<tr><td>R</td><td>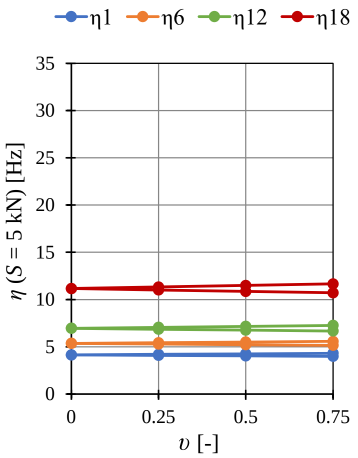
</td><td>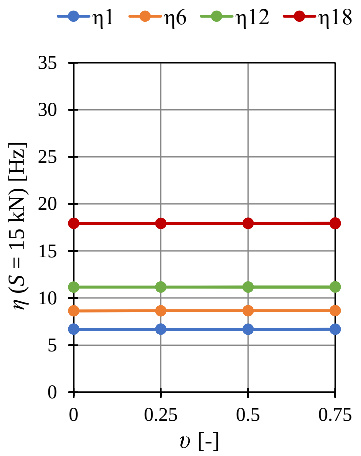
</td><td>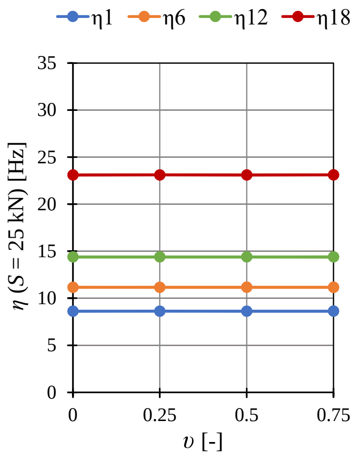
</td></tr>
<tr><td>M</td><td>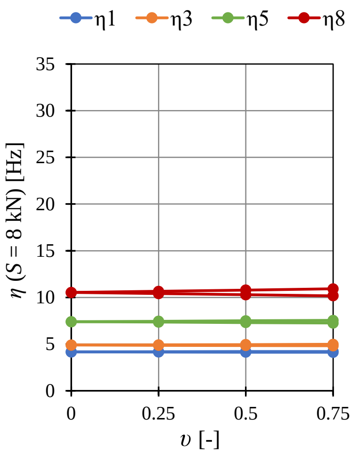
</td><td>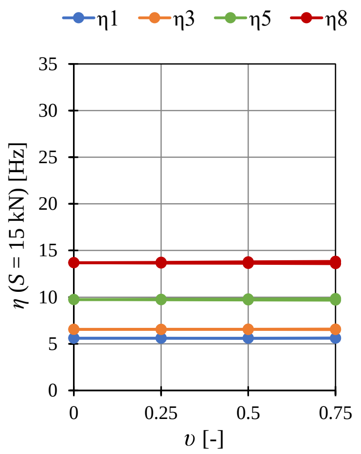
</td><td>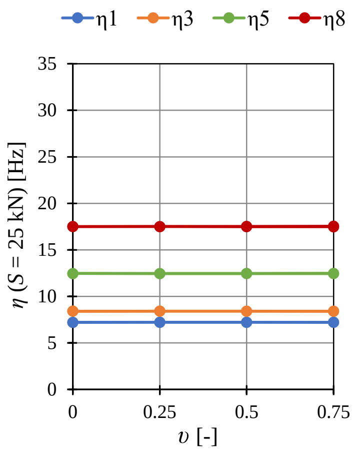
</td></tr>
</table>

Table 5.16. Limits of chosen four main instability regions of the RG 6A and MG 6A domes for P = 5 kN (R – RG 6A dome, M – MG 6A dome)

	S_{min} [kN]	$S = 40$ kN	$S_{max} = 50$ kN
R	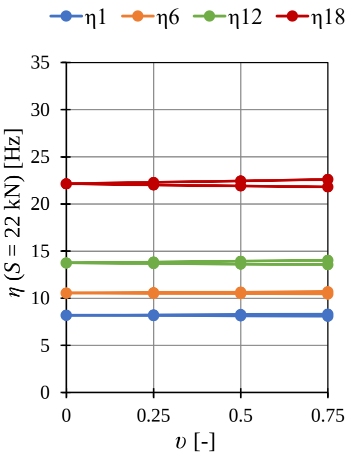	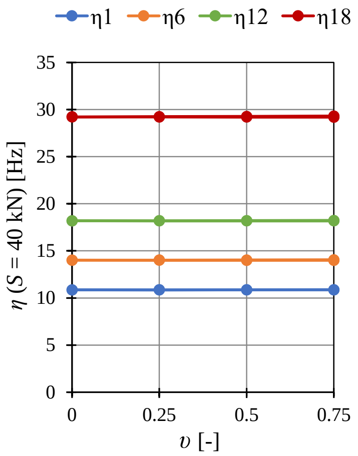	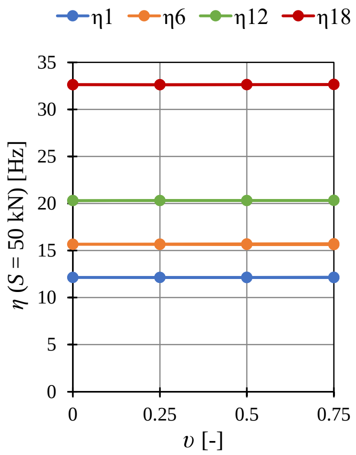
M	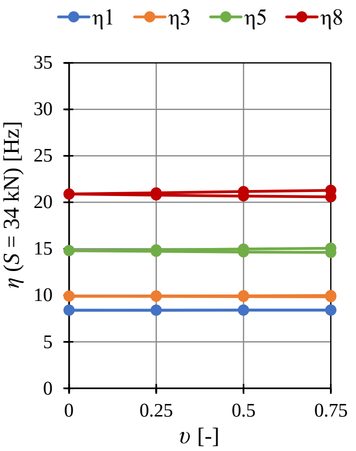	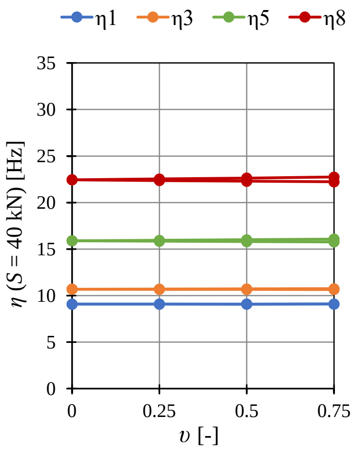	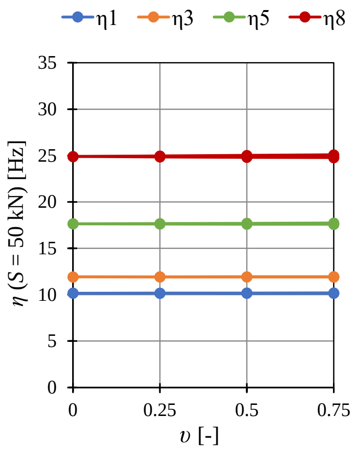

As in the case of natural frequencies, Geiger domes type A characterized by additional resonant frequencies dependent on the initial prestress level (see section 5.4.3). The RG 6A and MG 6A domes are characterized by three additional resonant frequencies, i.e., $\eta19$, $\eta20$, $\eta21$, and $\eta9$, $\eta10$, $\eta11$ respectively (Table 5.17). The additional frequencies do not depend on the pulsatility index υ, the boundaries of instability regions coincide. Nonetheless, the regular dome is more sensitive to change in the initial prestress level. The relative increase (RI) is about 36.69% - 41.74%, while for the modified dome it is around 32.58% - 37.47% (in the case P = 1 kN). The increase in the external load led to a decrease in the influence of the initial prestress. The RI is even three times smaller in the case of load P = 5 kN than for the P = 1 kN.

Table 5.17. Resonant frequencies of the RG 6A and MG 6A domes in the case of load position $\mathbf{P}^{(2)}$

	RG 6A				MG 6A			
	Resonant frequency $\eta(v = 0 \div 0.75) = \text{const.}$							
	$\eta 19$	$\eta 20$	$\eta 21$	$\eta 22$	$\eta 9$	$\eta 10$	$\eta 11$	$\eta 12$
P = 1 kN								
S_{min}	26.93	26.93	29.06	88.38	25.29	25.29	28.05	85.19
S_{max}	36.81	36.82	41.19	88.83	33.53	33.54	38.56	85.52
RI*	36.69%	36.72%	41.74%	0.51%	32.58%	32.62%	37.47%	0.39%
P = 5 kN								
S_{min}	31.24	31.24	34.44	88.56	30.76	30.78	35.09	85.39
S_{max}	36.85	36.89	41.27	88.83	33.58	33.61	38.65	85.52
RI*	17.96%	18.09%	19.83%	0.31%	9.17%	9.19%	10.15%	0.15%

RI* – relative increase: $[(\eta(\mathrm{S_{min}}) - \eta(S_{max}))/\eta(S_{min}) \cdot 100\%]$

Fig. 5.38 presents the impact of the initial prestress level on the range and distribution of instability regions. The change is measured by the nondimensional parameter λ. For each dome, the range of instability regions is equal to 1 for S_{min} level. In the case of the RG 6A dome (Fig. 5.38 a, b), the increase in the initial prestress level has greater impact on the areas than in the case of MG 6A dome (Fig. 5.38 c, d). For the P $= 1$ kN and $S = 15$ kN, the areas are smaller by about 95% and 68%, for RG 6A and MG 6A respectively (the changes are measured taking into account average value for four regions). The situation is similar for P $= 5$ kN and $S = 40$ kN, the average decrease is about 86% and 30%, for RG 6A and MG 6A respectively. In the case of the RG 6A dome, changes in the range of the second unstable region corresponded to the sixth resonant frequency $\eta 6$ should be noted. The increase of the initial prestress level results in the decrease of the area (up to 90% - 100%), and then in the significant increase. For the MG 6A dome, the behaviour of the first unstable region corresponded to the first resonant frequency $\eta 1$ is comparable.

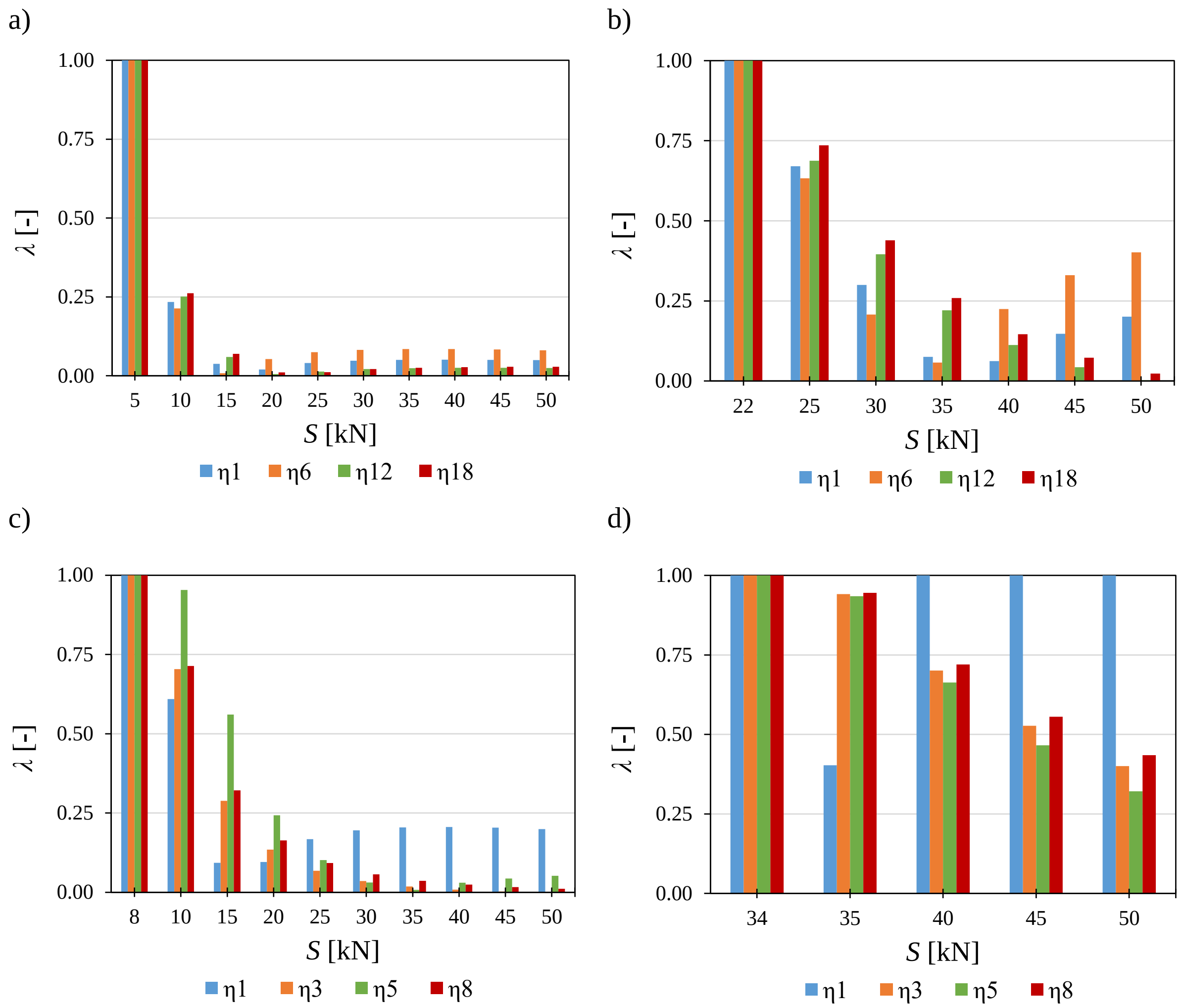

Fig. 5.38. Influence of the initial prestress level S on the range of unstable regions of: a) RG 6A for P = 1 kN, b) RG 6A for P = 5 kN, c) MG 6A for P = 1 kN, d) MG 6A for P = 5 kN

Conclusion of the comparison: In the case of type A domes, the probability of the occurrence of the unstable regions is low. Only in the case of S_{min} and low initial prestress level, there are unstable regions, however, the areas are small. Comparing the behaviour of regular and modified Geiger domes type A, it was noted that introducing additional circumferential cables is not affect the distribution of unstable regions. It means, the introducing of the additional cables is not necessary. Nevertheless, in the case of a regular dome, an initial prestress has a greater impact on the area of unstable regions, and the structure is characterized by higher resonant frequencies.

Example 2

<u>*Subject of the comparison:*</u> RG 6A (Fig. 5.39a) and RG 6B (Fig. 5.39b) domes – unstable regions

<u>*Aim of the comparison:*</u> (1) Does the initial prestress level affect unstable regions in the case of different dome types (closed (Fig. 5.39a) or open (Fig. 5.39b) upper section)? (2) Does the structure modification affect unstable regions in the case of different dome types (closed (Fig. 5.39a) or open (Fig. 5.39b) upper section)?

a) **RG 6A**
$\mathrm{P} = 1\ \mathrm{kN} \rightarrow S_{min} = 5\ \mathrm{kN}$
$\mathrm{P} = 5\ \mathrm{kN} \rightarrow S_{min} = 24\ \mathrm{kN}$

b) **RG 6B**
$\mathrm{P} = 1\ \mathrm{kN} \rightarrow S_{min} = 2\ \mathrm{kN}$
$\mathrm{P} = 5\ \mathrm{kN} \rightarrow S_{min} = 2\ \mathrm{kN}$

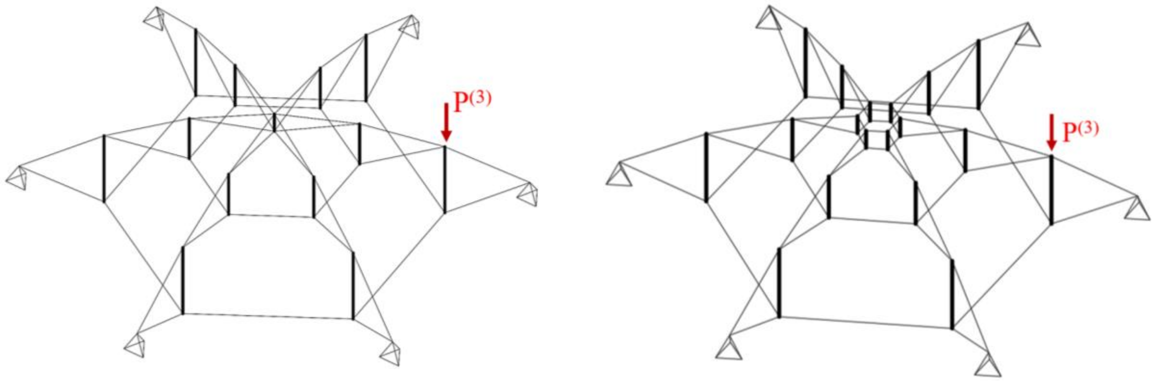

Fig. 5.39. External load application in the case of position $\mathbf{P}^{(3)}$ for: a) RG 6A, b) RG 6B

The second example concerns influence of the initial prestress level on the unstable regions of the RG 6A and RG 6B domes (difference is in the upper section). The dynamic behaviour of domes compared in the case of load position $\mathbf{P}^{(3)}$ for $\mathrm{P} = 1$ kN (Table 5.18) and $\mathrm{P} = 5$ kN (Table 5.19). The change in limits of instability regions is presented for three levels of initial prestress. In the case of low load value (Table 5.18), the S_{min} is on the similar level, however, the instability regions distribution is different. In the case of RG 6B dome, the initial prestress has a greater impact on the resonant frequencies and dome is characterized by the widest instability region corresponding to the last resonant frequency $\eta 31$. Nevertheless, the introducing of higher levels of initial prestress causes the coinciding of the limits of instability regions, and resonant frequencies η do not depend on the pulsatility index υ, and the risk of the excitation of unstable motion decreases. The increase of external load results in the increasing S_{min} value for the RG 6A dome, and widening of the limits of instability regions for both structures (Table 5.19). In the case of RG 6B dome, instability regions occur for each considered resonant frequency, and only for first ($\eta 1$) and last ($\eta 18$) for RG 6A dome. The increase of the initial prestress level results in the narrowing of located regions, nonetheless, small dependency of resonant frequencies η on the pulsatility index υ is noticed at high levels of prestress.

In the case of the domes type B, the number of resonant frequencies dependent on the initial prestress level is equal to the number of infinitesimal mechanisms. The additional frequencies do not depend neither on the pulsatility index υ, nor the initial prestress S (Table 5.20). The relative increase (RI) is about 0.53% - 0.55%, similarly to the independent frequency of the RG 6A dome ($\eta 22$).

Table 5.18. Limits of chosen four main instability regions of the RG 6A and RG 6B domes for P = 1 kN (A – RG 6A dome, B – RG 6B dome)

	S_{min} [kN]	S = 15 kN	S = 25 kN
A	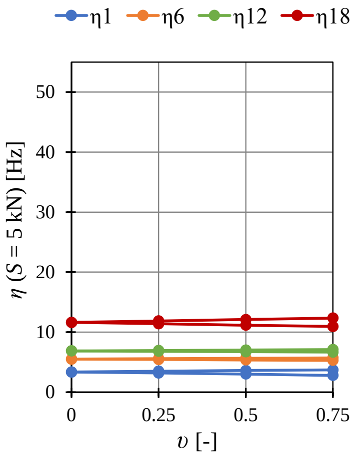	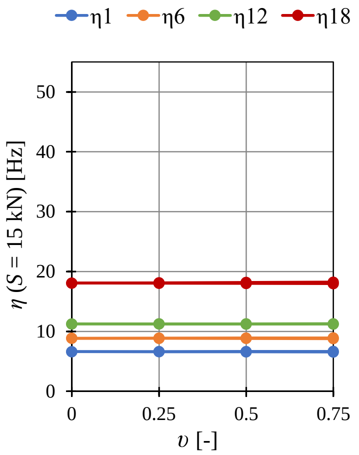	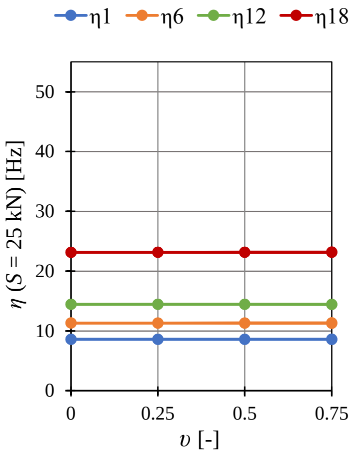
B	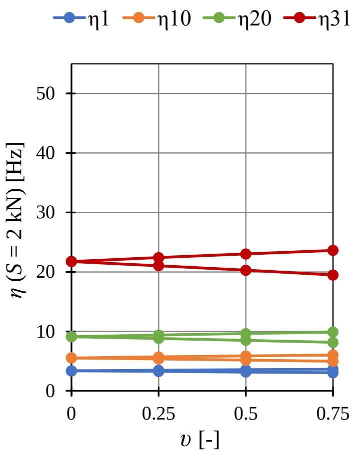	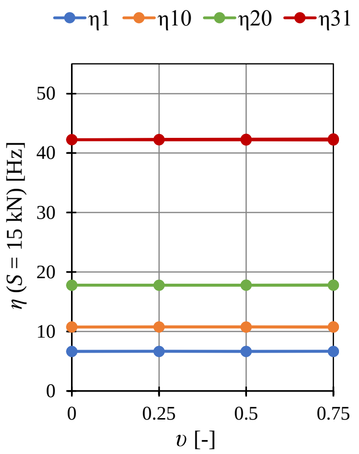	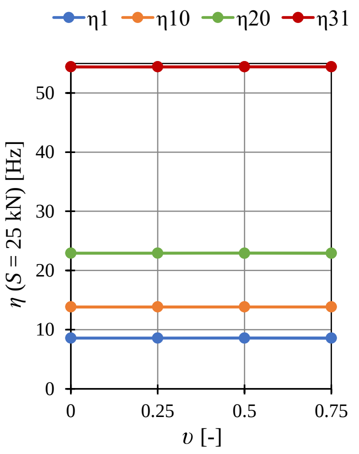

Table 5.19. Limits of chosen four main instability regions of the RG 6A and RG 6B domes for P = 5 kN (A – RG 6A dome, B – RG 6B dome)

	S_{min} [kN]	S_{min} + 10 kN	S_{min} + 20 kN
A	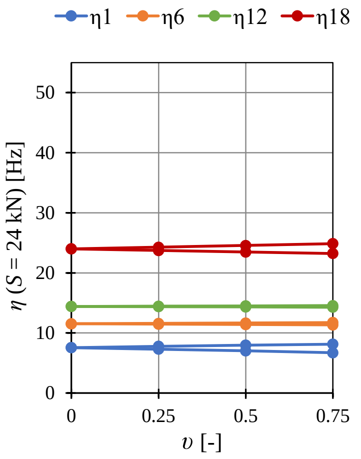	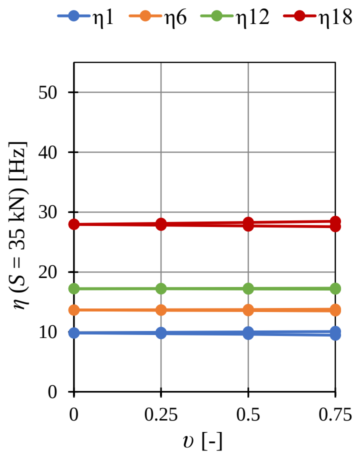	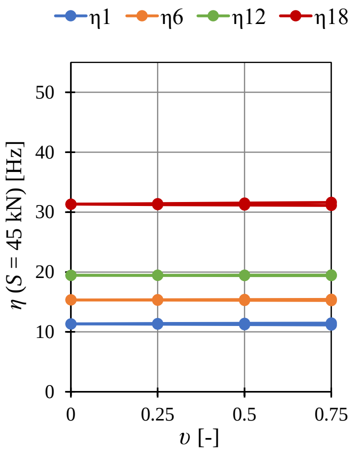
B	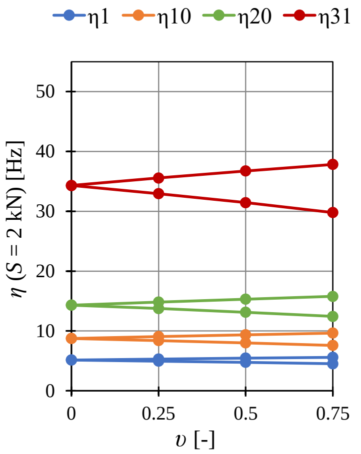	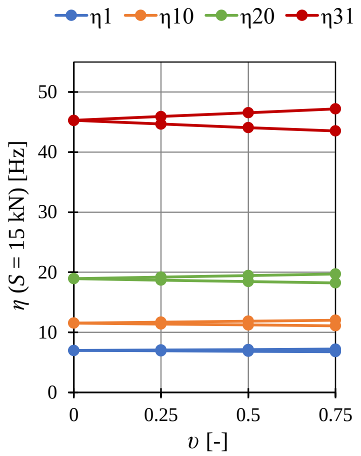	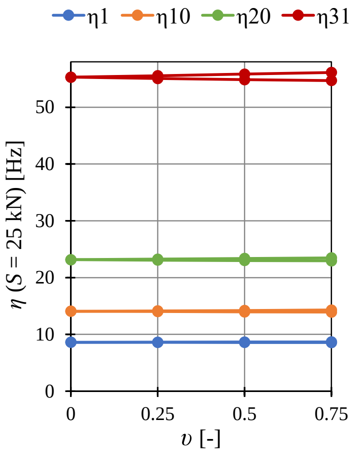

Table 5.20. Resonant frequencies of the RG 6A and RG 6B domes in the case of load position **P**$^{(3)}$

	RG 6A				**RG 6B**	
	Resonant frequency $\eta(\upsilon = 0 \div 0.75) = \text{const.}$					
	$\eta19$	$\eta20$	$\eta21$	$\eta22$	$\eta32$	$\eta33$
P = 1 kN						
S_{min}	26.79	26.90	28.94	88.38	83.77	180.25
S_{max}	36.79	36.83	41.18	88.83	84.21	181.25
RI*	37.33%	36.91%	42.29%	0.51%	0.53%	0.55%
P = 5 kN						
S_{min}	31.36	31.69	34.77	88.57	83.83	180.38
S_{max}	36.72	36.93	41.20	88.83	84.21	181.25
RI*	17.09%	16.54%	18.49%	0.29%	0.45%	0.48%

RI* – relative increase: $[(\eta(S_{min}) - \eta(S_{max}))/\eta(S_{min}) \cdot 100\%]$

Next, the impact of the initial prestress level on the range and distribution of instability regions is compared (Fig. 5.40). For the P = 1 kN and S = 15 kN, the areas are smaller by about 80% and 96%, for RG 6A and RG 6B respectively (the changes are measured taking into account average value for four regions). The increase in the initial prestress level has greater impact on the areas of instability regions in the case of RG 6B dome. After introducing the increased external load P = 5 kN, the increase of the initial prestress level nonlinearly decreases the ranges of regions of RG 6B dome. In the case S = 35 kN, the areas are smaller by about 44% and 95%, for RG 6A and RG 6B respectively.

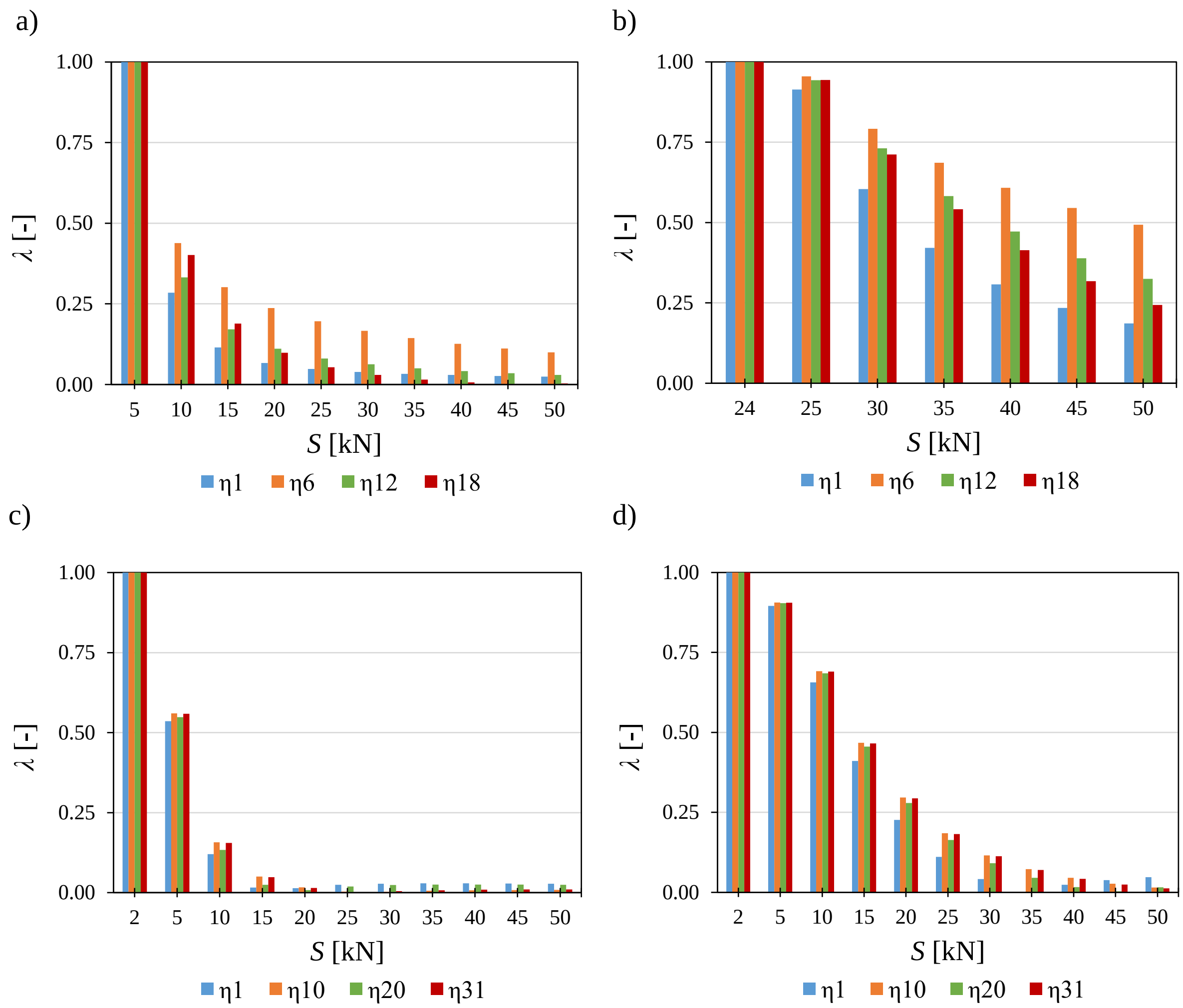

Fig. 5.40. Influence of the initial prestress level S on the range of unstable regions of: a) RG 6A for P = 1 kN, b) RG 6A for P = 5 kN, c) RG 6B for P = 1 kN, d) RG 6B for P = 5 kN

<u>*Conclusion of the comparison:*</u> The dynamic stability analysis of regular types A (RG 6A) and B (RG 6B) domes shows type B that dome (RG 6B) is characterized by bigger unstable regions and higher resonant frequencies. The risk of unstable excitation vibrations is much higher at low initial prestress levels. Nevertheless, introducing the higher prestress results in narrowing

the unstable regions of both domes and decreases the risk of the excitation of motion with increasing amplitudes.

Example 3

Subject of the comparison: RG 6B (Fig. 5.41a) and MG 6B (Fig. 5.41b) domes – unstable regions

Aim of the comparison: (1) Does the initial prestress level affect unstable regions for the type B domes? (2) Does the structure modification of type B domes (Fig. 5.41b) affect unstable regions?

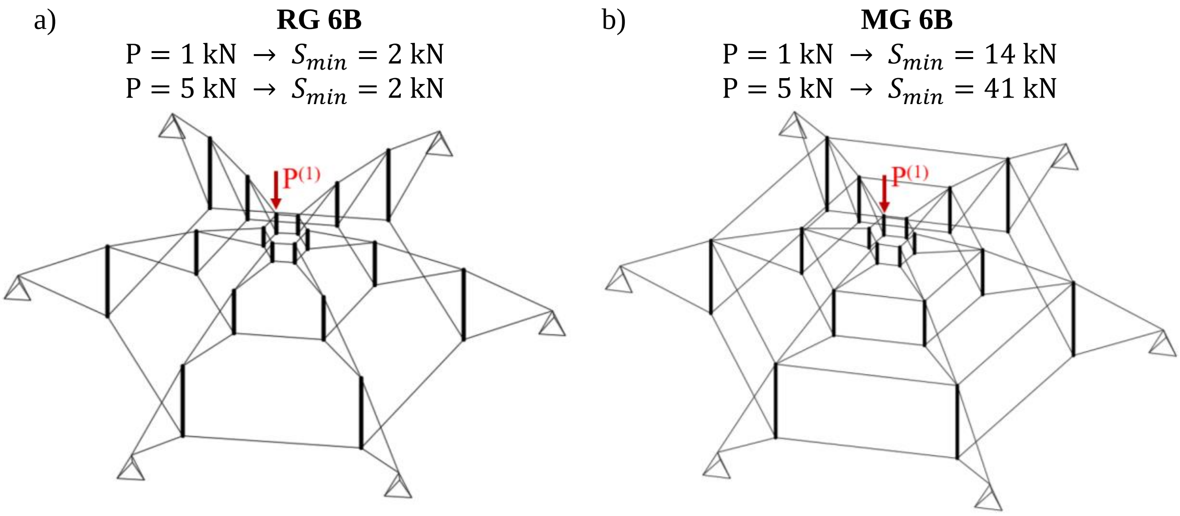

Fig. 5.41. External load application in the case of position $\mathbf{P}^{(1)}$ for: a) RG 6B, b) MG 6B

The third example aims to compare the dynamic response of the RG 6B and MG 6B domes. The dynamic stability analysis performed in the case of load position $\mathrm{P}^{(1)}$ for $\mathrm{P} = 1$ kN (Table 5.21) and $\mathrm{P} = 5$ kN (Table 5.22). The limits of instability regions are presented for three levels of initial prestress. Even the low external load ($\mathrm{P} = 1$ kN) cause the appearance of instability regions for considered domes. Nonetheless, in the case of the regular dome, instability regions occur for each considered resonant frequency, and for the modified dome – only for the last resonant frequency ($\eta 21$). It is worth to mention, that increasing of initial prestress by 10 kN resulted in complete narrowing of limit of instability regions of regular dome. For the modified one, the increasing resulted in the reduction of instability region for the last resonant frequency ($\eta 21$) and increased the limits of region for third considered resonant frequency ($\eta 14$). With the higher external load, the situation is similar. However, in the case of modified dome, the increasing of the initial prestress to $S_{max} = 50$ kN did not cause the narrowing of the instability region, and the risk of the excitation of motion with increasing amplitudes is still high. The situation is opposite for the regular dome. Comparing the resonant frequencies of the RG 6B and MG 6B for the same initial prestress level, the resonant frequencies of the regular dome are higher.

Domes of type B are characterized by greater instability regions compared to type A. Additionally, the instability regions correspond not only to the last resonant frequency. Fig. 5.42 presents instability regions corresponding to all resonant frequencies of the regular and modified dome in the case of the minimal prestress level, and $\mathbf{P}^{(3)}$ for P = 5 kN (in order to compare the behaviour on the same prestress level). Limits of most regions are concentrated in one area, creating a higher risk of occurring excitation vibrations.

Table 5.21. Limits of chosen four main instability regions of the RG 6B and MG 6B domes for P = 1 kN (R – RG 6B dome, M – MG 6B dome)

<table>
<tr><th></th><th>S_{min} [kN]</th><th>S_{min} + 10 kN</th><th>S_{min} + 20 kN</th></tr>
<tr><td>R</td>
<td>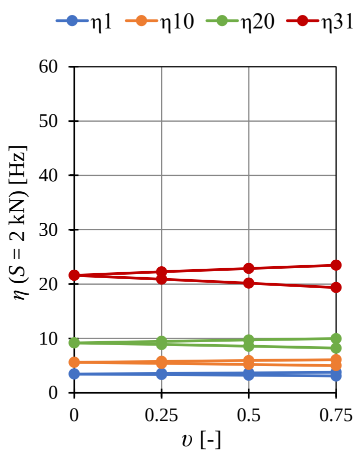
</td>
<td>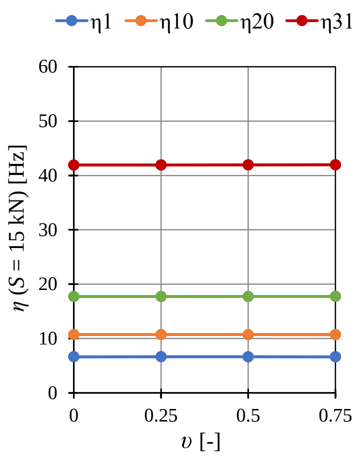
</td>
<td>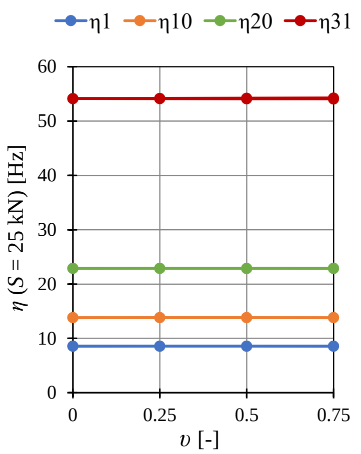
</td></tr>
<tr><td>M</td>
<td>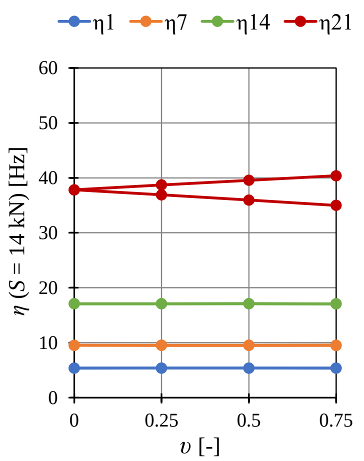
</td>
<td>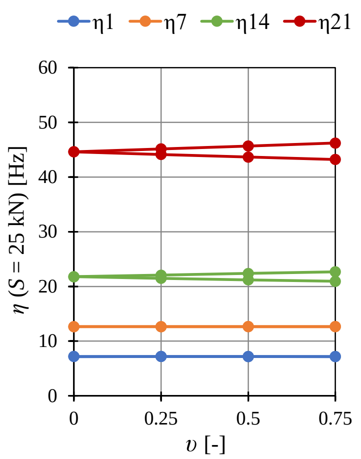
</td>
<td>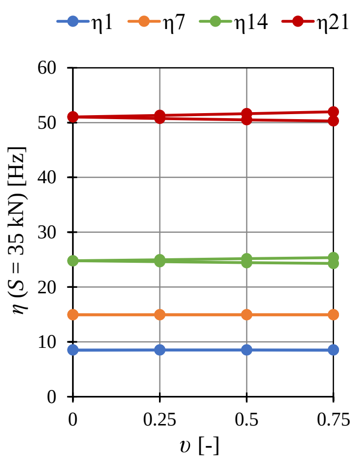
</td></tr>
</table>

Table 5.22. Limits of chosen four main instability regions of the RG 6B and MG 6B domes for P = 5 kN (R – RG 6B dome, M – MG 6B dome)

	S_{min} [kN]	S_{min} + 5 kN	S_{min} + 10 kN
R	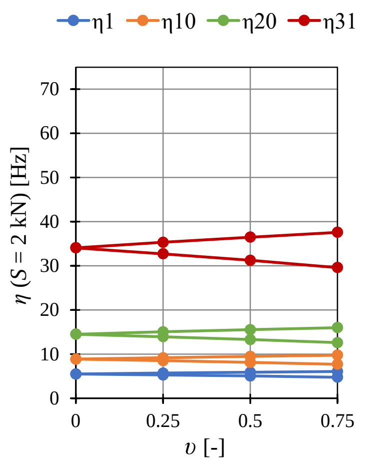	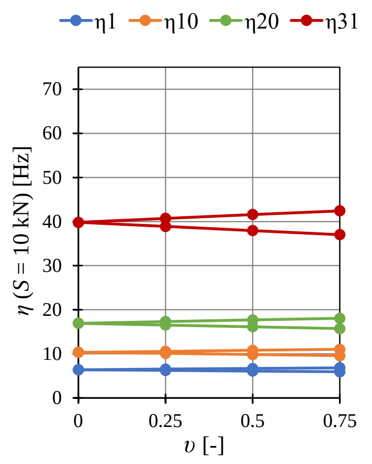	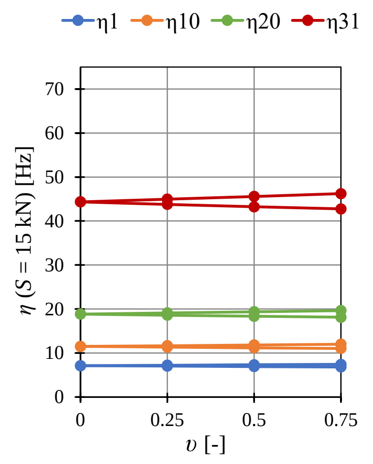
M	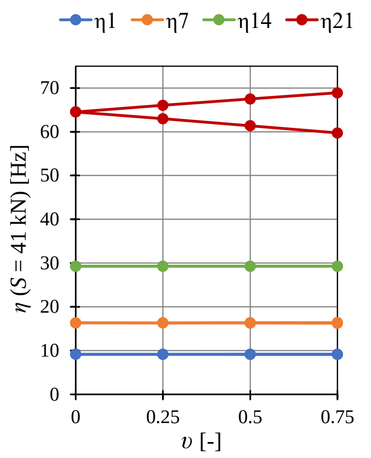	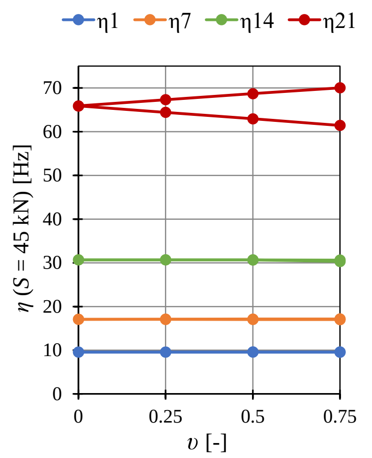	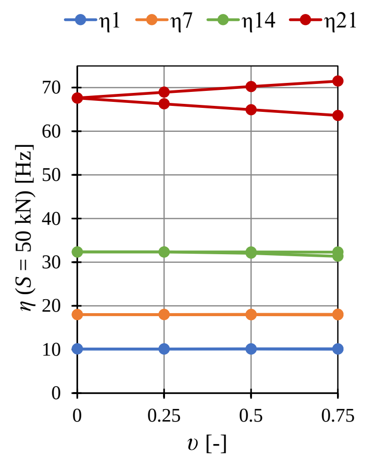

a) b)

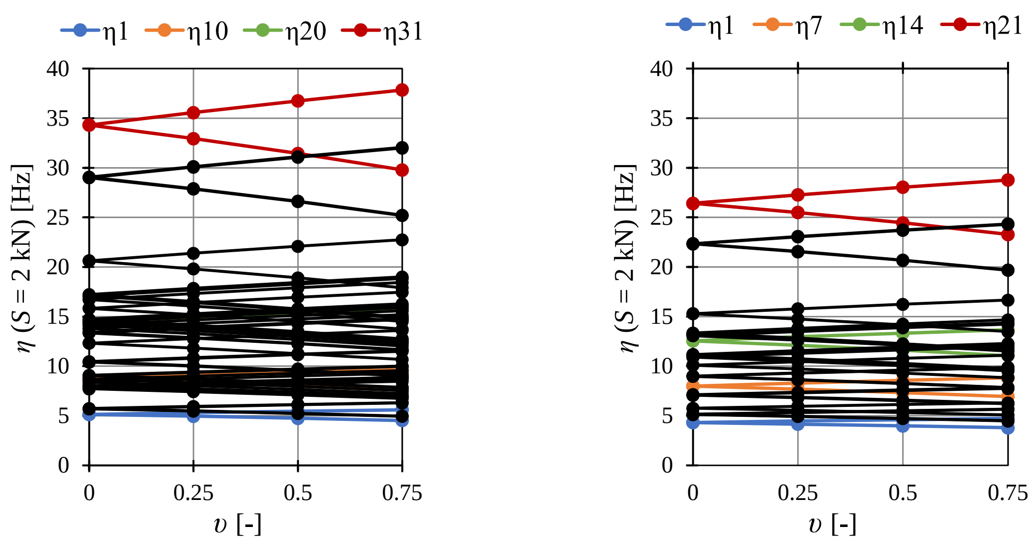

Fig. 5.42. Limits of all instability regions for the load P = 5 kN of: a) RG 6B, b) MG 6B

The impact of the initial prestress level on the range and distribution of instability regions is also compared (Fig. 5.43). In the case of regular dome, for P = 1 kN and S = 15 kN, the area of instability regions is decreased by 98% (the changes are measured taking into account the average value for four regions). In the situation P = 5 kN and S = 15 kN, the decrease is about 54%. For the modified dome and P = 1 kN, the increasing of the initial prestress level results in the decreasing areas that correspond to the frequencies $\eta 7$ and $\eta 21$, thus increasing for $\eta 1$ and $\eta 14$. Similarly, is in the case of higher external load.

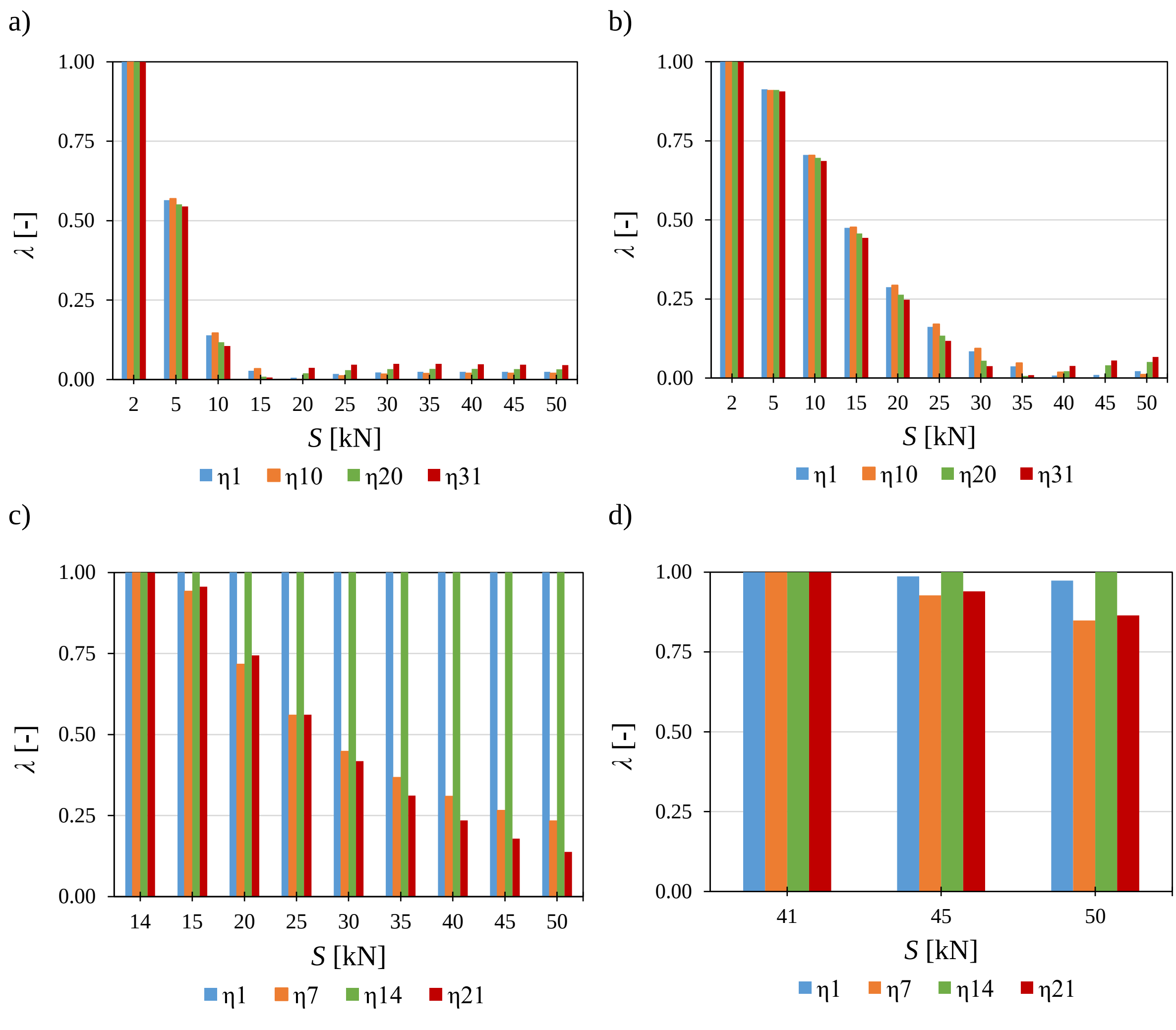

Fig. 5.43. Influence of the initial prestress level S on the range of unstable regions of: a) RG 6B P = 1 kN, b) RG 6B P = 5 kN, c) MG 6B P = 1 kN, d) MG 6B P = 5 kN

<u>*Conclusion of the comparison:*</u> Comparing the regular and modified Geiger domes, it was noted that modified domes are characterized by wider unstable regions. The increase of the load causes the lower impact of the initial prestress on the distribution of unstable regions in the case of the modified dome (MG 6B). Although the regular dome (RG 6B) is characterized by higher

resonant frequencies, the initial prestress has a greater impact on the area of unstable regions. In conclusion, the regular dome (RG 6B) is considered as more stable.

Example 4

Subject of the comparison: RG 6A, RG 6B, MG 6A, MG 6B – unstable regions

Aim of the comparison: (1) How do the load value and position affect the distribution of unstable regions? (2) For which dome the probability of the unstable regions is least likely to occur? (3) What is the most optimal recommended initial prestress level?

The summarized results present the distribution of instability regions that correspond to the last resonant frequency for each dome, in the case of different load situations (Fig. 5.44). The load is equal to 1 kN and 5 kN, whereas different load positions are defined as: 1,2, or 3. For example, in the charts the caption "RA 1(3)" stands for regular dome type A loaded with force 1 kN applied in position 3. The results are presented for the S_{min} level of prestress, in order to compare the distribution of widest regions. In the case of the domes type A (Fig. 5.44a, c), the limits of instability regions coincide, and resonant frequencies η do not depend on the pulsatility index υ, the risk of the excitation of unstable motion is low. Additionally, the increase in the external load causes an increase in the resonant frequencies. For the regular dome type B (Fig. 5.44b), the limits of instability regions are significantly wider and expand with higher external load. The position of the applied load in not affect the distribution of limits. The modified dome type B (Fig. 5.44d) is characterized by different behaviour compared to other domes. The distribution of instability regions is affected both by load value and position. The widest regions are in the case of load position $\mathbf{P}^{(1)}$, thus the narrowest in the case of load position $\mathbf{P}^{(2)}$.

Next, the influence of the initial prestress level on the areas of the unstable regions is studied (Fig. 5.45). In the case of regular type A dome (Fig. 5.45a), the impact of prestress can be noticed only for $\mathrm{P} = 5$ kN in the case of load position $\mathbf{P}^{(2)}$ (RA 5(2)) and $\mathbf{P}^{(3)}$ (RA 5(3)). In turn, in the case of the modified type A dome (Fig. 5.45c) only for $\mathrm{P} = 5$ kN in the case of load position $\mathbf{P}^{(2)}$ (MA 5(2)). The impact of prestress on areas of domes type B is nonlinear, on the other hand (Fig. 5.45b, d). The nonlinearity increases with the increasing of external load. Nonetheless, the influence of the initial prestress level is significantly smaller if $S > 30$ kN.

In the case of type B domes and load $\mathrm{P} = 1$ kN, the probability of occurrence of unstable regions is low. However, the situation is the opposite in the case of load $\mathrm{P} = 5$ kN. The size of unstable regions is comparable for different load positions for regular type B dome (RG B). On the other hand, the size of unstable regions of modified type B dome depends on load value and position, and can vary.

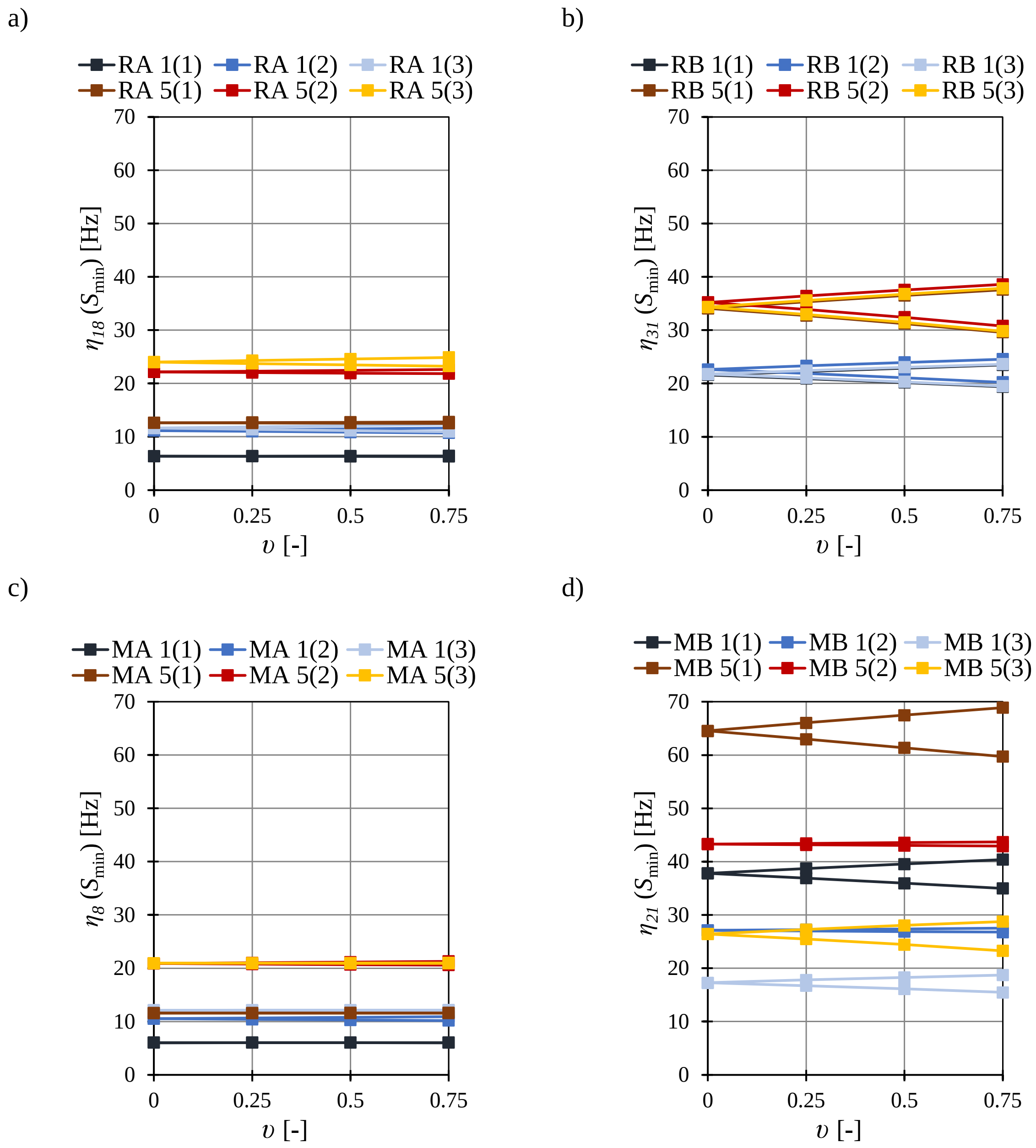

Fig. 5.44. Influence of the initial prestress level S on the range of last unstable region of: a) RG 6A, b) RG 6B, c) MG 6A, d) MG 6B

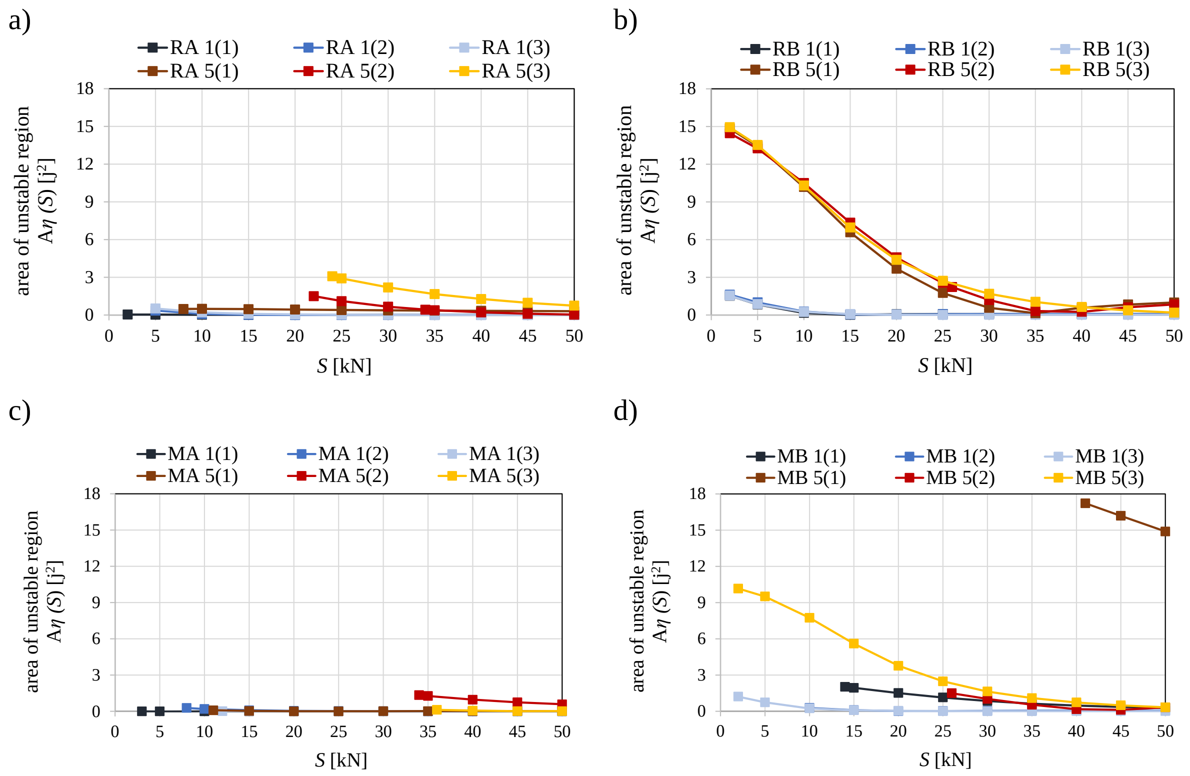

Fig. 5.45. Influence of the initial prestress level S on the area of unstable region A_η: a) RG 6A, b) RG 6B, c) MG 6A, d) MG 6B

<u>*Conclusion of the comparison:*</u> The load value and position have no effect in the case of the MG 6A dome. The situation is similar for the RG 6A dome. Both structures are characterized by narrow unstable regions. In turn, it is different in the case of type B domes. For the regular type B dome, the load value affects the unstable regions. Wherein, the bigger probability of the unstable regions to occur is in the case of a bigger load and lower initial prestress level (from $S = 0$ to $S = 30$ kN), and the unstable regions are the same regardless the load position. In turn, the unstable regions of the modified type B dome depend both on the value and position of the load. It should be noted, that in the case of modified type B, load position $\mathbf{P}^{(1)}$, and force 5 kN (MB 5(1)), the probability of the occurrence of the unstable regions is high and not depending on the initial prestress level. The probability of the occurrence of the unstable regions is getting smaller with an increasing of the initial prestress level (for each dome, except example MB 5(1)). The most optimal recommended initial prestress level is above $S = 25$ kN.

5.5. Summary

The behaviour of the Geiger dome can be controlled by adjusting the initial prestress level. The structure's response to the external load conditions highly depends on the dome type. The impact of the load is the most significant at low values of the initial prestress. The Geiger dome is more susceptible to the asymmetrical load, which causes displacements consistent with infinitesimal mechanisms. In the case of a symmetrical load, the displacements are smaller and insensitive to the prestress. The static analysis results that additional circumferential cables in the structure do not improve stiffness nor reduce displacements. Thus, the regular layout is considered as a better solution due advantage related to the weight of the structure. Comparing the differences in the upper sections, the regular dome with an open upper section (RG 6B) is characterized by the lowest level of minimum prestress, higher dependency on the initial prestress level adjustment, and higher ability to control the static parameters.

In the case of the dynamic analysis, the natural frequencies level of the type A domes (RG ngA and MG ngA domes) were not related to the number of load-bearing girders of the structure. Additionally, only these types of structures were characterized by the additional natural frequencies depending on the initial prestress level, unlike the type B domes (RG ngB and MG ngB). Comparing the free frequencies of the considered structures, the biggest discrepancy remains at the low levels of the initial prestress. The biggest discrepancy between natural and free frequency was noticed in the case of RG 6B dome (up to 55%). In the case of this type of dome, the same level of minimum prestress occurs despite the load value or position. Nonetheless, for each considered dome, at the maximum prestress level $S = 50$ kN the values of the natural and free frequencies were comparable (the discrepancy up to 11%).

The dynamic stability analysis showed that the type B domes (RG 6B and MG 6B) are characterized by wider unstable regions in comparison to type A domes. In the case of the RG 6A and MG 6A domes, the instability regions occur only at the low values of the initial prestress, and get completely narrow with its increase. In turn, for the RG 6B and MG 6B domes, the impact of the initial prestress is lower. The number of unstable regions depends on the number of infinitesimal mechanisms. The type B domes characterized by the higher number of infinitesimal mechanisms, thus higher number of unstable regions. Additionally, they are concentrated close to each other, and some of them coincide, which results in a higher risk of occurring excitation vibrations. The MG 6B dome is the most sensitive to the change in the resonant frequencies, whereas the MG 6A dome is the least sensitive. It means, the additional circumferential cables (MG 6B) introduced a negative impact on the dynamic stability of type B domes.

The conducted analyses proved that the most optimum solution to be considered is that the RG 6B dome, which is characterized by the lowest minimum prestress level, and unstable regions depend on the load value only. It is worth to mention, that the RG 6B dome was patented by Geiger [115].

6. Levy domes

6.1. Introduction

Shortly after the first tensegrity dome appeared, Matthys Levy presented a second design. In 1992, Levy proposed the project of a Georgia Dome in a quasi-linear shape for the Atlanta Olympic Games [139]. Unlike the Geiger dome, Levy's dome was a triangular dome in which cables and struts were not in the same plane. The Georgia Dome was called the first Hypar-Tensegrity Dome [193]. The structure with a 233.5 m span, consisted of a triangulated network of cables attached at strut nodes (Fig. 6.1). The characteristic design of Georgia Dome generated a lot of interest in the scientific world. The analysis of this structure was the main topic of different research [76, 140, 194].

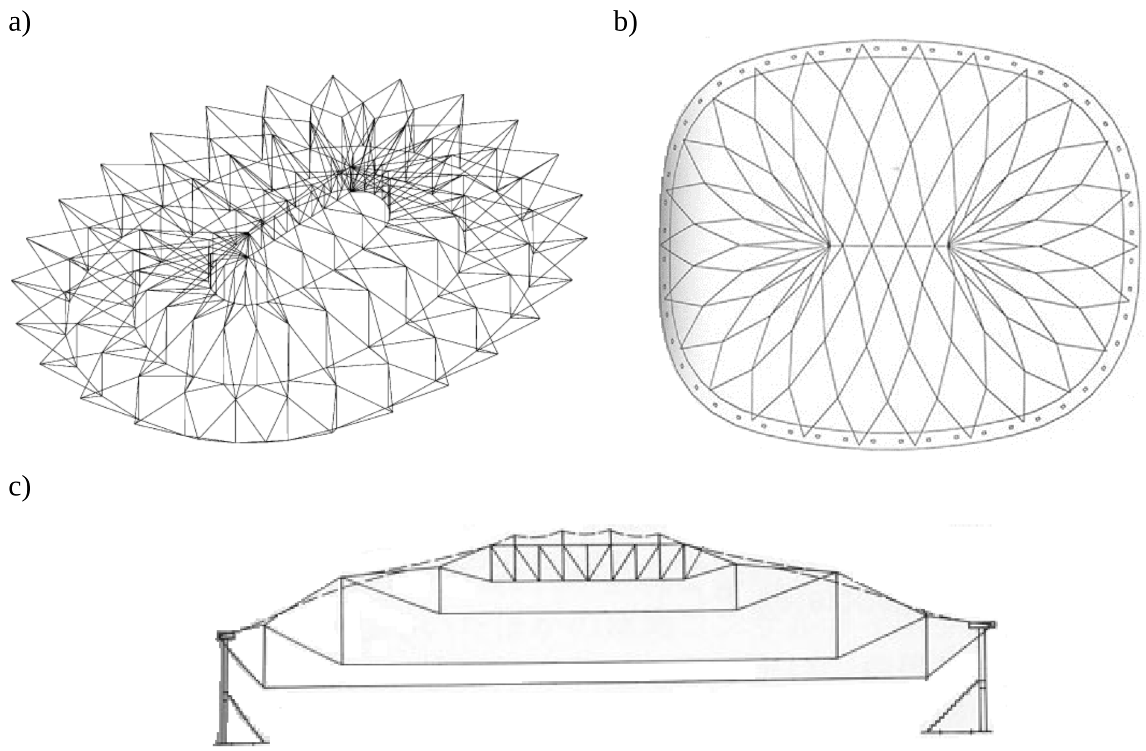

Fig. 6.1. Design of a Georgia dome [195]: a) 3D view, b) plan view, c) load-bearing girder

The original Levy's structure was modified by different researchers in order to perform the analysis of a new form of cable-strut dome. The shape was simplified to the regular dome-like structure and the upper section was presented in the form of a single strut or an open hoop, retaining the original triangulated network of cables (Fig. 6.1).

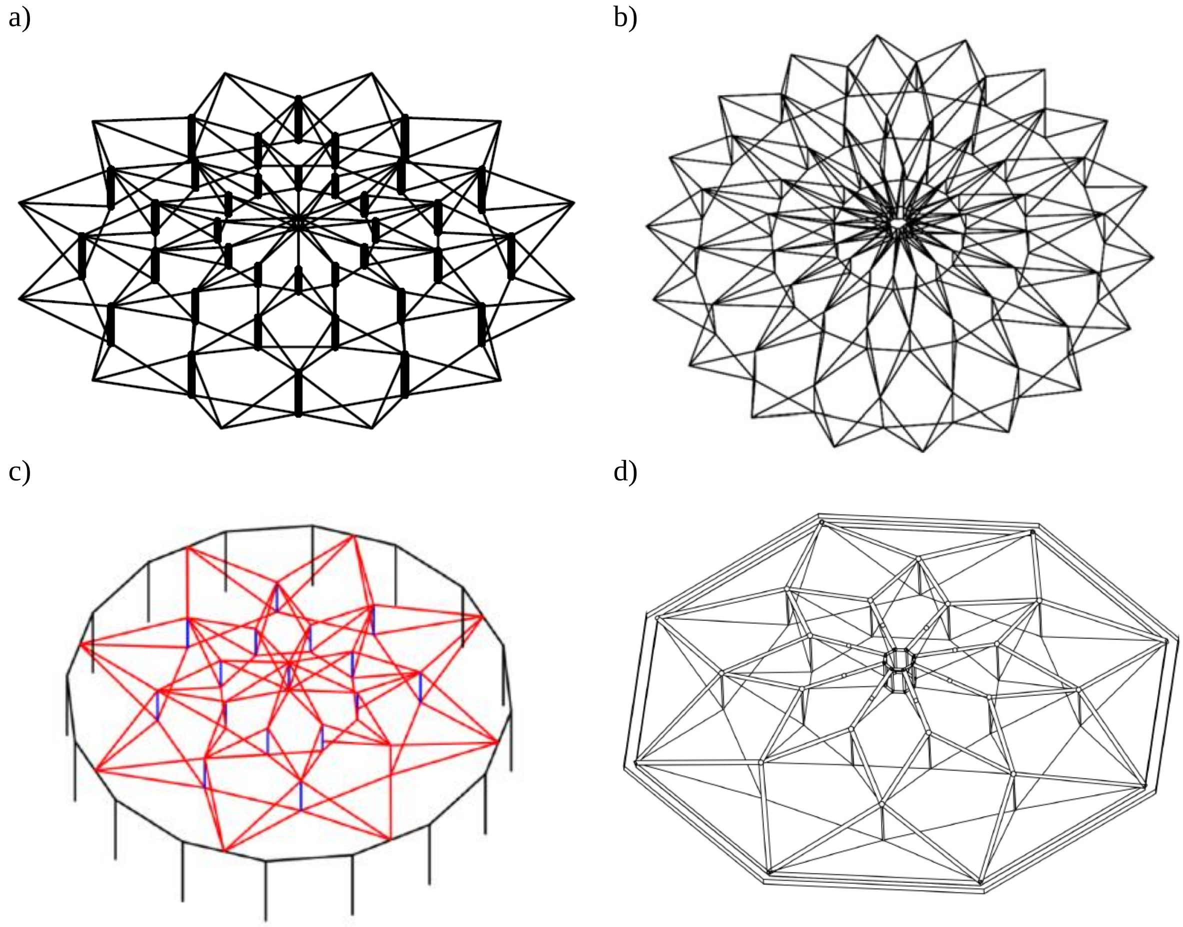

Fig. 6.2. Design transformations of Levy dome: a) shape presented by [85], b) shape presented by [196], c) shape presented by [197], d) shape presented by [198]

Due to complex geometry and statically indeterminacy, the main challenge in the analysis of the Levy dome is a calculation of the correct force distribution in the elements. A lot of research focused on this problem and several solutions were introduced. Dong et al. presented the nodal equilibrium equations-based method [199], the method based on the linear adjustment theory was proposed by Zhang et al. [196], as well as the *DSVD* (*Double Singular Value Decomposition*) method by Yuan et al. [180], and others [168, 181, 200, 201]. Further research was concerned with collapse resistance [186, 202, 203], design optimization [187, 204, 205], and the influence of different kinds of external loads [185, 206]. Most of the papers are subjected to the experimental studies of the Levy dome, e.g., shape forming process [85, 174], active control [197, 207], and new structural solutions [198, 208]. Unlike the Geiger dome, the static and dynamic analysis of the Levy dome is the subject of a few numbers of papers. Among others, the static analysis was considered in [209-211], and the dynamic analysis in [202, 204, 212].

This work aims to present the results of a complete static and dynamic analysis of the Levy dome. This type of cable-strut domes consisted of a system of repeating spatial load-bearing girders connected with lower circumferential cables. The domes with different geometry of a load-bearing girder and different numbers of load-bearing girders are concerned. Similarly to the Geiger dome, the girder is presented in two variants, i.e., close upper section (type A) and open upper section (type B). The names of analyzed domes are acronyms: L – Levy dome, the number – the number of load-bearing girders, and letter A or B – girders type, e.g., "L 6A" is the Levy dome with 6 load-bearing girders type A.

6.2. Geometrical design

Unlike the Geiger dome, the Levy dome consists of uniformly distributed spatial load-bearing girders. The proposed geometrical designs include the own solutions (section 6.2.1) and solutions known from the literature (section 6.2.2). Only the first ones are the subject of further static and dynamic analysis.

6.2.1. Proposed design solutions

The first proposed design covers the geometry of small-scale domes. In contrast to small-scale Geiger domes, the elements of the load-bearing girder are not in the same plane. The elements are divided into three groups, i.e., grid cables (elements: 1, 2, 3, 4, 5, 6), circumferential cables (C1, C2, C3, C4), and struts (S1, S2, S3). Fig. 6.3 presents the geometry of a repetitive spatial load-bearing girder of a Levy dome with a closed upper section (type A) (Fig. 6.3a), and an open one (type B) (Fig. 6.3b). The node coordinates of girders are presented for domes type A (Table 6.1) and type B (Table 6.2). The considered domes are 12 m wide and 3.25 m heigh. The support is in every node of the lowest section of girder. The geometry of a Levy dome is significantly different from regular Geiger domes. The hoops are rotated relative to each other, so the struts are not located in one plane. The cables create a network of spatial triangles connected with struts. The geometry of Levy dome type A and B, consisted of six load-bearing girders is presented in Fig. 6.4. The additional modification of the geometry is an increase in the number of load-bearing girders. The domes with 8, 10, and 12 girders are also considered (Fig. 6.5).

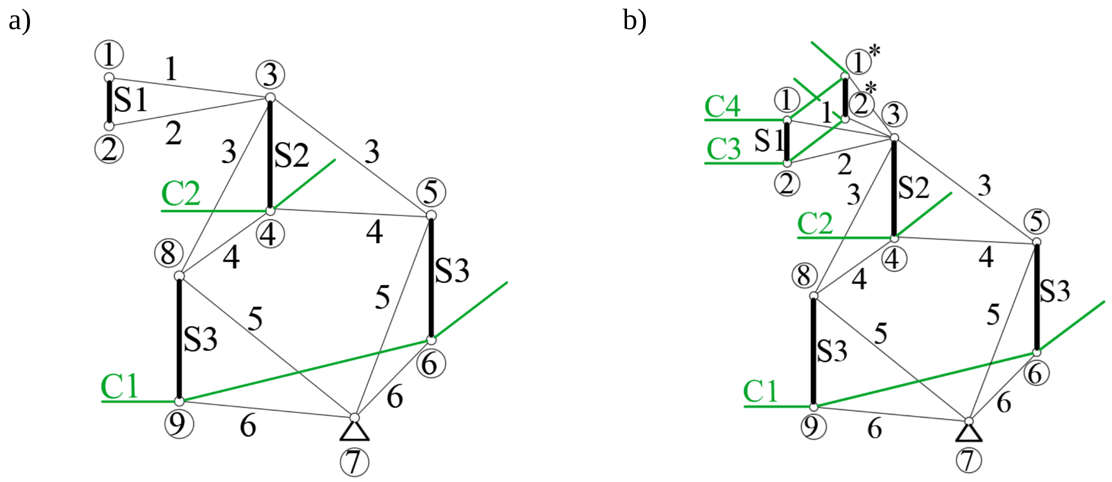

Fig. 6.3. Load-bearing girder of the Levy dome: a) type A, b) type B

Table 6.1. Node coordinates [m] of the load-bearing girder of the Levy dome type A

No. of node	**1**	**2**	**3**	**4**	**5**	**6**	**7**	**8**	**9**
x	0		2		$4 \cdot \cos\alpha$		6	$4 \cdot \cos\alpha$	
y	0		0		$4 \cdot (-\sin\alpha)$		0	$4 \cdot \sin\alpha$	
z	2.1	1.5	1.85	0.45	1.15	-1.15	0	1.15	-1.15

Table 6.2. Node coordinates [m] of the load-bearing girder of the Levy dome type B

No. of node	**1**	**2**	**1***	**2***	**3**	**4**	**5**	**6**	**7**	**8**	**9**
x	$0.5 \cdot \cos\alpha$		$0.5 \cdot \cos\alpha$		2		$4 \cdot \cos\alpha$		6	$4 \cdot \cos\alpha$	
y	$0.5 \cdot \sin\alpha$		$0.5 \cdot (-\sin\alpha)$		0		$4 \cdot (-\sin\alpha)$		0	$4 \cdot \sin\alpha$	
z	2.1	1.5	2.1	1.5	1.85	0.45	1.15	-1.15	0	1.15	-1.15

Note! Calculations must be performed in radians.

where ng – number of girders, and α is calculated as:

$$\alpha = (ng - 1) \cdot \alpha_{add} + \frac{\alpha_{add}}{2}, \quad \alpha_{add} = (\frac{360}{ng})/180 \cdot \pi \qquad (6.1)$$

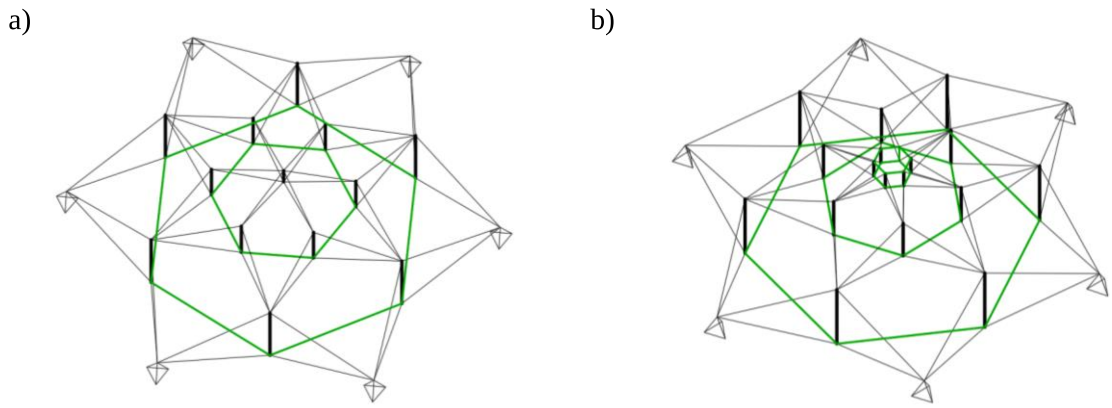

Fig. 6.4. Levy dome: a) 6A, b) 6B

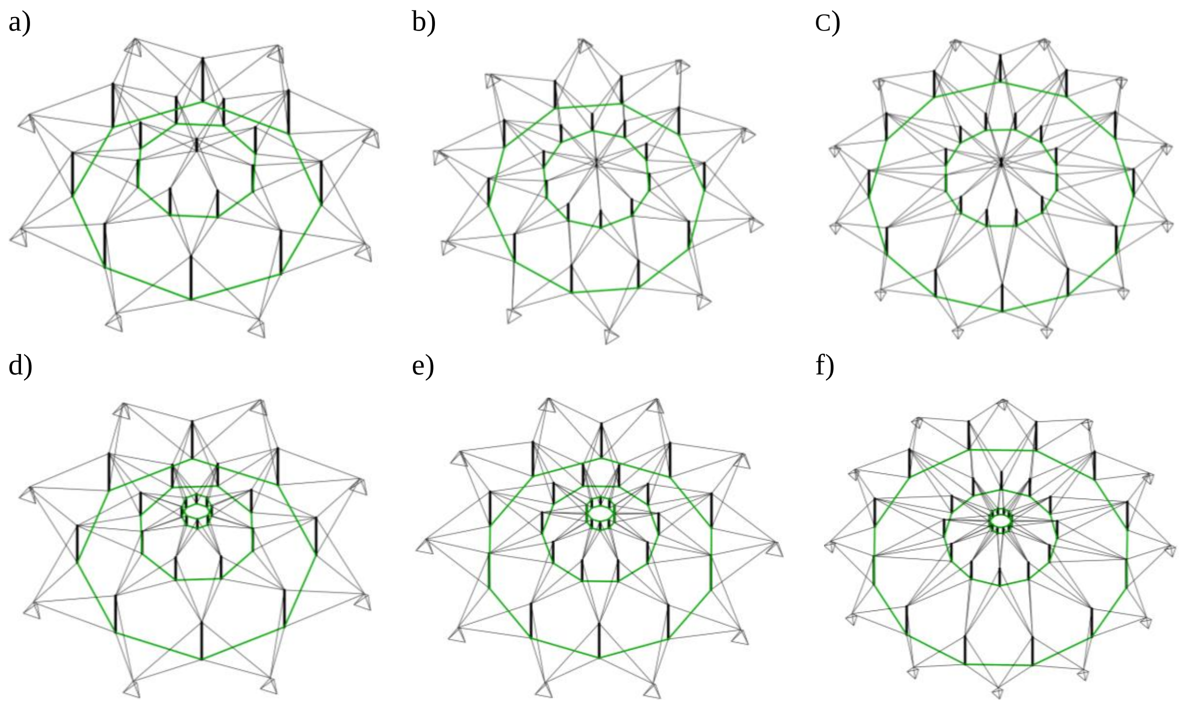

Fig. 6.5. Levy dome: a) 8A, b) 10A, c) 12A, d) 8B, e) 10B, f) 12B

6.2.2. Solutions from the literature

The examples of the Levy dome presented in the literature contain different solutions for the load-bearing girder and cable system. Three examples of domes with different geometry are shown. Firstly, the dome presented by Chen&Feng [212] (Fig. 6.6) is considered. The structure is a large-span dome with a width of 100 m and a height of 8.2 m, consisted of 12 spatial load-bearing girders, and the open upper section of the girder (L 12B). Unlike the solution presented in 6.2.1, some groups of elements are divided into subgroups (groups of elements 6 and C) (Fig. 6.6b). The node coordinates for the load-bearing girder are presented in Table 6.3.

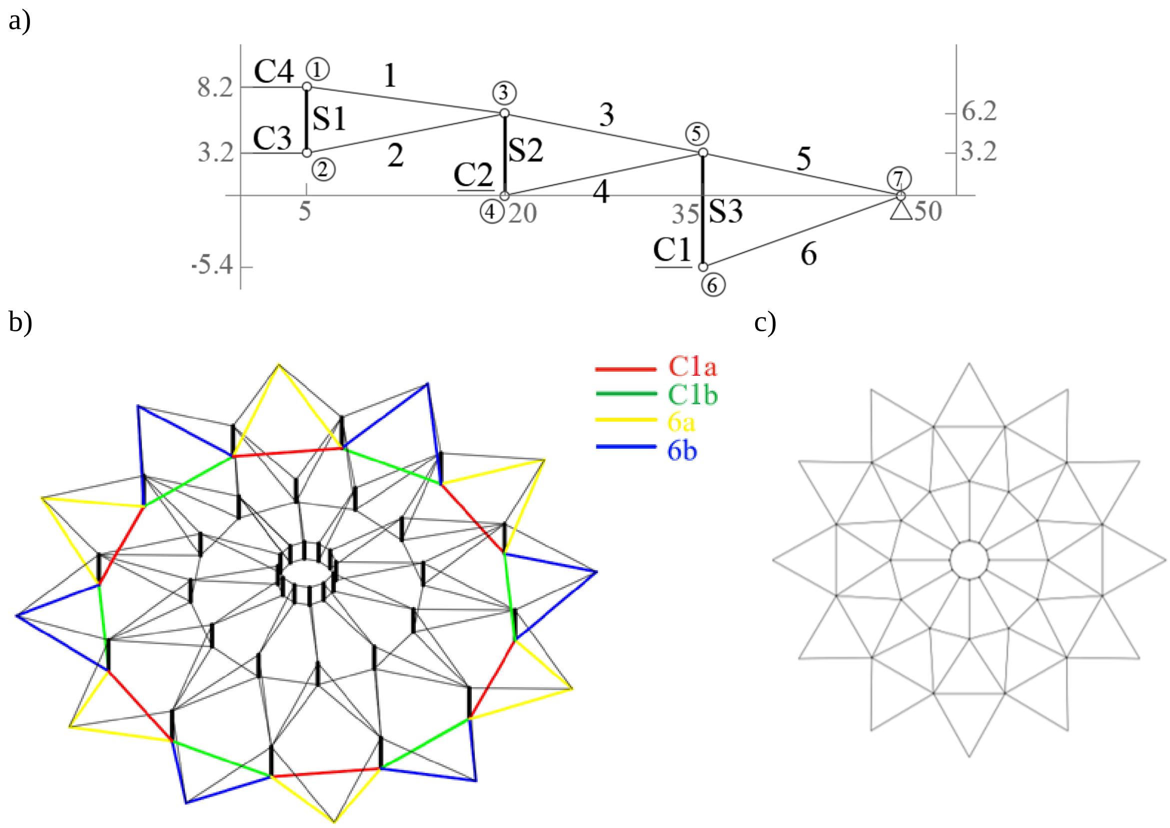

Fig. 6.6. Levy dome by [212]: a) geometry of a girder, b) 3D view, c) top view

Table 6.3. Node coordinates [m] of the load-bearing girder of the Levy dome by [212]

No. of node	**1**	**2**	**3**	**4**	**5**	**6**	**7**	**8**	**9**
x	5		20		33.81		50	33.81	
y	0		0		9.1		0	-9.1	
z	8.2	3.2	6.2	0	3.2	-5.4	0	3.2	-5.4

The second example is dome presented by Yuan et al. [180] (Fig. 6.7). The analyzed dome is 80 m wide and 9.8 m high, consists of six load-bearing girders, with closed upper section (L 6A). The structure is supported in every external node of the girder.

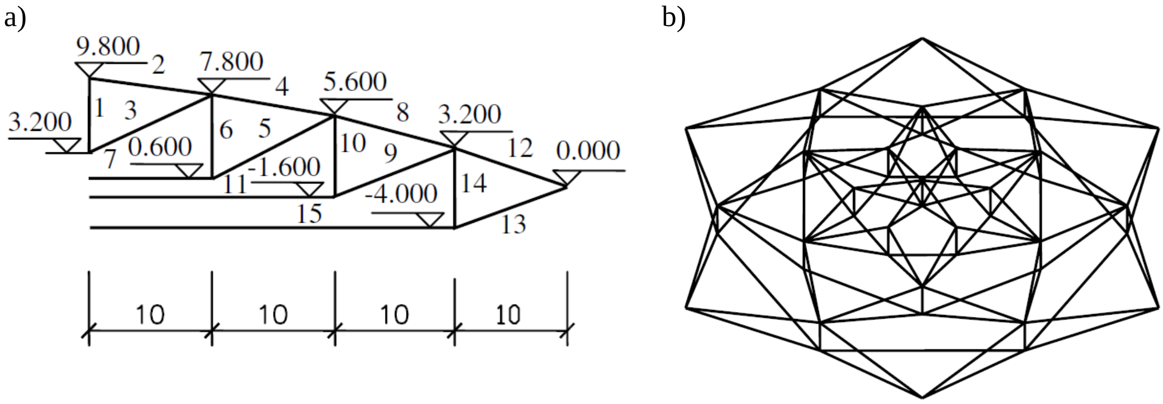

Fig. 6.7. Levy dome by [180]: a) geometry of a girder, b) 3D view

The third example is presented by Li et al. [206] (Fig. 6.8). The dome is approximately 1 m wide and 0.2 m high, consists of eight load-bearing girders, with closed upper section (L 8A). The structure is considered as a prototype for further analyses. The examples provided in the literature mostly focus on different girder solutions, while the cable network remains the same. The dimensions of the girder are selected individually by each researcher in terms of the performed analyses.

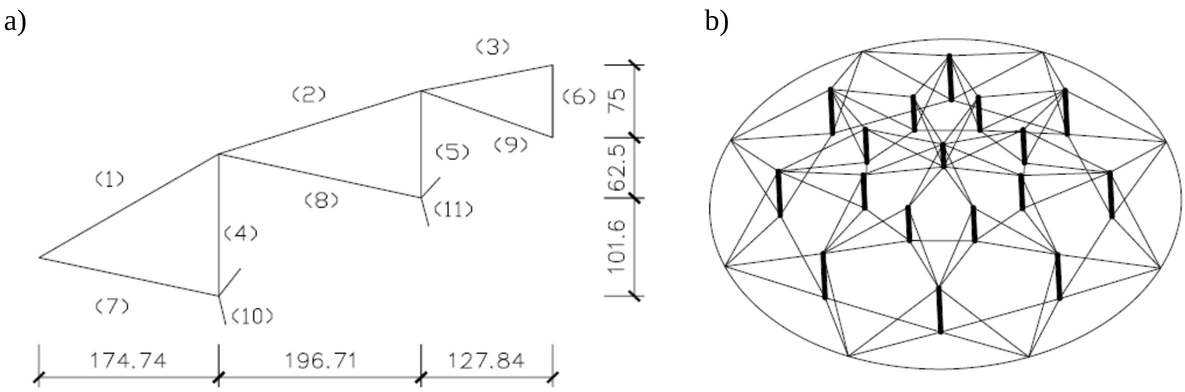

Fig. 6.8. Levy dome by [206]: a) geometry of a girder, b) 3D view

6.3. Qualitative analysis

Like in the case of the Geiger dome, qualitative analysis of the Levy dome relies on the identification of existing infinitesimal mechanisms and self-stress states. Due to a complex cable network, the Levy dome is considered as statically indeterminate tensegrity structure. The identification of self-equilibrium forces is performed using the spectral analysis (section 6.3.1), and genetic algorithm in comparison to methods from the literature (section 6.3.2).

6.3.1. Spectral analysis of truss matrices

The spectral analysis of truss matrices allowed to determine the number of existing self-stress states and infinitesimal mechanisms of Levy domes (see section 4.2.1). The summarized results for considered structures, i.e., L ngA, L ngB where $ng = \{6, 8, 10, 12\}$ number of load-bearing girders, are contained in Table 6.4.

Table 6.4. Results of the qualitative analysis of Levy domes

No. of the load-bearing girders (ng)	No. of nodes	No of d.o.f	No. of elements (n)	No. of struts (ns)	No. of mechanisms (nm)	No. of self-stress states (nst)
Type A						
6	32	78	85	13	0	7
8	42	102	113	17	0	11
10	52	126	141	21	0	15
12	62	150	169	25	0	19
Type B						
6	42	42	114	18	1	7
8	56	56	152	24	1	9
10	70	70	190	30	1	11
12	84	84	228	36	1	13

The domes type A featured by existence of the self-stress states and absence of infinitesimal mechanisms. The number of infinitesimal mechanisms of dome type B is always one, regardless the number of girders. The number of existing self-stress states for both dome types is depending on number of load-bearing girders and can be calculated as:

$$\begin{aligned} &\text{type A:}\ \ nst = ns - 6; \\ &\text{type B:}\ \ nst = ns - 2 \cdot ng + 1 \end{aligned} \tag{6.2}$$

The superimposed self-stress states (Table 6.5) were used for further analysis for Levy domes. The values of obtained self-stress states were normalized in the way that force in the longest strut is equal to -1. The infinitesimal mechanism identified in type B domes is located in the upper section of the dome (Fig. 6.9).

Table 6.5. Values of self-stress state $\mathbf{y}_S$ of the Levy domes

Type A						Type B					
el.	$\mathbf{y}_S$	**el.**	$\mathbf{y}_S$	**el.**	$\mathbf{y}_S$	**el.**	$\mathbf{y}_S$	**el.**	$\mathbf{y}_S$	**el.**	$\mathbf{y}_S$
S1	$-0.147^{(6)}$ $-0.308^{(8)}$ $-0.465^{(10)}$ $-0.616^{(12)}$	**1**	$0.197^{(6)}$ $0.311^{(8)}$ $0.375^{(10)}$ $0.414^{(12)}$	**C1**	$1.040^{(6)}$ $1.753^{(8)}$ $2.401^{(10)}$ $3.016^{(12)}$	**S1**	$-0.031^{(6)}$ $-0.050^{(8)}$ $-0.061^{(10)}$ $-0.068^{(12)}$	**1**	$0.100^{(6)}$ $0.157^{(8)}$ $0.189^{(10)}$ $0.209^{(12)}$	**C1**	$1.040^{(6)}$ $1.753^{(8)}$ $2.401^{(10)}$ $3.016^{(12)}$
S2	$-0.161^{(6)}$ $-0.218^{(8)}$ $-0.248^{(10)}$ $-0.264^{(12)}$	**2**	$0.142^{(6)}$ $0.224^{(8)}$ $0.270^{(10)}$ $0.298^{(12)}$	**C2**	$0.336^{(6)}$ $0.691^{(8)}$ $1.032^{(10)}$ $1.359^{(12)}$	**S2**	$-0.161^{(6)}$ $-0.218^{(8)}$ $-0.248^{(10)}$ $-0.264^{(12)}$	**2**	$0.073^{(6)}$ $0.114^{(8)}$ $0.137^{(10)}$ $0.151^{(12)}$	**C2**	$0.336^{(6)}$ $0.691^{(8)}$ $1.032^{(10)}$ $1.359^{(12)}$
S3	-1.000	**3** **4**	$0.295^{(6)}$ $0.372^{(8)}$ $0.406^{(10)}$ $0.424^{(12)}$	**C4**		**S3**	-1.000	**3** **4**	$0.295^{(6)}$ $0.372^{(8)}$ $0.406^{(10)}$ $0.424^{(12)}$	**C3**	$0.109^{(6)}$ $0.252^{(8)}$ $0.396^{(10)}$ $0.534^{(12)}$
		5 **6**	$1.491^{(6)}$ $1.303^{(8)}$ $1.204^{(10)}$ $1.147^{(12)}$	**C6**				**5** **6**	$1.491^{(6)}$ $1.303^{(8)}$ $1.204^{(10)}$ $1.147^{(12)}$	**C4**	$0.154^{(6)}$ $0.353^{(8)}$ $0.554^{(10)}$ $0.748^{(12)}$

$^{(6)}$ dome with 6 girders; $^{(8)}$ dome with 8 girders; $^{(10)}$ dome with 10 girders; $^{(12)}$ dome with 12 girders

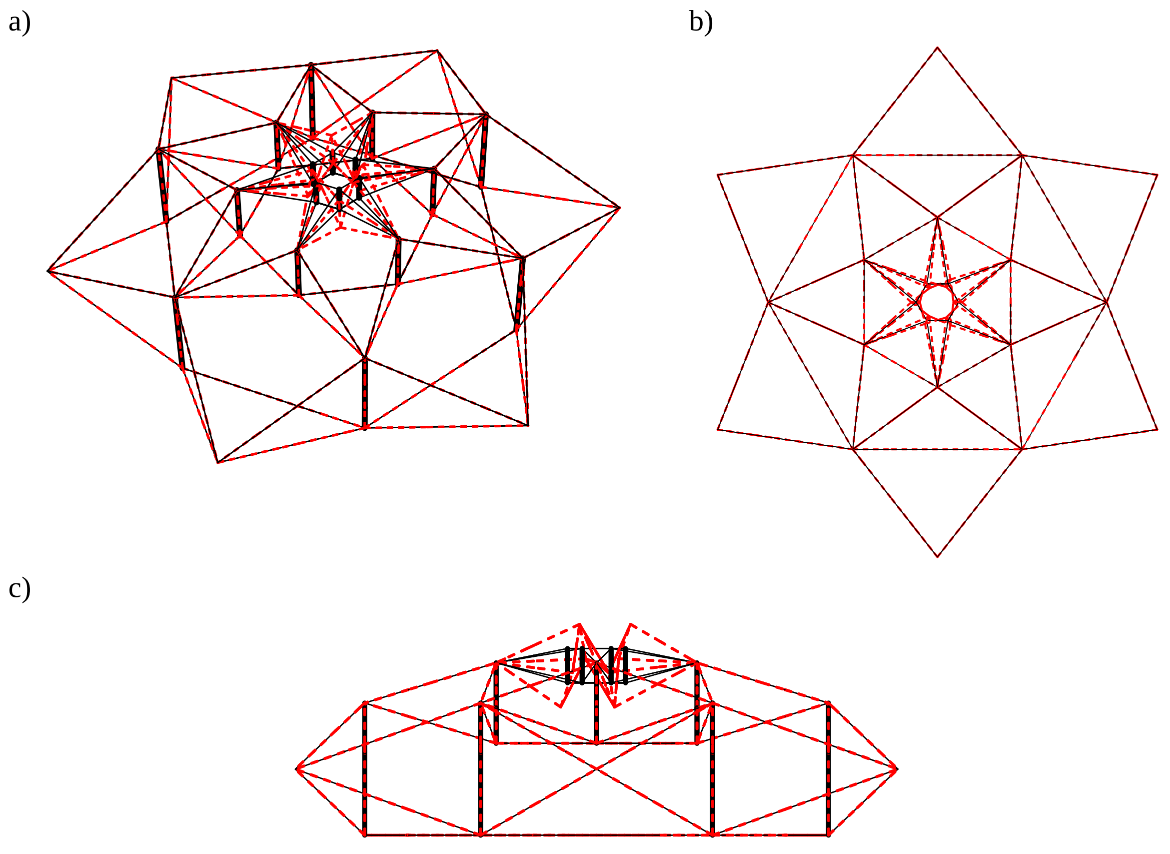

Fig. 6.9. Form of infinitesimal mechanism of L 6B dome: a) 3D view, b) top view, c) side view

The qualitative analysis of Levy domes determined following tensegrity features, i.e., the dome is a truss (*T*), with a continuous net of tensed cables (*C*), and discontinues net of compressed struts (*D*) surrounded by cables, and it features the existence of the self-stress state (*SS*) and infinitesimal mechanism (*M*) (only in case of dome type B). Nonetheless, not every existing self-stress state stiffens the mechanism and a superimposed self-stress state must be introduced to the structure. Therefore, the analyzed Levy domes type A are classified as structures with tensegrity features class 2, and Levy domes type B are classified as structures with tensegrity features class 1.

6.3.2. Genetic algorithm

The qualitative analysis of the Levy type B dome (L 12B) (Fig. 6.6) was also performed using the genetic algorithm. A set of self-equilibrated forces was described using the procedure presented in Section 4.2.2. Two series of calculations are performed using the following parameters:

- population size: 1000 (Series 1), 1100 (Series 2),
- number of generations: 100 (Series 1), 150 (Series 2),
- solutions in the population: 200 (Series 1), 250 (Series 2),
- number of genes: equals the number of groups of elements.

The values obtained by the genetic algorithm were compared to the exact values from the spectral analysis (section 6.3.1), and the one presented by Chen&Feng in [212]. Summarized results are provided in Table 6.6. The original values from the paper (Original) were normalized (Norm.) in such a way that the value in the longest strut is equal to -1 for comparison.

Table 6.6. Values of self-stress state of the Levy dome obtained by different methods

Groups of Elements	Chen & Feng [212]			Present Study				
	Original	Norm.	*Relative Error*	Exact Solution	GA Series 1	*Relative Error*	GA Series 2	*Relative Error*
1	392	1.285	23%	1.044	0.431	59%	0.675	35%
2	248	0.813	15%	0.704	0.459	35%	0.390	45%
3	644	2.111	105%	1.032	0.525	49%	0.627	39%
4	688	2.256	133%	0.969	0.962	1%	0.963	1%

Table 6.6. Values of self-stress state of the Levy dome obtained by different methods - Continued

Groups of Elements		Chen & Feng [212]			Present Study				
		Original	**Norm.**	***Relative Error***	**Exact Solution**	**GA Series 1**	***Relative Error***	**GA Series 2**	***Relative Error***
5		1343	4.403	57%	2.809	2.097	25%	2.234	20%
6	**a**	901	2.954	276%	0.786	0.190	76%	0.281	64%
	b			12%	2.639	2.805	6%	2.934	11%
C1	**a**	1637	5.367	47%	3.644	2.664	27%	2.916	20%
	b			8%	4.986	4.542	9%	4.874	2%
C2		1307	4.285	37%	3.124	3.067	2%	3.093	1%
C3		469	1.538	15%	1.333	0.884	34%	0.727	45%
C4		750	2.459	23%	2.000	0.838	58%	1.282	36%
S1		−52	−0.170	23%	−0.138	−0.074	46%	−0.083	40%
S2		−126	−0.413	20%	−0.345	−0.289	16%	−0.270	22%
S3		−305	−1.000	0%	−1.000	−1.000	0%	−1.000	0%

The values provided in [212] are not meeting the criteria of the node equilibrium, and the relative errors are up to 276%. The differences may occur due to a different classification of groups of elements. In the case of the genetic algorithm, the accuracy of the obtained results is highly dependent on the parameters of the algorithm, higher convergence could be achieved by increasing these parameters. Obtained values are considered satisfactory in the case of second series, and meet the requirement of stable equilibrium (the equilibrium of nodes is close to zero).

6.4. Quantitative analysis

The quantitative analysis of Levy domes examines the influence of the initial prestress level on the behaviour of the structure under external load. As in the case of the Geiger dome, the material properties and cross-sections of the elements are essential for consideration. It is assumed that cables are made of steel S460N. The "Type A" cables with a Young modulus of 210 GPa [192] are used. The struts are made of hot-finished circular hollow sections (steel S355J2) with a Young modulus of 210 GPa. The density of steel is equal $\rho = 7860\ \mathrm{kg/m^3}$.

The quantitative analysis is performed in terms of static, dynamic, and dynamic stability analyses. Each type of the analysis concerns the small-scale domes. Static analysis is performed for the small-scale domes consisted of six load-bearing girders (section 6.2.1). The qualitative analysis of small-scale domes, i.e., identifying existing self-stress states and infinitesimal mechanisms was performed in Section 6.3.2. Dynamic analysis concerns domes consisting of different numbers of load-bearing girders, i.e., 6, 8, 10, and 12 girders. In turn, dynamic stability analysis is provided for small-scale Geiger domes considered in the static analysis.

The consideration of small-scale domes includes two variants of the geometry, i.e., L 6A and L 6B (Fig. 6.4). The cables with the diameter $\phi = 20$ mm and load-bearing capacity $N_{Rd} = 110.2$ kN are taken into account. For struts, there are rods with a diameter $\phi = 76.1$ mm and thickness $t = 2.9$ mm with lengths 0.6 m, 1.4 m, and 2.3 m and load-bearing capacity $N_{Rd} = 224.3$ kN, 170.5 kN, and 107.1 kN respectively. The external load is considered in different positions, e.g., in $\mathbf{P}^{(i)}$, where $i = 1, 2, 3$ (Fig. 6.10), and different values, i.e., $\mathbf{P}^{(i)} = \{1\ \mathrm{kN},\ 5\ \mathrm{kN}\}$. Similarly to the Geiger dome, the minimum prestress level of the Levy domes is highly dependent on the load value and position (Table 6.7). In turn, the value of the maximum prestress level (S_{max}) depends on the load-bearing capacity of the most stressed elements. For all structures, it was assumed as S_{max} = 50 kN. The maximum effort of cables is $W_{max,C}$ = 0.7, and the maximum effort of struts is $W_{max,S}$ = 0.48.

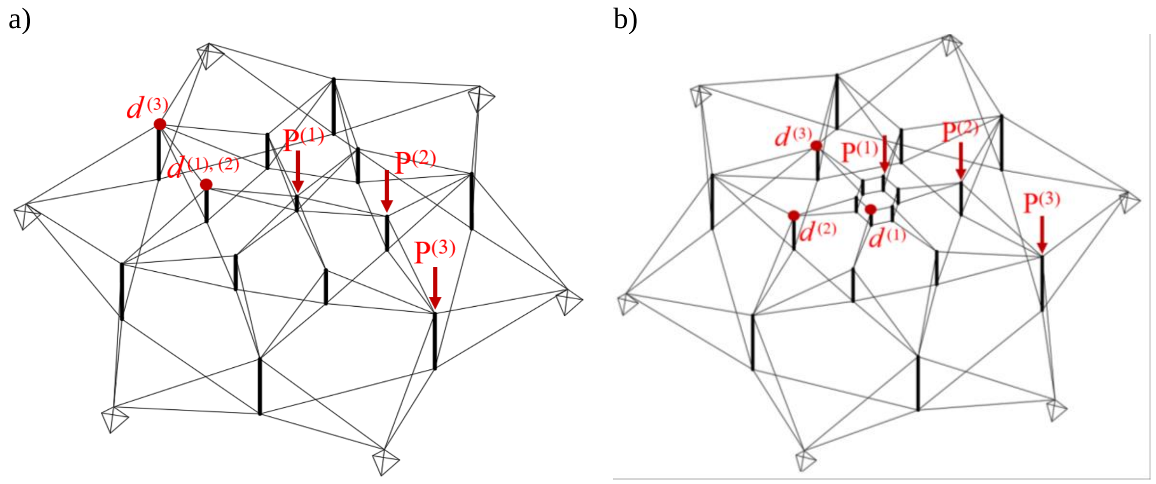

Fig. 6.10. Position of the external load on the girder: a) type A, b) type B

Table 6.7. The S_{min} values for Levy domes under external load

A	Load value						B	Load value					
	$P=1$ kN			$P=5$ kN				P = 1 kN			P = 5 kN		
	Load position			Load position				Load position			Load position		
	$\mathbf{P}^{(1)}$	$\mathbf{P}^{(2)}$	$\mathbf{P}^{(3)}$	$\mathbf{P}^{(1)}$	$\mathbf{P}^{(2)}$	$\mathbf{P}^{(3)}$		$\mathbf{P}^{(1)}$	$\mathbf{P}^{(2)}$	$\mathbf{P}^{(3)}$	$\mathbf{P}^{(1)}$	$\mathbf{P}^{(2)}$	$\mathbf{P}^{(3)}$
	S_{min} [kN]			S_{min} [kN]				S_{min} [kN]			S_{min} [kN]		
	4	9	1	18	42	5		22	10	3	-	50	12

A – type A, B – type B

Note!

In the case of the Levy dome, selected profiles were not sufficient to identify the S_{min} level for the load position $\mathbf{P}^{(1)}$ (for P $=5$ kN), and $S_{min}=S_{max}$ for the load position $\mathbf{P}^{(2)}$ (for P $=5$ kN). It was decided to increase the cross-section of the elements. The cables with the diameter $\phi=27$ mm and load-bearing capacity $N_{Rd}=206.7$ kN were selected instead. For struts, there are rods with a diameter $\phi=82.5$ mm and thickness $t=3.2$ mm with lengths 0.6 m, 1.4 m, and 2.3 m and load-bearing capacity $N_{Rd}=297.6$ kN, 233.4 kN, and 154.0 kN respectively. For all structures, it was assumed as S_{max} = 120 kN. The maximum effort of cables is $W_{max,C}$ = 0.9, and the maximum effort of struts is $W_{max,S}$ = 0.48. Further analysis was carried out using updated cross-sections.

Table 6.8. The updated S_{min} values for Levy domes under external load

A	Load value						B	Load value					
	$P=1$ kN			$P=5$ kN				P = 1 kN			P = 5 kN		
	Load position			Load position				Load position			Load position		
	$\mathbf{P}^{(1)}$	$\mathbf{P}^{(2)}$	$\mathbf{P}^{(3)}$	$\mathbf{P}^{(1)}$	$\mathbf{P}^{(2)}$	$\mathbf{P}^{(3)}$		$\mathbf{P}^{(1)}$	$\mathbf{P}^{(2)}$	$\mathbf{P}^{(3)}$	$\mathbf{P}^{(1)}$	$\mathbf{P}^{(2)}$	$\mathbf{P}^{(3)}$
	S_{min} [kN]			S_{min} [kN]				S_{min} [kN]			S_{min} [kN]		
	4	9	1	18	42	5		22	10	3	95	50	12

A – type A, B – type B

Additionally, the static analysis of the realistic-scale Levy dome is performed. The realistic-scale dome geometry was obtained by the rescaling of the small-scale dome, and resulted in the same self-stress values (Table 6.5).

In the charts the following symbols are used: II – second-order theory, III – third-order theory, 1 – external load equal to 1 kN, 5 – external load equal to 5 kN, s – struts, c – cables, A – type A, B – type B, L1 – realistic dome with symmetrical load, L2 – realistic dome with asymmetrical load. The caption "A 1(II)" stands for the Levy dome type A loaded with force 1 kN analyzed using the second-order theory, and "L1 (II)" stands for the Levy dome with symmetrical load analyzed using the second-order theory.

6.4.1. Static analysis of small-scale domes

Similarly to the Geiger dome, static analysis of the Levy domes concerns the impact of the initial prestress on the behaviour of the structure under time-independent external load. Particularly, the displacements (q_y, q_z), maximum effort of structure W_{max}, and stiffness parameter GSP are studied under the influence of the prestress. The displacements are measured for the node located on the girder opposite to the location of the loaded node (node d depends on the position of load) (Fig. 6.10). The examples provided below are to compare the static response of the L 6A and L 6B domes in the case of different load positions. Firstly, the load position $\mathbf{P}^{(1)}$ is considered (Example 1), then the load position $\mathbf{P}^{(2)}$ (Example 2), and finally the load position $\mathbf{P}^{(3)}$ (Example 3).

Example 1

<u>*Subject of the comparison:*</u> L 6A (Fig. 6.11a) and L 6B (Fig. 6.11b) domes, load position $\mathbf{P}^{(1)}$ – behaviour under the external load

<u>*Aim of the comparison:*</u> (1) Whether the design solution (close or open upper section) of the structure matter in the case of load position $\mathbf{P}^{(1)}$? (2) Which dome (Geiger or Levy) is more sensitive in the case of the load position $\mathbf{P}^{(1)}$?

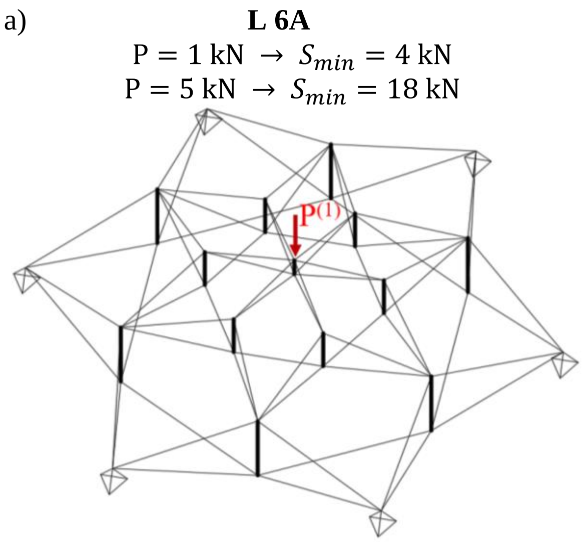

Fig. 6.11. External load application in the case of position $\mathbf{P}^{(1)}$ for: a) L 6A, b) L 6B

The first considered example examines the influence of the initial prestress on the static parameters in the case of the load position $\mathbf{P}^{(1)}$. The external load is located in the upper section of the dome, i.e., where the infinitesimal mechanism is located for the dome type B. The impact of the initial prestress on the plane displacement q_y (Fig. 6.12) and vertical displacement q_z (Fig. 6.13) is considered. In the case of the dome type A, the displacements are insensitive to the change in the prestress. The situation is opposite for the dome type B. The influence of the initial prestress level is nonlinear. The results obtained from the second-order theory and third-order theory are convergent only for the lower load in the high prestress range ($S = 70 \div 120$ kN). It is worth mentioning, that increasing of the external load results in the change of the direction of the plane displacement q_y (Fig. 6.12b). The influence of the initial prestress level on the maximum effort of elements W_{max} (Fig. 6.14) is linear for both structures. The GSP parameter of the dome type A (Fig. 6.15a) is constant at value 1 and is not depending on the prestress. For the dome type B (Fig. 6.15b), the relation between GSP parameter and initial prestress level is linear. The increasing in the external load results in the decrease of the stiffness of the structure up to 60% (for $S = 120$ kN).

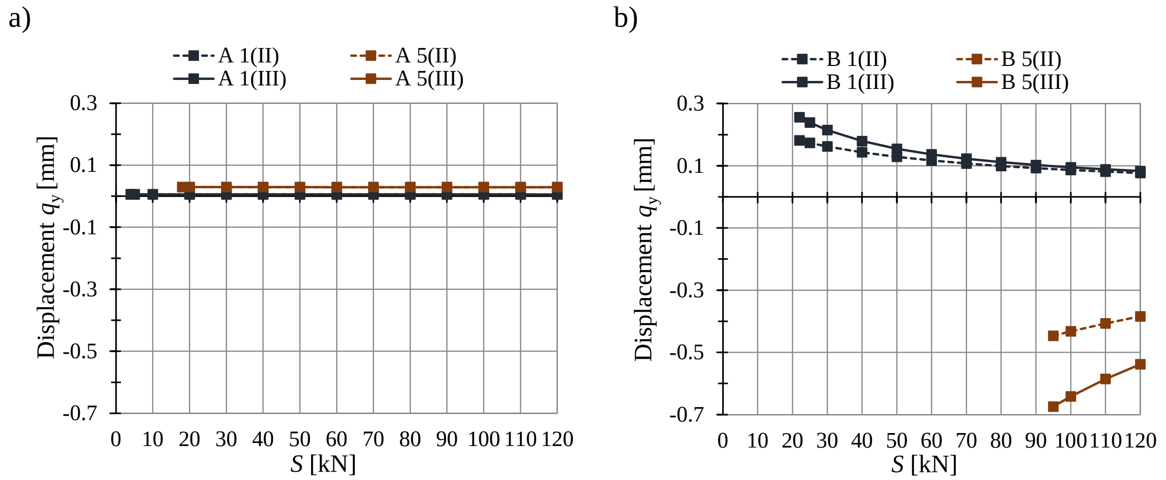

Fig. 6.12. Impact of the initial prestress S on the displacement q_y in the case of the load position $\mathbf{P}^{(1)}$ for: a) L 6A, b) L 6B

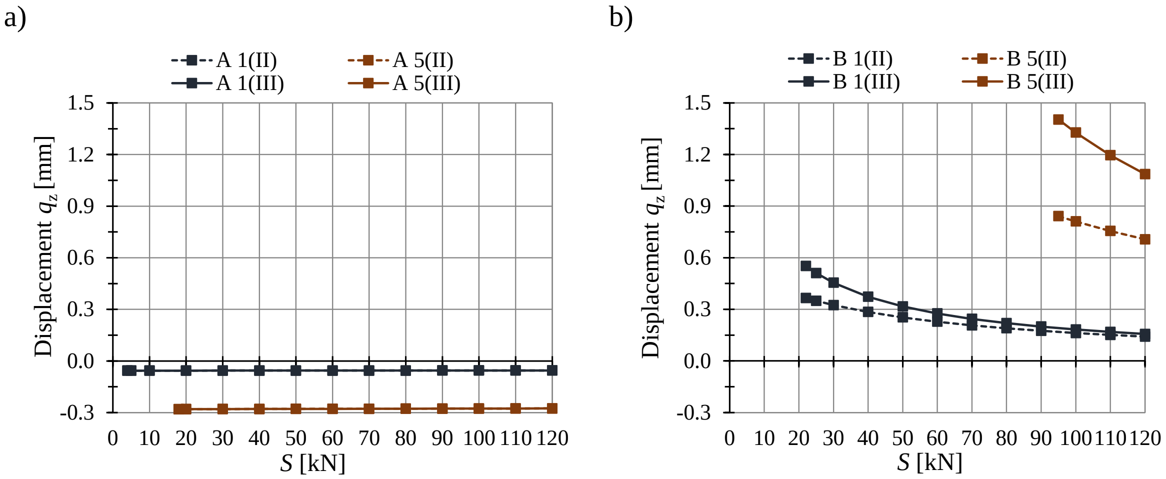

Fig. 6.13. Impact of the initial prestress S on the displacement q_z in the case of the load position $\mathbf{P}^{(1)}$ for: a) L 6A, b) L 6B

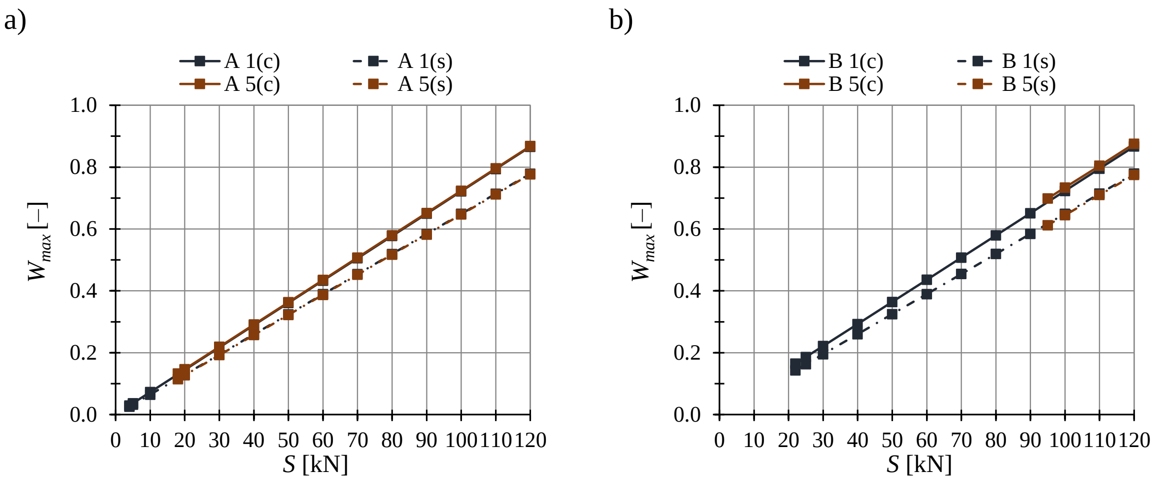

Fig. 6.14. Impact of the initial prestress S on the maximum effort of structure W_{max} in the case of the load position $\mathbf{P}^{(1)}$ for: a) L 6A, b) L 6B

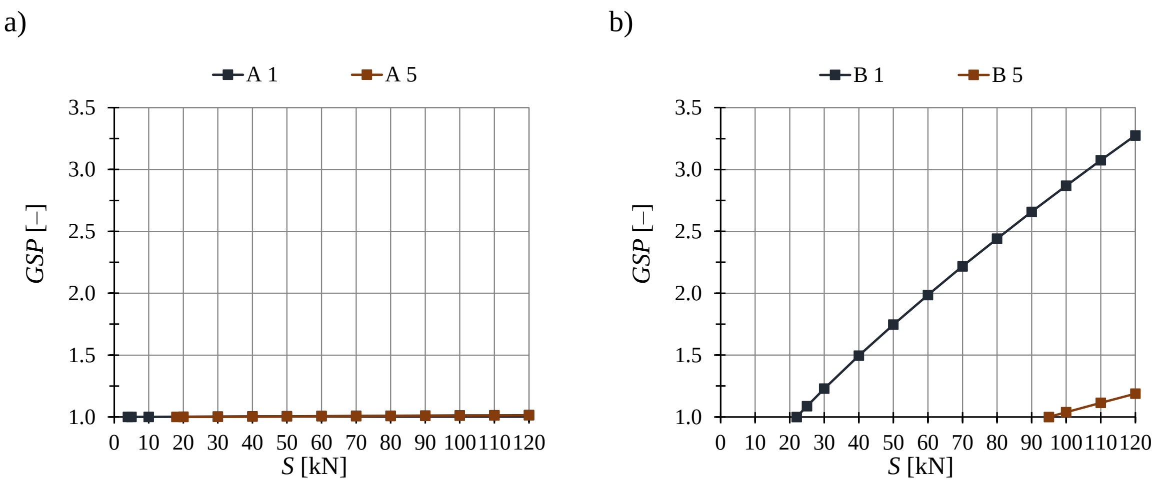

Fig. 6.15. Impact of the initial prestress S on the GSP parameter in the case of the load position $\mathbf{P}^{(1)}$ for: a) L 6A, b) L 6B

<u>*Conclusion of the comparison:*</u> The load positioned in the upper section is significant for the Levy dome type B due to a localization of the infinitesimal mechanism (Fig. 6.9). Unlike the dome type A, the L 6B dome is sensitive to the change of the initial prestress level and external load. Comparing the behavior of the Geiger dome and Levy dome for the same load position (section 5.4.1: *Example 1*), it can be noticed that Levy dome type A behaves similarly to the Geiger domes RG 6A and MG 6A, i.e., the prestress has no impact on the displacements or stiffness of the structure. The Levy dome type B is characterized by a high impact of the initial prestress level and bigger displacements.

Example 2

<u>*Subject of the comparison:*</u> L 6A (Fig. 6.16a) and L 6B (Fig. 6.16b) domes, load position $\mathbf{P}^{(2)}$ – behaviour under external load

<u>*Aim of the comparison:*</u> Whether the design solution (close or open upper section) of the structure matter in the case of load position $\mathbf{P}^{(2)}$? (2) Which dome (Geiger or Levy) is more sensitive in the case of the load position $\mathbf{P}^{(2)}$?

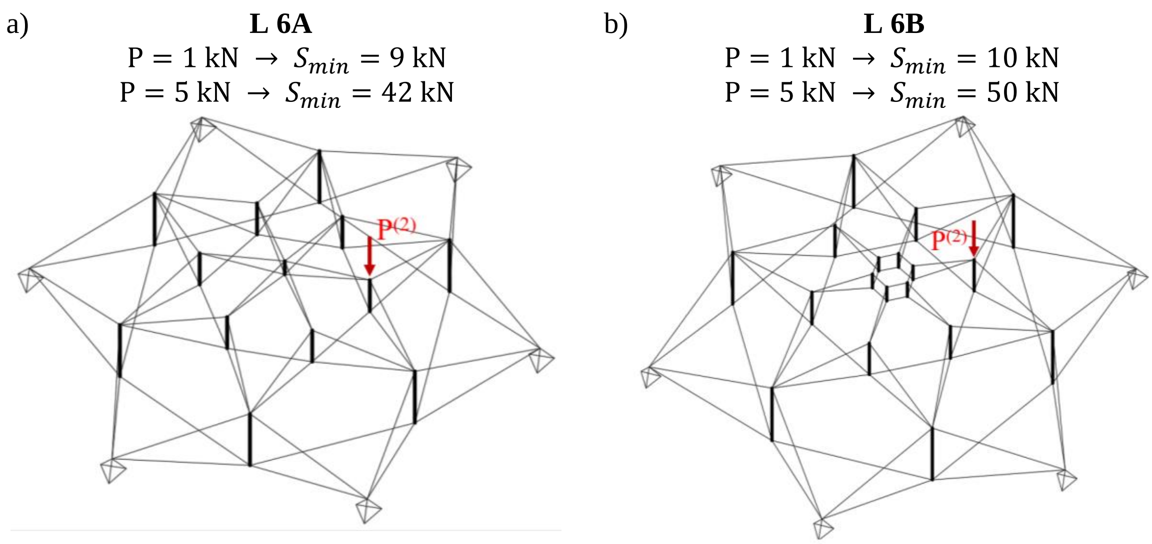

Fig. 6.16. External load application in the case of position $\mathbf{P}^{(2)}$ for: a) L 6A, b) L 6B

The second example considers the load position $\mathbf{P}^{(2)}$. The consideration includes the impact of the initial prestress level on the plane displacement q_x (Fig. 6.17) and vertical displacement q_z (Fig. 6.18). In contrast to *Example 1*, the biggest displacements are obtained for the L 6A dome, whereas the displacements of the L 6B dome are almost constant and insensitive to the change in the external load. The results obtained using second-order theory and third-order theory are fully convergent for both domes. The influence of the initial prestress level on the maximum effort of structure W_{max} (Fig. 6.19) is linear, as well as on the *GSP* parameter (Fig. 6.20). Nevertheless, for the L 6B dome and P = 1 kN (Fig. 6.20b) the nonlinearity can be noticed and the graph has a reverse behaviour. The increasing of the external load resulted in the decreasing of the stiffness up to 7% and 17%, for L 6A and L 6B domes respectively.

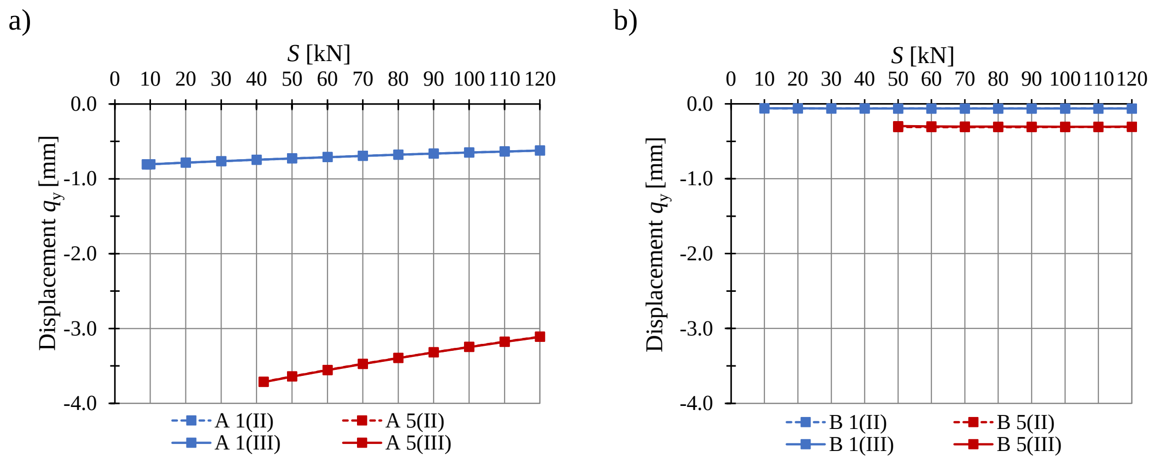

Fig. 6.17. Impact of the initial prestress S on the displacement q_y in the case of the load position $\mathbf{P}^{(2)}$ for: a) L 6A, b) L 6B

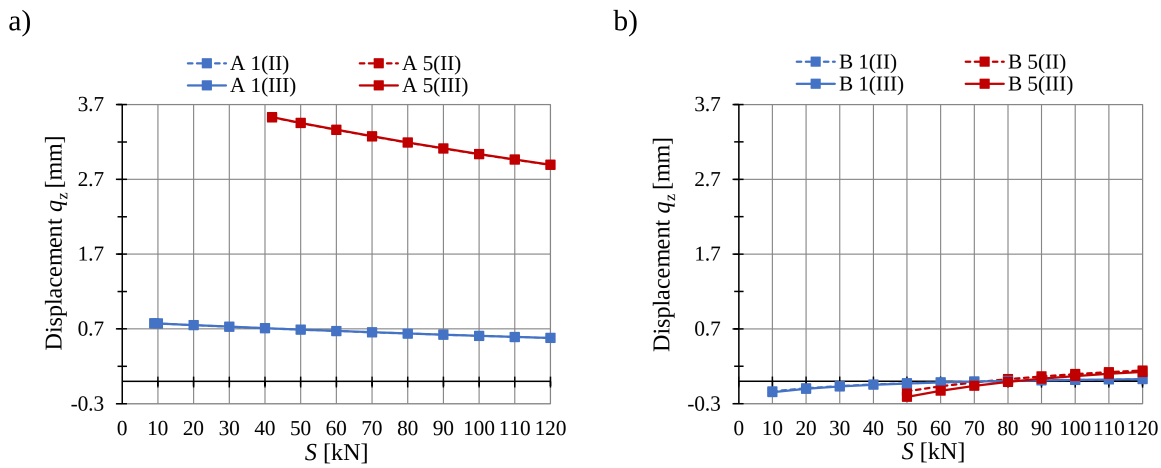

Fig. 6.18. Impact of the initial prestress S on the displacement q_z in the case of the load position $\mathbf{P}^{(2)}$ for: a) L 6A, b) L 6B

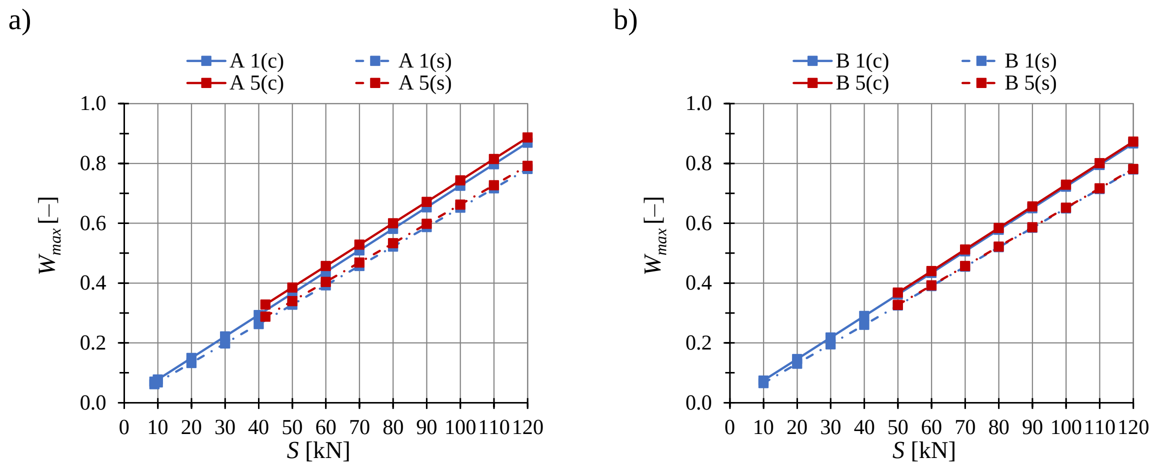

Fig. 6.19. Impact of the initial prestress S on the maximum effort of structure W_{max} in the case of the load position $\mathbf{P}^{(2)}$ for: a) L 6A, b) L 6B

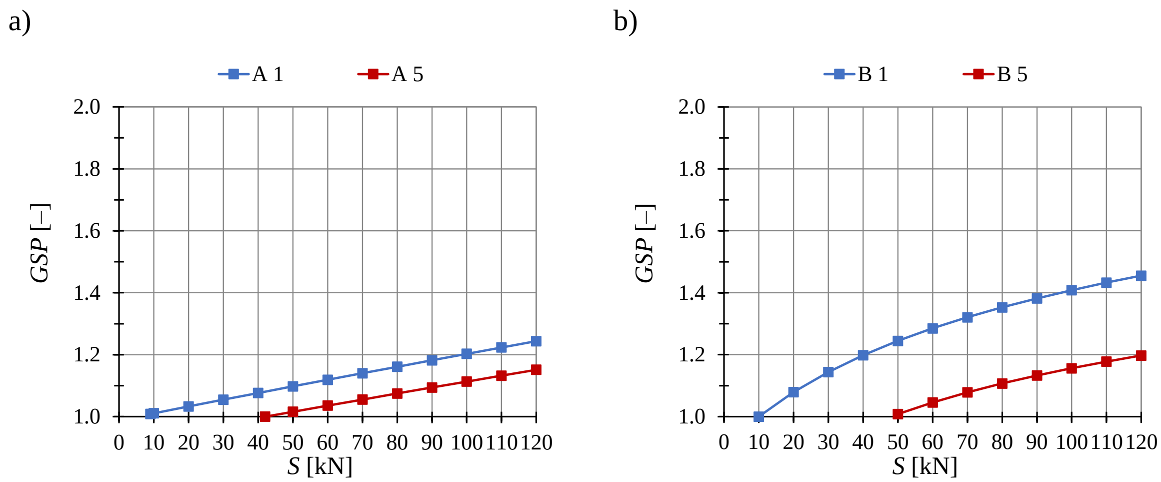

Fig. 6.20. Impact of the initial prestress S on the GSP parameter in the case of the load position $\mathbf{P}^{(2)}$ for: a) L 6A, b) L 6B

Conclusion of the comparison: Despite the absence of the infinitesimal mechanism in the L 6A dome, the influence of the initial prestress level on the displacements and stiffness of the structure can be noticed. Because the load is positioned further away from the localization of the mechanism (Fig. 6.9), the L 6B dome is almost insensitive to the change in the initial prestress, and displacements are considerably lower in comparison to the L 6A dome. Nonetheless, Geiger domes are more sensitive to the change in the initial prestress level, i.e., characterized by bigger displacements and higher stiffness of the structure.

Example 3

<u>*Subject of the comparison:*</u> L 6A (Fig. 6.21a) and L 6B (Fig. 6.21b) domes, load position $\mathbf{P}^{(3)}$ – behaviour under external load

<u>*Aim of the comparison:*</u> Whether the design solution (close or open upper section) of the structure matter in the case of load position $\mathbf{P}^{(3)}$? (2) Which dome (Geiger or Levy) is more sensitive in the case of the load position $\mathbf{P}^{(3)}$?

a) **L 6A**
$\mathrm{P} = 1\ \mathrm{kN} \rightarrow S_{min} = 1\ \mathrm{kN}$
$\mathrm{P} = 5\ \mathrm{kN} \rightarrow S_{min} = 5\ \mathrm{kN}$

b) **L 6B**
$\mathrm{P} = 1\ \mathrm{kN} \rightarrow S_{min} = 3\ \mathrm{kN}$
$\mathrm{P} = 5\ \mathrm{kN} \rightarrow S_{min} = 12\ \mathrm{kN}$

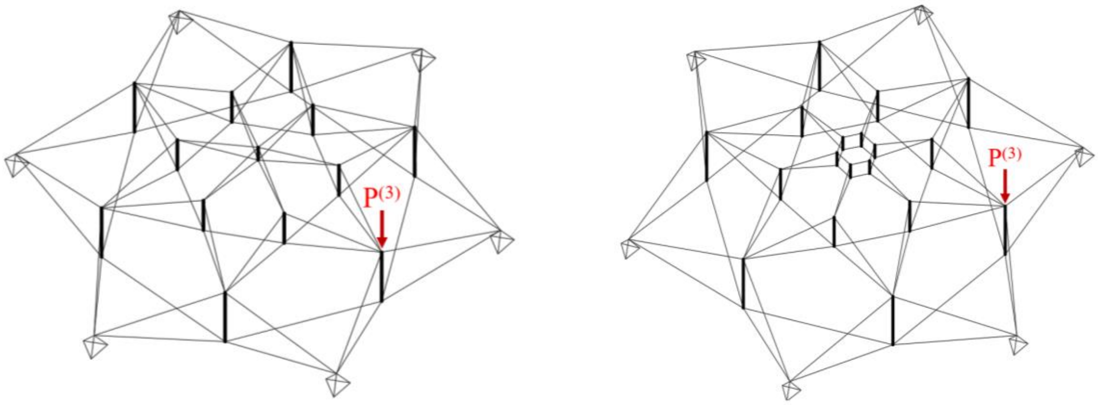

Fig. 6.21. External load application in the case of position $\mathbf{P}^{(3)}$ for: a) L 6A, b) L 6B

The third example focuses on the influence of the initial prestress in the case of the load position $\mathbf{P}^{(3)}$. In this situation, the external load positioned furthest from the localization of the infinitesimal mechanism in the L 6B dome. The impact of the initial prestress on the displacements q_y (Fig. 6.22) and q_z (Fig. 6.23) is considered. Similarly to the *Example 2*, the L 6A dome is characterized by biggest displacements, nonetheless, the displacements are even three times smaller than in the *Example 2*. The influence of the initial prestress is linear. In the case of L 6B, the displacements are almost constant, insensitive to the change in the external load and initial prestress level. The maximum effort of structure W_{max} (Fig. 6.24) and the GSP parameter (Fig. 6.25) have linear behaviour as well. The increase in the external load is not affecting the stiffness of the structure, which remains on the same level $GSP = 1.07 \div 1.14$.

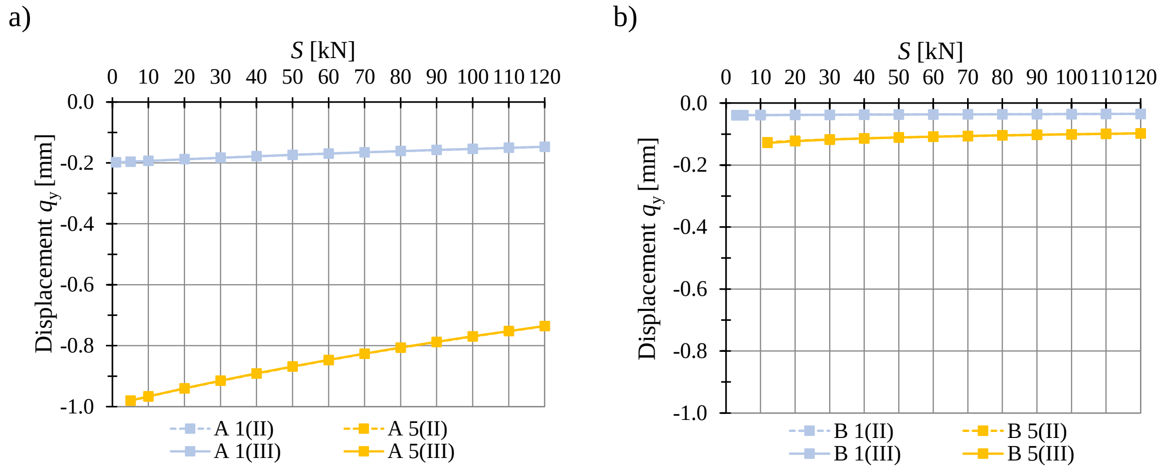

Fig. 6.22. Impact of the initial prestress S on the displacement q_y in the case of the load position $\mathbf{P}^{(3)}$ for: a) L 6A, b) L 6B

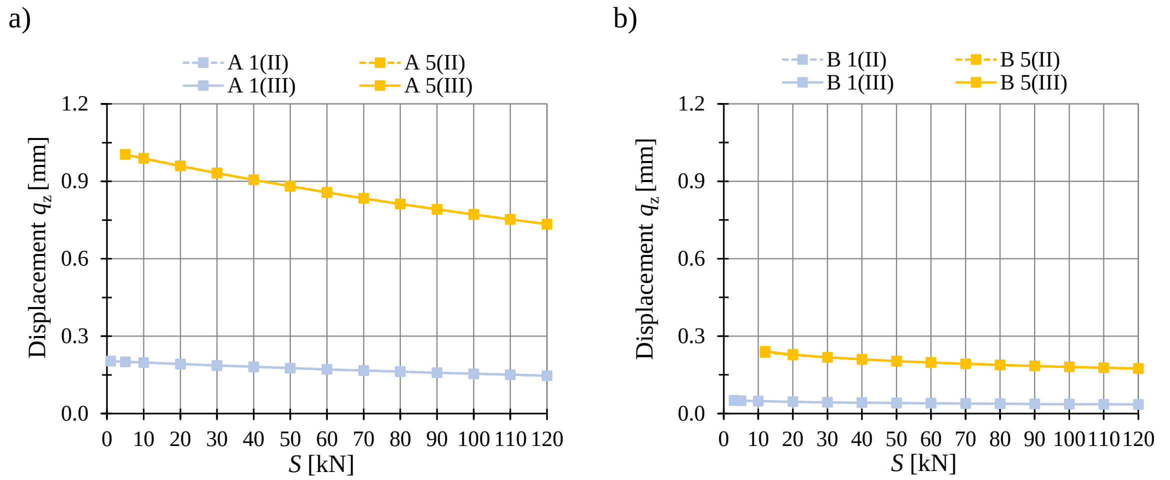

Fig. 6.23. Impact of the initial prestress S on the displacement q_z in the case of the load position $\mathbf{P}^{(3)}$ for: a) L 6A, b) L 6B

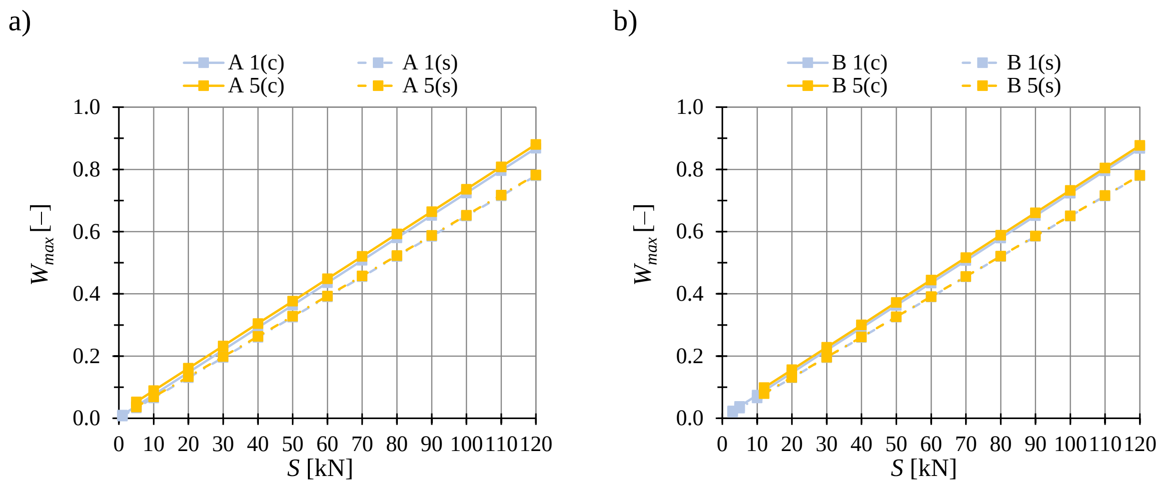

Fig. 6.24. Impact of the initial prestress S on the maximum effort of structure W_{max} in the case of the load position $\mathbf{P}^{(3)}$ for: a) L 6A, b) L 6B

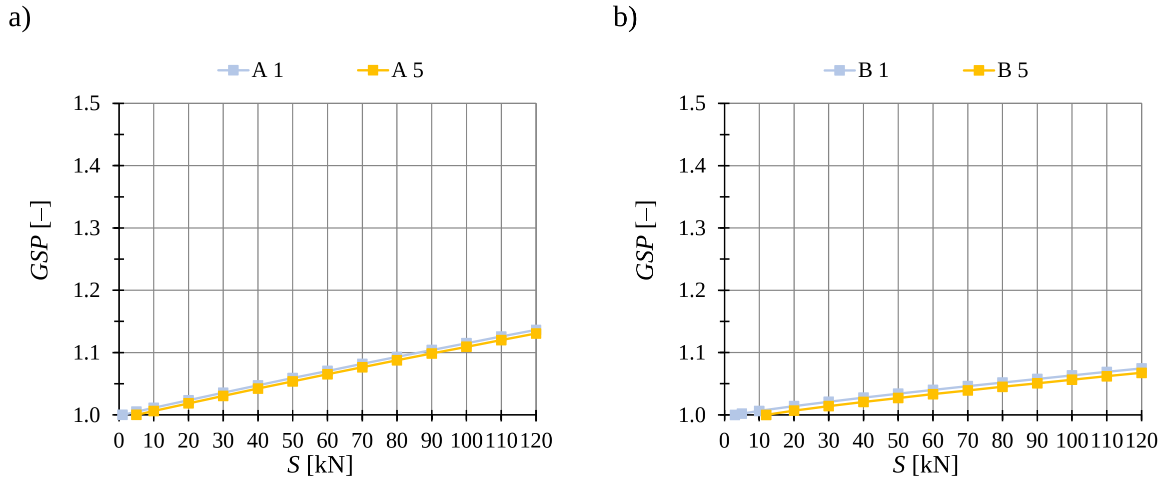

Fig. 6.25. Impact of the initial prestress S on the GSP parameter in the case of the load position $\mathbf{P}^{(3)}$ for: a) L 6A, b) L 6B

<u>*Conclusion of the comparison:*</u> Despite the fact that L 6B dome is characterized by the self-stress state and infinitesimal mechanism, in the case of external load position $\mathbf{P}^{(3)}$, the initial prestress has almost no impact on the static parameters of the dome, as well as external load value. In turn, the Geiger dome with the same load conditions is characterized by the higher sensitivity to the change in the initial prestress level.

6.4.2. Static analysis of the realistic-scale dome

The one geometry is chosen for the realistic-scale dome, i.e., realistic-scale type A Levy dome consisted of six load-bearing girders (L 6A) (Fig. 6.4a). The dome is 20 m wide and 3.5 m high (Fig. 6.26). The structure consists of 85 elements, i.e., 13 struts and 72 cables. The struts are designed as tubes CHS 108x4.5. Due to the different lengths, the struts were divided into three groups, i.e., six struts of 3.83 m length, six struts of 2.33 m length, and one strut of 1 m length, with the maximum load-bearing capacity of $N_{Rd} = 224$ kN, 402 kN, and 499 kN, respectively. In turn, the cables are assumed to be made of "D36" with a maximum load-bearing capacity of $N_{Rd} = 367.5$ kN. The external load application and value was the same as in the case of realistic Geiger dome (section 5.4). The load was applied symmetrically (L1) (Fig. 5.30a) and asymmetrically (L2) (Fig. 5.30b). The minimum prestress level for the dome is equal to S_{min}= 11 kN, whereas the maximum prestress level was assumed as S_{max} = 190 kN. The maximum effort of structure is W_{max} = 0.91.

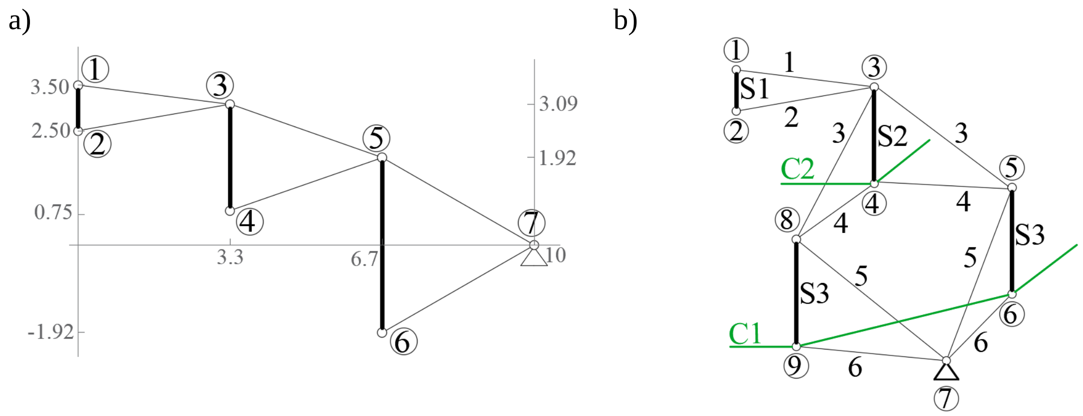

Fig. 6.26. Load-bearing girder of the realistic Levy dome: a) cross section, b) 3D view

As in the case of the Geiger dome, the impact of the initial prestress level S on the displacements q_x and q_z of the top node 1 (Fig. 6.26), maximum effort of structure W_{max}, and stiffness parameter GSP of the realistic Levy dome is considered.

Unlike the Geiger dome, the impact of the initial prestress level on the plane displacement q_x (Fig. 6.27a) is linear, and on vertical displacement q_z (Fig. 6.27b) – is absent. The results obtained using the second-order theory and third-order theory are fully convergent even at the low levels of initial prestress. The asymmetrical load type (L1) affects only the plane displacement q_x, whereas vertical displacements are insensitive to the load type. The maximum effort of the structure W_{max} (Fig. 6.27) increased linearly, the effort for both load types is the same. The GSP parameter, on the other hand, depend on the external load nature. Comparing to the Geiger dome, the stiffness is significantly lower, i.e., $GSP = 7$ and $GSP = 1.23$, for Geiger and Levy dome respectively (in the case of asymmetrical load). The decrease is up to 82%. In the case of symmetrical load, the GSP parameter is constant at value 1.

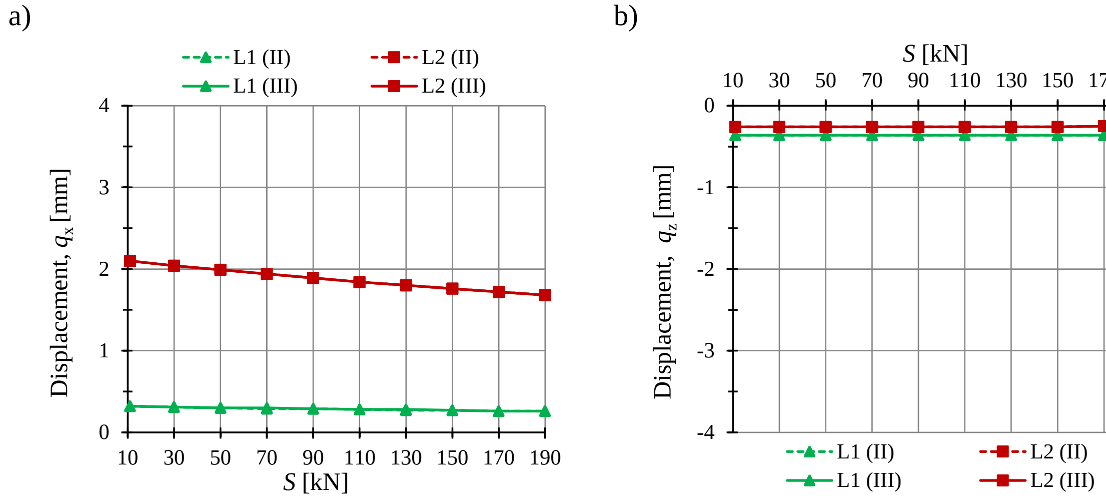

Fig. 6.27. Impact of the initial prestress S on the displacement: a) q_x, b) q_z

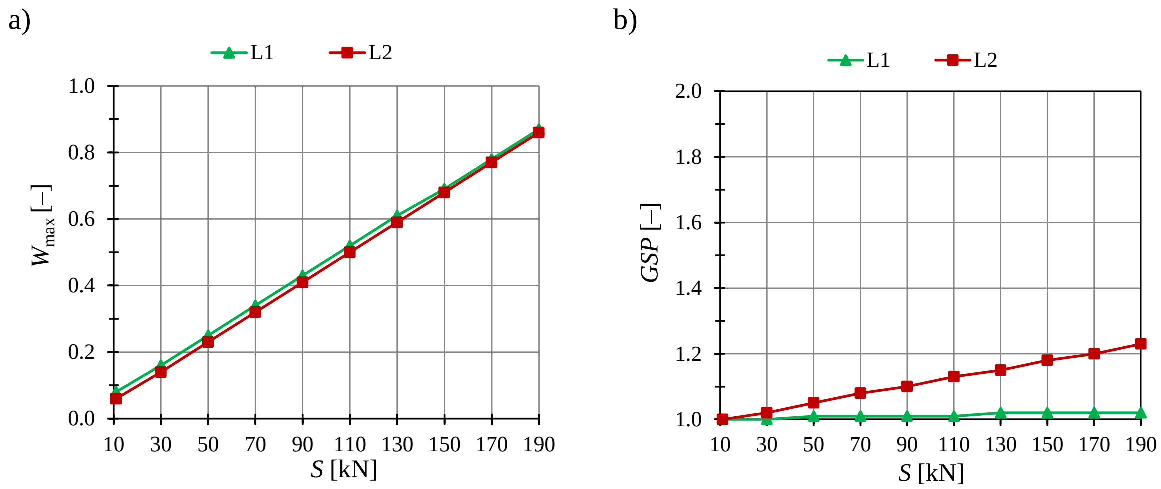

Fig. 6.28. Impact of initial prestress S on the: a) maximum effort of structure W_{max}, b) GSP parameter

Due to a lack of the infinitesimal mechanism, the considered Levy dome is insensitive to the change in the initial prestress level. The impact of the different types of external load is significantly lower comparing to the Geiger dome. The analysis can be carried out using the second-order theory.

6.4.3. Dynamic analysis

The dynamic analysis of Levy dome concerns the impact of the initial prestress level on natural and free frequencies of the structure. The section is divided onto analysis of natural frequencies correspond to the infinitesimal mechanism (Example 1), additional natural frequencies that depend on the initial prestress (Example 2), and free frequencies (Example 3).

Example 1

Subject of the comparison: L ngA, L ngB domes ($ng = \{6,8,10,12\}$) - natural frequency correspond to the infinitesimal mechanism

Aim of the comparison: (1) How does the initial prestress level impact the natural frequency correspond to the infinitesimal mechanism? (2) Whether the number of load-bearing girders impacts the natural frequency corresponding to the infinitesimal mechanism? (3) How does the design solution (open or closed upper section) impact the dome behaviour?

The analysis concerns the small-scale Levy domes from the section 6.4.1. Considered structure consist of different number of load-bearing girders (ng), i.e., $ng = \{6,8,10,12\}$. The qualitative analysis, i.e., the identification of self-stress states and infinitesimal mechanisms, was performed in section 6.3.1. In the case of type A Levy domes (L ngA) the number of infinitesimal mechanisms (nm) is equal to zero. In turn, the L ngB dome characterized by one natural frequency $f1$ that correspond to one infinitesimal mechanism. Fig. 6.29 presents the influence of the initial prestress level on the first natural frequency $f1$ of considered domes. The first natural frequency $f1$ of type A domes is not related to the mechanism and the absence of the initial prestress is not equal to zero natural frequency. Thus, the increasing of the initial prestress level causes small linear increasing of natural frequencies L ngA domes. It is worth to mention, the natural frequencies $f1$ for domes with 8, 10, and 12 load-bearing girders remain on the same level $f1 = 16.5 \div 18.3$ Hz. In turn, for the L 6A dome it equals $f1 = 12.8 \div 13.7$ Hz (Fig. 6.29a).

For the domes type B, zero prestress ($S = 0$) results in zero frequencies (Fig. 6.29b). The increase in the number of load-bearing girders affecting only natural frequencies related to the infinitesimal mechanism, and the impact of the initial prestress level is nonlinear. The discrepancy between the first natural frequency $f1$ values is around $11 \div 12$ Hz for S_{max}. In the case of $S = 0$, the forms of vibrations realize the forms of infinitesimal mechanisms. Fig. 6.30 presents forms of vibrations of the Levy domes type B.

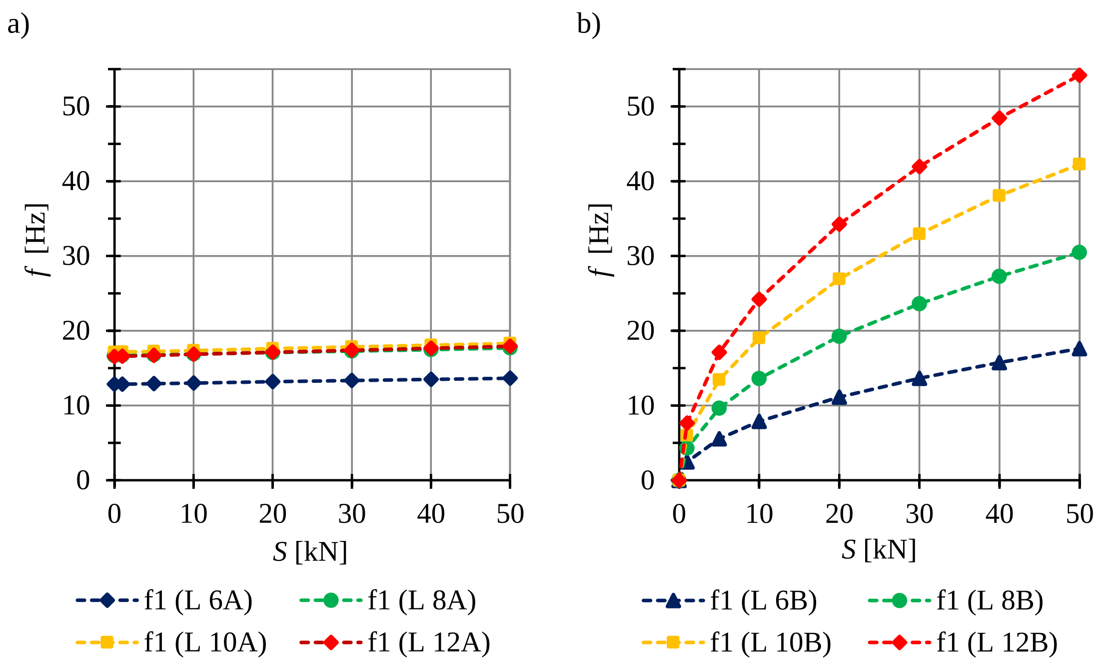

Fig. 6.29. Influence of the initial prestress S on the first natural frequency $f1$ of: a) L ngA, b) L ngB,

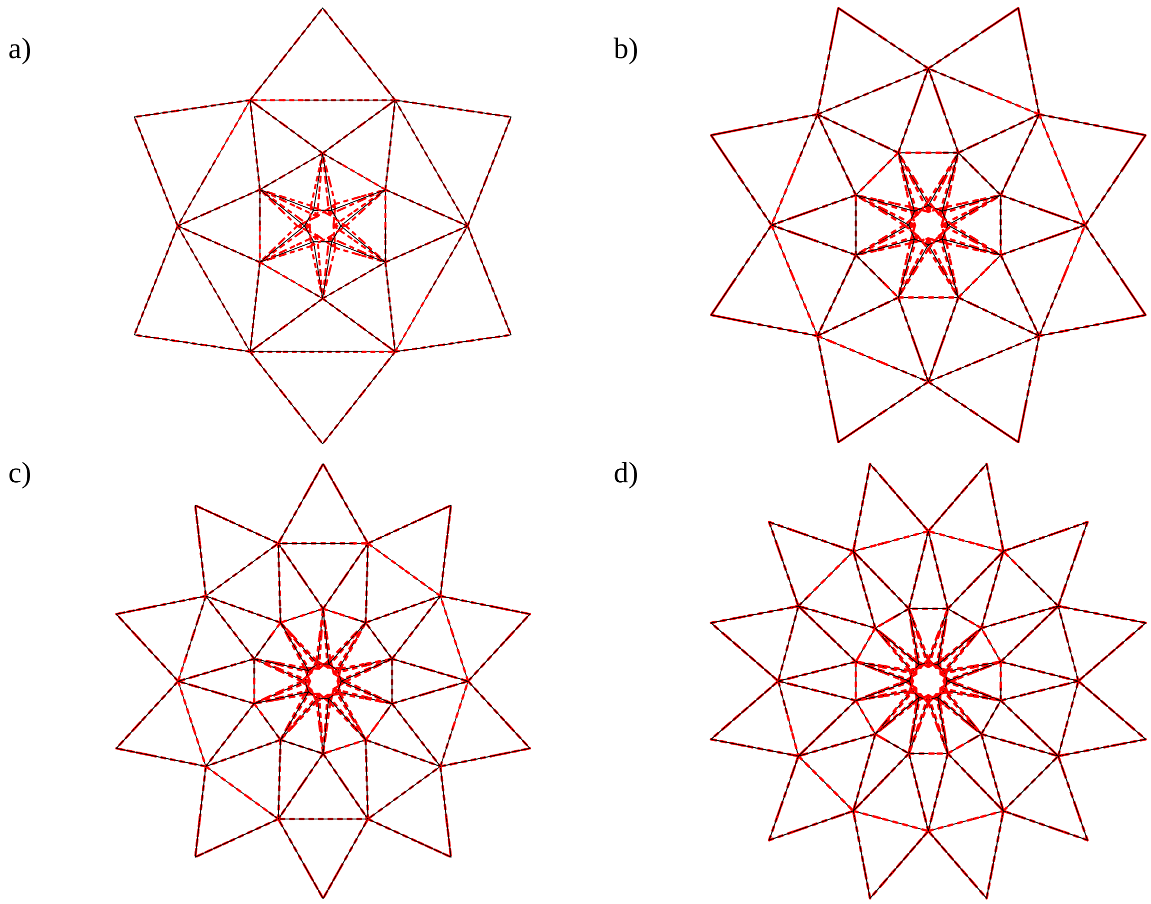

Fig. 6.30. Forms of vibrations for the L ngB dome: a) L 6B, b) L 8B, c) L 10B, d) L 12B

Conclusion of the comparison: The natural frequency corresponding to the infinitesimal mechanisms is characterized by a high sensitivity to the change in the initial prestress level. Additionally, the impact of the prestress is nonlinear. The number of load-bearing girders affects only the first natural frequency $f1$ of the type B domes (open section).

The first natural frequency $f1$ of the type A dome remains on the similar level, nonetheless small linear impact of the initial prestress level is present. Only the increasing of the number of load-bearing girders from six to eight effected the first natural frequency $f1$ of the type A dome.

Example 2

Subject of the comparison: L ngA, L ngB domes ($ng = \{6,8,10,12\}$) - additional natural frequencies dependent on the initial prestress level

Aim of the comparison: (1) Whether the initial prestress level impacts the next natural frequencies that not correspond to the infinitesimal mechanism? (2) Whether the number of load-bearing girders impacts the natural frequencies that not correspond to the infinitesimal mechanisms? (3) How does the design solution (open or close upper section) impact the dome behaviour?

The natural frequencies of the type A Levy domes do not correspond to the infinitesimal mechanisms, and the next natural frequencies ($f2$, $f3$, $f4$, $f5$) were considered for this example. As in the case of the type A Geiger domes, the type B Levy domes (L ngB) are characterized by additional natural frequencies depending on the initial prestress level. The number of dependent frequencies f_{total} depends on the number of girders (ng):

$$f_{total} = f_{nm} + f_{add}; \quad f_{add} = (ng - 4) \tag{6.3}$$

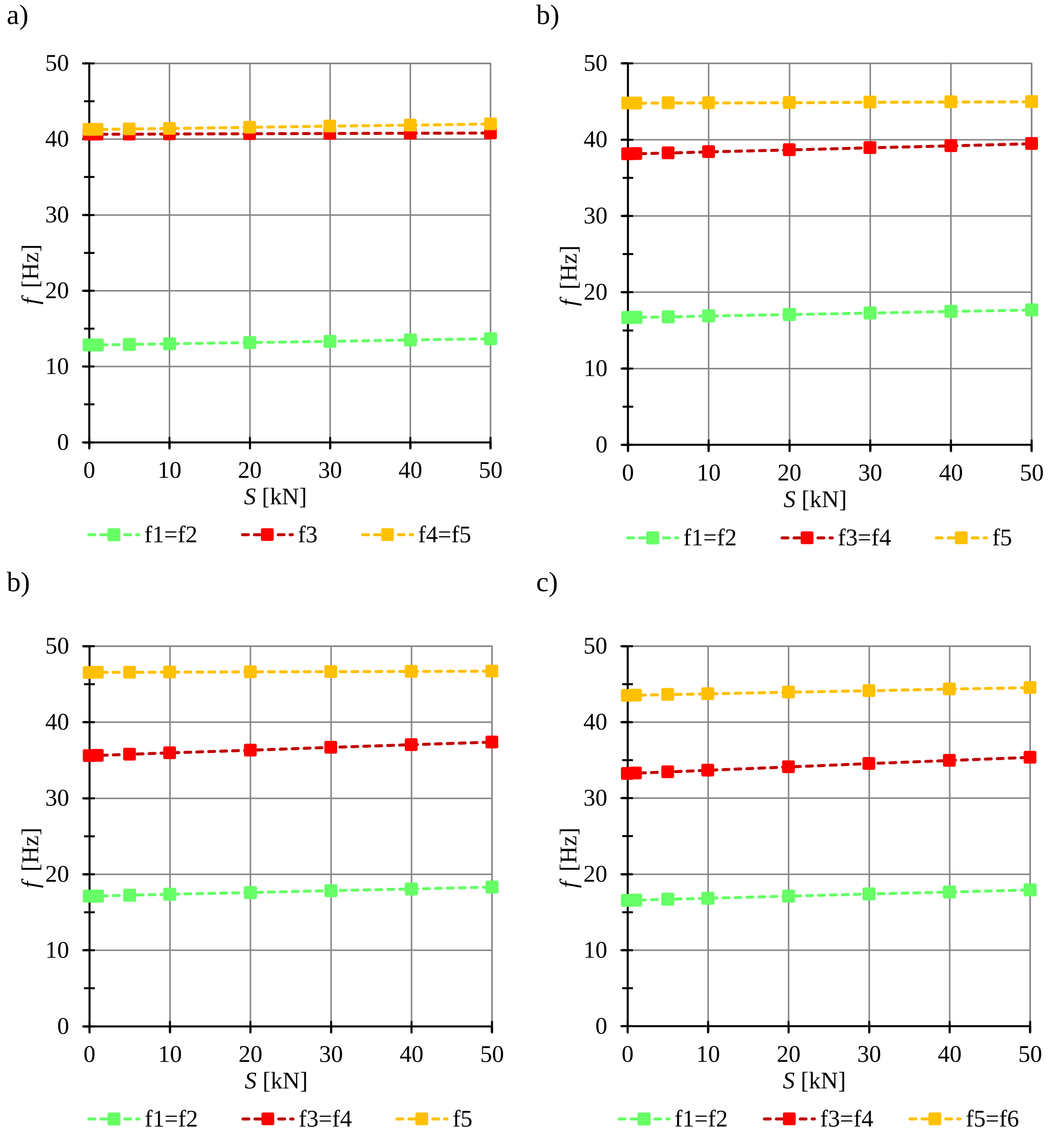

Fig. 6.31. Influence of the initial prestress S on the natural frequencies f of: a) L 6A, b) L 8A, c) L 10A, d) L 12A

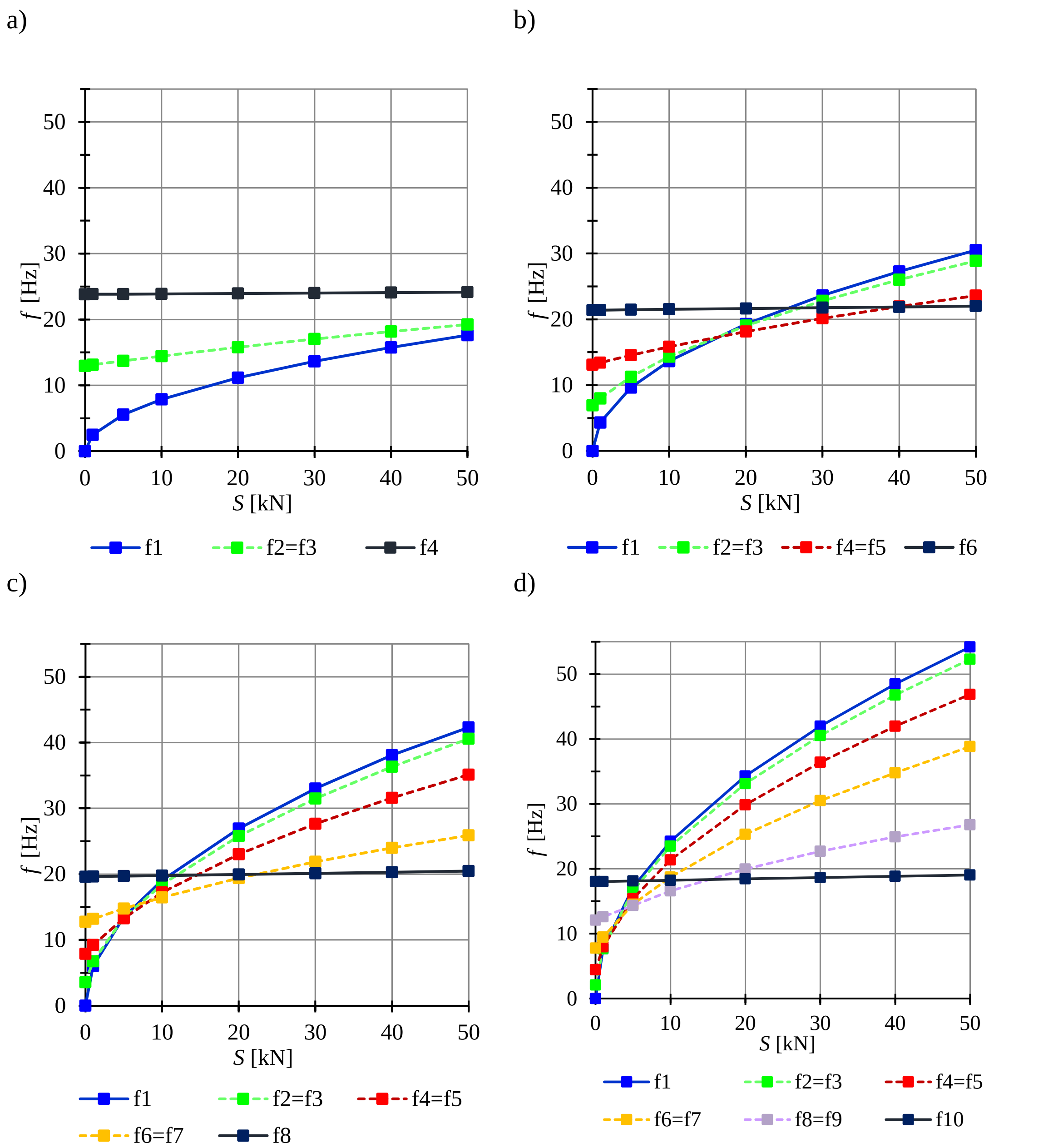

Fig. 6.32. Influence of the initial prestress S on the natural frequencies f_{nm}, f_{add}, and $f_{total+1}$ of: a) L 6B, b) L 8B, c) L 10B, d) L 12B

Fig. 6.31 and Fig. 6.32 present the natural frequencies of Levy domes. The L ngA domes natural frequencies are not corresponded to the mechanism, yet a small linear dependency on the initial prestress level can be noticed (Fig. 6.31). The number of load-bearing girder also effects the value of natural frequencies. As in the case of the Geiger domes, some frequencies characterized by same values but different forms of vibrations. The influence of the initial prestress is higher for higher frequencies.

In turn, the natural frequencies of the L ngB domes depend nonlinearly on the initial prestress level (Fig. 6.32). The first frequency is the one corresponding to the infinitesimal mechanism (f_{nm}), next are that additional dependent on the prestress (f_{add}), and first independent of prestress ($f_{total+1}$). Similarly to the Geiger domes, in the case of zero prestress ($S = 0$), the frequency f_{nm} is equal to zero, and after introducing prestress S the values f_{nm} increase in nonlinear way. For the frequencies f_{add} the absence of prestress is not resulted in zero values and the frequencies also increase nonlinearly. Nonetheless, nonlinearity and sensitivity to the changes in the initial prestress decreases for the higher frequencies. The value of the first independent frequency is on the similar level $f_{total+1} = 18.4$ Hz ÷ 23.9 Hz.

Conclusion of the comparison: In the case of type A Levy domes (L ngA) all natural frequencies characterized by the small linear dependency on the initial prestress level.

In turn, for the L ngB domes, the number of additional natural frequencies that depend on the initial prestress level highly depend on the number of load-bearing girders.

Example 3

Subject of the comparison: L 6A, L 6B domes - free frequencies

Aim of the comparison: (1) How does the initial prestress level impact free frequencies? (2) How do the value and position of load impact free frequencies?

The analysis of free frequencies of the Levy domes contains results for first frequency $f_1(P)$ of L 6A dome (Table 6.9) and L 6B dome (Table 6.9). In the case of L 6A dome, the values of natural frequency $f_1(0)$ and free frequencies $f_1(P)$ are identical for each case of load value and position. The lowest values of the S_{min} are noticed for the load position $\mathbf{P}^{(2)}$. In turn, for the L 6B dome, the lowest values of the S_{min} are for the load position $\mathbf{P}^{(1)}$ (the localization of the infinitesimal mechanism). The further the load from this position, the higher the value of the minimum prestress level.

The biggest discrepancy between natural and free frequencies is noticeable for the L 6B in the case P = 5 kN. Depending on the position, it is approximately 2%, 12%, or 4% (for $\mathbf{P}^{(1)}$, $\mathbf{P}^{(2)}$, and $\mathbf{P}^{(3)}$ respectively), in the case of minimum prestress level S_{min}. The increasing of the initial prestress level results in the convergence of the values of natural and free frequencies. In the case of the prestress level $S = 100$ kN, the difference is around 0.3%, 6%, and 1% (for $\mathbf{P}^{(1)}$, $\mathbf{P}^{(2)}$, and $\mathbf{P}^{(3)}$ respectively). In turn, for the $S = 120$ kN values are fully convergent for each load value and position.

Table 6.9. First natural $f_i(0)$ and free $f_i(P)$ frequency [Hz] for the L 6A dome

S [kN]	$f_1(0)$	$f_1(P)$					
		$\mathbf{P}^{(1)}$		$\mathbf{P}^{(2)}$		$\mathbf{P}^{(3)}$	
		1 kN	5 kN	1 kN	5 kN	1 kN	5 kN
0	12.84						
1	12.86					12.86	
4	12.91	12.91				12.91	
5	12.92	12.92		12.92		12.92	12.92
9	12.99	12.99		12.99		12.99	12.99
10	13.01	13.01		13.00		13.01	13.00
18	13.14	13.14	13.14	13.14		13.14	13.13
20	13.17	13.18	13.18	13.17		13.18	13.17
30	13.34	13.34	13.34	13.34		13.34	13.33
40	13.50	13.50	13.51	13.50		13.50	13.50
42	13.53	13.54	13.53	13.54	13.52	13.53	13.53
50	13.67	13.67	13.67	13.66	13.65	13.66	13.66
60	13.83	13.83	13.83	13.82	13.81	13.82	13.81
70	13.98	13.98	13.98	13.98	13.96	13.98	13.98
80	14.14	14.14	14.14	14.13	14.12	14.14	14.13
90	14.29	14.29	14.29	14.29	14.27	14.29	14.36
100	14.44	14.44	14.44	14.44	14.42	14.44	14.44
110	14.59	14.59	14.59	14.59	14.57	14.59	14.59
120	14.74	14.74	14.74	14.74	14.72	14.74	14.73

Table 6.10. First natural $f_i(0)$ and free $f_i(P)$ frequency [Hz] for the L 6B dome

S [kN]	$f_1(0)$	$f_1(P)$					
		$\mathbf{P}^{(1)}$		$\mathbf{P}^{(2)}$		$\mathbf{P}^{(3)}$	
		1 kN	5 kN	1 kN	5 kN	1 kN	5 kN
0	0.00						
1	2.49						
3	4.32					4.23	
5	5.57					5.51	
10	7.88			7.51		7.84	
12	8.63			8.29		8.56	8.26
20	11.15			10.88		11.11	10.84
22	11.69	11.54		11.38		11.64	11.35
30	13.65	13.53		13.42		13.62	13.38

Table 6.10. First natural $f_i(0)$ and free $f_i(P)$ frequency [Hz] for the L 6B dome - Continued

S [kN]	$f_1(0)$	$f_1(P)$					
		$\mathbf{P}^{(1)}$		$\mathbf{P}^{(2)}$		$\mathbf{P}^{(3)}$	
		1 kN	5 kN	1 kN	5 kN	1 kN	5 kN
40	15.76	15.65		15.55		15.74	15.49
48	17.25	17.17		17.05	15.16	17.23	16.98
50	17.62	17.53		17.41	15.53	17.59	17.34
60	19.31	19.22		19.07	17.23	19.28	18.98
70	20.85	20.77		20.55	18.75	20.81	20.42
80	22.13	22.01		21.81	20.11	22.08	21.66
90	23.01	22.91		22.85	21.35	22.98	22.70
95	23.44	23.34	22.94	23.31	21.92	23.41	23.18
100	23.85	23.76	23.38	23.75	22.48	23.83	23.63
110	24.57	24.57	24.24	24.57	23.52	24.57	24.49
120	24.64	24.67	24.63	24.64	24.66	24.64	24.63

Conclusion of the comparison: In the comparison to the type A dome (L 6A), the free frequencies of the type B dome (L 6B) are highly dependent on the initial prestress level. The dependency on the load value and position is significant only in low levels of initial prestress, an increase in the initial prestress level results in a decrease in the sensitivity of the free frequencies to the load. In the case of type A dome (L 6A), the natural frequencies do not depend neither on the load value nor the position.

6.4.4. Dynamic stability analysis

The dynamic stability analysis of a small-scale Levy domes is considered. Particularly, the influence of the initial prestress level on the shape and range of unstable regions is analyzed. A few examples are provided in order to compare the behaviour of different domes under the periodic load. Firstly, the case of the load position $\mathbf{P}^{(1)}$ (Example 1), next the load position $\mathbf{P}^{(2)}$ (Example 2), and the load position $\mathbf{P}^{(3)}$ (Example 3). The consideration is concluded with summarized results (Example 4).

Example 1

Subject of the comparison: L 6A (Fig. 6.33a) and L 6B (Fig. 6.33b) domes, load position $\mathbf{P}^{(1)}$ – unstable regions

<u>*Aim of the comparison:*</u> (1) Does the initial prestress level affect unstable regions in the case of load position $\mathbf{P}^{(1)}$? (2) Does the design solution (close or open upper section) affect unstable regions in the case of load position $\mathbf{P}^{(1)}$?

a) **L 6A**
P = 1 kN → S_{min} = 4 kN
P = 5 kN → S_{min} = 18 kN

b) **L 6B**
P = 1 kN → S_{min} = 22 kN
P = 5 kN → S_{min} = 95 kN

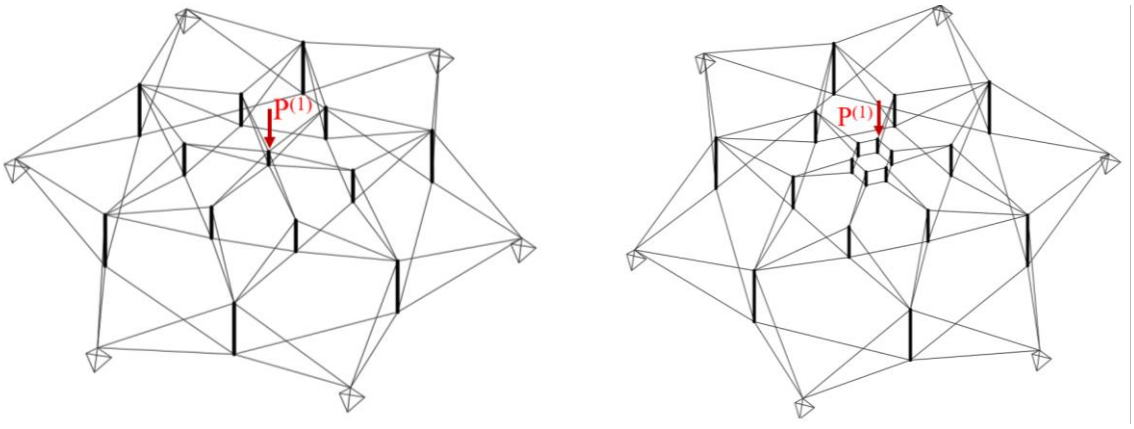

Fig. 6.33. External load application in the case of position $\mathbf{P}^{(1)}$ for: a) L 6A, b) L 6B

The first example concerns the impact of the initial prestress level on the unstable regions of L 6A and L 6B domes, in the case of the load position $\mathbf{P}^{(1)}$. The selected instability regions are presented for three levels of initial prestress, and two load variants P $=$ 1 kN and P $=$ 5 kN (Table 6.11). In the case of the L 6A dome, the initial prestress level has no impact on the resonant frequencies due to the absence of the infinitesimal mechanism, the frequency ($\eta 1$(A)) remains on the similar level $\eta 1$ = 25.8 Hz ÷27.7 Hz. The situation is opposite for the L 6B dome. The resonant frequency ($\eta 1$(B)) depend on both the initial prestress level and the external load. The small instability region can be noticed in the case of load variant P $=$ 5 kN for the S_{min} level of initial prestress.

The L 6B dome characterized by the additional resonant frequencies' dependent on the initial prestress level (see section 6.4.3). The frequencies $\eta 2$, $\eta 3$, $\eta 4$, and $\eta 5$ do not depend on the pulsatility index υ, the boundaries of instability regions coincide. Nonetheless, they are sensitive to change in the initial prestress level (Table 6.12). For the L 6A dome the situation is similar, however, the dependency on the initial prestress is significantly lover. The relative increase (RI) of L 6A dome is about 1.08% - 14.18%, while for L 6B it is around 56.64% - 6.19% (in the case P $=$ 1 kN). The increase in the external load led to a decrease in the influence of the initial prestress. The RI is even five times smaller in the case of load P $=$ 5 kN than for the P $=$ 1 kN for the L 6B dome (for frequencies $\eta 2$, $\eta 3$).

Table 6.11. Limits of first instability regions of the L 6A and L 6B domes for load position $\mathbf{P}^{(1)}$

	$S_{min}(\mathrm{A}) = 4$ kN $S_{min}(\mathrm{B}) = 22$ kN	$S = 40$ kN	$S = 60$ kN
1 kN	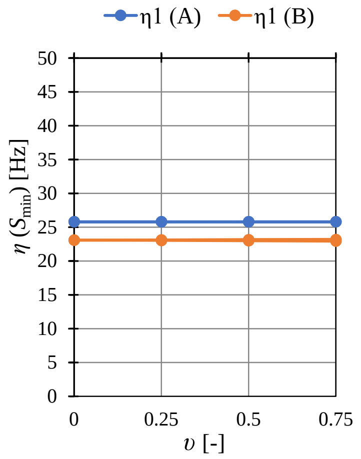	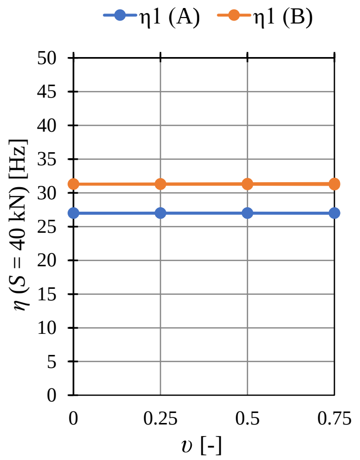	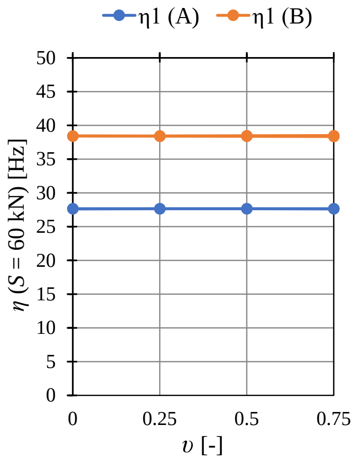
	$S_{min}(\mathrm{A}) = 18$ kN $S_{min}(\mathrm{B}) = 95$ kN	$S_{min} + 15$ kN	$S_{min} + 25$ kN
5 kN	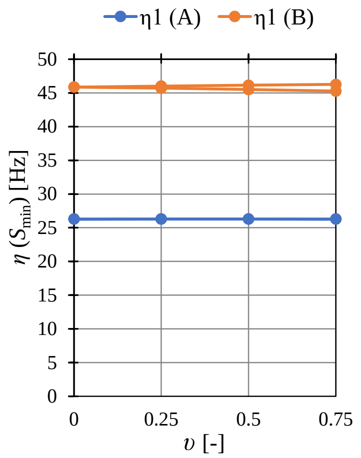	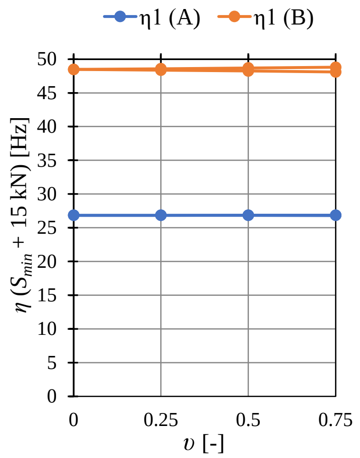	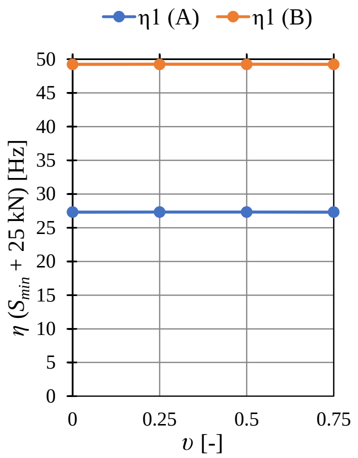

Table 6.12. Resonant frequencies of the L 6A and L 6B domes in the case of load position $\mathbf{P}^{(1)}$

	L 6A			**L 6B**				
	Resonant frequency $\eta(\upsilon = 0 \div 0.75) = \mathrm{const.}$							
	$\eta2$	$\eta3$	$\eta4$	$\eta2$	$\eta3$	$\eta4$	$\eta5$	$\eta6$
P = 1 kN								
S_{min}	25.82	81.33	82.67	31.57	32.38	47.93	47.95	74.10
S_{max}	29.48	82.21	85.97	49.28	50.72	50.90	54.48	74.71
RI*	14.18%	1.08%	3.99%	56.10%	56.64%	6.19%	13.62%	0.82%
P = 5 kN								
S_{min}	26.29	81.43	83.09	47.08	47.93	48.91	48.96	74.56
S_{max}	29.48	82.20	85.99	49.29	50.11	50.98	53.98	74.71
RI*	12.13%	0.95%	3.49%	4.69%	4.55%	4.23%	10.25%	0.20%

RI* – relative increase: $[(\eta(\mathrm{S_{min}}) - \eta(S_{max}))/\eta(S_{min}) \cdot 100\%]$

Fig. 6.34 presents the impact of the initial prestress level on the range and distribution of instability regions. The results are provided only for the L 6B dome. The instability regions of L 6A dome are insensitive to the change in the prestress. The increase of the initial prestress level results in the gradual reduction of the areas of instability regions, however, for the $S =$ 80 kN the unpredictable growth occurs (in the case P = 1 kN) (Fig. 6.34a). In the case of $S >$ 80 kN, the behaviour is the same to the case P = 5 kN (Fig. 6.34b). For both cases, the noticeable decrease in the area of the unstable region occurs at the level $S = 110 \div 115$ kN. The decrease is about 66% and 77%, for P = 1 kN and P = 5 kN respectively.

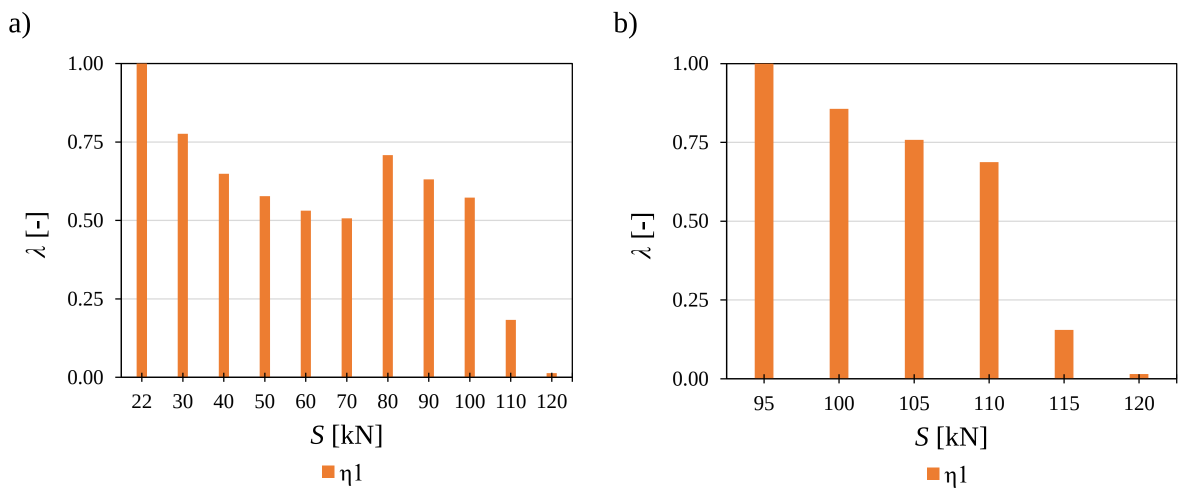

Fig. 6.34. Influence of the initial prestress level S on the range of unstable region of: a) L 6B for P = 1 kN, b) L 6B for P = 5 kN

<u>*Conclusion of the comparison:*</u> The dynamic stability analysis shows that the behaviour of L 6A and L 6B is completely different. The differences are related to the occurrence of the infinitesimal mechanisms. Whereas, the increasing of the initial prestress level results in the increasing of resonant frequencies values and narrowing of the unstable regions of type B dome. In turn, the type A dome is insensitive to the change. Additionally, the impact of the initial prestress level is greater as external load increases.

Example 2

<u>*Subject of the comparison:*</u> L 6A (Fig. 6.35a) and L 6B (Fig. 6.35b) domes, load position $\mathbf{P}^{(2)}$ – unstable regions

<u>*Aim of the comparison:*</u> (1) Does the initial prestress level affect unstable regions in the case of load position $\mathbf{P}^{(2)}$? (2) Does the design solution (close or open upper section) affect unstable regions in the case of load position $\mathbf{P}^{(2)}$?

a) **L 6A**
P = 1 kN $\rightarrow$ S_{min} = 9 kN
P = 5 kN $\rightarrow$ S_{min} = 42 kN

b) **L 6B**
P = 1 kN $\rightarrow$ S_{min} = 10 kN
P = 5 kN $\rightarrow$ S_{min} = 50 kN

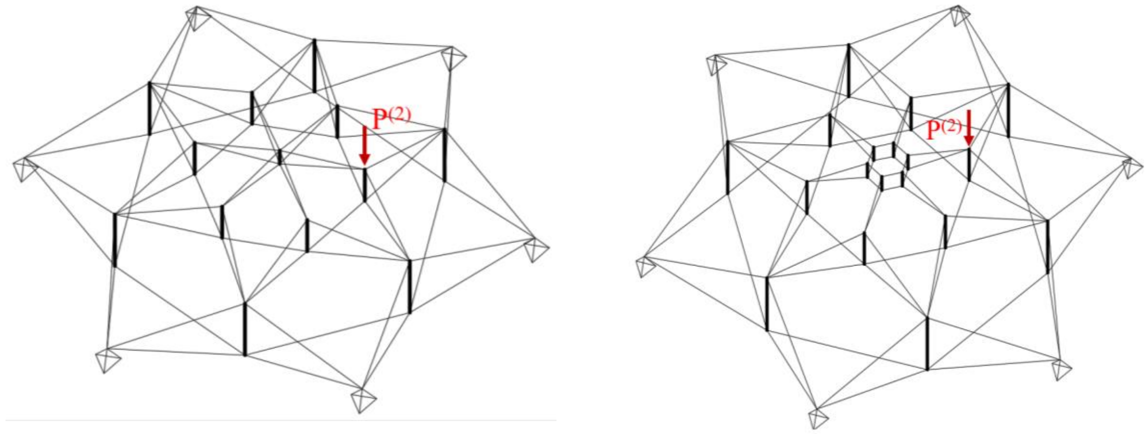

Fig. 6.35. External load application in the case of position $\mathbf{P}^{(2)}$ for: a) L 6A, b) L 6B

The second example concerns influence of the initial prestress level on the unstable regions in the case of load position $\mathbf{P}^{(2)}$ (Table 6.13). The dynamic behaviour is presented for load conditions P $=$ 1 kN and P $=$ 5 kN, and three levels of initial prestress. In this case, the S_{min} is on the similar level, however, the instability regions distribution is different. As in the Example 1, the resonant frequency $\eta 1$ of the L 6A is on the same level, do not depend on the pulsatility index υ, and the risk of the excitation of unstable motion decreases. In turn, for the L 6B dome, the increasing of external load resulted in the widening of the limits of instability region.

Next, the impact of the initial prestress level on the range and distribution of instability regions is compared (Fig. 6.36). Similarly to the Example 1, the behaviour of instability regions under the influence of the initial prestress level is characterized by the gradual reduction and then increase, in the case of P $=$ 1 kN. In the case of L 6B dome and P $=$ 1 kN, the noticeable reduction of unstable region area at level $S = 110$ kN was approximately 92%, and only 40% for the P $=$ 5 kN.

Fig. 6.37 presents instability regions corresponding to resonant frequencies dependent on the initial prestress level ($\eta 1$, $\eta 2$, $\eta 3$, $\eta 4$, $\eta 5$) and one independent frequency ($\eta 6$). Only the first three frequencies ($\eta 1$, $\eta 2$, and $\eta 3$) are characterized by the instability regions wide enough to increase the risk of occurring excitation of unstable motion. The complete narrowing of limit of instability regions is noticed for the frequencies $\eta 4$, $\eta 5$, and $\eta 6$.

Table 6.13. Limits of main instability regions of the L 6A and L 6B domes for load position $\mathbf{P}^{(2)}$

<table>
<tr><td></td><td>$S_{min}(\mathrm{A}) = 5$ kN
$S_{min}(\mathrm{B}) = 10$ kN</td><td>$S = 20$ kN</td><td>$S = 40$ kN</td></tr>
<tr><td>1 kN</td><td>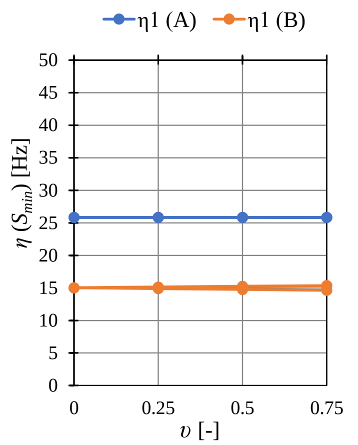
</td><td>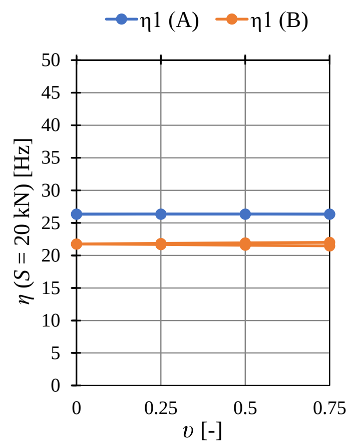
</td><td>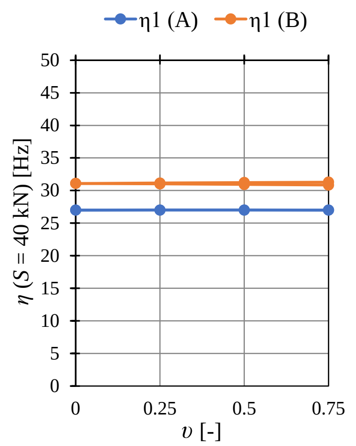
</td></tr>
<tr><td></td><td>$S_{min}(\mathrm{A}) = 42$ kN
$S_{min}(\mathrm{B}) = 48$ kN</td><td>$S = 80$ kN</td><td>$S = 110$ kN</td></tr>
<tr><td>5 kN</td><td>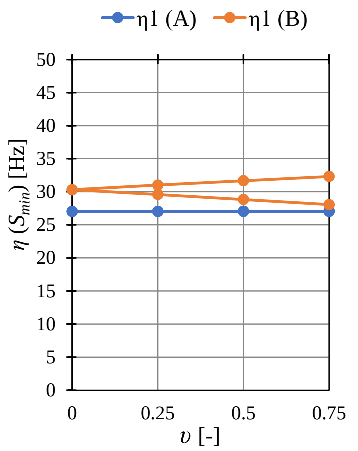
</td><td>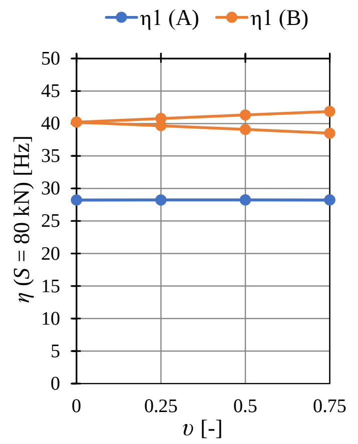
</td><td>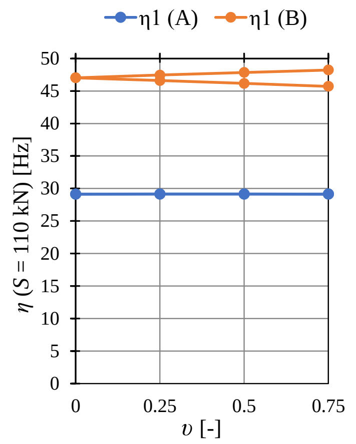
</td></tr>
</table>

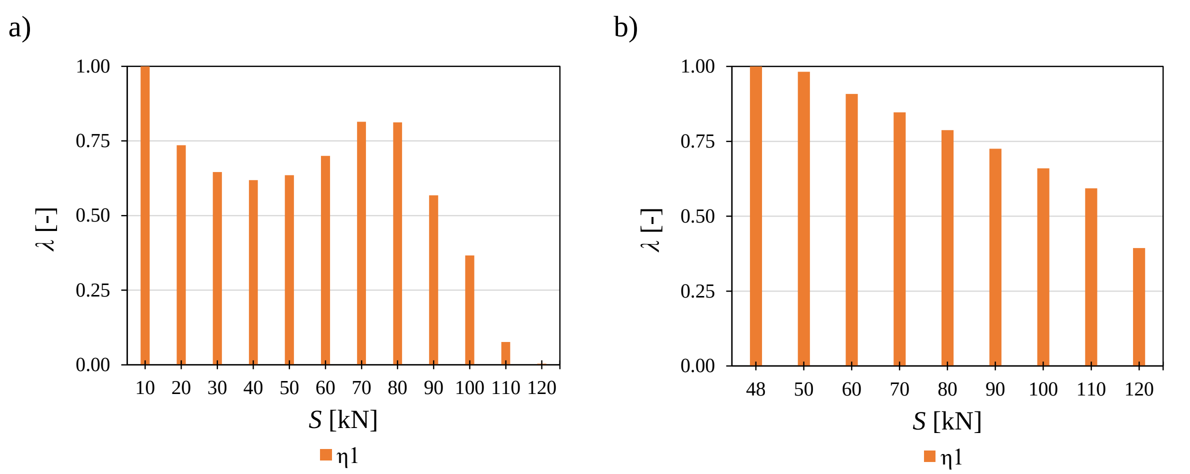

Fig. 6.36. Influence of the initial prestress level S on the range of unstable regions of: a) L 6B for P = 1 kN, b) L 6B for P = 5 kN

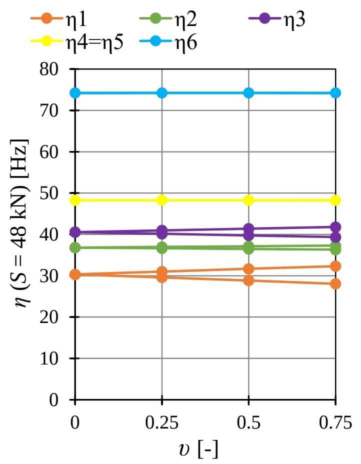

Fig. 6.37. Limits of six instability regions of the L 6B dome (S_{min} = 48 kN), for the load P = 5 kN

<u>*Conclusion of the comparison:*</u> The dynamic response of the L 6A dome remains the same in comparison to Example 1, while the L 6B dome is characterized by a wider unstable region that occurs even at the high level of the initial prestress. Comparing all resonant frequencies dependent on the initial prestress level, the one corresponding to the mechanism is characterized by the widest unstable region.

Example 3

<u>*Subject of the comparison:*</u> L 6A (Fig. 6.38a) and L 6B (Fig. 6.38b) domes, load position $\mathbf{P}^{(3)}$ – unstable regions

<u>*Aim of the comparison:*</u> (1) Does the initial prestress level affect unstable regions in the case of load position $\mathbf{P}^{(3)}$? (2) Does the design solution (close or open upper section) affect unstable regions in the case of load position $\mathbf{P}^{(3)}$?

a) **L 6A**
P = 1 kN → S_{min} = 1 kN
P = 5 kN → S_{min} = 5 kN

b) **L 6B**
P = 1 kN → S_{min} = 3 kN
P = 5 kN → S_{min} = 12 kN

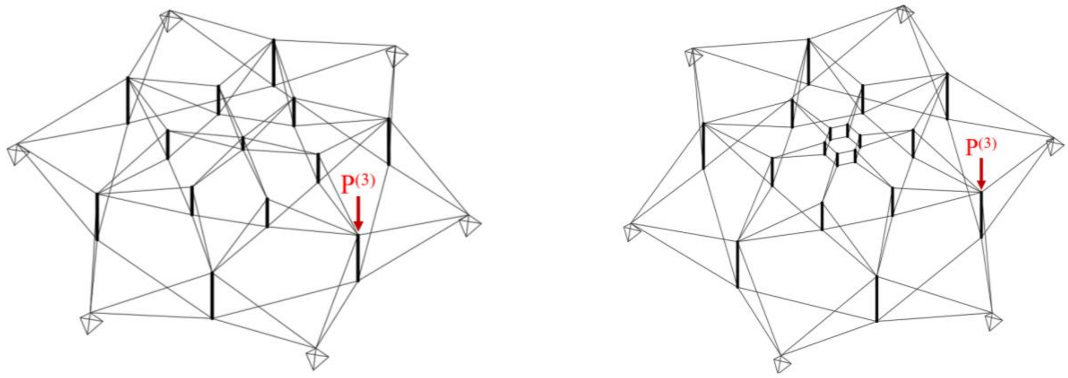

Fig. 6.38. External load application in the case of position $\mathbf{P}^{(1)}$ for: a) L 6A, b) L 6B

The next considered example concerns the dynamic behaviour of the considered domes in the case of the load position $\mathbf{P}^{(3)}$ (Table 6.14). The L 6B dome is characterized by the lowest resonant frequency level in comparison to Example 1 and Example 2, due to the fact that the external load is positioned farthest away from the infinitesimal mechanism. In the case of low load value, both domes are characterized by the absence of instability regions, however, the increased external load resulted in the occurrence of instability region of L 6B dome.

The impact of the initial prestress level on the distribution of the range and distribution of instability regions (Fig. 6.39) is similar to Example 1 and Example 2.

Table 6.14. Limits of main instability regions of the L 6A and L 6B domes for load position $\mathbf{P}^{(3)}$

<table>
<tr><td></td><td>$S_{min}(\mathrm{A}) = 1$ kN
$S_{min}(\mathrm{B}) = 3$ kN</td><td>$S = 20$ kN</td><td>$S = 40$ kN</td></tr>
<tr><td>1 kN</td><td>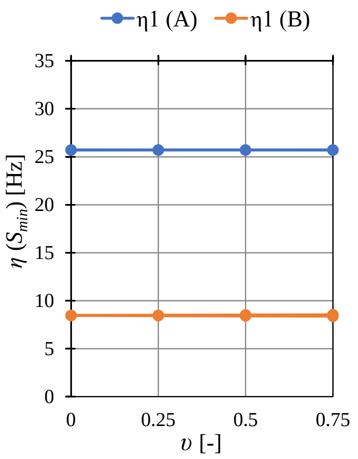
</td><td>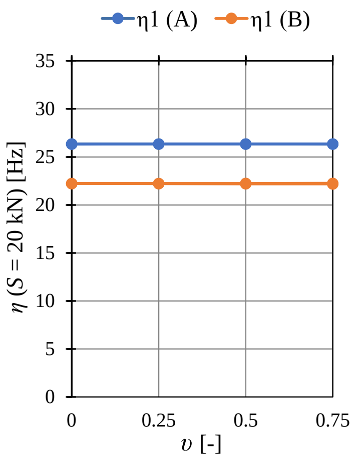
</td><td>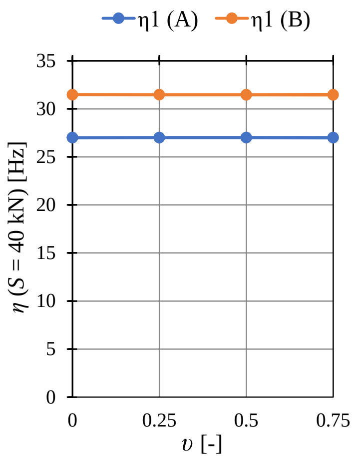
</td></tr>
<tr><td></td><td>$S_{min}(\mathrm{A}) = 5$ kN
$S_{min}(\mathrm{B}) = 12$ kN</td><td>$S = 30$ kN</td><td>$S = 50$ kN</td></tr>
<tr><td>5 kN</td><td>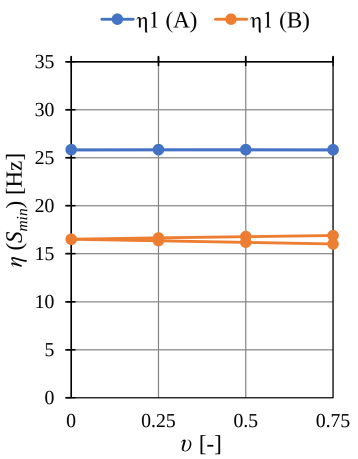
</td><td>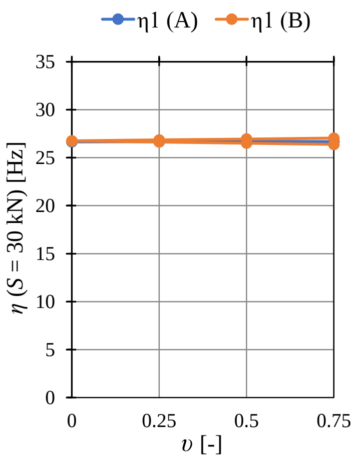
</td><td>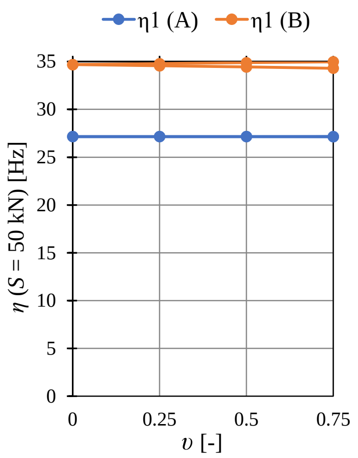
</td></tr>
</table>

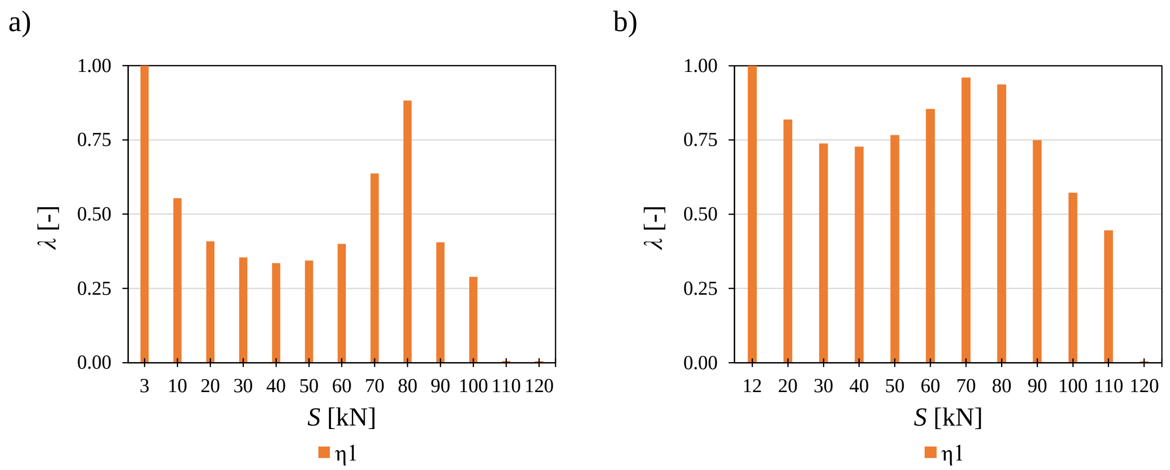

Fig. 6.39. Influence of the initial prestress level S on the range of unstable region of: a) L 6B for P = 1 kN, b) L 6B for P = 5 kN

<u>*Conclusion of the comparison:*</u> In the comparison to Example 2, the L 6B characterized by the smaller unstable regions, whilst the behaviour of L 6A dome remains the same. The occurrence of unstable regions noticed only at the low level of the initial prestress.

Example 4

<u>*Subject of the comparison:*</u> L 6A, L 6B – unstable regions

<u>*Aim of the comparison:*</u> (1) How do the load value and position affect the distribution of unstable regions? (2) For which dome the probability of the unstable regions is least likely to occur? (3) What is the most optimal recommended initial prestress level?

The summarized results present the distribution of instability regions that correspond to the first resonant frequency, in the case of different load situations (Fig. 6.40). The external load is equal to 1 kN (1) and 5 kN (5), whereas different load positions are defined as (1,2, or 3). The caption "LA 1(3)" stands for type A dome loaded with force 1 kN applied in position 3. The results are presented for the S_{min} level of prestress. In the case of type A dome (LA), neither load value nor position influences the level of resonant frequency. The limits of instability regions completely overlap. In turn, for the dome type B (LB), the resonant frequency depends on the external load. The load position $\mathbf{P}^{(1)}$ results in the highest resonant frequency, thus the widest instability region occurs in the situation $\mathbf{P}^{(2)}$ and P = 5 kN. The behaviour of L 6B dome is similar to the MG 6B dome (Geiger dome, modified, type B). The distribution of areas of instability regions is the same.

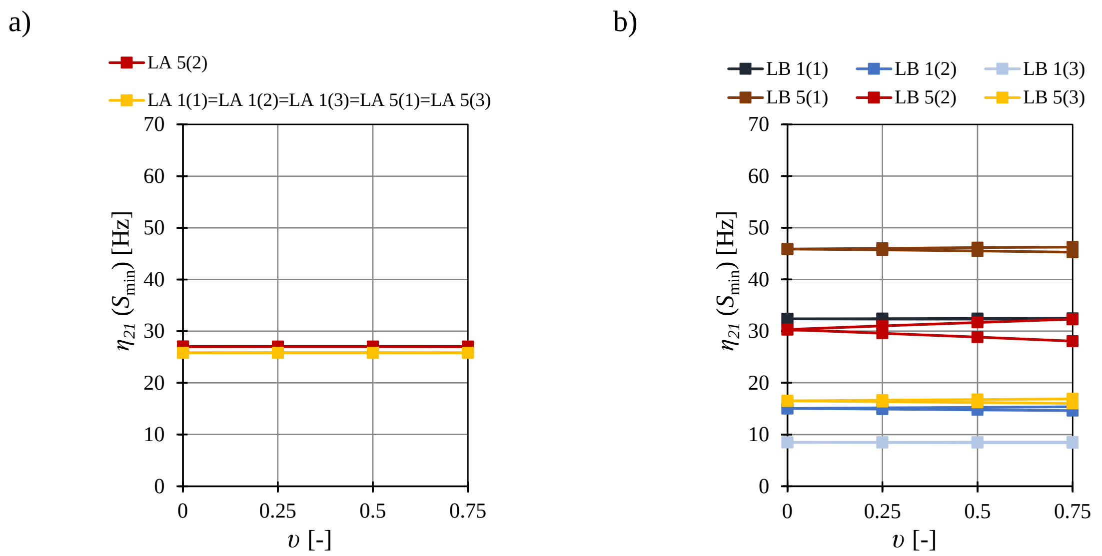

Fig. 6.40. Influence of the initial prestress level S on the range of unstable region of: a) L 6A, b) L 6B

The influence of the initial prestress level on the areas of the unstable regions is presented in Fig. 6.41. In the case of the LA dome, the impact of the initial prestress is absent, the behaviour is similar to the MG 6A dome (Geiger dome, modified, type A). In turn, the impact is nonlinear for the LB dome. However, the graph shape and the relation are different, than in the case of the MG 6B dome. The initial prestress level has an impact on the area of unstable regions even at the high levels of the prestress, unlike the Geiger dome.

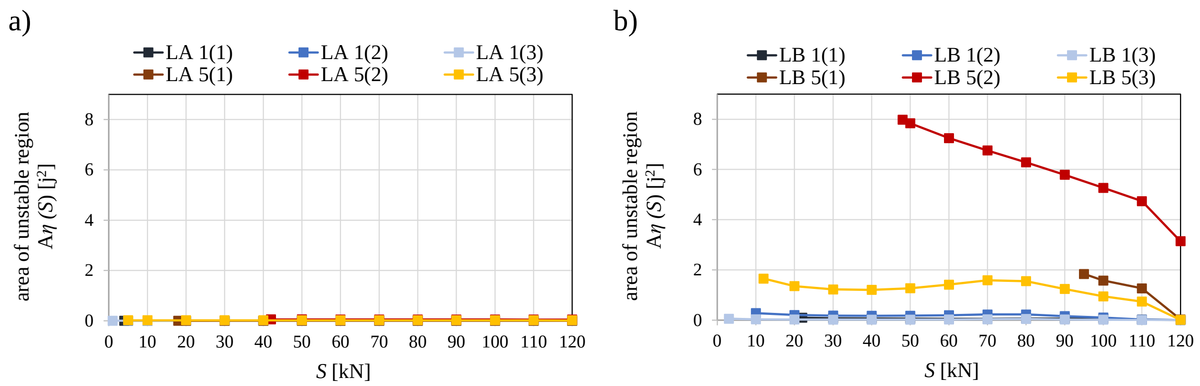

Fig. 6.41. Influence of the initial prestress level S on the area of unstable region A_η: a) L 6A, b) L 6B

Conclusion of the comparison: The load value and position have no impact on the unstable regions in the case of L 6A dome. In turn, for the L 6B dome the situation is opposite, however, only the load value effects the distribution of the unstable regions. Similarly to the Geiger domes, the probability of the occurrence of the unstable regions is getting smaller with an increasing of the initial prestress level, nonetheless, the level of prestress is significantly higher than in the case of Geiger domes. The most optimal recommended initial prestress level is above $S = 100$ kN.

6.5. Summary

The behaviour of the Levy dome is significantly different in comparison to the Geiger dome. The structures' response to the external load highly depends on the presence of the infinitesimal mechanism. The type A Levy dome (without the infinitesimal mechanism) behaves like a traditional rod-like structure, and the initial prestress level has little impact on the static parameters of the dome. In turn, type B Levy dome (with infinitesimal mechanism) behaves similarly to the Geiger dome, nonetheless, the impact of the initial prestress level is significantly smaller. Additionally, the type A dome characterized by the lower minimum prestress level.

The dynamic analysis of Levy domes shows, that the natural frequencies level of the type A domes is not related to the number of load-bearing girders of the structure, and only a little linear influence of the initial prestress level can be observed. On the other hand, in the case of type B domes, the natural frequencies level highly depends on a number of load-bearing girders and high nonlinear impact of the initial prestress level occurs. Additionally, the type B domes are characterized by the additional natural frequencies that depend on the initial prestress level. The situation is similar for free frequencies. In the case of type A Levy dome, free frequencies do not depend on neither the initial prestress level, nor load value or position. In turn, for the type B levy dome the situation is opposite, however at the maximum prestress level $S = 120$ kN the values of the natural and free frequencies are the same (the discrepancy less than 1%).

In the case of dynamic stability analysis, the occurrence of unstable regions is detected only for type B dome. The widest unstable region occurs in the case of load position $\mathbf{P}^{(\mathbf{2})}$ and $\mathrm{P} = 5$ kN, where the increase in the initial prestress level didn't result in the narrowing of limits. The limits of unstable regions of type A dome fully coincide, and the dome is insensitive to the change to the change in the resonant frequencies.

The results of the analysis show that the ability to control the dome behaviour by adjusting the initial prestress level is possible only for type B dome Levy dome. However, this dome is characterized by higher minimum prestress level and is more sensitive to the external load. In turn, for the type A dome initial prestress level has little impact, but the dome is less sensitive to the external load condition.

7. Conclusions

The dissertation thesis concerns the dynamic stability of tensegrity domes. The research was conducted in regard to the influence of the initial prestress level on the static parameters (displacements, stiffness, maximum effort) and dynamic parameters (natural and free frequencies of vibrations, unstable regions). The analysis of the two most known tensegrity domes, i.e., Geiger dome and Levy dome, was performed. The analyzed domes were presented with different number of load-bearing girders, structural modifications, and subjected to the different external load situations in order to compare structures response. The structural modification of the Geiger dome relies on changing the upper section of the dome, replacing the original open upper section with the single strut (closed upper section), and introducing additional circumferential cables. In terms of the Levy dome, only the modification of the upper section was introduced. The aim of the work was to answer the questions posed in Chapter 1 (research purpose and scope).

i. How does the initial prestress impact static parameters of the domes with and without infinitesimal mechanisms?

It is known from the literature, that initial prestress level impacts static parameters of the structure with infinitesimal mechanisms. This is in the case of Geiger domes under asymmetrical load. The Geiger domes are characterized by a dozen (several dozens) of infinitesimal mechanisms, the number of which depends on the number of load-bearing girders and design configuration. The mechanisms are related to the geometric variability of the entire dome. The influence of the initial prestress level on static parameters of Geiger domes is always significant. The impact on the displacements is nonlinear and greater at the low values of the initial prestress. The stiffness of the dome increases linearly, even up to 13 times. The exception is a symmetrical load applied on the dome. In this case, the influence of the initial prestress level is absent, because the resulting displacements are inconsistent with the infinitesimal mechanism.

In the case of Levy domes, only the dome type with an open upper section (type B Levy dome) was characterized by one infinitesimal mechanism. However, the mechanism is related only to the upper section of the dome. For the type B Levy dome (with the infinitesimal mechanism), the influence of the initial prestress is similar but significantly smaller. Depending on the load type, a small nonlinear or linear impact on the displacements was observed. The stiffness of the dome increases linearly only up to 3 times. In turn, for the type A Levy dome (without the infinitesimal mechanism), the low linear impact of the initial prestress level on the displacements and stiffness can be noticed, which in comparison to the Geiger domes is almost absent.

ii. *What is the relation between the initial prestress level and vibration frequencies that correspond to the infinitesimal mechanisms?*

The dynamic analysis of Geiger domes showed the nonlinear relation between natural frequencies corresponding to the mechanism and initial prestress level. In the case of type A domes (regular and modified), the number of load-bearing girders did not affect the level of natural frequencies, and frequencies were less sensitive to the change in the initial prestress level. In turn, for the type B Geiger domes, the situation is opposite. In the case of free frequencies of Geiger domes, the discrepancy between natural and free frequencies (for different load positions) was noticed only for low levels of initial prestress. The increase of the prestress results in the convergence of the values of frequencies.

In the case of the type B Levy dome, there is only one natural frequency corresponding to the infinitesimal mechanism, and the impact of the initial prestress level is nonlinear. For the free frequencies, the situation is similar to the Geiger domes. The type A Levy dome is not characterized by the mechanism, and therefore there are no frequencies correspond to the mechanism.

iii. *What is the relation between the initial prestress level and vibration frequencies that do not correspond to the infinitesimal mechanisms?*

During the dynamic analysis, it was noticed that some natural frequencies that do not correspond to the infinitesimal mechanisms are influenced by the initial prestress level. This is in the case of type A Geiger domes (regular and modified) and type B Levy domes. The number of these additional frequencies depends on the number of load-bearing girders of the dome. In the case of Geiger domes, the impact of the initial prestress on natural frequencies not corresponding to the infinitesimal mechanism was linear, thus, for the Levy dome – nonlinear. The influence of the initial prestress level increases with the number of load-bearing girders.

iv. *How does the initial prestress level influence the distribution and range of unstable regions?*

The dynamic stability analysis shows that the widest unstable regions occur at the minimum initial prestress level. Additionally, the widest regions are related to the last resonant frequency correspond to the mechanism. Nonetheless, an increasing of the prestress results in the complete or partial narrowing of the unstable regions. The resonant frequencies (unstable regions) of Geiger's dome are more sensitive to the change in the initial prestress level, thus increasing prestress to the maximum level resulted in a complete narrowing of areas of regions for each considered example. In turn, for the type B Levy dome, due to a little sensitivity to the change in the initial prestress level, some cases are characterized by wide unstable regions even at the maximum prestress. The type A Levy dome is not characterized by the presence of unstable regions and the initial prestress level has no impact on the resonant frequencies.

v. *How does the position and value of the external load influence the static and dynamic response of the dome?*

For the purpose of the analysis, several types of external load conditions were selected. The vertical force was applied in different positions on the load-bearing girder and two variants of the force values were presented. For the considered domes, different positions/values of the external load resulted in the change of the minimum prestress level. The exception was the Geiger patent dome (regular type B Geiger dome with 6 load-bearing girders). In the case of Geiger domes, significant was symmetrically distributed external load. This load type is inconsistent with the infinitesimal mechanisms of the dome, thus, the influence of the initial prestress level on static parameters is absent. For the type B Levy dome, the load positioned in the upper section requires the highest minimum prestress level. This is due to the location of one infinitesimal mechanism in the upper section of the dome. In turn, for the type A Levy dome, the load positioned in the middle section of the dome causes the higher minimum prestress level. For each considered dome, the greater impact on static and dynamic parameters had rather the load value than position.

vi. *How does the structural modification influence the static and dynamic response of the dome?*

In the case of the Geiger domes, the closed upper section resulted in the decreasing number of the infinitesimal mechanisms, thus, decreasing sensitivity to the change in the initial prestress. In turn, modification of cable layout (additional circumferential cables) didn't result in the improvement of the static response of the structure. Additionally, in the case of type B Geiger domes, extra cables introduced a negative impact on the dynamic stability of the dome.

The open upper section in the Levy domes (type B dome) results in the appearance of the infinitesimal mechanism, i.e., the ability to control static and dynamic parameters of the structure. It is worth mentioning, that type B Levy domes are characterized by significantly higher minimum prestress level and wide unstable regions. In terms of the dynamic response, type A Levy domes are more stable.

i. What are the design guidelines for the application of tensegrity domes?

The application of tensegrity domes in the real structure is a very demanding process. The existing tensegrity structures around the world are the ones without the infinitesimal mechanisms. In turn, the domes analyzed in this work characterized by the infinitesimal mechanisms, can be used for example for temporary structures, e.g., arenas, roofs, and festival facilities. In terms of applying these types of structures to real objects, additional analyses must be conducted (including experimental studies). The analyses must include the physical nonlinearity of cables and local stability analysis (the local buckling of single elements).

Conducted analysis confirmed the following hypothesis:

1. Control of static and dynamic parameters is only possible for tensegrity domes that exhibit an infinitesimal mechanism.
2. Structural modifications can both improve and impair domes' response to the external load.
3. The initial prestress affects the distribution of dynamic unstable regions in tensegrity domes subjected to periodic loads.

The consideration in the thesis is summarized in the Table 7.1:

Table 7.1. Summary of thesis considerations

	Geiger domes		**Levy domes**	
	Type A	**Type B**	**Type A**	**Type B**
Tensegrity features	• Self-stress states • Infinitesimal mechanisms	• Self-stress states • Infinitesimal mechanisms	• Self-stress state	• Self-stress state • Infinitesimal mechanism
Influence of the initial prestress level on following parameters:				
Static parameters				
Displacements	significant	significant	absent	insignificant
Maximum effort	significant	significant	significant	significant
Stiffness	significant	significant	insignificant	insignificant
Dynamic parameters				
Natural frequencies *and* **Free frequencies**	those, that correspond to the mechanism and additional dependent on the number of the load-bearing girders	those, that correspond to the mechanism	insignificant	those, that correspond to the mechanism and additional dependent on the number of the load-bearing girders
Unstable regions	significant	significant	absent	insignificant

List of figures

List of tables

References

1. Motro R. (2012) Tensegrity: from Art to Structural Engineering. *IASS-APCS Symposium, May 2012, Seoul, Sout Korea*.
2. Pugh A. (1976) *An introduction to tensegrity*. Berkley, USA: University of California Press.
3. Motro R. (2003) Tensegrity. Structural systems of the future. *Kogan Page Science, London and Sterling, VA.*
4. Skelton R.E., de Oliveira M.C. (2009) *Tensegrity systems*. San Diego, USA: Springer.
5. Snelson K. (2013) *Art and Ideas*. NY: Kenneth Snelson In Association With Marlborough Gallery.
6. Zhang J.Y., Ohsaki M. (2015) *Tensegrity Structures: Form, Stability, and Symmetry*. Springer, Japan.
7. Markocki B., Oleszek R. (2011) Konstrukcje tensegrity w zastosowaniu mostowym na przykładzie koncepcji kładki KL-3 nad trasą S-7 Salomea-Wolica. *VII Krajowa Konferencja Estetyka Mostów, Warszawa*.
8. Markocki B., Oleszek R. (2011) Koncepcja kładki dla pieszych o konstrukcji tensegrity w Magdalence koło Warszawy. *Inżynieria i Budownictwo*, **10**(2011): 553–557.
9. Bieniek Z. (2012) *Tensegrity – integrating tension in architectural systems (in polish)*. Rzeszów: Publishing house of the Rzeszów University of Technology, Monograph no. 96/12.
10. Bieniek Z. (2011) *Spojrzenie na rozwój i definicje systemów tensegrity*. Zeszyty Naukowe Politechniki Rzeszowskiej, Nr 276 Budownictwo i Inżynieria Środowiska 58, nr. 3/III.
11. Bieniek Z. (2009b) Space-filling tetrahedra, Symmetry: Art and Science. *The Journal of the International Society for the Interdisciplinary Study of Symmetry, Special Issue for the Conference of ISIS Symmetry Wrocław – Kraków, Poland, Lugosi G., Nagy D. [Eds.], September 14–19, 2009/1-4*: 44-47.
12. Bieniek Z. (2009a) A review of the Tensegrity Systems, Symmetry: Art and Science. *The Journal of the International Society for the Interdisciplinary Study of Symmetry, Special Issue for the Conference of ISIS Symmetry Wrocław and Cracow, Poland, Lugosi G., Nagy D. [Eds.], September 14-19, 2009/1-4*: 48-51.
13. Bieniek Z. (2015a) A mathematical model of the Class Theta tetrahedral tensegrity module. *Lightweight Structures in Civil Engineering – Contemporary Problems, XXI LSCE, Local Seminar of IASS Polish Chapter, Tarczewski R., Bieniek Z. [Eds.], Rzeszów University of Technology*: 9-16.
14. Bieniek Z. (2015b) Examples of cable-bar modular structures based on the Class-Theta tensegrity systems. *Journal of Civil Engineering and Architecture*, **9**: 1452-1462.
15. Bieniek Z. (2011a) Chosen Ideas of Geometrical Shaping of Modular Tensegrity Structures. *Structural Engineers World Congress, Como, Italy, Congress paper on CD*.
16. Bieniek Z., Mascolo I., Amendola A. (2018) On the design, elastic modeling and experimental characterization of novel tensegrity units. *PSU Research Review*, **2**(2): 145-151.
17. Modano M., et al. (2018) *Numerical and Analytical Approaches to the Self-Equilibrium Problem of Class θ = 1 Tensegrity Metamaterials*. Front. Mater. 5:5.
18. Gilewski W., Kasprzak A. (2011) Tensegrity w konstrukcjach mostowych. *Acta Scientiarum Polonorum Architectura*, **10**(3): 35-43.

19. Gilewski W., Kasprzak A. (2013) Tensegrity Form-finding via modal analysis. *T. Łodygowski i in. (eds.), 20th International Conference on Computer Methods in Mechanics, Short Papers, Poznań, TS02-27-28*.
20. Gilewski W., Kasprzak A. (2012) Introduction to mechanics of tensegrity modules. *Theoretical Foundation of Civil Engineering. Mechanics of Structures and Materials, Jemioło S., Lutomirski Sz., eds., OWPW, Warszawa, Tom 1*: 83-94.
21. Gilewski W., Kłosowska J., Obara P. (2016b) Verification of tensegrity properties of Kono Structure and Blur Building. *XXV Polish - Russian - Slovak Seminar –theoretical Foundation Of Civil Engineering*, **153**: 173-179.
22. Obara P., Kłosowska J., Gilewski W. (2019) Truth and myths about 2D tensegrity trusses. *Applied Sciences*, **9**(179): 1-19.
23. Gilewski W., Kłosowska J., Obara P. (2018) Self-stress control of real civil engineering tensegrity structures. *AIP Conference Proceedings 1922, 150004*.
24. Gilewski W., Kłosowska J., Obara P. (2019) Parametric analysis of some tensegrity structures. *MATEC Web of Conferences 262*, *10003. Krynica 2018*.
25. Gilewski W., Kłosowska J., Obara P. (2017) The influence of self-stress on the behavior of tensegrity-like real structure. *MATEC Web of Conferences 117, 00079. XXVI R-S-P Seminar 2017*.
26. Gilewski W., Kłosowska J., Obara P. (2016a) Form finding of tensegrity structures via Singular Value Decomposition of compability matrix. *Advances in Mechanics: Theoretical, Computational and Interdisciplinary Issues*: 191-195.
27. Gilewski W., Kłosowska J., Obara P. (2015) Applications of tensegrity structures in civil engineering. *Procedia Engineering*, **111**: 242–248.
28. Gilewski W., Kłosowska J., Obara P. (2015a) Application of singular value decomposition to qualitative analysis of trusses and tensegrity structures. *ACTA Scientarum Polonarum, Serie Architectura*, **14**: 3-20.
29. Kłosowska J., Obara P. (2016) *Analysis of Geiger and Fuller domes in terms of tensegrity features (in Polish)*. Research and Development of Young Scientists in Poland. Architecture and urban planning. Part 1.Volume: 1, 58-67.
30. Kasprzak A. (2014) *Assessment of the possibility of using tensegrity structures in bridge construction (in Polish)*. Doctoral dissertation, Publishing House of the Warsaw University of Technology, Warsaw.
31. Al Sabuoni-Zawadzka A. (2016) *Study of the possibilities of using intelligent structures in bridge construction (in Polish)*. Doctoral dissertation, Publishing House of the Warsaw University of Technology, Warsaw.
32. Kłosowska J. (2018) *Assessment of the possibility of using tensegrity structures in building construction (in Polish)*. Doctoral dissertation, Publishing House of Kielce University of Technology, Kielce.
33. Gilewski W., Al Sabouni-Zawadzka A. (2014) Control of tensegrity plate due to member loss. *Procedia Engineering*, **91**: 204-209.
34. Al Sabouni-Zawadzka A., Gilewski W. (2016a) On orthotropic properties of tensegrity structures. *Procedia Engineering*, **153**: 887-894.
35. Gilewski W., Al Sabouni-Zawadzka A. (2015) On possible applications of smart structures controlled by self-stress. *Archives of Civil and Mechanical Engineering*, **15**(2): 469-478.
36. Al Sabouni-Zawadzka A., Gilewski W. (2016b) Technical coefficients for continuum models of orthotropic tensegrity modules. *Advances in Mechanics: Theoretical, Computational and Interdisciplinary Issues, CRC Belkema, Taylor & Francis Group, London*: 197-200.

37. Al Sabouni-Zawadzka A., Gilewski W. (2018) Smart metamaterial based on the simplex tensegrity pattern. *Materials*, **11**(5).
38. Al Sabouni-Zawadzka A., Gilewski W. (2019) Soft and Stiff Simplex Tensegrity Lattices as Extreme Smart Metamaterials. *Materials*, **12**(187).
39. Małyszko L., Rutkiewicz A. (2020) Response of a Tensegrity Simplex in Experimental Tests of a Modal Hammer at Different Self-Stress Levels. *Applied Sciences*, **10**(23): 8733.
40. Małyszko L., Rutkiewicz A. (2019) The concept of application of tensegrity modeles in the steel towers structure (in Pol.). *Inżynieria i Budownictwo*, **75**(7-8): 331-334.
41. Małyszko L., Rutkiewicz A., Bilko P. (2018) Dynamic response of a tensegrity simplex in impact hammer tests. *In Proceeding of International Seminar Lightweight Structures in Civil Engineerin, XXIV LSCE*: 69-75.
42. Fuller R.B. (1954) Geodesic Domes. United States Patent US 2.682.235.
43. Gengnagel C. (2002) *Arbeitsblätter "Tensegrity", Munich: Fakultät für Architektur*. Technische Universität München.
44. Gomez-Jauregui V. (2009) Controversial Origins of Tensegrity. *Proceedings of the International Association for Shell and Spatial Structures (IASS) Symposium 2009, Valencia, A. Domingo, C. Lazaro (eds), Evolution i Trends in Design, Analysis i Construction of Shell i Spatial Structures, 28 September – 2 October 2009, Universidad Politechnica de Valencia*: 1642-152.
45. Snelson K. (1965) Continuous tension, discontinuous compression structures. United States Patent No 3,169,611.
46. Kenner H. (1976) *Geodesic Math and how to Use It*. University of California Press.
47. Calladine C.R. (1978) Buckminster Fuller's "tensegrity" structures and Clerk Maxwell's rules for the construction of stiff frames. *International Journal of Solids and Structures*, **14**: 161–172.
48. Calladine C.R. (1982) Modal stiffnesses of a pretensioned cable net. *International Journal of Solids and Structures*, **18**(10): 829–846.
49. Calladine C.R., Pellegrino S. (1991) First order infinitesimal mechanisms. *International Journal of Solids and Structures*, **27**: 505–515.
50. Pellegrino S. (1986) *Mechanics of kinematically indeterminate structures*. Ph.D. Thesis, University of Cambridge.
51. Pellegrino S. (1990) Analysis of prestressed mechanisms. *International Journal of Solids and Structures*, **26**: 1329–1350.
52. Hanaor A. (1987) Preliminary Investigation of Double-Layer Tensegrities. *in H.V. Topping (ed.), Proceedings of International Conference on the Design and Construction of Non-conventional Structures, Vol. 2, Edinburgh, Scotland, Civil-Comp Press*.
53. Hanaor A. (1991) Double-layer tensegrity grids: static load response. II – experimental study. *Journal of Structural Engineering*, **117**(6): 1675–1684.
54. Calladine C.R., Pellegrino S. (1986) Matrix analysis of statically and kinematically indeterminate frameworks. *International Journal of Solids and Structures*, **22**(4): 409–428.
55. Murakami H. (2001a) Static and dynamic analyses of tensegrity structures. Part 1. Nonlinear equations of motion. *International Journal of Solids and Structures*, **38**: 3599–3613.
56. Murakami H. (2001b) Static and dynamic analyses of tensegrity structures. Part 2. Quasi-static analysis. *International Journal of Solids and Structures*, **38**: 3615–3629.
57. Skelton R.E. (2005) Dynamics and control of tensegrity systems. *IUTAM Symposium on Vibration Control of Nonlinear Mechanisms and Structures, Springer*: 309–318.

58. Murakami H., Nishimura Y. (2001a) Static and dynamic characterization of regular truncated icosahedral and dodecahedral tensegrity modules. *International Journal of Solids and Structures*, **38**: 9359–9381.
59. Murakami H., Nishimura Y. (2001c) Static and dynamic characterization of some tensegrity modules. *Journal of Applied Mechanics*, **68**(1): 19–27.
60. Nishimura Y., Murakami H. (2001) Initial shape-finding and modal analyses of cyclic frustum tensegrity modules. *Computer methods in applied mechanics and engineering*, **190**(43-44): 5795–5818.
61. Gomez Estrada G., Bungartz H. J., Mohrdieck C. (2006) Numerical form-finding of tensegrity structures. *International Journal of Solids and Structures*, **43**: 6855–6868.
62. Koohestani K., Guest S.D. (2013) A new approach to the analytical and numerical form-finding of tensegrity structures. *International Journal of Solids and Structures*, **50**(19): 2995–3007.
63. Zhang J.Y., Ohsaki M. (2006) Adaptive force density method for form-finding problem of tensegrity structures. *International Journal of Solids and Structures*, **43**: 5658–5673.
64. Tibert A.G., Pellegrino S. (2003b) Review of Form-finding Methods for Tensegrity Structures. *International Journal of Space Structures*, **18**(4): 209-223.
65. Paul C., Lipson H., Cuevas F.V. (2005) Evolutionary Form-Finding of Tensegrity Structures. *Proceedings of the 2005 Conference: Genetic & Evolutionary Computation, Washington, USA*.
66. Tran H.C., Lee J. (2010) Advanced form finding for cable-strut structures. *International Journal of Solids and Structures*, **47**: 1785–1794.
67. Barnes M.R. (1999) Form-finding and analysis of tension structures by dynamic relaxation. *International Journal of Space Structures*, **14**(2).
68. Schek H. (1974) The force density method for form finding and computation of general networks. *Computer Methods in Applied Mechanics and Engineering*, **3**(1): 115-134.
69. Juan S.H., Tur J.M.M. (2008) Tensegrity frameworks: Static analysis review. *Mechanism and Machine Theory*, **43**(7): 859-881.
70. Sultan C. (2009) Tensegrity: 60 years of art, science and engineering. *Advances in Applied Mechanics*, **43**: 69-145.
71. Kebiche K., Kazi-Aoual M.N., Motro R. (1999) Geometrical non-linear analysis of tensegrity systems. *Engineering Structures*, **21**(9): 864–876.
72. Quirant J., Kazi-Aoual M.N., Motro R. (2003) Designing tensegrity systems: The case of a double layer grid. *Engineering Structures 25 (9)*, **25**(9): 1121–1130.
73. Hanaor A., Liao M.K. (1991) Double-layer tensegrity grids: static load response I – analytical study. *Journal of Structural Engineering*, **117**(6): 1660–1674.
74. Kono Y., Kunieda H. (1997b) Experimental Study On Static Load Responses Of Double Layer Tensegrity Grids. *Journal of Structural and Construction Engineering*, **502**: 93-97.
75. Faroughi S., Lee J. (2015) Analysis of tensegrity structures subject to dynamic loading using a Newmark approach. *Journal of Building Engineering*, **2**: 1-8.
76. Fu F. (2006) Non-linear static analysis and design of Tensegrity domes. *Steel and Composite Structures*, **6**(5): 417-433.
77. Bel Hadj Ali N., Rhode-Barbarigos L., Smith I.F.C. (2011) Analysis of clustered tensegrity structures using a modified dynamic relaxation algorithm. *International Journal of Solids and Structures*, **48**(5): 637-647.
78. Wu X., et al. (2020) Measuring full static displacements of cable domes based only on limited tested locations. *Applied Mathematical Modelling*, **77**: 1054-1064.
79. Masic M., Skelton R.E., Gill P.E (2006) Optimization of tensegrity structures. *International Journal of Solids and Structures*, **42**: 4687–4703.

80. Albertin A., et al. (2012) Genetic Algorithms in the Optimization of Cable Systems. *Newsleter EginSoft*, **9**(1): 30–33.
81. Biondini F., Malerba P. G., Quagliaroli M. (2011) Structural Optimization of Cable Systems by Genetic Algorithms. *The 2011 World Congress on Advances in Structural Engineering and Mechanics (ASEM'11+), Seoul, Korea, 18-22 September*.
82. Ashwear N., Tamadapu G., Eriksson A. (2016) Optimization of modular tensegrity structures for high stiffness and frequency separation requirements. *International Journal of Solids and Structures*, **80**: 297-309.
83. Zhang P., Feng J. (2017) Initial prestress design and optimization of tensegrity systems based on symmetry and stiffness. *International Journal of Solids and Structures*, **106-107**: 68-90.
84. Averseng J., Crosnier B. (2004) Static and dynamic robust control of tensegrity systems. *IASS 2004 Symposium on Shell and Spatial Structures – From Models to Realization*, **45**(3): 169-174.
85. Zhang A., Sun C., Jiang Z. (2018) Experimental study on the construction shape-forming process and static behaviour of a double strut cable dome. *Journal of Zhejiang University-SCIENCE A, Applied Physics & Engineering*, **19**(3): 225-239.
86. Fest E., et al. (2003) Adjustable Tensegrity Structures. *Journal of Structural Engineering*, **129**(4, April): 515–526.
87. Sultan C., Skelton R.E. (1997) Integrated design of controllable tensegrity structures. *Proceedings of the ASME international mechanical engineering congress and exposition*, **54**: 27-37.
88. Wroldsen A.S. (2007) *Modelling and Control of Tensegrity Structures*. Ph.D. Thesis, Department of Marine Technology, Norwegian University of Science and Technology.
89. Adam B., Smith I.F.C. (2006) Learning, Self-Diagnosis And Multi-Objective Control Of An Active Tensegrity Structure. *Advances in Engineering Structures, Mechanics & Construction*: 439-448.
90. Adam B., Smith I.F.C. (2007b) Tensegrity Active Control – Multi objective Approach. *Journal of Computing in Civil Engineering*, **21**(1, January): 3-10.
91. Adam B., Smith I.F.C. (2008a) Active tensegrity: a control framework for an adaptive civil engineering structure. *Computers & Structures*, **86**: 2215-2223.
92. Smith I.F.C. (2009) Control enhancements of a biomimetic structure. *Journal of Information Technology in Construction*, **14**: 229–236.
93. Smith I.F.C., Sychterz A., Veune N. (2017) Adaptive control of a deployable tensegrity structure. *Engineering Structures*, **152**: 14-23.
94. Averseng J., et al. (2005) Active control of a tensegrity plane grid. *Proceedings of the 44th IEEE Conference on Decision and Control, and the European Control Conference 2005, Seville, Spain, December 12–15*: 6830-6834.
95. Djouadi S., et al. (1998) Active control of tensegrity systems. *Journal of Aerospace Engineering*, **11**(2): 37–44.
96. Obara P., Tomasik J. (2021) Active Control of Stiffness of Tensegrity Plate-like Structures Built with Simplex Modules. *Materials*, **14**: 7888.
97. Oppenheim I.J., Williams W.O. (2001) Vibration of an elastic tensegrity structure. *European Journal of Mechanics and Solids*, **20**: 1023–1031.
98. Chen Y., Feng J. (2012b) Initial prestress distribution and natural vibration analysis of tensegrity structures based on group theory. *International Journal of Structural Stability and Dynamics*, **12**(2): 213-231.
99. Shekastehband B., Ayoubi M. (2019) Nonlinear dynamic instability behavior of tensegrity grids subjected to impulsive loads. *Thin-Walled Structures*, **136**: 1-15.

100. Ma S., Chen M., Skelton R.E. (2022) Dynamics and control of clustered tensegrity systems. *Engineering Structures*, **264**: 114391.
101. Tibert A.G., Pellegrino S. (2002) Deployable tensegrity reflectors for small satellites. *Journal of Spacecraft and Rockets*, **39**: 701–709.
102. Motro R. (1987) Tensegrity Systems for Double-Layer Space Structures. *in H.V. Topping (ed.), Proceedings of International Conference on the Design and Construction of Non-conventional Structures, Vol. 2, Edinburgh, Scotland, Civil-Comp Press*.
103. Tibert A.G. (2002) *Deployable tensegrity structures for space applications*. Ph. D. Thesis, Royal Institute of Technology, Stockholm, Sweden.
104. Sultan C., Corless M., Skelton R.E. (1999) Reduced prestressability conditions for tensegrity systems. *Conference: 40th Structures, Structural Dynamics, and Materials Conference*: 2300-2308.
105. Crawford L. (2016) *Transgender Architectonics: The shape of Change in Modernist Space*. Routledge.
106. Gomez-Jauregui V. (2004) *Tensegrity Structures and their Application to Architecture*. Master Thesis, School of Architecture Queen's University Belfast.
107. Fuller R.B. (1962) Tensile-integrity structures. United States Patent No 3.063.521.
108. Hanaor A. (1992) Aspects of design of double-layer tensegrity domes. *International Journal of Space Structures*, **7**(2): 1675–1684.
109. Pellegrino S. (1992) A Class of Tensegrity Domes. *International Journal of Space Structures*, **7**(2): 137–142.
110. Terry W.L. (1994) *Georgia Dome cable roof construction techniques*. John F. Abel, John W. Leonard, i Celina U. Penalba (ed.), Spatial, Lattice i tension structures: Proceeding of the IASS-ASCE International Symposium, New York, ASCE, .
111. Terry W.L. (1996) Tension braced dome structure. U.S. Patent No. 5,502,928.
112. Metodieva I.Y. (2014) Potential applications of tensegrity structures to bridge construction. *Proceedings of Second International Conference on Traffic and Transport Engineering, Belgrade*: 583–589.
113. Rhode-Barbarigos L., et al. (2009) Tensegrity modules for pedestrian bridges. *Proceedings of the International Association for Shell and Spatial Structures (IASS) Symposium 2009: Evolution and Trends in Design, Analysis and Construction of Shell and Spatial Structures, 28 September-2 October 2009, Universidad Politecnica Valencia, Spain, Domingo A., Lazaro C. (Eds.)*.
114. Rhode-Barbarigos L., et al. (2010) Designing tensegrity modules for pedestrian bridges. *Engineering Structures*, **32**(4): 1158–1167.
115. Geiger D.H. (1988) Roof structure. U.S. Patent No. 4,736,553.
116. Lazopoulos K.A., Lazopoulou N.K. (2006) Stability of tensegrity structure: application to cell mechanics. *Archive of Applied Mechanics*, **75**(3-4): 289–301.
117. Baudriller H., et al. (2006) Form-finding of complex tensegrity structures: application to cell cytoskeleton modeling. *Comptes Rendus Mecanique*, **334**(11): 662–668.
118. Cui T.J., Smith D.R., Liu R. (2010) *Metamaterials. Theory, Design and Applications*. Springer, New York, NY, USA Dordrecht, The Netherlands Heidelberg, Germany London, UK.
119. Engheta N., Ziolkowski R.W. (2006) *Metamaterials. Physics and Engineering Explorations*. Wiley-Interscience: New York, NY, USA.
120. Singh G., Ni R., Marwaha A. (2015) A review of metamaterials and its applications. *International Journal of Engineering Trends and Technology*, **19**: 305–310.
121. Zhang Q., et al. (2018) Tensegrity cell mechanical metamaterial with metal rubber. *Applied Physics Letters*, **113**: 031906.

122. Pałkowski S. (2015) Steel cable structures – examples of implementation (in Polish). *Bulider*, **1**: 59-61.
123. Ding M., et al. (2018) Experimental Study and Comparative Analysis of a Geiger-Type Ridge-Beam Cable Dome Structure. *International Journal of Civil Engineering*, **16**: 1739-1755.
124. Obara P., Solovei M. (2023) Assessment of the impact of the number of girders on the dynamic behaviour of Geiger dome. *Archives of Civil Engineering*, **LXIX**(3): 597-611.
125. Kim S.D., Sin I.A. (2014) A Comprative Analysis of Dynamic Instability Characterictic of Geiger-Typed Cable Dome Structures by Load Condition. *Journal of Korean Association for Spatial Structures*, **14**(1): 85-91.
126. Wang Z., Yuan X., Dong S. (2010) Simple approach for force finding analysis of circular Geiger domes with consideration of self-weight. *Journal of Constructional Steel Research*, **66**: 317-322.
127. Sultan C., Corless M., Skelton R.E. (2002) Linear dynamics of tensegrity structures. *Engineering Structures*, **24**: 671–685.
128. Williamson D., Skelton R.E., Han J.H. (2003a) Equilibrium conditions of a tensegrity structure. *International Journal of Solids and Structures*, **40**: 6347-6367.
129. Williamson D., Skelton R.E., Han J.H. (2003b) Equilibrium conditions of class 1 tensegrity structures. *Revue Francaise de Genie*, **7**: 291-310.
130. Rastorfer D. (1988) Structural Gymnastic for the Olympics. *Architectural Record*, (September, 1988).
131. Geiger D.H., Stefaniuk A., Chen D. (1986) The Design and Construction of two Cable Domes for the Korean Olympics. *Shells, Membranes and Space Frames*, (Proceedings IASS Symposium, Osaka, 1986).
132. Tuchman J.L., Ho-Chul S. (1986) Olympic domes first in their kind. *Engineering News Record*, (March 6,1986).
133. Pelczarski M. (2013) About shaping the roof structure of the Spodek hall in Katowice. Reflections from interviews with Professor Wacław Zalewski. *Architectus*, **2**(34): 69-82.
134. Zalewski W. (2006) Shaping Structures.
135. Allen E., Zalewski W. (2009) *Form and Forces: Designing Efficient, Expressive Structures*. Hoboken N.J: John Wiley & Sons.
136. *https://www.bryla.pl/bryla/56,85301,8496801,Architektura_w_Katowicach_TOP_10___przewodnik_po_najciekawszych,,ga.html* [access 11.05.2024].
137. *https://wyborcza.pl/51,82983,27059823.html#S.galeria-K.C-B.1-L.1.duzy* [access 11.05.2024].
138. *https://www.wz-structure.org/supersam* [access 11.05.2024].
139. Gerardo C., Levy M. P. (1992) *Analysis of the Georgia dome cable roof*. Proc., Eighth Conf. of Computing in Civil Engineering and Georgraphic Information Systems Symp., ASCE, Reston, VA.
140. Melaragno M. (1993) Tensegrities for skeletal domes: The Georgia Dome; A case study. *Periodica polytechnica ser. Architecture*, **37**(1-4): 73-79.
141. Levy M.P. (1991) Floating fabric over Georgia dome. *Civil Engineering ASCE*, **61**: 34-37.
142. Levy M.P. (1994) The Georgia dome and beyond: achieving lightweight-longspan structures. *Spatial, Lattice and Tension Structures: Proceedings of the IASS-ASCE International Symposium 1994, Held in Conjunction with the ASCE Structures Congress XII*: 560-562.

143. Kawaguchi K., Ohya S., Vormus S. (2011) Long-Term Monitoring of White Rhino, Building with Tensegrity Skeletons. *35th Annual Symposium of IABSE / 52nd Annual Symposium of IASS / 6th International Conference on Space Structures: Taller, Longer, Lighter - Meeting growing demand with limited resources, London, United Kingdom, September 2011*.
144. Kawaguchi K., Lu Z.-Y. (2002) Construction of three-strut tension systems. *G.A.R. Parke, P. Disney (eds), Space Structures 5, vol. 1, Civil-Comp Press, Guildford*.
145. Kawaguchi K., Ohya S., Vormus S. (2009) Monitoring of full scale tensegrity skeletons under temperature change. *Symposium of the International Association for Shell and Spatial Structures - IASS*: 224-231.
146. Argyris J.H., Scharpf D.W. (1972) Large deflection analysis of prestressed networks. *Journal of the Structural Division*, **98**(3): 633-654.
147. Pagitz M., Mirats Tur J.M. (2009) Finite element based form finding algorithm. *International Journal of Solids and Structures*, **46**(17): 3235-3240.
148. Obara P. (2019) *Dynamics and dynamic stability of tensegrity structures (in Polish)*. Kielce, Polska: Kielce University of Technology.
149. Motro R. (1984) Forms and forces in tensegrity systems. *H. Nooshin (ed.), Proceedings of Third International Conference on Space Structures, Elsevier*: 180-185.
150. Tran H.C., Lee J. (2011d) Geometrical and material nonlinear analysis of tensegrity structures. *Acta Mechanical Science*, **27**(6): 938-949.
151. Obara P., Tomasik J. (2021) Parametric Analysis of Tensegrity Plate-Like Structures: Part 2—Quantitative Analysis. *Applied Sciences*, **11**: 602.
152. Obara P., Tomasik J. (2020) Parametric Analysis of Tensegrity Plate-Like Structures: Part 1—Qualitative Analysis. *Applied Sciences*, **10**: 7042.
153. Koohestani K. (2012) Form-finding of tensegrity structures via genetic algorithm. *International Journal of Solids and Structures*, **49**(5): 739-747.
154. Ma Q., et al. (2018) Step-by-step unbalanced force iteration method for cable-strut structure with irregular shape. *Engineering Structures*, **177**: 331-344.
155. Obara P., Solovei M., Tomasik J. (2023) Qualitative and quantitative analysis of tensegrity domes. *Bulletin of the Polish Academy of Sciences Technical Sciences*, **71**(1): e144574.
156. Yahamoto M., et al. (2011) A Genetic algorithm based form-finding for tensegrity structure. *Proceedia Engineering*, **14**: 2949-2956.
157. Lee S., Lee J., Kang J. (2017) A Genetic Algorithm Based Form-finding of Tensegrity Structures with Multiple Self-stress States. *Journal of Asian Architecture and Building Engineering*, **16**(1): 155-162.
158. Xu X., Luo Y. (2010) Form-finding of non-regular tensegrities using a genetic algorithm. *Mechanics Research Communications*, **37**: 85-91.
159. Ma S., Yuan X.F., Xie S.D. (2019) A new Genetic Algorithm-based topology optimization method of tensegrity tori. *KSCE Journal of Civil Engineering*, **23**: 2136-2147.
160. Uzun F. (2016) Form-finding of free-form tensegrity structures by genetic algorithm-based total potential energy optimization. *Advances in Civil Engineering*, **20**: 784-796.
161. Lee S., Woo B.H., Lee J. (2014) Self-stress design of tensegrity grid structures using genetic algorithm. *International Journal of Mechanical Sciences*, **79**: 38-46.
162. Bel Hadj Ali N., et al. (2010) Design optimization and dynamic analysis of a tensegrity-based footbridge. *Engineering Structure*, **32**: 3650-3659.
163. Faroughi S., Lee J. (2014) Geometrical nonlinear analysis of tensegrity based on a co-rotational method. *Advances in Structural Engineering*, **17**(1): 41-51.

164. Obara P., Tomasik J. (2023) Dynamic Stability of Tensegrity Structures-Part II: The Periodic External Load. *Materials*, **16**(13): 4564.
165. Kim S.D., Kim. H.S., Baek I.S. (2001) Effects by bracing reinforcement on the instability phenomenon of cable domes. *Journal of the Korean Association for Spatial Structures*, **1**(2): 75-83.
166. Atig M., El Ouni M.H., Kahla N.B (2019) Dynamic stability analysis of tensegrity systems. *European Journal of Environmental and Civil Engineering*, **23**(6): 675-692.
167. Saitoh M., et al. (1994) Design and Conctruction of Tension Strut Dome. *IEEE Journal of Solid-state Circuits*, **1**: 67-78.
168. Malerba P.G., Patelli M., Quagliaroli M. (2012) An Extended Force Density Method for the form finding of cable systems with new forms. *Structural Engineering and Mechanics*, **42**(2): 191-210.
169. Ahmed E.A., Nassef A.O., El Damatty A.A. (2023) NURBS-based form-finding algorithm for double-curvature cable domes. *Engineering Structures*, **283**: 115877.
170. Chen L.M., et al. (2022) Design Optimisation of a Cable–Strut Tensile Structure According to the Importance of Elements. *Buildings*, **12**: 1528.
171. Xue S., Li X., Li X. (2024) Geometry-force interactive design and optimization method of cable dome structures. *Thin-Walled Structures*, **111977**.
172. Deng H., Jiang Q.F., Kwan A.S.K. (2005) Shape finding of incomplete cable-strut assemblies containing slack and prestressed elements. *Computer and Structures*, **83**: 1767-1779.
173. Gao Z., Xue S., Wang T. (2018) Four-step Tensioning Construction Method and Experimental Study for Rigid Bracing Dome. *International Journal of Steel Structures*, **18**(1): 281-291.
174. Ye J., Feng R., Kan Y. (2012) Simulation of construction shape-forming process of cable domes. *Science China: Technological Sciences*, **55**(1): 101-116.
175. Jia Y., et al. (2023) A Comparative Study on the Stability Performance of the Suspen-Dome, Conventional Cable Dome, and Ridge-Beam Cable Dome. *Buildings*, **13**: 2019.
176. Xue Y., et al. (2023) A new configuration of Geiger-type cable domes with sliding ridge cables: Computational framework and structural feasibility investigation. *Engineering Structures*, **286**: 116028.
177. Guo J., et al. (2023) Study on the Nonlinear Stability and Parametric Analysis of a Tensile–Beam Cable Dome. *Symmetry*, **15**: 1690.
178. Jiang Z., et al. (2019) Catenary equation-based approach for force finding of cable domes. *International Journal of Steel Structures*, **19**: 283-292.
179. Chen L., et al. (2020) Identification and Adjustment of the Pretension Deviation in Cable-Strut Tensile Structures. *Journal of Civil Engineering*, **24**(1): 143-152.
180. Yuan X., Chen L., Dong S. (2007) Prestress design of cable domes with new forms. *International Journal of Solids and Structures*, **44**: 2773-2782.
181. Yuan X.F., Dong S.L. (2003) Integral feasible prestress of cable dom. *Computers and Structures*, **81**: 2111-2119.
182. Obara P., Solovei M., Tomasik J. (2023) Genetic Algorithms a Tool for the Determination of the Self-Stress States of Tensegrity Domes. *Applied Sciences*, **13**(9): 5267.
183. Zhao Y., et al. (2022) Control method for determining feasible pre-stresses of cable-struts structure. *Thin-Walled Structures*, **174**: 109159.
184. Yan X., et al. (2019) Mechanical properties of a hybrid cable dome under non-uniform snow distribution. *Journal of Constructional Steel Research*, **153**: 519-532.
185. Zheng J., Yuan X., Dong S. (2007) Failure mode and behaviour analysis of two types of cable domes. *Engineering Mechanics*, **24**(1): 44-50.

186. Chen L., et al. (2022) Analysis and Evaluation of the Progressive Collapse Behaviour of a Cable Dome Structure. *Buildings*, **12**(10): 1700.
187. Chen L.M., et al. (2023) Optimisation of Cable Dome Structure Design for Progressive Collapse Resistance. *Applied Sciences*, **13**(4): 2086.
188. Chen L.M., et al. (2023) Analysis and Evaluation of the Progressive Collapse of Cable Dome Structures Induced by Joint Damage. *Buildings*, **13**: 2072.
189. K.Y. Volokh, Vilnay O., Averbuh I. (2003) Dynamics of Cable Structures. *Journal of Engineering Mechanics*, **129**(2): 175-180.
190. Wu X., Deng H., Zhu D. (2017) Mode shape expansions for the dynamic testing of cable domes considering random pretension deviations. *Journal of Sound and Vibration*, **394**: 155-170.
191. Obara P., Solovei M. (2024) Parametric dynamic analysis of tensegrity cable-strut domes. *Journal of Theoretical and Applied Mechanics*.
192. EN 1993-1-11: 2006. Eurocode 3: Design of streel structures - Part 1-11: Design of structures with tension and components.
193. Levy M.P. (1989) Hypar-tensegrity dome. *In Proceeding of International Symposium on Sports Architecture, Beijing, China*: 157-162.
194. Fu F. (2005) Structural behavior and design methods of Tensegrity domes. *Journal of Constructional Steel Research*, **61**: 23-35.
195. *https://www.tensinet.com/index.php/component/tensinet/?view=project&id=3755* [access 11.05.2024].
196. Zhang L., Chen W., Dong S. (2007) Initial pre-stress finding procedure and structural performance research for Levy cable dome based on linear adjustment theory. *Journal of Zhejiang University SCIENCE A*, **8**(9): 1366-1372.
197. Zhang H., et al. (2023) Active control experiments on a Levy cable dome. *Engineering Structures*, **278**: 115450.
198. Ding M., et al. (2021) Experimental Investigation and Numerical Simulation of a Levy Hinged-Beam Cable Dome. *Buildings*, **11**(3): 110.
199. Dong S.I., Wang Z., Yuan X. (2009) A simplified calculation method for initial prestress of Levy cable domes with the consideration of self-weight. *Engineering Mechanics*, **26**(4): 1-6.
200. Tran H.C., Park H.S., Lee J. (2012) A unique feasible mode of prestress design for cable domes. *Finite Elements in Analysis and Design*, **59**: 44-54.
201. Zhu M., et al. (2023) Artificial neural network-aided force finding of cable dome structures with diverse integral self-stress states-framework and case study. *Engineering Structures*, **285**: 116004.
202. Liu R., et al. (2022) On the Collapse Resistance of the Levy Type and the Loop-Free Suspen-Dome Structures After Accidental Failure of Cables. *International Journal of Steel Structures*, **22**(5): 585-596.
203. Zhang W., Li P. (2022) Progressive collapse analysis of Levy type open cable domes. *In Proceedings of the IASS 2022 Symposium affiliated with APCS 2022 conference, Innovation·Sustainability·Legacy, 19 – 22 September 2022, Beijing, China*, **4**: 1-10.
204. Ma S., et al. (2020) Design and analysis of deployable clustered tensegrity cable domes. *Proceedings of the IASS Annual Symposium 2020/21 and the 7th International Conference on Spatial Structures*.
205. Xue Y., et al. (2023) Mechanical Analysis of Frictional Continuous Cable Systems Considering the Influence of Load Path. *Journal of Engineering Mechanics*, **149**(2): 04022111.
206. Li Y., et al. (2009) Wind tunnel test on Levy type cable dome. *The Seventh Asia-Pacific Conference on Wind Engineering, November 8-12, 2009, Taipei, Taiwan*.

207. Kmet S., Mojdis M. (2015) Adaptive Cable Dome. *Journal of Structural Engineering*, **14**(9): 04014225.
208. Zhang A., et al. (2023) Experimental study on static performance of fully assembled ridge-tube threading cable with annular-struts cable dome. *Engineering Structures*, **288**: 116194.
209. Lv H., et al. (2023) Conformation and static performance analysis of pentagonal three-four strut hybrid open-type cable dome. *Advanced Steel Construction*, **19**(4): 403-410.
210. Kmet S., Mojdis M. (2014) Adaptive cable dome. *Journal of Structural Engineering*, **141**(9): 04014225.
211. Ding M., et al. (2015) Design and static analysis of a composite rigidrigid-roof structure. *In Proceedings of the International Association for Shell and Spatial Structures (IASS) Symposium 2015, Amsterdam*, **8**: 1-11.
212. Chen Y., Feng J. (2012a) Generalized eigenvalue analysis of symmetric prestressed structures using group theory. *Journal of Computing in Civil Engineering*, **26**(4): 488-497.

APPENDICES

Appendix A – Spectral analysis of Geiger dome (RG 6B) (Mathematica environment)

```
In[666]:= lp = 6; (*liczba dzwigarow nosnych*)

lwp = 7; (*liczba wezlow dzwigara*)
lep = 9; (*liczba elementow dzwigara*)
ll = 4; (*liczba lacznikow*)
lz = 3; (*liczba zastrzalow*)

xl = {5., 5.0, 20., 20., 40., 40., 60} * 10^(-1); (*wspolrzedne dzwigara*)
zl = {21., 15., 18.5, 4.5, 11.5, -11.5, 0} * 10^(-1);

x = Table[0, {lwp * lp}];
    tabela
y = Table[0, {lwp * lp}];
    tabela
z = Table[0, {lwp * lp}];
    tabela

Do[
rób
  (
   x[[i]] = xl[[i]];
   z[[i]] = zl[[i]]
  ),
  {i, lwp}
]

als = 360 / lp;
als = als / 180 * Pi;
                  pi
Do[
rób
  (
   np = i * lwp;
   Do[
   rób
    (
     al = i * als;
     x[[np + j]] = xl[[j]] * Cos[al];
                             cosinus
     y[[np + j]] = xl[[j]] * Sin[al];
                             sinus
     z[[np + j]] = zl[[j]]
    ),
    {j, lwp}
   ]
  ),
  {i, lp - 1}
]

p1l = {1, 3, 5, 3, 5, 7, 2, 4, 6};
p2l = {2, 4, 6, 1, 3, 5, 3, 5, 7};
```

```
lwe = lp * (lep + ll); (*liczba wszystkich elementow*)
p1 = Table[0, {lwe}];
     tabela
p2 = Table[0, {lwe}];
     tabela

k = 0;
Do[
rób
  (
   k++;
   p1[[i]] = p1l[[i]];
   p2[[i]] = p2l[[i]]
  ),
  {i, lz}
]

Do[
rób
  (
   Do[
   rób
    (
     k++;
     p1[[k]] = p1l[[j]] + i * lwp;
     p2[[k]] = p2l[[j]] + i * lwp
    ),
    {j, lz}
   ]
  ),
  {i, lp - 1}
]

Do[
rób
  (
   k++;
   p1[[k]] = p1l[[i]];
   p2[[k]] = p2l[[i]]
  ),
  {i, lz + 1, lep}
]

Do[
rób
  (
   Do[
   rób
    (
     k++;
```

```
      p1[[k]] = p1l[[j]] + i * lwp;
      p2[[k]] = p2l[[j]] + i * lwp),
     {j, lz + 1, lep}
    ]
   ),
   {i, lp - 1}
  ]

li = {1, 2, 4, 6};
Do[
   (
    Do[
      (
       k++;
       p1[[k]] = li[[j]] + (i - 1) * lwp;
       p2[[k]] = p1[[k]] + lwp
      ),
      {j, ll}
     ]
    ),
    {i, lp - 1}
   ];

Do[
  (
   k++;
   p1[[k]] = li[[j]] + (lp - 1) * lwp;
   p2[[k]] = li[[j]]
  ),
  {j, ll}
 ]

lwz = lz * lp; (*liczba wszystkich zastrzalow*)
lw = lwp * lp;
(*geometria calej kopuly*)
wezly = {Thick, Table[Text[Style[i, {Larger, Bold}],
        {x[[i]] + 0.005, y[[i]] + 0.005, z[[i]] + 0.008}], {i, 1, lw}]};
prety = {Thick, Table[Text[Style[i, {Larger, Bold}],
       {(x[[p1[[i]]]] + x[[p2[[i]]]]) / 2 + 0.05, (y[[p1[[i]]]] + y[[p2[[i]]]]) / 2 + 0.05,
        (z[[p1[[i]]]] + z[[p2[[i]]]]) / 2 + 0.05}], {i, 1, lwe}]};
zastrzaly = {Thickness[0.01], Table[Line[{{x[[p1[[i]]]], y[[p1[[i]]]], z[[p1[[i]]]]},
        {x[[p2[[i]]]], y[[p2[[i]]]], z[[p2[[i]]]]}}], {i, 1, lwz}]};
ciegna = {Thickness[0.002], Table[Line[{{x[[p1[[i]]]], y[[p1[[i]]]], z[[p1[[i]]]]},
         {x[[p2[[i]]]], y[[p2[[i]]]], z[[p2[[i]]]]}}], {i, lwz + 1, lwe}]};
```

```
Graphics3D[{zastrzaly, ciegna, Red, wezly}]
trójwymiarowa grafika               czerwony
```

Out[690]=

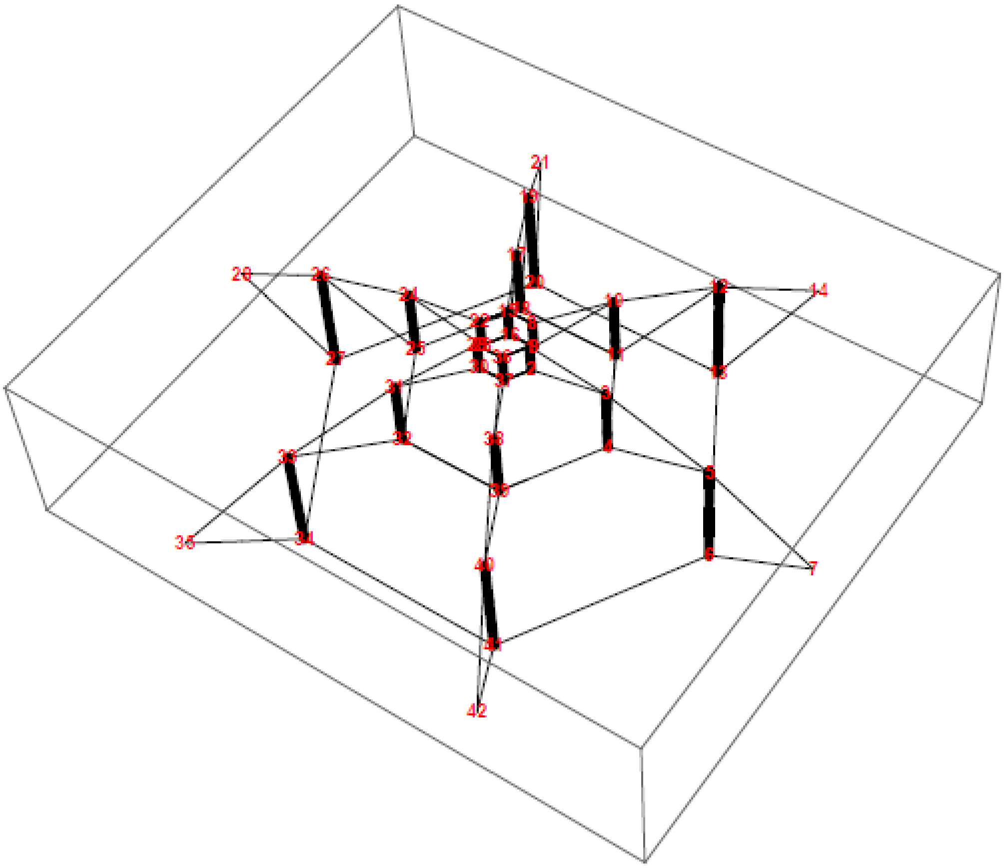


```
In[691]:= dane;
le = lwe;
lw = lw;
odebrane stopnie swobody;
odebrane stopnie swobody;
loss = 3 * lp;
toss = Table[0, {loss}];
        tabela
nwo = lwp; (*numer pierwszego wezla obwodowego*)
Do[
rób
  (
   toss[[3 * i - 2]] = 3 * nwo - 2;
   toss[[3 * i - 1]] = 3 * nwo - 1;
   toss[[3 * i]] = 3 * nwo;
   nwo = nwo + 7;
  ),
  {i, lp}
]
charakterystyki elementów;
```

```
e = Table[210000000, {le}];
    tabela
a = Table[0, {le}];
    tabela
ac = 3.14159 * 10^(-4);
az = 6.88 * 10^(-4);
cięgna;
Do[
róbo
  (
   a[[i]] = ac;
  ),
  {i, lwz + 1, lwe}
 ];
zastrzały;
Do[
rób
  (
   a[[i]] = az;
  ),
  {i, 1, lwz}
 ];
stopnie swobody;
llss = 6;
lgss = 3 * lw;
tablica wszystkich stopni swobody;
tss = Table[i, {i, lgss}];
      tabela
niezerowe stopnie swobody;
lnss = lgss - loss;
tnss = Table[0, {lnss}]; inicjowanie tablicy niezerowych stopni swobody;
       tabela
ii = 1;
Do[
rób
  (
   c = 1;
   Do[
   rób
    (
     If[tss[[i]] == toss[[j]], (j = loss; c = 0)]
     operator warunkowy
    ),
    {j, loss}
   ];
   If[c == 1, (tnss[[ii]] = tss[[i]]; ii++)]
   operator warunkowy
  ),
  {i, lgss}
 ];

obliczenia macierzy sztywnościli linowej i macierzy wydłużeń;
```

```
B = Table[0, {le}, {lgss}];
    tabela
Bt = Table[0, {lgss}, {le}];
     tabela
n = Table[0, {llss}];
    tabela
Do[
rób
  (
   w1 = p1[[i]];
   w2 = p2[[i]];
   x1 = x[[w1]];
   y1 = y[[w1]];
   z1 = z[[w1]];
   x2 = x[[w2]];
   y2 = y[[w2]];
   z2 = z[[w2]];
   L = Sqrt[(x2 - x1) * (x2 - x1) + (y2 - y1) * (y2 - y1) + (z2 - z1) * (z2 - z1)];
       pierwiastek kwadratowy
   cx = (x2 - x1) / L;
   cy = (y2 - y1) / L;
   cz = (z2 - z1) / L;
   n[[3]] = 3 * w1;
   n[[2]] = n[[3]] - 1;
   n[[1]] = n[[3]] - 2;
   n[[6]] = 3 * w2;
   n[[5]] = n[[6]] - 1;
   n[[4]] = n[[6]] - 2;
   macierz odkształceń;
   B[[i, n[[1]]]] = -cx;
   B[[i, n[[2]]]] = -cy;
   B[[i, n[[3]]]] = -cz;
   B[[i, n[[4]]]] = cx;
   B[[i, n[[5]]]] = cy;
   B[[i, n[[6]]]] = cz;
   transponowana macierz odkształceń;
   sz = e[[i]] * a[[i]] / L;
   Bt[[n[[1]], i]] = -cx * sz;
   Bt[[n[[2]], i]] = -cy * sz;
   Bt[[n[[3]], i]] = -cz * sz;
   Bt[[n[[4]], i]] = cx * sz;
   Bt[[n[[5]], i]] = cy * sz;
   Bt[[n[[6]], i]] = cz * sz;
  ),
  {i, le}
 ];
MatrixForm[B];
postać macierzy
macierz sztywności liniowej;
k = Bt.B;
MatrixForm[k];
postać macierzy
```

```
        postać macierzy
        d = B.Bt;
        MatrixForm[d];
        postać macierzy

In[730]:= Length[toss];
          długość

In[731]:= warunki brzegowe;
          macierz sztywności liniowej;
          nk = k;
          Do[
          rób
            (
             ii = toss[[i]];
             Do[
             rób
              (
               nk[[ii, j]] = 0;
               nk[[j, ii]] = 0;
              ),
              {j, lgss}
             ];
             nk[[ii, ii]] = 1;
            ),
            {i, loss}
           ];
          MatrixForm[nk];
          postać macierzy
          macierz wydłużeń (wybieranie kolumn z macierzy);
          nB = Table[0, {le}, {lnss}];
               tabela
          Do[
          rób
            (
             ii = tnss[[i]];
             Do[
             rób
              (
               nB[[j, i]] = B[[j, ii]];
              ),
              {j, le}
             ]
            ),
            {i, lnss}
           ];
          nB // MatrixForm;
                postać macierzy
          nd = nB.Transpose[nB];
                  transpozycja
          nd // MatrixForm;
                postać macierzy
```

```
In[742]:= ANALIZA SPEKTRALNA;
macierzy sztywnosci;
wnk = Eigenvalues[nk];
      |wartości własne macierzy
nk0 = Table[0, {lgss}];
      |tabela
lzk = 0;
Do[
|rób
  If [Abs[wnk[[i]]] < 10^-5, (lzk++; nk0[[lzk]] = i;)],
  |o··· |wartość bezwzględna
  {i, lgss}
 ];
wwnk = Eigenvectors[nk];
       |wektory własne
wwk = Table[0, {lzk}, {lgss}];
      |tabela
Do[
|rób
  (
   ii = nk0[[i]];
   Do[
   |rób
    (
     wwk[[i, k]] = wwnk[[ii, k]]
    ),
    {k, lgss}]
  ),
  {i, lzk}
 ];
nk0
MatrixForm[wwk];
|postać macierzy
(*liczba mechanizmow infinitezymalnych*)
Out[751]= {96, 97, 98, 99, 100, 101, 102, 103, 104, 105, 106, 107, 108, 109, 110, 111, 112, 113,
 114, 115, 116, 117, 118, 119, 120, 121, 122, 123, 124, 125, 126, 0, 0, 0, 0, 0, 0,
 0, 0, 0, 0, 0, 0, 0, 0, 0, 0, 0, 0, 0, 0, 0, 0, 0, 0, 0, 0, 0, 0, 0, 0, 0, 0, 0, 0, 0, 0,
 0, 0, 0, 0, 0, 0, 0, 0, 0, 0, 0, 0, 0, 0, 0, 0, 0, 0, 0, 0, 0, 0, 0, 0, 0, 0, 0, 0, 0, 0,
 0, 0, 0, 0, 0, 0, 0, 0, 0, 0, 0, 0, 0, 0, 0, 0, 0, 0, 0, 0, 0, 0, 0, 0, 0, 0, 0, 0, 0, 0}
```

```
In[753]:= ANALIZA SPEKTRALNA;
          macierzy d;
          wartości i wektory własne;
          wnd = Eigenvalues[nd];
                |wartości własne macierzy
          n0 = Table[0, {le}];
               |tabela
          lz = 0;
          Do[
          |rób
            If[Abs[wnd[[i]]] < 10^(-5), (lz++; n0[[lz]] = i;)],
            |·· |wartość bezwzględna
            {i, le}
           ];
          wwnd = Eigenvectors[nd];
                 |wektory własne
          ww = Table[0, {lz}, {le}];
               |tabela
          Do[
          |rób
            (
             ii = n0[[i]];
             Do[
             |rób
               (
                ww[[i, k]] = wwnd[[ii, k]]
               ),
               {k, le}]
            ),
            {i, lz}
           ];
          n0
          ww
          (*liczba stanow samonaprezenia*)

Out[763]= {78, 0, 0, 0, 0, 0, 0, 0, 0, 0, 0, 0, 0, 0, 0, 0, 0, 0, 0, 0, 0, 0, 0, 0,
           0, 0, 0, 0, 0, 0, 0, 0, 0, 0, 0, 0, 0, 0, 0, 0, 0, 0, 0, 0, 0, 0, 0, 0, 0, 0, 0,
           0, 0, 0, 0, 0, 0, 0, 0, 0, 0, 0, 0, 0, 0, 0, 0, 0, 0, 0, 0, 0, 0, 0, 0, 0, 0, 0}

Out[764]= {{-0.0087896, -0.0316426, -0.103968, -0.0087896, -0.0316426, -0.103968, -0.0087896,
            -0.0316426, -0.103968, -0.0087896, -0.0316426, -0.103968, -0.0087896, -0.0316426,
            -0.103968, -0.0087896, -0.0316426, -0.103968, 0.0534651, 0.0957849, 0.208575,
            0.0386816, 0.0957849, 0.208575, 0.0534651, 0.0957849, 0.208575, 0.0386816,
            0.0957849, 0.208575, 0.0534651, 0.0957849, 0.208575, 0.0386816, 0.0957849, 0.208575,
            0.0534651, 0.0957849, 0.208575, 0.0386816, 0.0957849, 0.208575, 0.0534651,
            0.0957849, 0.208575, 0.0386816, 0.0957849, 0.208575, 0.0534651, 0.0957849,
            0.208575, 0.0386816, 0.0957849, 0.208575, 0.0527376, 0.0376697, 0.0904073,
            0.180815, 0.0527376, 0.0376697, 0.0904073, 0.180815, 0.0527376, 0.0376697,
            0.0904073, 0.180815, 0.0527376, 0.0376697, 0.0904073, 0.180815, 0.0527376,
            0.0376697, 0.0904073, 0.180815, 0.0527376, 0.0376697, 0.0904073, 0.180815}}
```

```
In[765]:=
     (*stan samonaprezenia: wartosci w elementach*)

In[766]:= (*normalizacja stanu samonaprezenia*)
     wy0p = ww[[1]] / 0.10396843891541534`

Out[766]= {-0.0845411, -0.304348, -1., -0.0845411, -0.304348, -1., -0.0845411,
      -0.304348, -1., -0.0845411, -0.304348, -1., -0.0845411, -0.304348,
      -1., -0.0845411, -0.304348, -1., 0.514243, 0.921288, 2.00613, 0.372051,
      0.921288, 2.00613, 0.514243, 0.921288, 2.00613, 0.372051, 0.921288, 2.00613,
      0.514243, 0.921288, 2.00613, 0.372051, 0.921288, 2.00613, 0.514243, 0.921288,
      2.00613, 0.372051, 0.921288, 2.00613, 0.514243, 0.921288, 2.00613, 0.372051,
      0.921288, 2.00613, 0.514243, 0.921288, 2.00613, 0.372051, 0.921288, 2.00613,
      0.507246, 0.362319, 0.869565, 1.73913, 0.507246, 0.362319, 0.869565, 1.73913,
      0.507246, 0.362319, 0.869565, 1.73913, 0.507246, 0.362319, 0.869565, 1.73913,
      0.507246, 0.362319, 0.869565, 1.73913, 0.507246, 0.362319, 0.869565, 1.73913}

In[767]:= pierwszy wektor własny;
     macierz sztywnosci geometrycznej;
     wy0 = wy0p;
     kg = Table[0, {lgss}, {lgss}];
          tabela
     Do[
     rób
       (
        w1 = p1[[ne]];
        w2 = p2[[ne]];
        x1 = x[[w1]];
        y1 = y[[w1]];
        z1 = z[[w1]];
        x2 = x[[w2]];
        y2 = y[[w2]];
        z2 = z[[w2]];
        L = Sqrt[(x2 - x1) * (x2 - x1) + (y2 - y1) * (y2 - y1) + (z2 - z1) * (z2 - z1)];
            pierwiastek kwadratowy
        cx = (x2 - x1) / L;
        cy = (y2 - y1) / L;
        cz = (z2 - z1) / L;
        n[[3]] = 3 * w1;
        n[[2]] = n[[3]] - 1;
        n[[1]] = n[[3]] - 2;
        n[[6]] = 3 * w2;
        n[[5]] = n[[6]] - 1;
        n[[4]] = n[[6]] - 2;
        S = wy0[[ne]];
        mian = cx^2 + cy^2;
        If[mian != 0,
        operator warunkowy
         k11 = (cy^2 + cx^2 * cz^2) / mian;
         k12 = (cy * cx * (cz^2 - 1)) / mian;
```

```
    k13 = -cx * cz;
    k22 = (cx^2 + cy^2 * cz^2) / mian;
    k23 = -cy * cz;
    k33 = (cx^2 + cy^2);
    kge = {{k11 * S/L, k12 * S/L, k13 * S/L, -k11 * S/L, -k12 * S/L, -k13 * S/L},
      {k12 * S/L, k22 * S/L, k23 * S/L, -k12 * S/L, -k22 * S/L, -k23 * S/L},
      {k13 * S/L, k23 * S/L, k33 * S/L, -k13 * S/L, -k23 * S/L, -k33 * S/L},
      {-k11 * S/L, -k12 * S/L, -k13 * S/L, k11 * S/L, k12 * S/L, k13 * S/L},
      {-k12 * S/L, -k22 * S/L, -k23 * S/L, k12 * S/L, k22 * S/L, k23 * S/L},
      {-k13 * S/L, -k23 * S/L, -k33 * S/L, k13 * S/L, k23 * S/L, k33 * S/L}},
    kge = {{S/L, 0, 0, -S/L, 0, 0}, {0, S/L, 0, 0, -S/L, 0}, {0, 0, 0, 0, 0, 0},
      {-S/L, 0, 0, S/L, 0, 0}, {0, -S/L, 0, 0, S/L, 0}, {0, 0, 0, 0, 0, 0}};
   Do[
   rób
    Do[
    rób
     kg[[n[[i]], n[[j]]]] += kge[[i, j]],
     {j, llss}
    ],
    {i, llss}
   ]
  ),
  {ne, le}
 ];
warunki brzegowe macierzy sztywności geometrycznej;
nkg = kg;
Do[
rób
  (
   ii = toss[[i]];
   Do[
   rób
    (
     nkg[[ii, j]] = 0;
     nkg[[j, ii]] = 0;
    ),
    {j, lgss}
   ];
   nkg[[ii, ii]] = 1;
  ),
```

```
  {i, loss}
 ];
MatrixForm[nkg];
postać macierzy
ANALIZA SPEKTRALNA;
sumy macierzy sztywności liniowej i geometrycznej;
Eigenvalues[nk + nkg]
wartości własne macierzy
(*sprzawdzenie macierzy sztywnosci: wszystkie wartosci wieksze od zera*)
```

```
Out[778]= {484 004., 483 996., 483 996., 483 961., 483 961., 483 903., 395 841., 395 840., 336 466.,
 336 466., 334 641., 334 641., 238 424., 238 424., 224 814., 224 814., 217 299., 214 638.,
 214 503., 214 503., 210 283., 210 283., 208 092., 172 510., 155 177., 151 387., 151 387.,
 141 519., 141 519., 139 384., 134 053., 132 897., 132 897., 119 172., 119 172., 105 276.,
 98 960.3, 93 442.2, 93 442.2, 85 154.6, 85 154.6, 82 347.9, 71 937.9, 71 937.9, 70 476.6,
 49 480.5, 48 165.7, 48 165.7, 45 537.1, 45 537.1, 44 423.8, 40 935.7, 40 193.5, 40 193.5,
 39 805.2, 39 805.2, 33 875.8, 29 712.3, 25 925.4, 25 925.4, 21 704., 21 704., 19 384.7,
 16 813.2, 16 813.2, 14 348.6, 14 348.6, 7389.69, 7389.69, 5938.48, 4171.17, 3929.32,
 3929.32, 2911.33, 2702.48, 2702.48, 471.585, 3.7304, 2.84541, 2.84541, 2., 2., 2.,
 2., 2., 2., 2., 2., 2., 2., 2., 2., 2., 2., 2., 2., 2., 2., 1.93299, 1.86807, 1.66524,
 1.66524, 1.64563, 1.64563, 1.55407, 1.4153, 1.4153, 1.39782, 1.36609, 1.10727,
 1.10727, 1.02535, 1.02535, 0.860558, 0.778693, 0.717084, 0.717084, 0.63758,
 0.63758, 0.547374, 0.540744, 0.540744, 0.399974, 0.320809, 0.320809, 0.290196}
```

```
(*sprawdzenie rownowagi w wezlach*)
```

```
In[780]:= equ[p1_, p2_, x_, y_, z_, wy0p_, element_] :=
  Module[{w1, w2, x1, y1, z1, x2, y2, z2, L, cx, cy, cz, sum1, sum},
  moduł
   (sum = 0;
    Do[
    rób
     w1 = p1[[i]];
     w2 = p2[[i]];
     x1 = x[[w1]];
     y1 = y[[w1]];
     z1 = z[[w1]];
     x2 = x[[w2]];
     y2 = y[[w2]];
     z2 = z[[w2]];
     L = ((x2 - x1)^2 + (y2 - y1)^2 + (z2 - z1)^2)^0.5;
     cx = (x2 - x1) / L;
     cy = (y2 - y1) / L;
     cz = (z2 - z1) / L;
     sum1 = cx * wy0p[[i]] + cy * wy0p[[i]] + cz * wy0p[[i]];
     If [element == p1[[i]], sum = sum + sum1, sum = sum];
     operator warunkowy
     If[element == p2[[i]], sum = sum - sum1, sum = sum], {i, Length[p1]}];
     operator warunkowy                                          długość
    sum)]

sumequ = 0;
Do[
rób
  sumequ2 = equ[p1, p2, x, y, z, wy0p, i];
  Print[i, "-", sumequ2];
  drukuj
  sumequ += sumequ2^2
     sumequ += sumequ2^2
  , {i, {1, 2, 3, 4, 5, 6, 8, 9, 10, 11, 12, 13, 15, 16, 17, 18, 19, 20,
    22, 23, 24, 25, 26, 27, 29, 30, 31, 32, 33, 34, 36, 37, 38, 39, 40, 41}}];
sumequ
output2 = 1 / (sumequ^0.5 + 0.00001)
```

$1 - 2.88658 \times 10^{-15}$

$2 - 8.32667 \times 10^{-16}$

$3 - -2.55351 \times 10^{-15}$

$4 - -3.9968 \times 10^{-15}$

$5 - 1.33227 \times 10^{-15}$

$6 - -4.44089 \times 10^{-16}$

$8 - 3.33067 \times 10^{-16}$

$9 - -4.44089 \times 10^{-16}$

$10 - -3.10862 \times 10^{-15}$

$11 - -2.66454 \times 10^{-15}$

$12 - 6.66134 \times 10^{-16}$

$13 - 2.44249 \times 10^{-15}$

$15 - -3.33067 \times 10^{-16}$

$16 - 2.77556 \times 10^{-16}$

$17 - -2.02616 \times 10^{-15}$

$18 - -2.44249 \times 10^{-15}$

$19 - -1.44329 \times 10^{-15}$

$20 - -6.21725 \times 10^{-15}$

$22 - 5.55112 \times 10^{-16}$

$23 - 3.60822 \times 10^{-16}$

$24 - -2.27596 \times 10^{-15}$

$25 - -9.99201 \times 10^{-16}$

$26 - -6.66134 \times 10^{-16}$

$27 - 2.55351 \times 10^{-15}$

$29 - -2.9976 \times 10^{-15}$

$30 - 2.88658 \times 10^{-15}$

$31 - -5.55112 \times 10^{-17}$

$32 - -1.77636 \times 10^{-15}$

$33 - 9.99201 \times 10^{-16}$

$34 - -5.77316 \times 10^{-15}$

$36 - 8.88178 \times 10^{-16}$

$37 - 2.22045 \times 10^{-16}$

$38 - -1.52656 \times 10^{-16}$

$39 - -8.88178 \times 10^{-16}$

$40 - 2.44249 \times 10^{-15}$

$41 - 5.32907 \times 10^{-15}$

Out[783]= 2.1237×10^{-28}

Out[784]= 100 000.

Appendix B – Genetic algorithm (Python environment)

```
import pygad
import numpy as np
import scipy.linalg as la

def equ(p1, p2, x, y, z, wy02, element):
    sum = 0
    for i in range(len(p1)):
        w1 = p1[i]
        w2 = p2[i]
        x1 = x[w1 - 1]
        y1 = y[w1 - 1]
        z1 = z[w1 - 1]
        x2 = x[w2 - 1]
        y2 = y[w2 - 1]
        z2 = z[w2 - 1]
        L = ((x2 - x1) ** 2 + (y2 - y1) ** 2 + (z2 - z1) ** 2) ** 0.5
        cx = (x2 - x1) / L
        cy = (y2 - y1) / L
        cz = (z2 - z1) / L
        sum1 = cx * wy02[i] + cy * wy02[i] + cz * wy02[i]
        if element == p1[i]:
            #print(i + 1)
            #print(sum1)
            sum = sum + sum1
            #print(sum)
        elif element == p2[i]:
            #print(i + 1)
            #print(-sum1)
            sum = sum - sum1
            #print(sum)
    return sum

def fitness_func(solution, solution_idx):
    # Calculating the fitness value of each solution in the current population.
    # The fitness function calculates the sum of products between each input
and its corresponding weight.

    b1 = 1
    b2 = 1
    b3 = 1

    #kilka modułów
    le = 78
    lw = 42
#pierwszy i ostatni numer wezla
    p1 = [15, 8, 7, 36, 29, 22, 37, 14, 9, 16, 23, 30, 25, 32, 39, 35, 11, 18, \
27, 34, 41, 13, 20, 6, 36, 7, 22, 15, 8, 29, 21, 24, 38, 17, 10, 31, \
35, 42, 25, 26, 18, 19, 11, 12, 39, 40, 32, 33, 27, 28, 41, 5, 6, 1, \
20, 3, 4, 34, 13, 2, 37, 7, 8, 15, 22, 29, 21, 24, 31, 10, 38, 17, \
42, 19, 40, 12, 26, 33]

    p2 = [8, 7, 36, 29, 22, 15, 14, 9, 16, 23, 30, 37, 32, 39, 35, 11, 18, 25, \
34, 41, 6, 20, 27, 13, 38, 21, 24, 17, 10, 31, 14, 23, 37, 16, 9, 30, \
```

```
42, 21, 26, 24, 19, 17, 12, 10, 40, 38, 33, 31, 28, 26, 5, 40, 1, 42, \
3, 19, 33, 4, 2, 12, 36, 14, 9, 16, 23, 30, 35, 25, 32, 11, 39, 18, \
6, 20, 41, 13, 27, 34]
#wspolrzedne
   x1 = [6.00,3.00,-3.00,-3.00,3.00,4.00,0.50,0.25,0.25,1.00,1.00,2.00,2.00
,\
        0.50,-0.25,-0.25,-1.00,-1.00,-2.00,-2.00,2.00,-0.50,-0.50,-2.00,-2.00
,\
        -4.00,-4.00,-6.00,-0.25,-0.25,-1.00,-1.00,-2.00,-2.00,2.00,0.25,0.25,
1.00,\
        1.00,2.00,2.00,4.00]

   y1 = [0.0,5.20,5.20,-5.20,-5.20,0.0,0.0,0.43,0.43,1.73,1.73,3.46,3.46,0.0
,0.43,\
        0.43,1.73,1.73,3.46,3.46,0.0,0.0,0.0,0.0,0.0,0.0,0.0,0.0,-0.43,-0.43,-
1.73,\
        -1.73,-3.46,-3.46,0.0,-0.43,-0.43,-1.73,-1.73,-3.46,-3.46,0.0]

   z1 = [0.0,0.0,0.0,0.0,0.0,-1.15,2.10,2.10,1.50,1.85,0.45,1.15,-1.15,1.50
,\
        2.10,1.50,1.85,0.45,1.15,-1.15,1.85,2.10,1.50,1.85,0.45,1.15,-1.15,\
        0.0,2.10,1.50,1.85,0.45,1.15,-1.15,0.45,2.10,1.50,1.85,0.45,1.15,-1.
15,1.15]

   x = [element * b1 for element in x1]
   y = [element * b2 for element in y1]
   z = [element * b3 for element in z1]

   toss = [1,2,3,4,5,6,7,8,9,10,11,12,13,14,15,82,83,84]
   loss = len(toss)

   e = np.ones(le) * 210000000
   a = np.ones(le) * 1 * 10 ** (-4)
   # liczba ciegien
   for i in range(60):
      a[i] = 1 * 10 ** (-4)

   llss = 6
   lgss = 3 * lw

   tss = np.arange(0, lgss) + 1
   lnss = lgss - loss
   tnss_def = np.arange(0, lgss) + 1

   for j in range(loss):
      for i in range(len(tnss_def)):
         if tnss_def[i] == toss[j]:
            tnss_def[i] = 0

   tnss = np.zeros(lgss - loss)

   j = 0
   for i in range(len(tnss_def)):
```

```
    if tnss_def[i] != 0:
        tnss[j] = tnss_def[i]
        j += 1

B = np.zeros((le, lgss))
Bt = np.zeros((lgss, le))
Btsz = np.zeros((lgss, le))
n = [0, 0, 0, 0, 0, 0]

for i in range(le):
    w1 = p1[i]
    w2 = p2[i]
    x1 = x[w1 - 1]
    y1 = y[w1 - 1]
    z1 = z[w1 - 1]
    x2 = x[w2 - 1]
    y2 = y[w2 - 1]
    z2 = z[w2 - 1]
    L = ((x2 - x1) ** 2 + (y2 - y1) ** 2 + (z2 - z1) ** 2) ** 0.5
    cx = (x2 - x1) / L
    cy = (y2 - y1) / L
    cz = (z2 - z1) / L
    n[2] = 3 * w1 - 1
    n[1] = 3 * w1 - 2
    n[0] = 3 * w1 - 3
    n[5] = 3 * w2 - 1
    n[4] = 3 * w2 - 2
    n[3] = 3 * w2 - 3
    B[i][int(n[0])] = -cx
    B[i][int(n[1])] = -cy
    B[i][int(n[2])] = -cz
    B[i][int(n[3])] = cx
    B[i][int(n[4])] = cy
    B[i][int(n[5])] = cz
    Bt[int(n[0])][i] = -cx
    Bt[int(n[1])][i] = -cy
    Bt[int(n[2])][i] = -cz
    Bt[int(n[3])][i] = cx
    Bt[int(n[4])][i] = cy
    Bt[int(n[5])][i] = cz
    sz = e[i] * a[i] / L
    Btsz[int(n[0])][i] = -cx * sz
    Btsz[int(n[1])][i] = -cy * sz
    Btsz[int(n[2])][i] = -cz * sz
    Btsz[int(n[3])][i] = cx * sz
    Btsz[int(n[4])][i] = cy * sz
    Btsz[int(n[5])][i] = cz * sz

k = Bt.dot(B)
kk = Btsz.dot(B)
# d = B.dot(Bt)

nk = k
```

```
    for i in range(len(tss)):
        for j in range(loss):
            if (i + 1) == toss[j]:
                for ii in range(lgss):
                    if ii == i:
                        nk[i][i] = 1
                    else:
                        nk[i][ii] = 0
                        nk[ii][i] = 0

    nkk = kk
    for i in range(len(tss)):
        for j in range(loss):
            if (i + 1) == toss[j]:
                for ii in range(lgss):
                    if ii == i:
                        nk[i][i] = 1
                    else:
                        nk[i][ii] = 0
                        nk[ii][i] = 0

    ii = 0
    nB = np.zeros((le, lnss))
    for i in range(lnss):
        ii = tnss[i]
        for j in range(le):
            nB[j][i] = B[j][int(ii - 1)]
    nd = nB.dot(np.transpose(nB))

    for i in range(len(tss)):
        for j in range(loss):
            if (i + 1) == toss[j]:
                for ii in range(lgss):
                    if ii == i:
                        nk[i][i] = 1
                    else:
                        nk[i][ii] = 0
                        nk[ii][i] = 0

#grupowanie elementow
    max_ss = max(solution)
    wy02 = np.zeros(le)

    np.put(wy02, np.arange(0,6), solution[0] / max_ss)
    np.put(wy02, np.arange(6,12), solution[1] / max_ss)
    np.put(wy02, np.arange(12,18), solution[2] / max_ss)
    np.put(wy02, np.arange(18,24), solution[3] / max_ss)
    np.put(wy02, np.arange(24,30), solution[4] / max_ss)
    np.put(wy02, np.arange(30,36), solution[5] / max_ss)
    np.put(wy02, np.arange(36,48), solution[6] / max_ss)
    np.put(wy02, np.arange(48,60), solution[7] / max_ss)
    np.put(wy02, np.arange(60,66), -solution[8] / max_ss)
    np.put(wy02, np.arange(66,72), -solution[9] / max_ss)
```

```
    np.put(wy02, np.arange(72,78), -solution[10] / max_ss)

#sprawdzenie rownowagi wezlow
    print("Przyjęty self-stress: \nss = " + str(wy02))
    wy0 = wy02

    sum_equ = 0
    c = [6,7,8,9,10,11,12,13,14,15,16,17,18,19,20,21,22,23,24,25,26,27,29,
30,31,32,33,34,35,36,37,38,39,40,41,42,43,44,45,46,47,48,49,50,51,52,53
54,55,56,57,58,59,60,61,62,63,64,65,66,67,68,69,70,71,72,73,74,75,76,77
78]
    for i in c:
        sum_equ2 = equ(p1, p2, x, y, z, wy02, i)
        sum_equ += sum_equ2 ** 2

    output2 = 1 / (sum_equ ** 0.5 + 0.00001)

    print("suma wezly")
    print(sum_equ)

    kg = np.zeros((lgss, lgss))
    nn = np.zeros(llss)
    for i in range(le):
        w1 = p1[i]
        w2 = p2[i]
        x1 = x[w1 - 1]
        y1 = y[w1 - 1]
        z1 = z[w1 - 1]
        x2 = x[w2 - 1]
        y2 = y[w2 - 1]
        z2 = z[w2 - 1]
        L = ((x2 - x1) ** 2 + (y2 - y1) ** 2 + (z2 - z1) ** 2) ** 0.5
        nn[2] = 3 * w1 - 1
        nn[1] = 3 * w1 - 2
        nn[0] = 3 * w1 - 3
        nn[5] = 3 * w2 - 1
        nn[4] = 3 * w2 - 2
        nn[3] = 3 * w2 - 3
        S = wy0[i]
        kge = S / L * np.array([[1, 0, 0, -1, 0, 0],
                        [0, 1, 0, 0, -1, 0],
                        [0, 0, 1, 0, 0, -1],
                        [-1, 0, 0, 1, 0, 0],
                        [0, -1, 0, 0, 1, 0],
                        [0, 0, -1, 0, 0, 1]])
        for j in range(llss):
            for ii in range(llss):
                kg[int(nn[ii])][int(nn[j])] += kge[ii][j]

    nkg = kg
    for i in range(len(tss)):
        for j in range(loss):
            if (i + 1) == toss[j]:
```

```
            for ii in range(lgss):
                if ii == i:
                    nkg[i][i] = 1
                else:
                    nkg[i][ii] = 0
                    nkg[ii][i] = 0

    kt1 = np.add(nkg, nkk)
    nkt1 = kt1
    for i in range(len(tss)):
        for j in range(loss):
            if (i + 1) == toss[j]:
                for ii in range(lgss):
                    if ii == i:
                        nkt1[i][i] = 1
                    else:
                        nkt1[i][ii] = 0
                        nkt1[ii][i] = 0

    wnkg_eigvals, wnkg_eigvecs = la.eig(nkt1)
    # print("Wartości własne stycznej macierzy sztywności: " + str(np.sort(np.
real(wnkg_eigvals))))
    wnkg_positive = False
    for i in range(len(wnkg_eigvals)):
        if wnkg_eigvals[i] >= 0:
            wnkg_positive = True
        else:
            wnkg_positive = False
            break

    if wnkg_positive:
        wnkg_str = "Zidentyfikowany mechanizm jest infinitezymalny"
        wnkg_red = [x for x in wnkg_eigvals if x != 1]
        # output = min(wnkg_red)
        output = 1
        print(wnkg_red)

    else:
        wnkg_str = "Mechanizm nie jest stabilizowany przez stan
samonaprężenia"
        output = 0
        print(wnkg_str)

    print("równowaga", output2)
    print("Kt", output)

    fitness = output2 * output
    return fitness

fitness_function = fitness_func

num_generations = 1100 # Number of generations.
num_parents_mating = 150 # Number of solutions to be selected as parents
```

```
in the mating pool.
sol_per_pop = 250 # Number of solutions in the population.
num_genes = 11

init_range_low = 0.01
init_range_high = 0.99

parent_selection_type = "sss" # Type of parent selection.
keep_parents = -1 # Number of parents to keep in the next population. -1
means keep all parents and 0 means keep nothing.

crossover_type = "uniform" # Type of the crossover operator.

# Parameters of the mutation operation.
mutation_type = "random" # Type of the mutation operator.
mutation_percent_genes = 20 # Percentage of genes to mutate. This
parameter has no action if the parameter mutation_num_genes exists or
when mutation_type is None.

last_fitness = 0
def callback_generation(ga_instance):
   global last_fitness
   print("Generation = {generation}".format(generation=ga_instance.
generations_completed))
   print("Fitness    = {fitness}".format(fitness=ga_instance.best_solution
()[1]))
   print("Change     = {change}".format(change=ga_instance.
best_solution()[1] - last_fitness))
   last_fitness = ga_instance.best_solution()[1]

# Creating an instance of the GA class inside the ga module. Some
parameters are initialized within the constructor.
ga_instance = pygad.GA(num_generations=num_generations,
                       num_parents_mating=num_parents_mating,
                       fitness_func=fitness_function,
                       sol_per_pop=sol_per_pop,
                       num_genes=num_genes,
                       init_range_low=init_range_low,
                       init_range_high=init_range_high,
                       parent_selection_type=parent_selection_type,
                       keep_parents=keep_parents,
                       crossover_type=crossover_type,
                       mutation_type=mutation_type,
                       mutation_percent_genes=mutation_percent_genes,
                       random_mutation_min_val=0,
                       random_mutation_max_val=1.0,
                       on_generation=callback_generation)

# Running the GA to optimize the parameters of the function.
ga_instance.run()

# After the generations complete, some plots are showed that summarize the
 how the outputs/fitenss values evolve over generations.
```

```
ga_instance.plot_result()

# Returning the details of the best solution.
solution, solution_fitness, solution_idx = ga_instance.best_solution()
print("Parameters of the best solution : {solution}".format(solution=
solution))
print("Fitness value of the best solution = {solution_fitness}".format(
solution_fitness=solution_fitness))
print("Index of the best solution : {solution_idx}".format(solution_idx=
solution_idx))

#prediction =
#print("Predicted output based on the best solution : {prediction}".format(
prediction=prediction))

if ga_instance.best_solution_generation != -1:
   print("Best fitness value reached after {best_solution_generation}
generations.".format(best_solution_generation=ga_instance.
best_solution_generation))

# Saving the GA instance.
filename = 'genetic' # The filename to which the instance is saved. The
name is without extension.
ga_instance.save(filename=filename)

# Loading the saved GA instance.
loaded_ga_instance = pygad.load(filename=filename)
loaded_ga_instance.plot_fitness()

string = ""
print(solution)
for i in solution:
   string = string + str(i) + ","
print (string)
```

Example of the solution calculated for Geiger dome (RG 6B)

```
Parameters of the best solution : [1.06641286 0.83229971 1.93267036 3.9547615  1.10785665 0.84460437
 2.06033303 4.5027814  0.16996956 0.66759805 2.26572047]
Fitness value of the best solution = 21.61694475071151
Index of the best solution : 0
Best fitness value reached after 1029 generations.
[1.06641286 0.83229971 1.93267036 3.9547615  1.10785665 0.84460437
 2.06033303 4.5027814  0.16996956 0.66759805 2.26572047]
1.0664128629564233,0.8322997050273251,1.9326703582156897,3.9547614959700583,1.1078566466637918,0.8446

Process finished with exit code 0
```

Version Control   Run   TODO   Problems   Terminal   Python Packages   Python Console

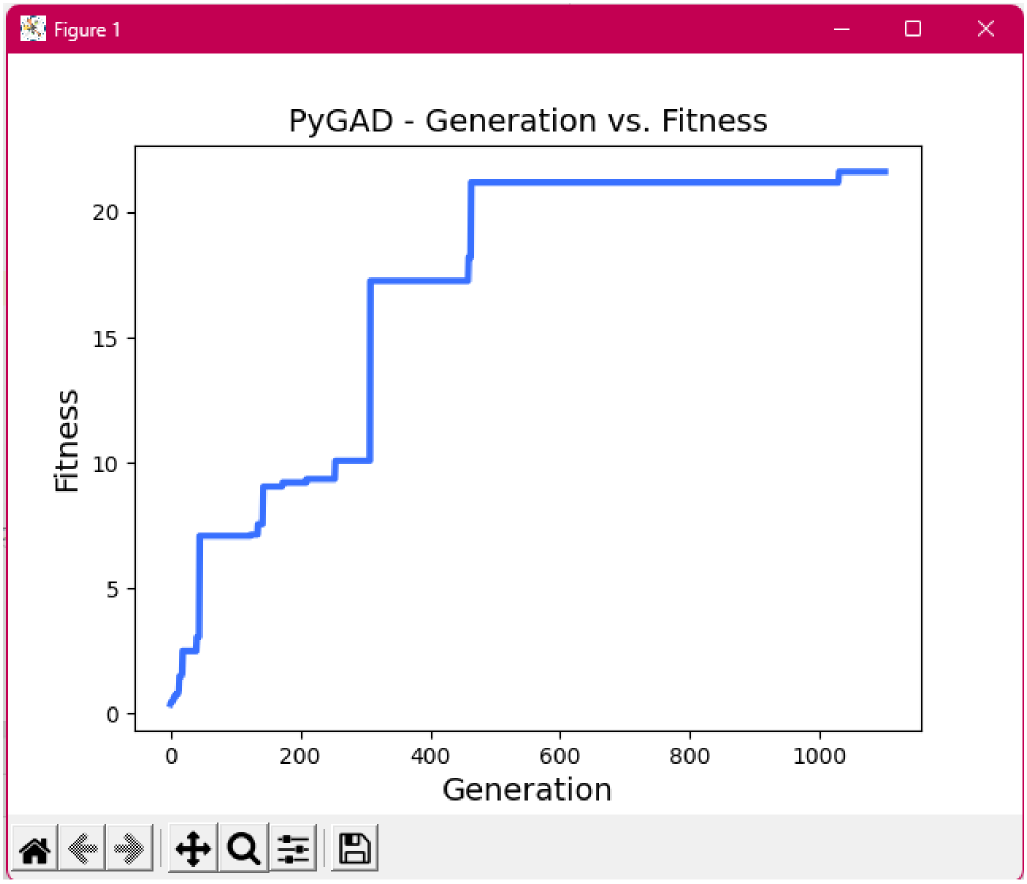

Appendix C – Dynamic stability analysis of Geiger dome (RG 6B) (Mathematica environment)

```
ClearAll["Global`*"];
wyczyść wszystko

MKlin[p1_, p2_, x_, y_, z_, e_, a_, le_, loss_, toss_, lgss_] := Module[
                                                                  moduł
   (*
     q       -   wektor przemieszczen, dla liniowych zagadnien musi byc 0,
   dla nieliniowych jest inicjowany ostatnimi przyblizeniami;
     p1,p2 -    wektory numerow poczatkowych i koncowych wezlow  pretow;
     x,y,z -    wektory wspolzednych wezlow;
     e      -   wektor modulow Younga poszczegolnych pretow;
     a      -   wektor pol przekrojow poprzecznych poszczegolnych pretow;
     sne    -   wektor sil samonaprezen elementow (pretow);
     msne   -   mnoznik samonaprezen;
     le     -   liczba elementow;
     loss   -   liczba odebranych stopni swobody;
     toss   -   wektor odebranych stopni swobody;
     lgss   -   liczba globalnych stopni swobody;
   *)
   {
    Kl, Ks, Ku1, Ku2, Kge, Kg, T, u, w1, w2,
    x1, y1, z1, x2, y2, z2, x21, y21, z21, lxy, l, sa, ca, sb, s,
    cb, T1, se, q1, q2, ql1, ql2, dq, ea11, ea21, ea31, sl, i,
    j, I1, I2, wi, ko, wd, kd, wm, km, Tt, nkg, ii
   },
   (
    Kl = Table[0, {6}, {6}];
         tabela
    Kge = Table[0, {6}, {6}]; (*macierz sztywnosci elemntu w ukladzie globalnym *)
          tabela
    Kg = Table[0, {lgss}, {lgss}]; (*globalna maciesz sztywnosci *)
         tabela
    T = Table[0, {6}, {6}];
        tabela
    (*macierz transformacji elementu - z globalnego do lokalnego*)

    Do[
    rób
     (
      w1 = p1[[i]];
      w2 = p2[[i]];
      x1 = x[[w1]];
      y1 = y[[w1]];
      z1 = z[[w1]];
      x2 = x[[w2]];
      y2 = y[[w2]];
      z2 = z[[w2]];
      x21 = (x2 - x1);
      y21 = (y2 - y1);
      z21 = (z2 - z1);
```

```
lxy = Sqrt[x21 * x21 + y21 * y21];
      pierwiastek kwadratowy
l = Sqrt[x21 * x21 + y21 * y21 + z21 * z21];
    pierwiastek kwadratowy

If[lxy != 0,
operator warunkowy
 sa = z21 / l; ca = lxy / l; sb = y21 / lxy; cb = x21 / lxy;
 T1 = {{ca * cb, ca * sb, sa}, {-sb, cb, 0}, {-sa * cb, -sa * sb, ca}},
 T1 = {{0, 0, -1}, {-1, 0, 0}, {0, 1, 0}}
];

se = {3 * w1 - 2, 3 * w1 - 1, 3 * w1, 3 * w2 - 2, 3 * w2 - 1, 3 * w2};

ea1l = e[[i]] * a[[i]] / l;
ea2l = ea1l / l;
ea3l = ea2l / l;

Do[Do[Do[Do[
rób rób rób rób
     (
      wi = 3 * (wd - 1);
      ko = 3 * (kd - 1);
      T[[wi + wm, ko + km]] = T1[[wm, km]];
     )
     , {km, 3}], {wm, 3}], {kd, 2}], {wd, 2}
];

Do[Do[
rób rób
   (
    T[[wm, km]] = T[[km, wm]] = 0;
   )
   , {km, 4, 6}], {wm, 1, 3}
];

Kl[[1, 1]] = Kl[[4, 4]] = ea1l;
Kl[[4, 1]] = Kl[[1, 4]] = -Kl[[1, 1]];
Kge = Kl;
Tt = Transpose[T];
     transpozycja
Kge = Tt.Kge.T;
Do[Do[
   rób
   (
    Kg[[se[[wm]], se[[km]]]] += Kge[[wm, km]];
   )
   , {km, 6}], {wm, 6}
 ]
),
{i, le}
```

```
  ];

  nkg = Kg;
  Do[
  rób
   (
    ii = toss[[i]];
    Do[
    rób
     (
      nkg[[ii, j]] = 0;
      nkg[[j, ii]] = 0;
     ),
     {j, lgss}
    ];
    nkg[[ii, ii]] = 1;
   ),
   {i, loss}
  ];
  nkg
 )
];


MKgeom[p1_, p2_, x_, y_, z_, e_, a_, sne_, msne_, le_, loss_, toss_, lgss_] := Module[
                                                                              moduł
 {
  Kl, Ks, Kge, Kg, T, u, w1, w2, x1,
  y1, z1, x2, y2, z2, x21, y21, z21, lxy, l, sa, ca, sb, s,
  cb, T1, se, q1, q2, ql1, ql2, dq, ea11, ea21, ea31, sl, i,
  j, I1, I2, wi, ko, wd, kd, wm, km, Tt, nkg, ii
 },
 (
  Kl = Ks = Table[0, {6}, {6}];
            tabela
  Kge = Table[0, {6}, {6}]; (*macierz sztywnosci elemntu w ukladzie globalnym *)
        tabela
  Kg = Table[0, {lgss}, {lgss}]; (*globalna maciesz sztywnosci *)
       tabela
  T = Table[0, {6}, {6}];
      tabela
  (*macierz transformacji elementu - z globalnego do lokalnego*)
  u = Table[0, {3}];
      tabela

  Do[
  rób
   (
    w1 = p1[[i]];
    w2 = p2[[i]];
    x1 = x[[w1]];
```

```
    y1 = y[[w1]];
    z1 = z[[w1]];
    x2 = x[[w2]];
    y2 = y[[w2]];
    z2 = z[[w2]];
    x21 = (x2 - x1);
    y21 = (y2 - y1);
    z21 = (z2 - z1);
    lxy = Sqrt[x21 * x21 + y21 * y21];
          pierwiastek kwadratowy
    l = Sqrt[x21 * x21 + y21 * y21 + z21 * z21];
        pierwiastek kwadratowy

    se = {3 * w1 - 2, 3 * w1 - 1, 3 * w1, 3 * w2 - 2, 3 * w2 - 1, 3 * w2};
    (*stoponie swobody element*)

    s = sne[[i]];
    sl = msne * s / l;

    Do[Ks[[j, j]] = sl, {j, 6}];
    rób
    Do[Ks[[j, j + 3]] = Ks[[j + 3, j]] = -sl, {j, 3}];
    rób

    Kge = Ks;

    Do[Do[
    ···  rób
      (
       Kg[[se[[wm]], se[[km]]]] += Kge[[wm, km]];
      )
      , {km, 6}], {wm, 6}
    ]
  ),
  {i, le}
];

nkg = Kg;
Do[
rób
  (
    ii = toss[[i]];
    Do[
    rób
      (
       nkg[[ii, j]] = 0;
       nkg[[j, ii]] = 0;
      ),
      {j, lgss}
    ];
    nkg[[ii, ii]] = 1;
```

```
      ),
      {i, loss}
     ];
     nkg
    )
   ];

 MM[p1_, p2_, x_, y_, z_, e_, a_, ro_, le_, loss_, toss_, lgss_] := Module[
                                                                    moduł
    (*ro    -   wektor gęstości,
      le    -   liczba elementow;*)
    {w1, w2, x1, x2, y1, y2, z1, z2, x21, y21, z21, l, se, Me, M, nM, i, j, ii, wm, km},
    (M = Table[0, {lgss}, {lgss}];
         tabela
     Do[
     rób
      w1 = p1[[i]];
      w2 = p2[[i]];
      x1 = x[[w1]];
      y1 = y[[w1]];
      z1 = z[[w1]];
      x2 = x[[w2]];
      y2 = y[[w2]];
      z2 = z[[w2]];
      x21 = (x2 - x1);
      y21 = (y2 - y1);
      z21 = (z2 - z1);
      l = Sqrt[x21 * x21 + y21 * y21 + z21 * z21];
          pierwiastek kwadratowy
      se = {3 * w1 - 2, 3 * w1 - 1, 3 * w1, 3 * w2 - 2, 3 * w2 - 1, 3 * w2};
      Me = ro[[i]] * a[[i]] * l / 6 * {{2, 0, 0, 1, 0, 0},
          {0, 2, 0, 0, 1, 0},
          {0, 0, 2, 0, 0, 1},
          {1, 0, 0, 2, 0, 0},
          {0, 1, 0, 0, 2, 0},
          {0, 0, 1, 0, 0, 2}};
      Do[Do[
      rób rób
        M[[se[[wm]], se[[km]]]] += Me[[wm, km]];
        , {km, 6}], {wm, 6}
      ],
      {i, le}];
     nM = M;
     Do[
     rób
      (
       ii = toss[[i]];
       Do[
       rób
        (
         nM[[ii, j]] = 0;
```

```
        nM[[j, ii]] = 0;
       ),
       {j, lgss}
      ];
      nM[[ii, ii]] = 1;
     ),
     {i, loss}
    ];
    nM
   )
  ];

Sily[tob_, si_, sne_, msne_, le_, lgss_, p1_, p2_, x_, y_, z_] := Module[
                                                                   moduł
   {T, f, i, j, w1, w2, x1, y1, z1, x2, y2, z2, x21, y21, z21,
    lxy, l, sa, ca, sb, cb, T1, ms, wi, wd, ko, kd, wm, km, Tt, pp, se, p},
   (*tob   -   tablica numerow obciazonych stopni swobody - sily zewnetrzne;
     si    -
    tablica wartosci sil zewnetrznych odpowiednich stopniom swobody z tob; *)
   (
    T = Table[0, {6}, {6}];
        tabela
    f = Table[0, {6}];
        tabela
    p = Table[0, {lgss}];
        tabela

    (*obciazenie zewnetrzne w ukladzie globalnym*)
    Do[p[[tob[[i]]]] += si[[i]], {i, Length[tob]}];
    rób                               długość
    p
   )
  ];


SilyPrety[qp_, p1_, p2_, x_, y_, z_, e_, a_, le_, loss_, toss_] := Module[
                                                                      moduł
   (*qp     -   wektor przemieszczen, dla liniowych zagadnien musi byc 0,
   dla nieliniowych jest inicjowany ostatnimi przyblizeniami;*)
   {
    q, SP, i, j, T, u, w1, w2, x1, y1, z1, x2, y2, z2, x21, y21, z21, lxy, l, sa, ca, sb,
    cb, T1, se, q1, q2, ql1, ql2, dq, l1, l11, eps
   },
   (
    T = Table[0, {6}, {6}];
        tabela
    (*macierz transformacji elementu - z globalnego do lokalnego*)
    SP = Table[0, {le}]; (*wektor sil w pretach*)
         tabela
    u = Table[0, {3}];
        tabela
```

```
q = qp;
Do[q[[toss[[i]]]] = 0, {i, loss}];
rób

Do[
rób
 (
  w1 = p1[[i]];
  w2 = p2[[i]];
  x1 = x[[w1]];
  y1 = y[[w1]];
  z1 = z[[w1]];
  x2 = x[[w2]];
  y2 = y[[w2]];
  z2 = z[[w2]];
  x21 = (x2 - x1);
  y21 = (y2 - y1);
  z21 = (z2 - z1);
  lxy = Sqrt[x21 * x21 + y21 * y21];
        pierwiastek kwadratowy
  l = Sqrt[x21 * x21 + y21 * y21 + z21 * z21];
      pierwiastek kwadratowy

  If[lxy != 0,
  operator warunkowy
   sa = z21 / l; ca = lxy / l; sb = y21 / lxy; cb = x21 / lxy;
   T1 = {{ca * cb, ca * sb, sa}, {-sb, cb, 0}, {-sa * cb, -sa * sb, ca}},
   T1 = {{0, 0, -1}, {-1, 0, 0}, {0, 1, 0}}
  ];

  se = {3 * w1 - 2, 3 * w1 - 1, 3 * w1, 3 * w2 - 2, 3 * w2 - 1, 3 * w2};
  (*stoponie swobody element*)
  q1 = {{q[[se[[1]]]]}, {q[[se[[2]]]]}, {q[[se[[3]]]]}};
  q2 = {{q[[se[[4]]]]}, {q[[se[[5]]]]}, {q[[se[[6]]]]}};

  ql1 = T1.q1;
  ql2 = T1.q2;
  dq = ql2 - ql1;

  Do[u[[j]] = dq[[j, 1]], {j, 3}];
  rób

  (*zdjecie, poczatek*)
  l1 = Sqrt[u[[2]] * u[[2]] + u[[3]] * u[[3]] + (l + u[[1]]) * (l + u[[1]])];
         pierwiastek kwadratowy
  l11 = l1 / l;
  eps = (l11 * l11 - 1) / 2;
  SP[[i]] = e[[i]] * a[[i]] * eps * l11
  (*zdjecie, koniec*)
```

```
      ),
      {i, le}
     ];

     SP
    )
   ];

MK[q_, p1_, p2_, x_, y_, z_, e_, a_, sne_, msne_, le_, loss_, toss_, lgss_] := Module[
                                                                                  moduł
    {
     Kl, Ks, Ku1, Ku2, Kge, Kg, T, u, w1, w2,
     x1, y1, z1, x2, y2, z2, x21, y21, z21, lxy, l, sa, ca, sb, s,
     cb, T1, se, q1, q2, ql1, ql2, dq, ea11, ea21, ea31, sl, i,
     j, I1, I2, wi, ko, wd, kd, wm, km, Tt, nkg, ii
    },
    (
     Kl = Ks = Ku1 = Ku2 = Table[0, {6}, {6}];
                           tabela
     Kge = Table[0, {6}, {6}]; (*macierz sztywnosci elemntu w ukladzie globalnym *)
           tabela
     Kg = Table[0, {lgss}, {lgss}]; (*globalna maciesz sztywnosci *)
          tabela
     T = Table[0, {6}, {6}];
         tabela
     (*macierz transformacji elementu - z globalnego do lokalnego*)
     u = Table[0, {3}];
         tabela

     Do[
     rób
      (
       w1 = p1[[i]];
       w2 = p2[[i]];
       x1 = x[[w1]];
       y1 = y[[w1]];
       z1 = z[[w1]];
       x2 = x[[w2]];
       y2 = y[[w2]];
       z2 = z[[w2]];
       x21 = (x2 - x1);
       y21 = (y2 - y1);
       z21 = (z2 - z1);
       lxy = Sqrt[x21 * x21 + y21 * y21];
             pierwiastek kwadratowy
       l = Sqrt[x21 * x21 + y21 * y21 + z21 * z21];
           pierwiastek kwadratowy

       If[lxy != 0,
       operator warunkowy
        sa = z21 / l; ca = lxy / l; sb = y21 / lxy; cb = x21 / lxy;
```

```
 T1 = {{ca * cb, ca * sb, sa}, {-sb, cb, 0}, {-sa * cb, -sa * sb, ca}},
 T1 = {{0, 0, -1}, {-1, 0, 0}, {0, 1, 0}}
];

se = {3 * w1 - 2, 3 * w1 - 1, 3 * w1, 3 * w2 - 2, 3 * w2 - 1, 3 * w2};
(*stoponie swobody element*)
q1 = {{q[[se[[1]]]]}, {q[[se[[2]]]]}, {q[[se[[3]]]]}};
q2 = {{q[[se[[4]]]]}, {q[[se[[5]]]]}, {q[[se[[6]]]]}};

ql1 = T1.q1;
ql2 = T1.q2;
dq = ql2 - ql1;

ea1l = e[[i]] * a[[i]] / l;
ea2l = ea1l / l;
ea3l = ea2l / l;

Kl[[1, 1]] = Kl[[4, 4]] = ea1l;
Kl[[4, 1]] = Kl[[1, 4]] = -Kl[[1, 1]];

s = sne[[i]];
sl = msne * s / l;

Do[u[[j]] = dq[[j, 1]], {j, 3}];
rób
(*sl=ea1l*u[[1]];*)
Do[Ks[[j, j]] = sl, {j, 6}];
rób
Do[Ks[[j, j + 3]] = Ks[[j + 3, j]] = -sl, {j, 3}];
rób

I1 = {
   {3 * u[[1]], u[[2]], u[[3]]},
   {2 * u[[2]], 0, 0},
   {2 * u[[3]], 0, 0}
 };

I2 = {
   {u[[1]] * u[[1]], u[[1]] * u[[2]], u[[1]] * u[[3]]},
   {u[[1]] * u[[2]], u[[2]] * u[[2]], u[[2]] * u[[3]]},
   {u[[1]] * u[[3]], u[[2]] * u[[3]], u[[3]] * u[[3]]}
 };

Do[Do[Do[Do[
rób rób rób rób
     (
      wi = 3 * (wd - 1);
      ko = 3 * (kd - 1);
      Ku1[[wi + wm, ko + km]] = ea2l * I1[[wm, km]];
      Ku2[[wi + wm, ko + km]] = ea3l * I2[[wm, km]];
      (*poprawione*)
```

```
          T[[wi + wm, ko + km]] = T1[[wm, km]];
         )
         , {km, 3}], {wm, 3}], {kd, 2}], {wd, 2}
    ];

    Do[Do[
    rób rób
       (
        Ku1[[wm, km]] = -Ku1[[wm, km]];
        Ku1[[km, wm]] = -Ku1[[km, wm]];
        Ku2[[wm, km]] = -Ku2[[wm, km]];
        Ku2[[km, wm]] = -Ku2[[km, wm]];
        T[[wm, km]] = T[[km, wm]] = 0;
       )
       , {km, 4, 6}], {wm, 1, 3}
    ];

    Kge = Kl + Ks + Ku1 / 2. + Ku2 / 2.;
    Tt = Transpose[T];
         transpozycja
    Kge = Tt.Kge.T;

    Do[Do[
    rób rób
       (
        Kg[[se[[wm]], se[[km]]]] += Kge[[wm, km]];
       )
       , {km, 6}], {wm, 6}
    ]
   ),
   {i, le}
  ];

  nkg = Kg;
  Do[
  rób
   (
    ii = toss[[i]];
    Do[
    rób
     (
      nkg[[ii, j]] = 0;
      nkg[[j, ii]] = 0;
     ),
     {j, lgss}
    ];
    nkg[[ii, ii]] = 1;
   ),
   {i, loss}
  ];
  nkg
```

```
  )
 ];

MKsty[q_, p1_, p2_, x_, y_, z_, e_, a_, sne_, msne_, le_, loss_, toss_, lgss_] := Module[
                                                                                   moduł
  {
   Kl, Ks, Ku1, Ku2, Kp, Kge, Kg, T, u, w1,
   w2, x1, y1, z1, x2, y2, z2, x21, y21, z21, lxy, l, sa, ca, sb, s,
   cb, T1, se, q1, q2, ql1, ql2, dq, ea11, ea21, ea31, sl, su,
   i, j, I1, I2, wi, ko, wd, kd, wm, km, Tt, nkg, ii
  },
  (
   Kl = Ks = Ku1 = Ku2 = Kp = Table[0, {6}, {6}];
                              tabela
   Kge = Table[0, {6}, {6}]; (*macierz sztywnosci elemntu w ukladzie globalnym *)
         tabela
   Kg = Table[0, {lgss}, {lgss}]; (*globalna maciesz sztywnosci *)
        tabela
   T = Table[0, {6}, {6}];
       tabela
   (*macierz transformacji elementu - z globalnego do lokalnego*)
   u = Table[0, {3}];
       tabela
   Do[
   rób
    (
     w1 = p1[[i]];
     w2 = p2[[i]];
     x1 = x[[w1]];
     y1 = y[[w1]];
     z1 = z[[w1]];
     x2 = x[[w2]];
     y2 = y[[w2]];
     z2 = z[[w2]];
     x21 = (x2 - x1);
     y21 = (y2 - y1);
     z21 = (z2 - z1);
     lxy = Sqrt[x21 * x21 + y21 * y21];
           pierwiastek kwadratowy
     l = Sqrt[x21 * x21 + y21 * y21 + z21 * z21];
         pierwiastek kwadratowy
     If[lxy != 0,
     operator warunkowy
      sa = z21 / l; ca = lxy / l; sb = y21 / lxy; cb = x21 / lxy;
      T1 = {{ca * cb, ca * sb, sa}, {-sb, cb, 0}, {-sa * cb, -sa * sb, ca}},
      T1 = {{0, 0, -1}, {-1, 0, 0}, {0, 1, 0}}
     ];

     se = {3 * w1 - 2, 3 * w1 - 1, 3 * w1, 3 * w2 - 2, 3 * w2 - 1, 3 * w2};
     (*stoponie swobody element*)
     q1 = {{q[[se[[1]]]]}, {q[[se[[2]]]]}, {q[[se[[3]]]]}};
```

```
q2 = {{q[[se[[4]]]]}, {q[[se[[5]]]]}, {q[[se[[6]]]]}};

ql1 = T1.q1;
ql2 = T1.q2;
dq = ql2 - ql1;

ea1l = e[[i]] * a[[i]] / l;
ea2l = ea1l / l;
ea3l = ea2l / l;

Kl[[1, 1]] = Kl[[4, 4]] = ea1l;
Kl[[4, 1]] = Kl[[1, 4]] = -Kl[[1, 1]];

s = sne[[i]];
sl = msne * s / l;

Do[u[[j]] = dq[[j, 1]], {j, 3}];
rób
(*sl=ea1l*u[[1]];*)
Do[Ks[[j, j]] = sl, {j, 6}];
rób
Do[Ks[[j, j + 3]] = Ks[[j + 3, j]] = -sl, {j, 3}];
rób

su = (u[[1]] * u[[1]] + u[[2]] * u[[2]] + u[[3]] * u[[3]] / 2);
Do[Kp[[j, j]] = su * ea3l, {j, 6}];
rób
Do[Kp[[j, j + 3]] = Ks[[j + 3, j]] = -su * ea3l, {j, 3}];
rób

I1 = {
   {3 * u[[1]], u[[2]], u[[3]]},
   {u[[2]], u[[1]], 0},
   {u[[3]], 0, u[[1]]}
  };

I2 = {
   {u[[1]] * u[[1]], u[[1]] * u[[2]], u[[1]] * u[[3]]},
   {u[[1]] * u[[2]], u[[2]] * u[[2]], u[[2]] * u[[3]]},
   {u[[1]] * u[[3]], u[[2]] * u[[3]], u[[3]] * u[[3]]}
  };

Do[Do[Do[Do[
··  rób rób rób
     (
      wi = 3 * (wd - 1);
      ko = 3 * (kd - 1);
      Ku1[[wi + wm, ko + km]] = ea2l * I1[[wm, km]];
      Ku2[[wi + wm, ko + km]] = ea3l * I2[[wm, km]];
      (*poprawione*)
      T[[wi + wm, ko + km]] = T1[[wm, km]];
```

```
        )
        , {km, 3}], {wm, 3}], {kd, 2}], {wd, 2}
    ];

    Do[Do[
    |… |rób
      (
       Ku1[[wm, km]] = -Ku1[[wm, km]];
       Ku1[[km, wm]] = -Ku1[[km, wm]];
       Ku2[[wm, km]] = -Ku2[[wm, km]];
       Ku2[[km, wm]] = -Ku2[[km, wm]];
       T[[wm, km]] = T[[km, wm]] = 0;
      )
      , {km, 4, 6}], {wm, 1, 3}
    ];

    Kge = Kl + Ks + Ku1 + Ku2 + Kp;
    Tt = Transpose[T];
         |transpozycja
    Kge = Tt.Kge.T;

    Do[Do[
    |… |rób
      (
       Kg[[se[[wm]], se[[km]]]] += Kge[[wm, km]];
      )
      , {km, 6}], {wm, 6}
    ]
   ),
   {i, le}
  ];

  nkg = Kg;
  Do[
  |rób
   (
    ii = toss[[i]];
    Do[
    |rób
     (
      nkg[[ii, j]] = 0;
      nkg[[j, ii]] = 0;
     ),
     {j, lgss}
    ];
    nkg[[ii, ii]] = 1;
   ),
   {i, loss}
  ];
  nkg
 )
```

```
  ];


Newton[sl_, tsl_, qg_, p_, p1_, p2_, x_, y_,
   z_, e_, a_, sne_, msne_, le_, loss_, toss_, lgss_] := Module[
                                                        moduł
   (* tsl   -   tablica numerow sledzonych przemieszczen; *)
   {KK, krs, ws, qp, tkrs, A, ff, tz, is, stop, fp, f, q1, KK1, f1, eps, dp, i, j, q, tpo},
   q = qg;

   is = 0;
   ws = 10^(-6); (*warunek stopu*)
   KK = MK[q, p1, p2, x, y, z, e, a, sne, msne, le, loss, toss, lgss];
   qp = q;
   q = LinearSolve[KK, p];
       rozwiąż układ równań liniowych
   (*q=Inverse[KK].p;*)
        macierz odwrotna

   If[sl == 1,
   operator warunkowy
    Print["iteracja ", is];
    drukuj
    tpo = Table[0, {Length[tsl]}];
          tabela   długość
    Do[tpo[[i]] = q[[tsl[[i]]]],
    rób
     {i, Length[tsl]}];
         długość
    Print[ScientificForm[tpo]]
          postać wykładnicza
   ];


   A = Table[0, {lgss}, {lgss}];
       tabela
   ff = Table[0, {lgss}];
        tabela
   (*tablica znacznikow odebrania stopnia swobody 1-nieodebrany, 0-odebrany*)
   tz = Table[1, {lgss}]; Do[tz[[toss[[i]]]] = 0, {i, loss}];
        tabela            rób
   stop = 1;

   While[ stop > ws,
   podczas
    (
     is++;
     KK = MK[q, p1, p2, x, y, z, e, a, sne, msne, le, loss, toss, lgss];
     f = KK.q;
     fp = f - p;

     A = MKsty[q, p1, p2, x, y, z, e, a, sne, msne, le, loss, toss, lgss];
```

```
      eps = LinearSolve[A, fp];
              rozwiąż układ równań liniowych
      (*eps=Inverse[A].fp;*)
               macierz odwrotna
      qp = q;
      q = qp - eps;

      If[sl == 1,
      operator warunkowy
       Print["iteracja ", is];
       drukuj
       tpo = Table[0, {Length[tsl]}];
             tabela    długość
       Do[tpo[[i]] = q[[tsl[[i]]]],
       rób
        {i, Length[tsl]}];
            długość
       Print[ScientificForm[tpo]]
              postać wykładnicza
      ];

      dp = 0;
      Do[(dp += eps[[j]] * eps[[j]]), {j, lgss}];
      rób
      stop = Sqrt[dp];
             pierwiastek kwadratowy
      If[is > 100000, Print["Przekroczona liczba dopuszczalnch iteracji"];
                      drukuj
       Break[];
       przerwij operacje
      ismax = is;
     )
    ];
    q
   ];

NewtonRaphson[sl_, tsl_, qg_, p_, p1_, p2_, x_,
   y_, z_, e_, a_, sne_, msne_, le_, loss_, toss_, lgss_] := Module[
                                                            moduł
   {q, ws, qp, KK, f, dQ, stop, is, lpwe, dq, dp, i, tpo},
   q = qg; (*przemieszczeni oczatkowe, zerowe*)
   ws = 10^(-4); (*warunek stopu*)

   is = 0;
   (*rozwiazanie liniowe - pierwsza iteracja, poczatek*)
   qp = q; (*poprzednie przyblizenie rozwiazania*)
   KK = MKsty[q, p1, p2, x, y, z, e, a, sne, msne, le, loss, toss, lgss];
   q = LinearSolve[KK, p];
       rozwiąż układ równań liniowych

   If[sl == 1,
   operator warunkowy
```

```
 Print["iteracja ", is];
 drukuj
 tpo = Table[0, {Length[tsl]}];
       tabela    długość
 Do[tpo[[i]] = q[[tsl[[i]]]],
 rób
  {i, Length[tsl]}];
     długość
 Print[ScientificForm[tpo]]
       postać wykładnicza
];

KK = MK[q, p1, p2, x, y, z, e, a, sne, msne, le, loss, toss, lgss];
f = KK.q;
dQ = p - f;
(*rozwiazanie liniowe - pierwsza iteracja, koniec*)

(*dlugos wektora przyrostu obciazenia, poczatek*)
dp = 0;
Do[(dp += dQ[[j]] * dQ[[j]]), {j, lgss}];
rób
stop = Sqrt[dp];
       pierwiastek kwadratowy
(*dlugos wektora przyrostu obciazenia, konic*)

(*iteracyjny proces NR, poczatek*)
While[ stop > ws,
podczas
 (
  is++;
  KK = MKsty[q, p1, p2, x, y, z, e, a, sne, msne, le, loss, toss, lgss];
  dq = LinearSolve[KK, dQ];
       rozwiąż układ równań liniowych
  q = q + dq;

  If[sl == 1,
  operator warunkowy
   Print["iteracja ", is];
   drukuj
   tpo = Table[0, {Length[tsl]}];
         tabela    długość
   Do[tpo[[i]] = q[[tsl[[i]]]],
   rób
    {i, Length[tsl]}];
       długość
   Print[ScientificForm[tpo]];
         postać wykładnicza
  ];

  KK = MK[q, p1, p2, x, y, z, e, a, sne, msne, le, loss, toss, lgss];
  f = KK.q;
  dQ = p - f;
```

```
      dp = 0;
      Do[(dp += dQ[[j]] * dQ[[j]]), {j, lgss}];
      róβ
      stop = Sqrt[dp];
             pierwiastek kwadratowy
      If[is > 50000, Print["Przekroczona liczba dopuszczalnch iteracji"];
                     drukuj
       Break[]];
       przerwij operacje
     )
    ];
    q
   ];

str = OpenRead[ToFileName[{NotebookDirectory[]}, "plik_wsadowyR6B.txt"]];
      otwórz do odczytu      katalog notatnika
le = Read[str, Number];
     czytaj    liczba
lw = Read[str, Number];
     czytaj    liczba
x = y = z = Table[0, {lw}];
            tabela
Do[x[[is]] = Read[str, Number], {is, lw}];
rób          czytaj    liczba
Do[y[[is]] = Read[str, Number], {is, lw}];
rób          czytaj    liczba
Do[z[[is]] = Read[str, Number], {is, lw}];
rób          czytaj    liczba

p1 = p2 = e = a = sne = Table[0, {le}];
                        tabela
Do[p1[[is]] = Read[str, Number], {is, le}];
rób           czytaj    liczba
Do[p2[[is]] = Read[str, Number], {is, le}];
rób           czytaj    liczba
Do[e[[is]] = Read[str, Number], {is, le}];
             czytaj    liczba
Do[a[[is]] = Read[str, Number], {is, le}];
rób          czytaj    liczba
loss = Read[str, Number];
       czytaj    liczba

toss = Table[0, {loss}];
       tabela
Do[toss[[is]] = Read[str, Number], {is, loss}];
rób             czytaj    liczba
Do[sne[[is]] = Read[str, Number], {is, le}];
rób            czytaj    liczba
Close[str];
zamknij strumień
ro = Table[7860, {le}];
     tabela
wy0 = sne;
```

```
lgss = 3 * lw;
msnei = {30};
P = -1;
Pt = Range[0, 1, 1 / 3] * 0.75 * P
      zakres

qq = qq2 = mSwP = mF = mOmega = Table[0, {Length[msnei]}];
                                tabela      długość
qq0 = qq02 = mOmega0 = Table[0, {Length[msnei]}];
                       tabela      długość
qq3 = qq4 = Table[0, {Length[Pt]}];
            tabela      długość
mOmega2 = mOmega3 = Table[0, {Length[msnei]}, {Length[Pt]}];
                    tabela      długość          długość
q0 = Table[0, {lgss}];
     tabela
tob = {1 * 3}
tsl = {24 * 3};  (*tablica sledzonch stopni swobody*)
si1 = P; (*obciazenie w kiloNiutonach*)

Do[
róב
 msne = msnei[[ii]]; (*mnożnik stanu samonaprężenia*)
 Print["mnożnik ", msne];
 drukuj

 p0 = Table[0, {lgss}];
      tabela
 KK = MK[q0, p1, p2, x, y, z, e, a, sne, msne, le, loss, toss, lgss];
 q02 = LinearSolve[KK, p0];
       rozwiąż układ równań liniowych
 qq02[[ii]] = q02;
 If[ii == 1,
 operator warunkowy
  q00 = Newton[0, tsl, q02, p0, p1, p2, x, y, z, e, a, sne, msne, le, loss, toss, lgss],
  q00 =
   Newton[0, tsl, qq0[[ii - 1]], p0, p1, p2, x, y, z, e, a, sne, msne, le, loss, toss, lgss]
 ];
 qq0[[ii]] = q00;

 tpo0 = Table[0, {Length[tsl]}];
        tabela      długość
 Do[tpo0[[i]] = q00[[tsl[[i]]]],
 rób
  {i, Length[tsl]}];
      długość
 Print["wyniki  ", ScientificForm[tpo0]];
                   postać wykładnicza
 Print["iteracja ", ismax];
 drukuj
 Print["q=", q00];
 drukuj
 (*************sily w pretach**************)
```

```
SwP0 = SilyPrety[q00, p1, p2, x, y, z, e, a, le, loss, toss];
ssf0 = SwP0 + msne * sne;
Print["sily w pretach ", ssf0];
drukuj
(*sprawdzenie, poczatek*)
KK = MK[q00, p1, p2, x, y, z, e, a, sne, msne, le, loss, toss, lgss];
Sly = KK.q00;
prog = 10^(-3); (*ponizej tej wartosci elementy beda zerowane*)
Do[If[Abs[Sly[[i]]] < prog, Sly[[i]] = 0], {i, lgss}];
    ··· wartość bezwzględna
Print["spr ", N[Sly, 3]];
              przybliżenie numeryczne
(*sprawdzenie*)
(*dynamika*)
Kdyn0 = MK[q0, p1, p2, x, y, z, e, a, ssf0, 1, le, loss, toss, lgss];
M = MM[p1, p2, x, y, z, e, a, ro, le, loss, toss, lgss];

omega0 = Sort[(Eigenvalues[{Kdyn0, M}] * 1000)^0.5 / 2 / Pi];
         sortuj  wartości własne macierzy              pi
For[d = Length[omega0], d > 0, d--,
        długość
 {If[Abs[omega0[[d]] - 5.0329] < 0.0001, omega0[[d]] = Sequence[]]}];
  ··· wartość bezwzględna                              kolejność argumentów
mOmega0[[ii]] = omega0;
Print["częstotliwości drgan własnych", omega0];
drukuj

si = Table[si1, {Length[tob]}];
     tabela     długość
Do[si[[i]] = si1, {i, Length[tob]}];
                      długość
p = Sily[tob, si, sne, msne, le, lgss, p1, p2, x, y, z];
KK = MK[q0, p1, p2, x, y, z, e, a, sne, msne, le, loss, toss, lgss];
q2 = LinearSolve[KK, p];
     rozwiąż układ równań liniowych
qq2[[ii]] = q2;
If[ii == 1,
operator warunkowy
 q = Newton[0, tsl, q2, p, p1, p2, x, y, z, e, a, sne, msne, le, loss, toss, lgss],
 q = Newton[0, tsl, qq[[ii - 1]], p, p1, p2, x, y, z, e, a, sne, msne, le, loss, toss, lgss]
];
qq[[ii]] = q;

(*macierze*)
MacSty = MKsty[q, p1, p2, x, y, z, e, a, sne, msne, le, loss, toss, lgss];
MacSie = MK[q, p1, p2, x, y, z, e, a, sne, msne, le, loss, toss, lgss];

tpo = Table[0, {Length[tsl]}];
      tabela    długość
Do[tpo[[i]] = q[[tsl[[i]]]],
rób
 {i, Length[tsl]}];
    długość
```

```
Print["wyniki  ", ScientificForm[tpo]];
                  postać wykładnicza
Print["iteracja ", ismax];
drukuj
Print["q=", q];
drukuj
(************sily w pretach*************)
SwP = SilyPrety[q, p1, p2, x, y, z, e, a, le, loss, toss];
ssf = SwP + msne * sne;
Print["sily w pretach ", ssf];
drukuj
mSwP[[ii]] = SwP;
(*sprawdzenie, poczatek*)
KK = MK[q, p1, p2, x, y, z, e, a, sne, msne, le, loss, toss, lgss];
Sly = KK.q;
prog = 10^(-3); (*ponizej tej wartosci elementy beda zerowane*)
Do[If[Abs[Sly[[i]]] < prog, Sly[[i]] = 0], {i, lgss}];
   ···  wartość bezwzględna
Print["spr ", N[Sly, 3]];
              przybliżenie numeryczne
(*sprawdzenie*)
(*dynamika*)
Kdyn = MK[q0, p1, p2, x, y, z, e, a, ssf, 1, le, loss, toss, lgss];
Kg = MKgeom[p1, p2, x, y, z, e, a, ssf, 1, le, loss, toss, lgss];
Kl = MKlin[p1, p2, x, y, z, e, a, le, loss, toss, lgss];
M = MM[p1, p2, x, y, z, e, a, ro, le, loss, toss, lgss];

omega1 = Sort[(Eigenvalues[{Kdyn, M}] * 1000)^0.5 / 2 / Pi];
          sortuj  wartości własne macierzy                 pi
For[d = Length[omega1], d > 0, d--,
        długość
 {If[Abs[omega1[[d]] - 5.0329] < 0.0001, omega1[[d]] = Sequence[]]}];
  ···  wartość bezwzględna                             kolejność argumentów
mOmega[[ii]] = omega1;
Print["częstotliwości drgan wymuszonych", omega1];
drukuj

Do[
rób
 si3 = Table[(P + 0.5 * Pt[[iii]]), {Length[tob]}];
       tabela                       długość
 Do[si3[[i]] = (P + 0.5 Pt[[iii]]), {i, Length[tob]}];
                                        długość
 p3 = Sily[tob, si3, sne, msne, le, lgss, p1, p2, x, y, z];
 q3 = Table[0., {lgss}];
      tabela
 Print[Pt[[iii]]];
 drukuj
 If[iii == 1,
 operator warunkowy
  q3 =
   Newton[0, tsl, qq[[ii]], p3, p1, p2, x, y, z, e, a, sne, msne, le, loss, toss, lgss],
```

```
 q3 = Newton[0, tsl, qq3[[iii - 1]], p3, p1, p2, x, y, z,
   e, a, sne, msne, le, loss, toss, lgss]
];
qq3[[iii]] = q3;
SwP3 = SilyPrety[q3, p1, p2, x, y, z, e, a, le, loss, toss];
ssf3 = SwP3 + msne * sne;

Kg3 = MKgeom[p1, p2, x, y, z, e, a, ssf3, 1, le, loss, toss, lgss];

omega2 = Sort[(Eigenvalues[{(Kl + Kg3), M / 4}] * 1000)^0.5 / 2 / Pi];
         sortuj  wartości własne macierzy                         pi
For[d = Length[omega2], d > 0, d--,
        długość
 {If[Abs[omega2[[d]] - 14.2353] < 0.0001, omega2[[d]] = Sequence[]]}];
  ⋯  wartość bezwzględna                               kolejność argumentów

mOmega2[[ii, iii]] = omega2;
Print["częstotliwość przy +Pt ", omega2];
drukuj

si4 = Table[(P - 0.5 * Pt[[iii]]), {Length[tob]}];
      tabela                        długość
Do[si4[[i]] = (P - 0.5 * Pt[[iii]]), {i, Length[tob]}];
                                         długość
p4 = Sily[tob, si4, sne, msne, le, lgss, p1, p2, x, y, z];
q4 = Table[0., {lgss}];
     tabela
If[iii == 1,
operator warunkowy
 q4 =
  Newton[0, tsl, qq[[ii]], p4, p1, p2, x, y, z, e, a, sne, msne, le, loss, toss, lgss
 q4 = Newton[0, tsl, qq4[[iii - 1]], p4, p1, p2, x, y, z,
   e, a, sne, msne, le, loss, toss, lgss]
];
qq4[[iii]] = q4;
SwP4 = SilyPrety[q4, p1, p2, x, y, z, e, a, le, loss, toss];
ssf4 = SwP4 + msne * sne;

Kg4 = MKgeom[p1, p2, x, y, z, e, a, ssf4, 1, le, loss, toss, lgss];

omega3 = N[Sort[(Eigenvalues[{(Kl + Kg4), M / 4}] * 1000)^0.5 / 2 / Pi], 4];
         ⋯ sortuj  wartości własne macierzy                         pi
For[d = Length[omega3], d > 0, d--,
dla     długość
 {If[Abs[omega3[[d]] - 14.2353] < 0.0001, omega3[[d]] = Sequence[]]}];
  ⋯  wartość bezwzględna                               kolejność argumentów

mOmega3[[ii, iii]] = omega3;
Print["częstotliwość przy -Pt ", omega3];
drukuj
```

```
 , {iii, 1, Length[Pt]}];
            długość
 ,
 {ii, Length[msnei]}]
       długość

Out[150]= {0., -0.25, -0.5, -0.75}

Out[156]= {3}

mnożnik 30

wyniki  {0.}

iteracja 1

q={0., 0., 0., 0., 0., 0., 0., 0., 0., 0., 0., 0., 0., 0., 0., 0., 0., 0., 0., 0., 0.,
  0., 0., 0., 0., 0., 0., 0., 0., 0., 0., 0., 0., 0., 0., 0., 0., 0., 0., 0., 0., 0.,
  0., 0., 0., 0., 0., 0., 0., 0., 0., 0., 0., 0., 0., 0., 0., 0., 0., 0., 0., 0., 0.,
  0., 0., 0., 0., 0., 0., 0., 0., 0., 0., 0., 0., 0., 0., 0., 0., 0., 0., 0., 0., 0.,
  0., 0., 0., 0., 0., 0., 0., 0., 0., 0., 0., 0., 0., 0., 0., 0., 0., 0., 0., 0., 0.,
  0., 0., 0., 0., 0., 0., 0., 0., 0., 0., 0., 0., 0., 0., 0., 0., 0., 0., 0., 0., 0.}

sily w pretach {-2.53623, -9.13043, -30., -2.53623, -9.13043, -30., -2.53623, -9.13043,
  -30., -2.53623, -9.13043, -30., -2.53623, -9.13043, -30., -2.53623, -9.13043, -30.,
  15.4273, 27.6386, 60.184, 11.1615, 27.6386, 60.184, 15.4273, 27.6386, 60.184, 11.1615,
  27.6386, 60.184, 15.4273, 27.6386, 60.184, 11.1615, 27.6386, 60.184, 15.4273, 27.6386,
  60.184, 11.1615, 27.6386, 60.184, 15.4273, 27.6386, 60.184, 11.1615, 27.6386, 60.184,
  15.4273, 27.6386, 60.184, 11.1615, 27.6386, 60.184, 15.2174, 10.8696, 26.087, 52.1739,
  15.2174, 10.8696, 26.087, 52.1739, 15.2174, 10.8696, 26.087, 52.1739, 15.2174, 10.8696,
  26.087, 52.1739, 15.2174, 10.8696, 26.087, 52.1739, 15.2174, 10.8696, 26.087, 52.1739}

spr {0, 0, 0, 0, 0, 0, 0, 0, 0, 0, 0, 0, 0, 0, 0, 0, 0, 0, 0, 0, 0, 0, 0, 0, 0, 0, 0, 0, 0, 0, 0, 0, 0,
  0, 0, 0, 0, 0, 0, 0, 0, 0, 0, 0, 0, 0, 0, 0, 0, 0, 0, 0, 0, 0, 0, 0, 0, 0, 0, 0, 0, 0, 0, 0,
  0, 0, 0, 0, 0, 0, 0, 0, 0, 0, 0, 0, 0, 0, 0, 0, 0, 0, 0, 0, 0, 0, 0, 0, 0, 0, 0, 0, 0, 0, 0,
  0, 0, 0, 0, 0, 0, 0, 0, 0, 0, 0, 0, 0, 0, 0, 0, 0, 0, 0, 0, 0, 0, 0, 0, 0, 0, 0, 0, 0, 0, 0}

częstotliwości drgan własnych
 {4.71503, 4.9531, 4.9531, 6.83724, 6.96388, 6.96388, 7.04104, 7.05945, 7.59237, 7.59237,
  7.82074, 7.82074, 8.93841, 8.93841, 10.539, 11.6654, 11.6654, 12.244, 12.4476, 12.5922,
  12.5922, 12.6134, 12.6134, 13.7178, 14.5335, 14.912, 14.912, 17.9385, 25.2469, 25.2469,
  29.8389, 42.0087, 90.4082, 90.5505, 90.5505, 112.701, 112.701, 118.694, 125.645, 125.645,
  131.411, 189.65, 189.65, 200.977, 200.977, 226.768, 251.439, 277.108, 277.108, 297.228,
  297.228, 305.045, 314.6, 345.188, 353.508, 353.508, 392.148, 392.148, 410.102, 410.102,
  487.845, 487.845, 509.772, 538.57, 575.405, 575.405, 581.531, 594.773, 594.773, 614.938,
  614.938, 623.711, 629.17, 636.58, 636.58, 663.661, 663.661, 667.932, 695.224, 733.471,
  733.471, 875.768, 875.768, 915.084, 928.291, 941.738, 941.738, 1005.44, 1005.44, 1048.06,
  1193.93, 1250.29, 1345.41, 1345.41, 1520.84, 1520.84, 1625.76, 1625.76, 1723.39,
  1922.44, 1922.44, 2009.25, 2036.65, 2081.03, 2081.03, 2251.11, 2251.11, 2353.41}

wyniki  {1.47032×10^-3}

iteracja 2
```

```
q={-0.00193766, -7.11402×10^-9, -0.00818949, 0.000296686, -5.07718×10^-8, -0.00818355,
  -0.00102248, -5.5495×10^-8, -0.0025456, 0.000275457, -1.00363×10^-8, -0.00254366,
  -0.000376403, -2.49715×10^-8, -0.000664961, 0.000372742, 7.86426×10^-9, -0.00066272,
  0., 0., 0., -0.00125361, 0.000331556, -0.00112344, 0.0000103019, -0.000220551,
  -0.00112186, -0.000720157, 0.0000919607, -0.000687676, 0.000148948, -0.0000676858,
  -0.000686766, -0.000292005, 0.0000139497, -0.000240574, 0.000304432, -0.0000268405,
  -0.000238742, 0., 0., 0., -0.00123441, 0.0000968307, 0.00270995, 0.0000227839,
  -0.0000425233, 0.00271127, -0.000699743, 0.000037915, 0.000890144, 0.000144041,
  -0.0000146778, 0.000890808, -0.000280609, 7.76446×10^-6, 0.000246987, 0.000293527,
  -5.18446×10^-6, 0.000248543, 0., 0., 0., -0.00105501, 7.6995×10^-8, 0.00392334,
  -0.0000523886, 2.81847×10^-8, 0.00392416, -0.000630107, 8.56022×10^-8, 0.00147032,
  0.000107776, -1.52947×10^-9, 0.00147085, -0.00025893, 3.47253×10^-8, 0.00044108,
  0.000262787, -1.67786×10^-8, 0.000442527, 0., 0., 0., -0.00123448, -0.000096718,
  0.00270967, 0.0000227067, 0.0000425359, 0.00271099, -0.000699863, -0.0000378181,
  0.000890085, 0.000144036, 0.0000146721, 0.00089075, -0.00028066, -7.72598×10^-6,
  0.000246973, 0.000293548, 5.16294×10^-6, 0.000248528, 0., 0., 0., -0.00125368,
  -0.000331533, -0.00112369, 0.000010225, 0.000220489, -0.00112211, -0.000720278,
  -0.0000919995, -0.000687746, 0.000148944, 0.0000676683, -0.000686836, -0.000292055,
  -0.0000139703, -0.000240586, 0.000304453, 0.0000268442, -0.000238754, 0., 0., 0.}

sily w pretach {-2.96502, -9.2687, -30.1331, -2.53371, -9.19563, -30.1102, -2.53315,
  -9.17268, -30.0932, -2.53274, -9.16559, -30.0872, -2.53315, -9.17268, -30.0932,
  -2.53371, -9.19563, -30.1102, 14.8038, 27.3106, 60.0402, 11.4758, 27.8348, 60.3939,
  14.8616, 27.3485, 60.0756, 11.4534, 27.8293, 60.3908, 14.8344, 27.3323, 60.0607,
  11.4651, 27.8318, 60.3917, 14.8284, 27.3258, 60.054, 11.4649, 27.8321, 60.3923,
  14.8344, 27.3323, 60.0607, 11.4651, 27.8318, 60.3917, 14.8616, 27.3485, 60.0756,
  11.4534, 27.8293, 60.3908, 14.6403, 11.164, 26.2688, 52.3541, 14.6303, 11.1655,
  26.2694, 52.3543, 14.6372, 11.1617, 26.2686, 52.3537, 14.6372, 11.1617, 26.2686,
  52.3537, 14.6303, 11.1655, 26.2694, 52.3543, 14.6403, 11.164, 26.2688, 52.3541}

spr {0, 0, -0.999999, 0, 0, 0, 0, 0, 0, 0, 0, 0, 0, 0, 0, 0, 0, 0, 0, 0, 0, 0, 0, 0, 0, 0, 0, 0, 0, 0, 0,
  0, 0, 0, 0, 0, 0, 0, 0, 0, 0, 0, 0, 0, 0, 0, 0, 0, 0, 0, 0, 0, 0, 0, 0, 0, 0, 0, 0, 0, 0, 0, 0,
  0, 0, 0, 0, 0, 0, 0, 0, 0, 0, 0, 0, 0, 0, 0, 0, 0, 0, 0, 0, 0, 0, 0, 0, 0, 0, 0, 0, 0, 0, 0, 0,
  0, 0, 0, 0, 0, 0, 0, 0, 0, 0, 0, 0, 0, 0, 0, 0, 0, 0, 0, 0, 0, 0, 0, 0, 0, 0, 0, 0, 0, 0, 0, 0}

częstotliwości drgan wymuszonych
 {4.70215, 4.9426, 4.94301, 6.80046, 6.92813, 6.93206, 7.00574, 7.06777, 7.574, 7.57539,
  7.79303, 7.79473, 8.9469, 8.94741, 10.5546, 11.6585, 11.6594, 12.2527, 12.3889, 12.5459,
  12.5494, 12.5571, 12.5602, 13.7364, 14.6044, 14.8289, 14.8322, 17.6106, 25.1126, 25.1147,
  29.6844, 42.0084, 90.4071, 90.5497, 90.5498, 112.697, 112.697, 118.686, 125.644, 125.644,
  131.408, 189.649, 189.649, 200.977, 200.977, 226.767, 251.44, 277.106, 277.107, 297.229,
  297.229, 305.044, 314.598, 345.188, 353.509, 353.509, 392.148, 392.148, 410.098, 410.099,
  487.845, 487.845, 509.772, 538.57, 575.406, 575.406, 581.53, 594.766, 594.768, 614.938,
  614.938, 623.712, 629.169, 636.581, 636.581, 663.661, 663.661, 667.923, 695.224, 733.469,
  733.469, 875.766, 875.766, 915.083, 928.287, 941.737, 941.737, 1005.44, 1005.44, 1048.06,
  1193.93, 1250.29, 1345.41, 1345.41, 1520.84, 1520.84, 1625.76, 1625.76, 1723.39,
  1922.44, 1922.44, 2009.24, 2036.64, 2081.03, 2081.03, 2251.11, 2251.11, 2353.41}

0.
```

częstotliwość przy +Pt

{9.4043, 9.8852, 9.88601, 13.6009, 13.8563, 13.8641, 14.0115, 14.1355, 15.148, 15.1508,
15.5861, 15.5895, 17.8938, 17.8948, 21.1093, 23.317, 23.3189, 24.5055, 24.7779, 25.0918,
25.0987, 25.1143, 25.1204, 27.4727, 29.2088, 29.6578, 29.6644, 35.2211, 50.2251, 50.2294,
59.3688, 84.0169, 180.814, 181.099, 181.1, 225.393, 225.393, 237.372, 251.288, 251.288,
262.817, 379.298, 379.298, 401.954, 401.954, 453.535, 502.879, 554.213, 554.213, 594.457,
594.458, 610.089, 629.196, 690.376, 707.018, 707.018, 784.296, 784.296, 820.197, 820.199,
975.691, 975.691, 1019.54, 1077.14, 1150.81, 1150.81, 1163.06, 1189.53, 1189.54, 1229.88,
1229.88, 1247.42, 1258.34, 1273.16, 1273.16, 1327.32, 1327.32, 1335.85, 1390.45, 1466.94,
1466.94, 1751.53, 1751.53, 1830.17, 1856.57, 1883.47, 1883.47, 2010.88, 2010.88, 2096.12,
2387.87, 2500.58, 2690.82, 2690.82, 3041.67, 3041.67, 3251.51, 3251.51, 3446.78,
3844.88, 3844.88, 4018.49, 4073.29, 4162.06, 4162.06, 4502.22, 4502.22, 4706.81}

częstotliwość przy -Pt

{9.4043, 9.8852, 9.88601, 13.6009, 13.8563, 13.8641, 14.0115, 14.1355, 15.148, 15.1508,
15.5861, 15.5895, 17.8938, 17.8948, 21.1093, 23.317, 23.3189, 24.5055, 24.7779, 25.0918,
25.0987, 25.1143, 25.1204, 27.4727, 29.2088, 29.6578, 29.6644, 35.2211, 50.2251, 50.2294,
59.3688, 84.0169, 180.814, 181.099, 181.1, 225.393, 225.393, 237.372, 251.288, 251.288,
262.817, 379.298, 379.298, 401.954, 401.954, 453.535, 502.879, 554.213, 554.213, 594.457,
594.458, 610.089, 629.196, 690.376, 707.018, 707.018, 784.296, 784.296, 820.197, 820.199,
975.691, 975.691, 1019.54, 1077.14, 1150.81, 1150.81, 1163.06, 1189.53, 1189.54, 1229.88,
1229.88, 1247.42, 1258.34, 1273.16, 1273.16, 1327.32, 1327.32, 1335.85, 1390.45, 1466.94,
1466.94, 1751.53, 1751.53, 1830.17, 1856.57, 1883.47, 1883.47, 2010.88, 2010.88, 2096.12,
2387.87, 2500.58, 2690.82, 2690.82, 3041.67, 3041.67, 3251.51, 3251.51, 3446.78,
3844.88, 3844.88, 4018.49, 4073.29, 4162.06, 4162.06, 4502.22, 4502.22, 4706.81}

-0.25

częstotliwość przy +Pt

{9.40193, 9.88347, 9.88439, 13.5925, 13.8486, 13.8574, 14.004, 14.1392, 15.1448, 15.1479,
15.5807, 15.5844, 17.8976, 17.8987, 21.1152, 23.3173, 23.3193, 24.5093, 24.7657, 25.0826,
25.0906, 25.1031, 25.1096, 27.48, 29.2252, 29.64, 29.6481, 35.1454, 50.1966, 50.2014,
59.3361, 84.0168, 180.814, 181.099, 181.099, 225.392, 225.393, 237.371, 251.288, 251.288,
262.816, 379.298, 379.298, 401.954, 401.954, 453.535, 502.88, 554.213, 554.213, 594.458,
594.458, 610.089, 629.195, 690.376, 707.018, 707.018, 784.296, 784.296, 820.196, 820.198,
975.691, 975.691, 1019.54, 1077.14, 1150.81, 1150.81, 1163.06, 1189.53, 1189.54, 1229.88,
1229.88, 1247.43, 1258.34, 1273.16, 1273.16, 1327.32, 1327.32, 1335.84, 1390.45, 1466.94,
1466.94, 1751.53, 1751.53, 1830.17, 1856.57, 1883.47, 1883.47, 2010.88, 2010.88, 2096.12,
2387.87, 2500.58, 2690.82, 2690.82, 3041.67, 3041.67, 3251.51, 3251.51, 3446.78,
3844.88, 3844.88, 4018.49, 4073.29, 4162.06, 4162.06, 4502.22, 4502.22, 4706.81}

częstotliwość przy -Pt

{9.40686, 9.88713, 9.88784, 13.6095, 13.8642, 13.8711, 14.0193, 14.1322, 15.1516, 15.154,
15.5918, 15.5948, 17.8904, 17.8913, 21.1039, 23.3172, 23.3189, 24.5021, 24.7907, 25.1015,
25.1074, 25.1261, 25.1318, 27.4661, 29.1919, 29.6762, 29.6816, 35.2983, 50.2548, 50.2585,
59.4028, 84.0169, 180.814, 181.1, 181.1, 225.394, 225.394, 237.374, 251.288, 251.288,
262.817, 379.298, 379.298, 401.954, 401.954, 453.535, 502.879, 554.213, 554.214, 594.457,
594.457, 610.089, 629.196, 690.376, 707.018, 707.018, 784.296, 784.296, 820.198, 820.2,
975.691, 975.691, 1019.54, 1077.14, 1150.81, 1150.81, 1163.06, 1189.53, 1189.54, 1229.88,
1229.88, 1247.42, 1258.34, 1273.16, 1273.16, 1327.32, 1327.32, 1335.85, 1390.45, 1466.94,
1466.94, 1751.53, 1751.53, 1830.17, 1856.58, 1883.47, 1883.47, 2010.88, 2010.88, 2096.12,
2387.87, 2500.58, 2690.82, 2690.82, 3041.68, 3041.68, 3251.51, 3251.51, 3446.78,
3844.88, 3844.88, 4018.49, 4073.29, 4162.06, 4162.06, 4502.22, 4502.22, 4706.81}

-0.5

```
częstotliwość przy +Pt
{9.39975, 9.88193, 9.88297, 13.5842, 13.8412, 13.851, 13.9968, 14.1433, 15.1418, 15.1453,
 15.5756, 15.5798, 17.9018, 17.9031, 21.1215, 23.3181, 23.3202, 24.5135, 24.754, 25.0738,
 25.0831, 25.0927, 25.0993, 27.4878, 29.2411, 29.6229, 29.6328, 35.0713, 50.1693, 50.1746,
 59.3048, 84.0168, 180.814, 181.099, 181.099, 225.392, 225.392, 237.369, 251.288, 251.288,
 262.816, 379.298, 379.298, 401.954, 401.954, 453.535, 502.88, 554.212, 554.212, 594.458,
 594.458, 610.089, 629.195, 690.376, 707.019, 707.019, 784.296, 784.296, 820.195, 820.198,
 975.691, 975.691, 1019.54, 1077.14, 1150.81, 1150.81, 1163.06, 1189.53, 1189.53, 1229.88,
 1229.88, 1247.43, 1258.34, 1273.16, 1273.16, 1327.32, 1327.32, 1335.84, 1390.45, 1466.94,
 1466.94, 1751.53, 1751.53, 1830.17, 1856.57, 1883.47, 1883.47, 2010.88, 2010.88, 2096.12,
 2387.87, 2500.58, 2690.82, 2690.82, 3041.67, 3041.67, 3251.51, 3251.51, 3446.78,
 3844.87, 3844.88, 4018.49, 4073.29, 4162.06, 4162.06, 4502.21, 4502.22, 4706.81}
częstotliwość przy -Pt
{9.40962, 9.88927, 9.88987, 13.6183, 13.8725, 13.8784, 14.0274, 14.1292, 15.1554, 15.1575,
 15.5979, 15.6005, 17.8873, 17.8881, 21.0988, 23.3178, 23.3193, 24.499, 24.804, 25.1116,
 25.1166, 25.1387, 25.1437, 27.46, 29.1746, 29.6953, 29.6996, 35.377, 50.2856, 50.2888,
 59.4381, 84.0169, 180.815, 181.1, 181.1, 225.395, 225.395, 237.376, 251.289, 251.289,
 262.818, 379.298, 379.298, 401.954, 401.954, 453.535, 502.879, 554.214, 554.214, 594.457,
 594.457, 610.089, 629.197, 690.376, 707.017, 707.017, 784.296, 784.296, 820.199, 820.2,
 975.691, 975.691, 1019.54, 1077.14, 1150.81, 1150.81, 1163.06, 1189.53, 1189.54, 1229.88,
 1229.88, 1247.42, 1258.34, 1273.16, 1273.16, 1327.32, 1327.32, 1335.85, 1390.45, 1466.94,
 1466.94, 1751.53, 1751.53, 1830.17, 1856.58, 1883.47, 1883.47, 2010.88, 2010.88, 2096.12,
 2387.87, 2500.58, 2690.82, 2690.82, 3041.68, 3041.68, 3251.52, 3251.52, 3446.78,
 3844.88, 3844.88, 4018.49, 4073.29, 4162.06, 4162.06, 4502.22, 4502.22, 4706.81}
-0.75
częstotliwość przy +Pt
{9.39777, 9.88061, 9.88176, 13.5762, 13.8341, 13.8449, 13.9899, 14.1476, 15.1392, 15.1431,
 15.571, 15.5754, 17.9064, 17.9078, 21.1283, 23.3192, 23.3216, 24.5181, 24.7429, 25.0655,
 25.0762, 25.0831, 25.0896, 27.4962, 29.2563, 29.6065, 29.6186, 34.9988, 50.1431, 50.1489,
 59.275, 84.0168, 180.814, 181.099, 181.099, 225.391, 225.391, 237.368, 251.288, 251.288,
 262.815, 379.298, 379.298, 401.954, 401.954, 453.535, 502.88, 554.212, 554.212, 594.458,
 594.458, 610.089, 629.194, 690.377, 707.019, 707.019, 784.296, 784.296, 820.194, 820.197,
 975.691, 975.691, 1019.54, 1077.14, 1150.81, 1150.81, 1163.06, 1189.53, 1189.53, 1229.88,
 1229.88, 1247.43, 1258.34, 1273.16, 1273.16, 1327.32, 1327.32, 1335.84, 1390.45, 1466.94,
 1466.94, 1751.53, 1751.53, 1830.17, 1856.57, 1883.47, 1883.47, 2010.88, 2010.88, 2096.12,
 2387.87, 2500.58, 2690.82, 2690.82, 3041.67, 3041.67, 3251.51, 3251.51, 3446.78,
 3844.87, 3844.88, 4018.49, 4073.28, 4162.06, 4162.06, 4502.21, 4502.22, 4706.81}
częstotliwość przy -Pt
{9.41256, 9.8916, 9.89209, 13.6273, 13.881, 13.8859, 14.0358, 14.1266, 15.1596, 15.1613,
 15.6043, 15.6065, 17.8846, 17.8853, 21.0943, 23.3189, 23.3201, 24.4963, 24.8179, 25.1224,
 25.1265, 25.1519, 25.1563, 27.4545, 29.157, 29.7151, 29.7185, 35.4571, 50.3175, 50.3202,
 59.4748, 84.017, 180.815, 181.1, 181.1, 225.396, 225.396, 237.377, 251.289, 251.289,
 262.819, 379.298, 379.298, 401.954, 401.954, 453.535, 502.879, 554.214, 554.214, 594.457,
 594.457, 610.089, 629.197, 690.376, 707.017, 707.017, 784.296, 784.296, 820.2, 820.201,
 975.691, 975.691, 1019.54, 1077.14, 1150.81, 1150.81, 1163.06, 1189.54, 1189.54, 1229.88,
 1229.88, 1247.42, 1258.34, 1273.16, 1273.16, 1327.32, 1327.32, 1335.85, 1390.45, 1466.94,
 1466.94, 1751.53, 1751.53, 1830.17, 1856.58, 1883.48, 1883.48, 2010.88, 2010.88, 2096.12,
 2387.87, 2500.59, 2690.82, 2690.82, 3041.68, 3041.68, 3251.52, 3251.52, 3446.78,
 3844.88, 3844.88, 4018.49, 4073.29, 4162.06, 4162.06, 4502.22, 4502.22, 4706.81}
```

```
qwybr = 24;
mMian = mGPS = mSC = mSZ = mWC = mWZ = muu = Table[0, {Length[msnei]}];
```

```
mq11 = mq22 = mq33 = mqq11 = mqq22 = mqq33 = Table[0, {Length[msnei]}];
                                             tabela    długość
qx = qy = qz = Table[0, {Length[msnei]}, {Length[qq[[1]]] / 3}];
               tabela    długość          długość
qmax = qmax2 = Table[0, {Length[msnei]}, {6}];
               tabela    długość
(*sily w pretach*)
Do[
rób
  msne = msnei[[ii]];
  Print["mnoznik ", msne];
  drukuj
  uu = mSwP[[ii]] + wy0 * msne;
  muu[[ii]] = uu;
  Print["siły w prętach ", uu];
  drukuj
  (*mianownik GPS*)
  q = qq[[ii]];
  Do[
  rób
   qx[[ii, iii]] = q[[3 * iii - 2]];
   qy[[ii, iii]] = q[[3 * iii - 1]];
   qz[[ii, iii]] = q[[3 * iii]],
   {iii, Length[q] / 3}];
         długość
  qmax[[ii, 1]] = 1000 * Max[qx[[ii, All]]];
                         maksimum   wszystko
  qmax[[ii, 2]] = 1000 * Min[qx[[ii, All]]];
                         minimum    wszystko
  qmax[[ii, 3]] = 1000 * Max[qy[[ii, All]]];
                         maksimum   wszystko
  qmax[[ii, 4]] = 1000 * Min[qy[[ii, All]]];
                         minimum    wszystko
  qmax[[ii, 5]] = 1000 * Max[qz[[ii, All]]];
                         maksimum   wszystko
  qmax[[ii, 6]] = 1000 * Min[qz[[ii, All]]];
                         minimum    wszystko
  qmax2[[ii, 1]] = Flatten[1000 * qq2[[ii, 3 * Ordering[qx[[ii, All]], -1] - 2]]];
                   spłaszcz                    pozycja w liście  wszystko
  qmax2[[ii, 2]] = Flatten[1000 * qq2[[ii, 3 * Ordering[qx[[ii, All]], 1] - 2]]];
                   spłaszcz                    pozycja w liście  wszystko
  qmax2[[ii, 3]] = Flatten[1000 * qq2[[ii, 3 * Ordering[qy[[ii, All]], -1] - 1]]];
                   spłaszcz                    pozycja w liście  wszystko
  qmax2[[ii, 4]] = Flatten[1000 * qq2[[ii, 3 * Ordering[qy[[ii, All]], 1] - 1]]];
                   spłaszcz                    pozycja w liście  wszystko
  qmax2[[ii, 5]] = Flatten[1000 * qq2[[ii, 3 * Ordering[qz[[ii, All]], -1]]]];
                   spłaszcz                    pozycja w liście  wszystko
  qmax2[[ii, 6]] = Flatten[1000 * qq2[[ii, 3 * Ordering[qz[[ii, All]], 1]]]];
                   spłaszcz                    pozycja w liście  wszystko
  Print["maksymalne przemieszczenie x ",
  drukuj
   1000 * Max[qx[[ii, All]]], ", i = ", Flatten[Ordering[qx[[ii, All]], -1]]];
          maksimum  wszystko             spłaszcz pozycja w liście  wszystko
```

```
Print["minimalne przemieszczenie x ", 1000 * Min[qx[[ii, All]]],
 ", i = ", Flatten[Ordering[qx[[ii, All]], 1]]];
Print["maksymalne przemieszczenie y ", 1000 * Max[qy[[ii, All]]],
 ", i = ", Flatten[Ordering[qy[[ii, All]], -1]]];
Print["minimalne przemieszczenie y ", 1000 * Min[qy[[ii, All]]],
 ", i = ", Flatten[Ordering[qy[[ii, All]], 1]]];
Print["maksymalne przemieszczenie z ", 1000 * Max[qz[[ii, All]]],
 ", i = ", Flatten[Ordering[qz[[ii, All]], -1]]];
Print["minimalne przemieszczenie z ", 1000 * Min[qz[[ii, All]]],
 ", i = ", Flatten[Ordering[qz[[ii, All]], 1]]];
mian = qq[[ii]].MK[qq[[ii]], p1, p2, x, y, z, e, a, sne,
   msnei[[ii]], le, loss, toss, lgss].qq[[ii]];
mMian[[ii]] = mian;
Print["mianownik GPS ", mian];
mGPS[[ii]] = qq[[1]].MK[qq[[1]], p1, p2, x, y,
    z, e, a, sne, msnei[[1]], le, loss, toss, lgss].qq[[1]] / mian;
Print["GPS ", mGPS[[ii]]];
mqq11[[ii]] = qq2[[ii]][[3 * qwybr - 2]] * 1000;
mqq22[[ii]] = qq2[[ii]][[3 * qwybr - 1]] * 1000;
mqq33[[ii]] = qq2[[ii]][[3 * qwybr]] * 1000;
Print["wybrane przemieszczenia II rzędu ", mqq11[[ii]], " ",
 mqq22[[ii]], " ",
 mqq33[[ii]]];

mq11[[ii]] = q[[3 * qwybr - 2]] * 1000;
mq22[[ii]] = q[[3 * qwybr - 1]] * 1000;
mq33[[ii]] = q[[3 * qwybr]] * 1000;
Print["wybrane przemieszczenia III rzędu ", mq11[[ii]], " ",
 mq22[[ii]], " ",
 mq33[[ii]]];

mSC[[ii]] = SetAccuracy[Max[uu], 2];
Print["maksymalna sila w ciegnach ",
 mSC[[ii]]];
Print[Ordering[uu, 1]];
```

```
  mSZ[[ii]] = SetAccuracy[Min[uu], 2];
              ⌊ustawić dokła··· ⌊minimum
  Print["minimalna sila w zastrzalach ",
  ⌊drukuj
   mSZ[[ii]]];
  Print[Ordering[uu, -1]];
        ⌊pozycja w liście
  mWC[[ii]] = SetAccuracy[Max[uu] / 110.2, 4];
              ⌊ustawić dokła··· ⌊maksimum
  Print["wytęzenie ciegien ",
  ⌊drukuj
   mWC[[ii]]];

  nrz = 3;
  nn = {-107.1, -170.5, -224.3}; (*nośności prętów*)

  r1 = Join[uu[[3 ;; 3]], uu[[6 ;; 6]],
       ⌊połącz
    uu[[9 ;; 9]], uu[[12 ;; 12]], uu[[15 ;; 15]], uu[[18 ;; 18]]];

  r2 = Join[uu[[2 ;; 2]], uu[[5 ;; 5]],
       ⌊połącz
    uu[[8 ;; 8]], uu[[11 ;; 11]], uu[[14 ;; 14]], uu[[17 ;; 17]]];

  r3 = Join[uu[[1 ;; 1]], uu[[4 ;; 4]],
       ⌊połącz
    uu[[7 ;; 7]], uu[[10 ;; 10]], uu[[13 ;; 13]], uu[[16 ;; 16]]];

  wz = Table[0, {Length[r1] + Length[r2] + Length[r3]}];
       ⌊tabela  ⌊długość     ⌊długość     ⌊długość
  Do[wz[[x]] = uu[[x]] / nn[[1]], {x, Length[r1]}];
                                      ⌊długość
  Do[wz[[x + Length[r1]]] = uu[[x + Length[r1]]] / nn[[2]], {x, Length[r2]}];
              ⌊długość             ⌊długość                    ⌊długość
  Do[wz[[x + Length[r1] + Length[r2]]] =
              ⌊długość     ⌊długość
    uu[[x + Length[r1] + Length[r2]]] / nn[[3]], {x, Length[r3]}];
            ⌊długość     ⌊długość                    ⌊długość

  mWZ[[ii]] = SetAccuracy[Min[wz], 4];
              ⌊ustawić dokła··· ⌊minimum
  Print["wytęzenie zastrzałow ",
  ⌊drukuj
   mWZ[[ii]]];
  Print["  "],
  ⌊drukuj
  {ii, Length[msnei]}];
       ⌊długość
r1
r2
r3
wz
```

```
w1 = Join[{{"qx3", "-qx3", "qy3", "-qy3", "qz3", "-qz3"}}, qmax];
      |połącz
w2 =
  Join[{{"qx2", "-qx2", "qy2", "-qy2", "qz2", "-qz2"}}, Flatten[qmax2, {{1}, {2, 3}}]];
  |połącz                                              |spłaszcz
w = Table[0, {Length[msnei] + 1}, {12}];
    |tabela    |długość
Do[Do[w[[j]][[2 i - 1]] = w2[[j, i]];
   |rób
   w[[j]][[2 i]] = w1[[j, i]], {i, 6}], {j, Length[msnei] + 1}];
                                            |długość

x1 = x2 = y1 = y2 = Table[0, {Length[Pt]}];
                    |tabela   |długość
Pola = lambda = Table[0, {Length[msnei]}];
                |tabela   |długość
(*n=7;*)
Do[
|rób
 Do[
 |rób
  Do[
  |rób
   y1[[i]] = mOmega2[[m, i, n]];
   y2[[i]] = mOmega3[[m, Length[Pt] + 1 - i, n]];
                        |długość
   y = Join[y1, y2[[1 ;; Length[Pt] - 1]]];
       |połącz         |długość
   x1[[i]] = Pt[[i]];
   x2[[i]] = Pt[[Length[Pt] + 1 - i]];
                 |długość
   x = Join[x1, x2[[1 ;; Length[Pt] - 1]]],
       |połącz         |długość
   {i, 1, Length[Pt]}];
          |długość
  area = 0;
Do[
|rób
If[i < 2 * Length[Pt] - 1,
|oper···   |długość
(pointX1 = x[[i]];
pointY1 = y[[i]];
pointX2 = x[[i + 1]];
pointY2 = y[[i + 1]]),
(pointX1 = x[[i]];
pointY1 = y[[i]];
pointX2 = x[[1]];
pointY2 = y[[1]])
];
area += pointX1 * pointY2 - pointX2 * pointY1;
, {i, 1, 2 * Length[Pt] - 1}];
              |długość
```

```
  Pola[[m]] = Abs[area / 2]
              wartość bezwzględna
  , {m, 1, Length[msnei]}];
              długość

 Do[lambda[[o]] = Pola[[o]] / Max[Pola]
 rób                          maksimum
  , {o, 1, Length[lambda]}];
              długość
 par1 = Join[{-Pt}, mOmega2[[All, All, n]]];
        połącz              ws···  wszystko
 par2 = Join[{Pt}, mOmega3[[All, All, n]]];
        połącz             ws···  wszystko
 par = Table[0, {Length[msnei] + 1}, {Length[Pt] * 2}];
       tabela    długość              długość
 Do[Do[par[[j]][[i]] = par1[[j, i]];
    rób
   par[[j]][[i + Length[Pt]]] = par2[[j, i]], {i, Length[Pt]}],
                 długość                           długość
  {j, Length[msnei] + 1}];
      długość
 SetDirectory[NotebookDirectory[]];
              katalog notatnika
 str = CreateFile[ToFileName[{Directory[]}, ToString[n] <> ".xlsx"]];
       stwórz plik            katalog      przemień na ciąg znaków
 Export[str, {Transpose[Join[List /@ Join[List /@ {ss}, msnei], par, 2]],
              transpozycja poł··· lista  poł··· lista
   Prepend[{Pola, lambda}, msnei]}]
   dołącz do początku
 , {n, 1, 31}]

(******************************************************)
Export[ToFileName[{NotebookDirectory[]}, "wyniki_III R6B.xlsx"],
                   katalog notatnika
  {"statyka 1" → Prepend[
                 dołącz do początku
     Transpose[{msnei, mqq11, mq11, mqq22, mq22, mqq33, mq33, mWC, mWZ, mGPS, mMian}],
     transpozycja
     {"ss", "wybrany węzeł x - II", "wybrany węzeł x - III", "wybrany węzeł y - II",
      "wybrany węzeł y - III", "wybrany węzeł z - II", "wybrany węzeł z - III",
      "wytężenie cięgna", "wytężenie zastrzały", "GPS", "mianownik"}],
   "statyka 2" → Join[List /@ Join[List /@ {ss}, msnei], w, 2], "N(P+S)" → Transpose[
                 poł··· lista  poł··· lista                            przybliżeni··· transpozycja
     Join[List /@ Join[List /@ {ss}, msnei], Join[{Range[1, le]}, muu], 2]], "N(P)" →
     poł··· lista  poł··· lista                połącz  zakres                      przybliżenie nu
    Transpose[Join[List /@ Join[List /@ {ss}, msnei], Join[{Range[1, le]}, mSwP], 2]],
              poł··· lista  poł··· lista                połącz  zakres
   "częstotliwości drgań własnych" → Join[List /@ Join[List /@ {ss}, msnei],
                                     poł··· lista  poł··· lista
     Join[{Range[1, Length[mOmega0[[1]]]]}, mOmega0], 2],
           zakres   długość
   "częstotliwości drgań wymuszonych" → Join[List /@ Join[List /@ {ss}, msnei],
                                        poł··· lista  poł··· lista
```

```
Join[{Range[1, Length[mOmega[[1]]]], mOmega], 2]}];
      zakres    długość
```

```
mnoznik 30

siły w prętach {-2.96502, -9.2687, -30.1331, -2.53371, -9.19563, -30.1102, -2.53315,
  -9.17268, -30.0932, -2.53274, -9.16559, -30.0872, -2.53315, -9.17268, -30.0932,
  -2.53371, -9.19563, -30.1102, 14.8038, 27.3106, 60.0402, 11.4758, 27.8348, 60.3939,
  14.8616, 27.3485, 60.0756, 11.4534, 27.8293, 60.3908, 14.8344, 27.3323, 60.0607,
  11.4651, 27.8318, 60.3917, 14.8284, 27.3258, 60.054, 11.4649, 27.8321, 60.3923,
  14.8344, 27.3323, 60.0607, 11.4651, 27.8318, 60.3917, 14.8616, 27.3485, 60.0756,
  11.4534, 27.8293, 60.3908, 14.6403, 11.164, 26.2688, 52.3541, 14.6303, 11.1655,
  26.2694, 52.3543, 14.6372, 11.1617, 26.2686, 52.3537, 14.6372, 11.1617, 26.2686,
  52.3537, 14.6303, 11.1655, 26.2694, 52.3543, 14.6403, 11.164, 26.2688, 52.3541}

maksymalne przemieszczenie x 0.372742, i = {6}

minimalne przemieszczenie x -1.93766, i = {1}

maksymalne przemieszczenie y 0.331556, i = {8}

minimalne przemieszczenie y -0.331533, i = {36}

maksymalne przemieszczenie z 3.92416, i = {23}

minimalne przemieszczenie z -8.18949, i = {1}

mianownik GPS 0.00818949

GPS 1.

wybrane przemieszczenia II rzędu -0.654605 -1.25695×10^-13 1.5186

wybrane przemieszczenia III rzędu -0.630107 0.0000856022 1.47032

maksymalna sila w ciegnach 60.4

{3}

minimalna sila w zastrzalach -30.1

{24}

wytęzenie ciegien 0.548

wytęzenie zastrzałow 0.011
```

```
Out[164]= {-30.1331, -30.1102, -30.0932, -30.0872, -30.0932, -30.1102}

Out[165]= {-9.2687, -9.19563, -9.17268, -9.16559, -9.17268, -9.19563}

Out[166]= {-2.96502, -2.53371, -2.53315, -2.53274, -2.53315, -2.53371}

Out[167]= {0.0276846, 0.0865425, 0.281355, 0.0236574, 0.0858602,
  0.281141, 0.0148572, 0.0537987, 0.1765, 0.0148548, 0.0537571, 0.176464,
  0.0112936, 0.0408947, 0.134165, 0.0112961, 0.040997, 0.134241}
```